NASA Tech Briefs

National
Aeronautics and
Space
Administration

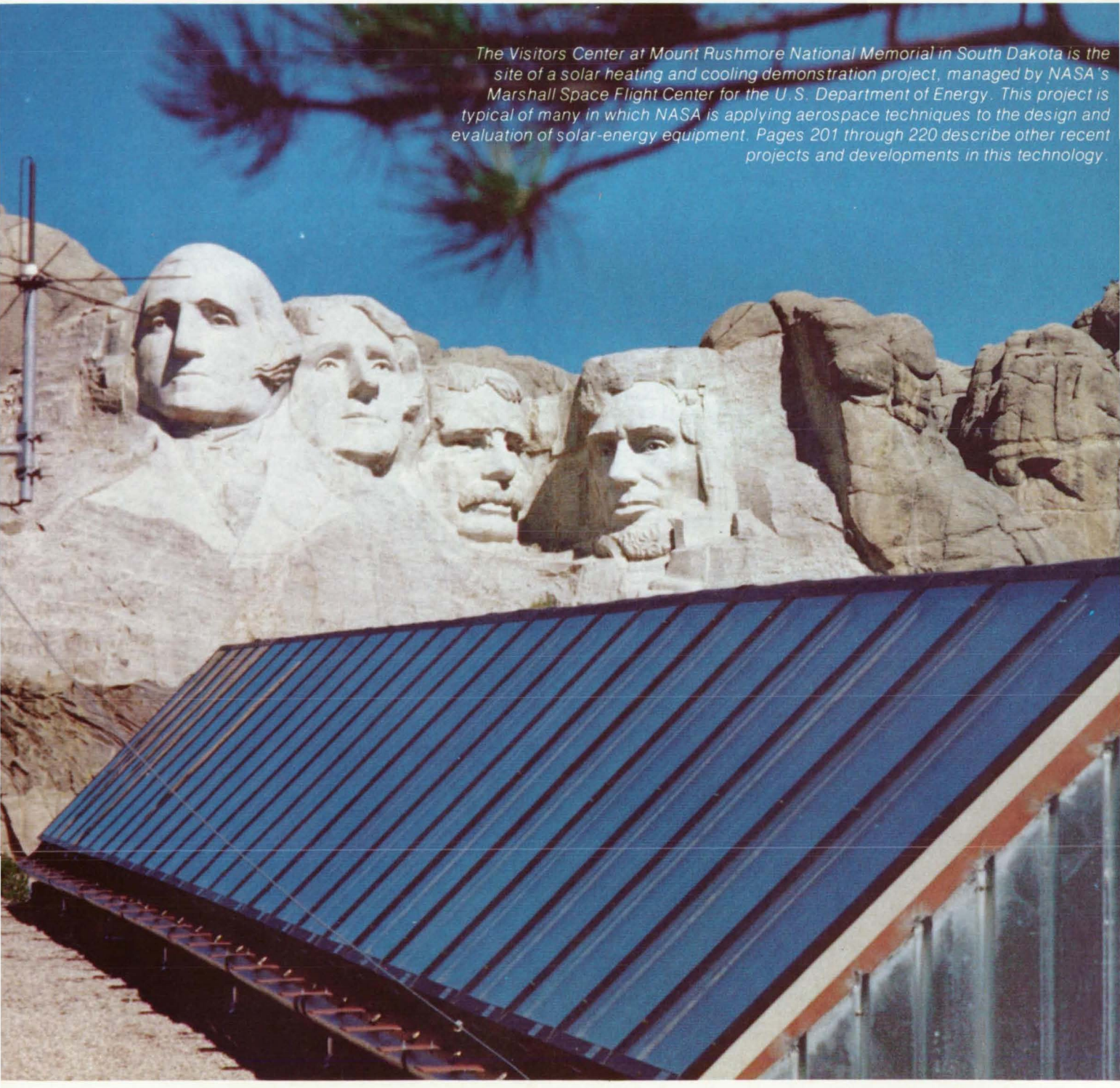

The Visitors Center at Mount Rushmore National Memorial in South Dakota is the site of a solar heating and cooling demonstration project, managed by NASA's Marshall Space Flight Center for the U.S. Department of Energy. This project is typical of many in which NASA is applying aerospace techniques to the design and evaluation of solar-energy equipment. Pages 201 through 220 describe other recent projects and developments in this technology.

Vol. 3, No. 2

SUMMER 1978

About the NASA Technology Utilization Program

The National Aeronautics and Space Act of 1958, which established NASA and the United States civilian space program, requires that "The Administration shall provide for the widest practicable and appropriate dissemination of information concerning its activities and the results thereof."

To help carry out this objective the NASA Technology Utilization (TU) Program was established in 1962. It offers a variety of valuable services to facilitate the transfer of aerospace technology to nonaerospace applications, thus assuring American taxpayers maximum return on their investment in space research; thousands of spinoffs of NASA research have already occurred in virtually every area of our economy.

The TU Program has worked for engineers, scientists, technicians, and businessmen. And it can work for you.

NASA Tech Briefs

Tech Briefs is published quarterly and is free to any U.S. citizen or organization. It is both a current-awareness medium and a problem-solving tool. Potential products ... industrial processes ... basic and applied research ... shop and lab techniques ... computer software ... new sources of technical data ... concepts ... you will find them all in NASA Tech Briefs. The first section highlights a few of the potential new products contained in Tech Briefs. The remainder of the volume is organized by technical category to help you quickly review new developments in your areas of interest. Finally, a subject index makes each issue a convenient permanent reference file.

Further Information on Innovations

Although many articles are complete in themselves, others are backed up by Technical Support Packages (TSP's). TSP's are available without charge and may be ordered by simply completing the enclosed TSP Request Card. Further information on some innovations is available for a nominal fee from other sources, as indicated at the ends of the articles. In addition, Technology Utilization Officers at NASA Field Centers will assist you directly when necessary. (See page A4.)

Patent Licenses

Many of the inventions described are under consideration for patents or have been patented by NASA. Unless NASA has decided not to apply for a patent, the patent status is described at the end of each article. For further information about the Patent Program see page A8.

Other Technology Utilization Services

To assist engineers, industrial researchers, business executives, city officials, and other potential users in applying space technology to their problems, NASA sponsors six Industrial Applications Centers. Their services are described on page A6. In addition, an extensive library of computer programs is available through COSMIC, the Technology Utilization Program's outlet for NASA-developed software. (See page A5.)

Applications Program

To help solve public-sector problems in such areas as safety, health, transportation, and environmental protection, NASA TU Applications Teams, staffed by professionals from a variety of disciplines, work with Federal agencies, local governments, and health organizations to identify critical problems amenable to technical solutions. Among their many significant contributions are a rechargeable heart pacemaker, a lightweight fireman's breathing apparatus, aids for the handicapped, and safer highways.

Reader Feedback

We hope you find the information in NASA Tech Briefs useful. A reader feedback card has been included because we want your comments and suggestions on how we can further help you apply NASA innovations and technology to your needs. Please use it, or if you need more space, write us a letter.

NASA Tech Briefs

National Aeronautics and Space Administration

SUMMER 1978
Volume 3, Number 2

NASA TU Services	A3	Technology Utilization services that can assist you in learning about and applying NASA technology.
New Product Ideas	A9	A summary of selected innovations of value to manufacturers for the development of new products.
Tech Briefs	163	**Electronic Components and Circuits**
	175	**Electronic Systems**
	185	**Physical Sciences**
	209	**Solar Energy**
	221	**Materials**
	235	**Life Sciences**
	255	**Mechanics**
	273	**Machinery**
	289	**Fabrication Technology**
	301	**Mathematics and Information Sciences**
Subject Index	307	Items in this issue are indexed by subject; a cumulative index will be published yearly.

COVERS: The photographs on the front and back covers illustrate recent developments by NASA and its contractors that resulted in commercial and nonaerospace spinoffs. Pages 201 through 220 describe recent NASA developments in solar energy, and the Water Monitor System [back cover] is described on pages 237 through 245.

About This NASA Publication

NASA Tech Briefs, a quarterly publication, is distributed free to U.S. citizens to encourage commercial application of U.S. space technology. For information on publications and services available through the NASA Technology Utilization Program, write to the Director, Technology Utilization Office, P. O. Box 8757, Baltimore/Washington International Airport, Maryland 21240.

"The Administrator of National Aeronautics and Space Administration has determined that the publication of this periodical is necessary in the transaction of the public business required by law of this Agency. Use of funds for printing this periodical has been approved by the Director of the Office of Management and Budget through December 31, 1978."

Change of Address

Change of Address: If you wish to have NASA Tech Briefs forwarded to your new address, use one of the Subscriptions cards enclosed in the back of this volume of NASA Tech Briefs. Be sure to check the appropriate box indicating change of address.

Communication Concerning Editorial Matter

For editorial comments or general communications about NASA Tech Briefs, you may use the self-addressed Feedback card in the back of NASA Tech Briefs, or write to: The Publications Manager, Technology Utilization Office (BTU-6), NASA Headquarters, Washington, DC 20546. Technical questions concerning specific articles should be directed to the Technology Utilization Officer of the sponsoring NASA Center (addresses listed on page A4).

NASA TECH BRIEFS Published Quarterly by the National Aeronautics and Space Administration, Technology Utilization Branch, Washington, DC.

Administrator: **Robert A. Frosch;** Chief, Technology Utilization Branch: **Louis Mogavero;** Publications Program Manager: **Judson O. Harrison III.**

Prepared for the National Aeronautics and Space Administration by **Logical Technical Services Corp.**: Editor-in-Chief: **Graham L. Gross;** Art Director: **Ernest Gillespie;** Managing Editor: **Jay Kirschenbaum;** Senior Editor: **Donald Blattner;** Chief Copy Editor: **Oden Browne;** Staff Editors: **Virginia Otis, Michael Polchaninoff, Johathan Rodgers, Ted Selinsky, George Watson;** Graphics: **Concetto Auditore, Douglas Dunn, Judy Tenenbaum;** Editorial & Production: **Richard Johnson, Sharon Britton, Rose Giglietti, Joan Shaw, Vincent Susinno, John Tucker, Madeline Tucker, Ernestine Walker, Carl Woolridge.**

NASA TU SERVICES

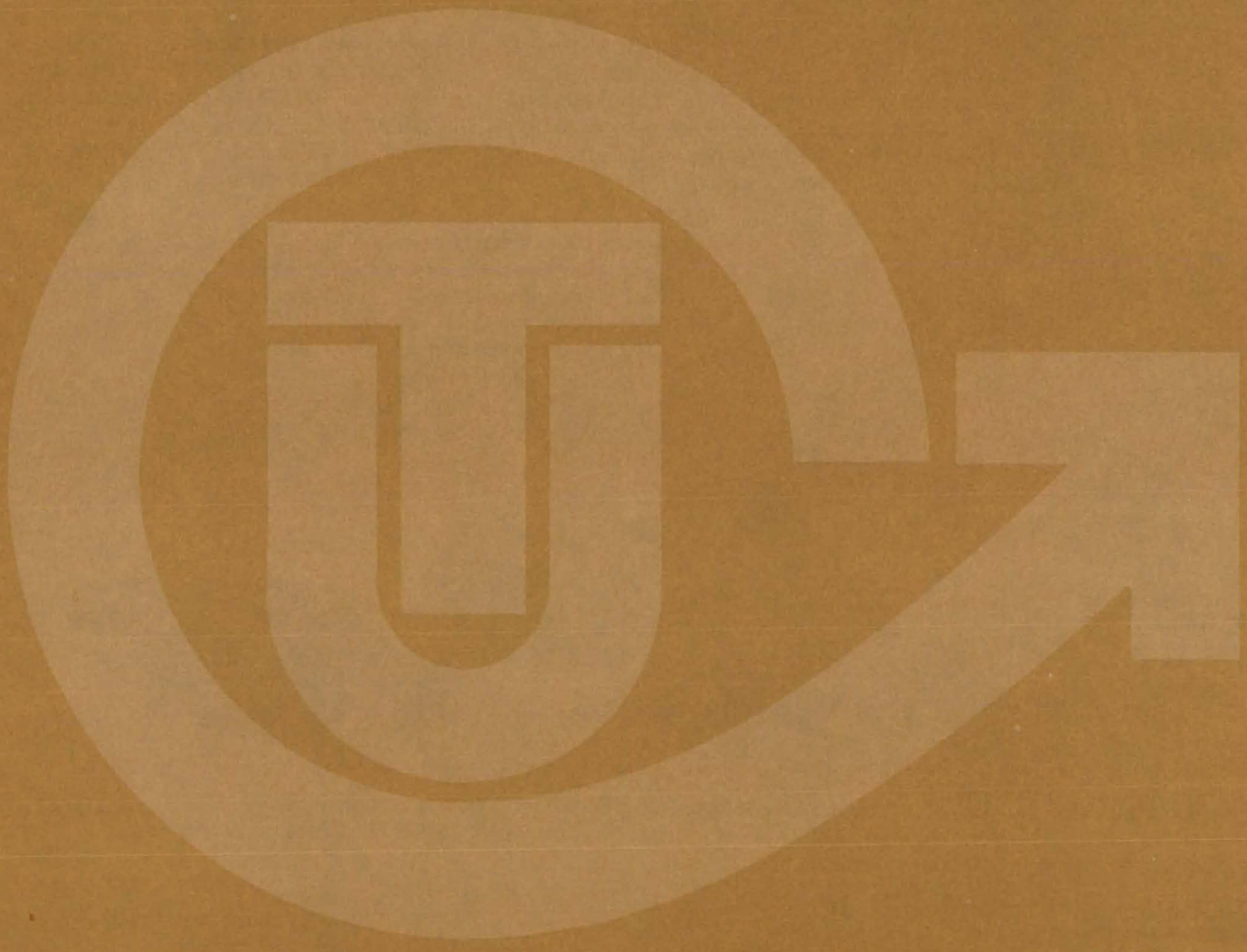

THE NASA TECHNOLOGY UTILIZATION OFFICERS

They will help you apply the innovations described in Tech Briefs.

The Technology Utilization Officer (TUO)
Each NASA Center has a Technology Utilization Officer — An applications engineer whose job is to help you make use of new technology developed at his center. He brings you the NASA Tech Briefs and other special publications, sponsors conferences, and arranges for expert assistance in solving technical problems.

Technical Assistance
Working together with NASA Scientists and Engineers and the Industrial Applications Centers, the center TUO's can answer specific questions about innovations and related NASA technology.

Technical Support Package (TSP's)
For many of the innovations described in Tech Briefs, the center TUO has prepared additional material that will help you in detailed evaluation and actual use or construction of the new technology. You may get TSP's free of cost by using the TSP Request Card or writing the center TUO.

Who to Contact. Of course, many technical questions about Tech Briefs are answered in the TSP's, but when no TSP is available, or you have further questions, write the Technology Utilization Officer at the center that sponsored the research at the address listed below.

Charles C. Kubokawa
Ames Research Center
Code AU: 240-2
Moffett Field, CA 94035
(415) 965-5554

Donald S. Friedman
Goddard Space Flight Center
Code 702.1
Greenbelt, MD 20771
(301) 982-6242

John T. Wheeler
Johnson Space Center
Code AT3
Houston, TX 77058
(713) 483-3809

Raymond J. Cerrato
John F. Kennedy Space Center
Code SA-RTP
Kennedy Space Center, FL 32899
(305) 867-2780

John Samos
Langley Research Center
Mail Stop 139A
Hampton, VA 23665
(804) 827-3281

Paul Foster
Lewis Research Center
21000 Brookpark Rd.
Cleveland, OH 44135
(216) 433-4000, Ext. 6832

Aubrey D. Smith
Marshall Space Flight Center
Code AT01
Marshall Space Flight Center, AL 35812
(205) 453-2224

John C. Drane
NASA Resident Legal Office-JPL
4800 Oak Grove Drive
Pasadena, CA 91103
(213) 354-6420

Gilmore H. Trafford
Wallops Flight Center
Wallops Island, VA 23337
(804) 824-3411, Ext 201

Louis Mogavero, Chief
Technology Utilization Branch
Code ETU-6
NASA Headquarters
Washington, DC 20546
(202) 755-2220

COSMIC

(Computer Software Management & Information Center)

AN ECONOMICAL SOURCE OF COMPUTER PROGRAMS DEVELOPED BY THE GOVERNMENT.

COSMIC is sponsored by NASA to give you access to over 1400 computer programs developed by NASA and the Department of Defense, and selected programs from other government agencies. It is one of the Nation's largest software libraries.

COSMIC charges very reasonable fees for programs to help cover part of their expenses—and NASA pays for the remainder. Programs generally cost from $500 to $1000, but a few are more expensive and many are less. Documentation is available separately and very inexpensively.

COSMIC collects and stores software packages, insures that they are complete, prepares special announcements (such as Tech Briefs), publishes an indexed software catalog, and reproduces programs for distribution. COSMIC helps customers to identify their software needs, follows up to determine the successes and problems, and provides updates and error corrections. In some cases, NASA engineers can offer guidance to users in installing or running a program.

COSMIC programs range from management (pert scheduling) to information science (retrieval systems) and computer operations (hardware and software). Hundreds of engineering programs perform such tasks as structural analysis, electronic circuit design, chemical analysis, and design of fluid systems. Others determine building energy requirements, optimize mineral exploration, and draw maps of water-covered areas using NASA satellite data. In fact, the chances are, if you use a computer, you can use COSMIC.

COSMIC is eager to help you get the programs you need. For more information about services or software available from COSMIC, fill out and mail the COSMIC Request Card in this issue.

COSMIC: Computer Software Management and Information Center

Suite 112, Barrow Hall, University of Georgia, Athens, Georgia 30602 Phone: (404) 542-3265

WHERE IS THE WORLD'S LARGEST BANK OF TECHNICAL DATA

?

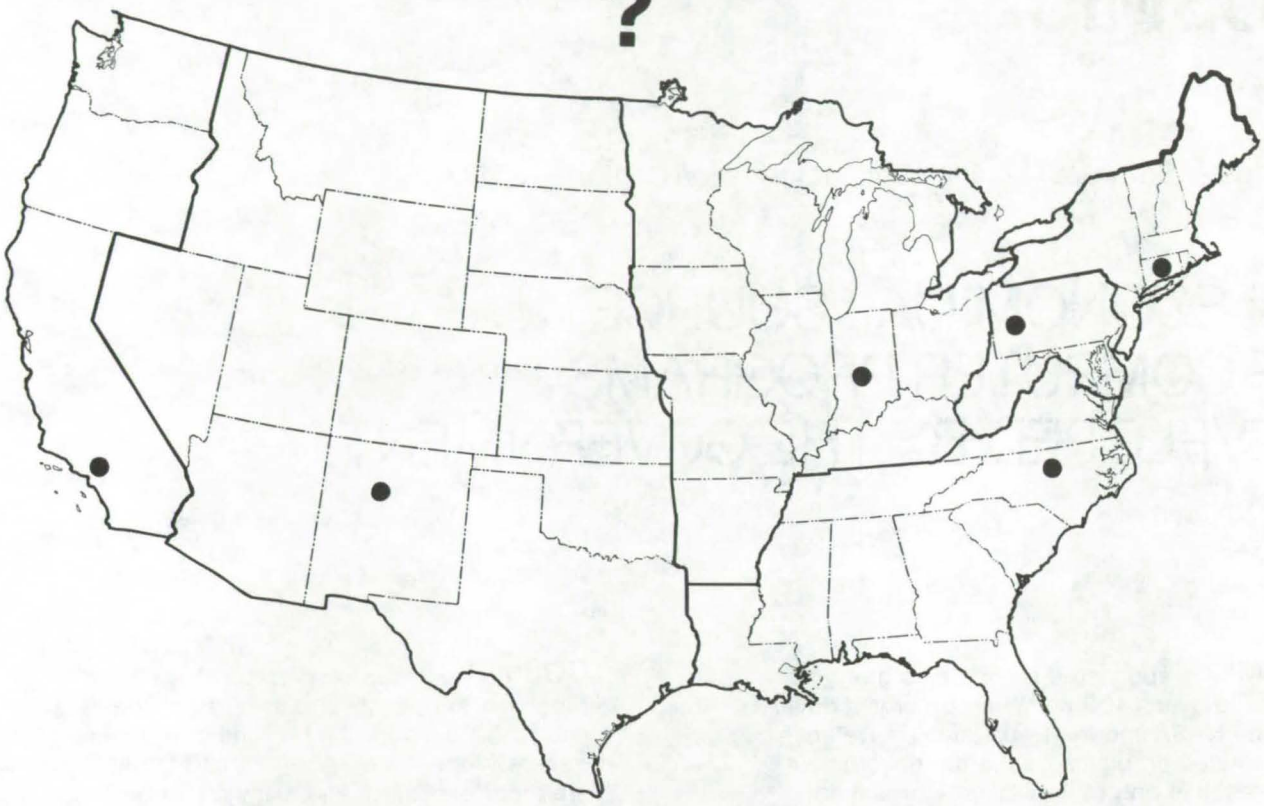

It's in Indianapolis and Pittsburgh, it's in Storrs, Connecticut and Research Triangle Park, North Carolina; and it's in Albuquerque and Los Angeles.

NASA IAC's — INDUSTRIAL

You can get more information and more data on more technical subjects through NASA's network of IAC's than anywhere else in the world. About 8,000,000 documents and growing at the rate of 50,000 more each month!

Major sources include:

- 750,000 NASA Technical Reports
- Selected Water Resources Abstracts
- NASA Scientific and Technical Aerospace Reports
- Air Pollution Technical Information Center
- NASA International Aerospace Abstracts
- Chem Abstracts Condensates
- Engineering Index
- Energy Research Abstracts
- NASA Tech Briefs
- Government Reports Announcements

and many other specialized files on food technology, textile technology, metallurgy, medicine, business, economics, social sciences, and physical science.

The IAC's are one of the most economical ways of staying competitive in today's world of exploding technology. The help available from the network ranges from literature searches through expert technical assistance.

Literature Searches

Help in designing your search, typically from 30 to 300 abstracts in as narrow or broad an area as you need, and complete reports when you need them. The most complete "search before research" available!

Current Awareness

Consult with our applications engineers to design your personal program — selected monthly or quarterly abstracts on new developments in your speciality. It's like having your own journal!

Technical Assistance

Our applications engineers will help you evaluate and apply your literature-search results. They can help find answers to your technical problems and put you in touch with scientists and engineers at NASA Field Centers.

To obtain more information about how NASA's IAC's can help you —
Check the IAC box on the TSP Request Card in this issue,
Or write or call the IAC nearest you.

APPLICATIONS CENTERS

How to get reports and other documents discussed in this issue of Tech Briefs

Many of the innovations in Tech Briefs are described in detail in reports available at a reasonable cost through one or more of the IAC's. To order a report, call or write the IAC referenced at the end of the Tech Brief article at the address below. Be sure to list the titles and accession numbers (N76-..., N75-..., etc.) of those you wish to purchase.

Aerospace Research Application Center (ARAC)
Indiana University-Purdue University at Indianapolis
1201 E. 38th St.
Indianapolis, IN 46205
E. Guy Buck, Director
(317) 264-4644

Knowledge Availability Systems Center (KASC)
University of Pittsburgh
Pittsburgh, PA 15260
Dr. Edmond Howie, Director
(412) 624-5211

New England Research Application Center (NERAC)
Mansfield Professional Park
Storrs, CT 06268
Dr. Daniel U. Wilde, Director
(203) 486-4533

North Carolina Science & Technology
Research Center (NC/STRC)
P. O. Box 12235
Research Triangle Park, NC 27709
Peter J. Chenery, Director
(919) 549-0671

Technology Application Center (TAC)
University of New Mexico
Albuquerque, NM 87131
Stanley A. Morain, Director
(505) 277-4000

Western Research Application Center (WESRAC)
901 Exposition Boulevard, Room 205
University of Southern California
University Park
Los Angeles, CA 90007
Radford King, Director
(213) 741-6132

NASA INVENTIONS AVAILABLE FOR LICENSING

Over 3,500 NASA inventions are available for licensing in the United States - both exclusive and nonexclusive.

Nonexclusive Licenses

Nonexclusive licenses for commercial use are encouraged to promote competition and to achieve the widest use of inventions. They must be used by a negotiated target date but are usually royalty free.

Exclusive Licenses

An exclusive license may be granted to encourage early commercial development of NASA inventions, especially when considerable private investment is required. These are generally for 5 to 10 years and usually require royalties based on sales or use.

The NASA patent licensing program also provides for licensing of NASA-owned foreign patents. In addition to inventions described in Tech Briefs, "NASA Patent Abstract Bibliography," containing abstracts of all NASA inventions, can be purchased from: National Technical Information Service, Springfield, Va., 22161. This document is updated semi-annually.

Patent Licenses and the NASA Tech Brief

Many of the inventions reported in Tech Briefs are patented or are under consideration for a patent at the time they are published. When this is the case, the current patent status is described at the end of the article; otherwise, there is no statement about patents. **If you want to know more about the patent program or are interested in license for a particular invention, write the Patent Counsel at the NASA Field Center** that sponsored the research. Be sure to refer to the NASA reference number in parenthesis at the end of the Tech Brief.

Robert F. Kempf
NASA Headquarters, Code GP-4
400 Maryland Ave., S.W.
Washington, DC 20546
(202) 755-3932

Darrell G. Brekke
Ames Research Center
Mail Code: 200-11A
Moffett Field, CA 94035
(415) 965-5104

John O. Tresansky
Goddard Space Flight Center
Mail Code: 204
Greenbelt, MD 20771
(301) 982-2351

Marvin F. Matthews
Lyndon B. Johnson Space Center
Mail Code: AM
Houston, TX 77058
(713) 483-4871

James O. Harrell
John F. Kennedy Space Center
Mail Code: SA-PAT
Kennedy Space Center, FL 32899
(305) 867-2544

Howard J. Osborn
Langley Research Center
Mail Code: 279
Hampton, VA 23665
(804) 827-3725

Norman T. Musial
Lewis Research Center
Mail Code: 500-311
21000 Brookpark Road
Cleveland, OH 44135
(216) 433-4000

Leon D. Wofford, Jr.
Marshall Space Flight Center
Mail Code: CC01
Marshall Space Flight Center, AL 35812
(205) 453-0020

Monte F. Mott
NASA Resident Legal Office
4800 Oak Grove Drive
Pasadena, CA 91103
(213) 354-2700

NEW PRODUCT IDEAS

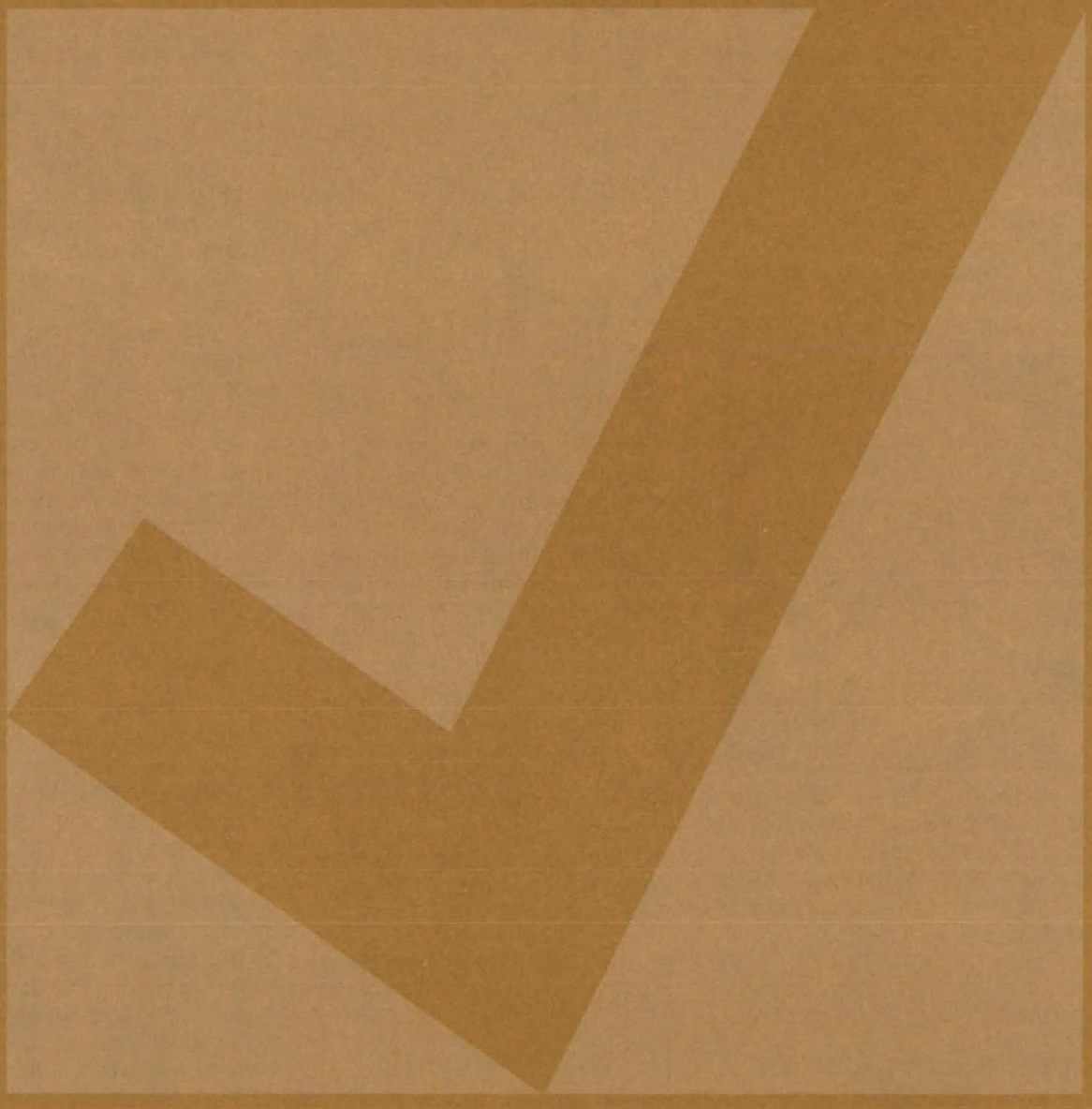

NEW PRODUCT IDEAS are just a few of the many innovations described in this issue of NASA Tech Briefs and having promising commercial applications. Each is discussed further on the referenced page in the appropriate section in this issue. If you are interested in developing a product from these or other NASA innovations, you can receive further technical information by requesting the TSP referenced at the end of the full-length article or by writing the Technology Utilization Office of the sponsoring NASA center (see page A4). NASA's patent-licensing program to encourage commercial development is described on page A8.

Wide-Angle Pinhole Camera

A hemispherical refracting element gives a pinhole camera a 180° field-of-view without compromising its simplicity and depth-of-field. The refracting element, located just behind the pinhole, bends light coming in from the sides so that it falls within the image area of the film. In contrast to earlier pinhole cameras that used water or other transparent fluids to widen the field,

this model is not subject to leakage and is easily loaded and unloaded with film. Moreover, by selecting glass with different indices of refraction, the field at the film plane can be widened or reduced.
(See page 192.)

Compact Ratchet Wrench

The manipulation of a ratchet wrench in tight spaces could be simplified by a proposed round ratchet wrench that would fit in the palm of the hand. Except for its compact design, the round wrench would be similar to conventional long-handle ratchet wrenches. Its drive end would be adapted to fit all conventional ratchet attachments, and a finger hole would be provided through which the turning direction could be selected.
(See page 281.)

Artificial Leg With Natural Gait

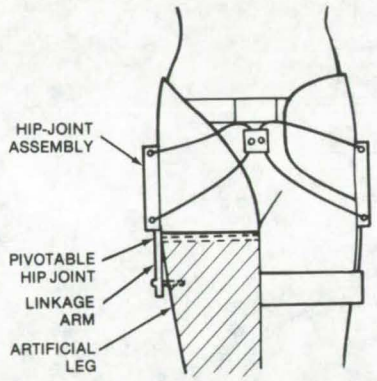

An improved artificial leg uses energy supplied by the normal leg to give the wearer a natural gait. A special actuator stores energy to rotate the artificial leg forward at just the right moment to give the correct stride cadence. The movement can be set 180° out of phase with the normal leg for walking, or in phase for sitting or rising. Two hip-joint assemblies containing fluid bladders that are connected by tubing are the primary components of the actuating mechanism. Fluid enters the bladder in the artificial leg to rotate a linkage and lift the leg in a motion similar to that of a natural leg.
(See page 246.)

Probes for Blood-Vessel and Spinal Interiors

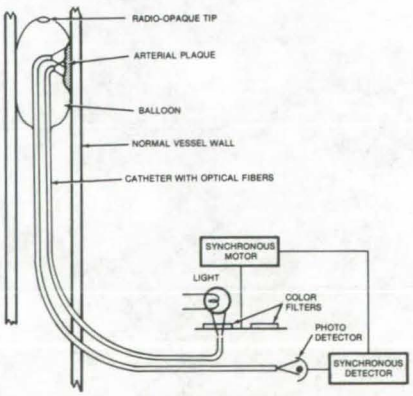

In vivo color-mapping of the interiors of blood vessels and spinal lumen is facilitated by two proposed probes that measure the intensity of light reflected off the vessel walls. One probe transmits the light through optical fibers; the other uses LED sources and a solid-state photodetector. The probes are contained in a thin catheter with a small inflatable balloon tip. Two or more wavelengths are bounced off the blood-vessel interior, and the spectrum of the returned light is analyzed to give a "picture" of the wall surface. The fiber-optics version using a very thin catheter can be used in spinal-lumen mapping. The light would be reflected off the lumen or neighboring nerve bundles, and the reflected wavelengths would be returned to an external sensor.
(See page 248.)

Magnetic Heat Pump

A method for pumping heat magnetically at room temperature may be more economical than existing refrigeration systems. The method uses the natural magnetothermal effect of gadolinium metal to establish a temperature gradient across the length of a tube. A regenerative cyclic process in which a gadolinium sample is magnetized and gives off heat at one end of the tube, and then is demagnetized at the other end to absorb heat, has established temperature gradients of 144° F in experiments near room temperature. Other materials with large magnetothermal effects can be used below room temperature. Possible commercial applications include freeze-drying and food processing, cold storage, and heating and cooling of buildings, plants, and ships.
(See page 190.)

Ultrasonic Extensometer Measures Bolt Preload

Conventional torque wrenches are not nearly as accurate as a new ultrasonic device for measuring the preload applied to a threaded fastener. The new device, which determines the transit time for an ultrasonic pulse to travel the length of the fastener and to return,

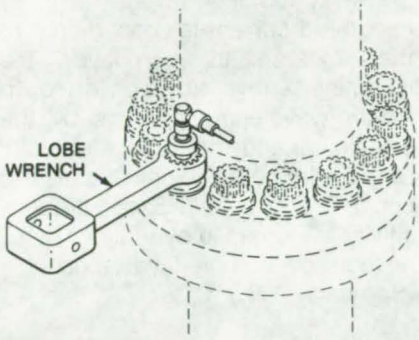

measures the applied torque (which is proportional to the elongation) to within 10 percent. This means lighter bolts can be selected to obtain the same safety factor, and substantial weight savings can be realized in large assemblies. The ultrasonic extensometer includes a piezoelectric transducer in an adapter that fits the head of the bolt. The total pulse transit time is measured electronically and is shown on a digital display.

(See page 278.)

Emergency Escape Device

With a few modifications, the device used to control the descent of the Lunar Roving Vehicle from the Lunar Module on the Moon's surface could be used in construction, shipping, safety exits, amusement parks, and other applications to lower people or equipment several hundred feet. The device consists of a reel controlled by a gear-and-ratchet mechanism. The payload is gently lowered as the cable is unwound from the reel. If developed for commercial applications, the mechanism could be fitted with a reel for cable storage and a cable guider to wind the cable uniformly on the reel.

(See page 278.)

Improved Transformer-Winding Method

Quieter, more efficient transformers may be possible by using an improved technique for installing the windings on the core. Instead of cutting the core to insert it through the windings, the wire is wound directly on the core with the help of a special bobbin and fixture. The core can therefore be shaped and impregnated before winding, eliminating the gaps produced during conventional transformer assembly. Stacking factors should be improved to 0.95 or better; and since assembly and disassembly are not necessary, the core would retain the shape it had after annealing.

(See page 291.)

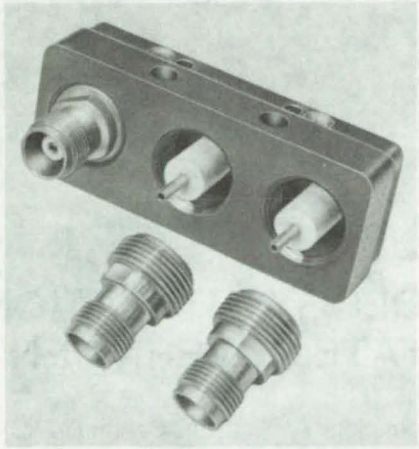

A new RF switch, designed for vacuum environments, can handle 5 kilowatts of microwave power. Arcing between the conductors is prevented by filling the gaps with Teflon, rather than with an inert gas as in conventional switches. Thus, the new switch is not susceptible to gas leakage, a problem faced by conventional switches in high-vacuum applications. A compact three-port switch, developed for microwave radar transmitters aboard spacecraft, is operated by depressing spring-mounted insulating pins that can be remotely actuated by a relay. When a pin is depressed, it routes the microwave signal to the selected output port.

(See page 168.)

Meter for Very Slow Flows

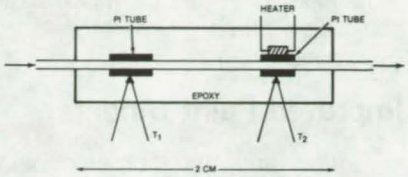

Flow rates as low as 0.5 ml/min are measured with a sensitivity of 0.01 ml/min by a new nonprotruding solid-state sensor, originally developed for NASA's Water-Quality Monitoring System. Its elements are simply a resistance heater, two thermistors, and a platinum tube, all encapsulated in an epoxy block. As the fluid flows down the tube, one thermistor measures the temperature at the inlet, while the second measures the temperature at the resistance heater, mounted farther along the flow path. The power needed to maintain a constant temperature differential between the sensors measures the flow velocity.

(See page 275.)

Wind-Wheel Electric-Power Generator

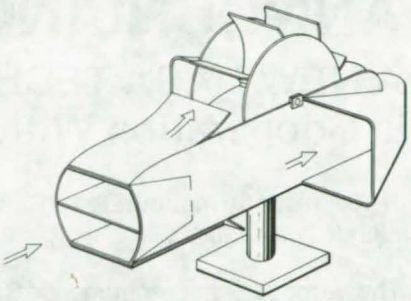

Wind energy is converted to rotary motion for the generation of electric power by a highly-efficient new wind wheel. In the new design, a special duct configuration integrates the available wind forces to maximize rotation. One forward-mounted duct, designed by using venturi principles, directs a high-velocity airflow at the rotor blades, while a second duct channels additional air toward the blades. Two side-mounted ducts also create a turning force. These side ducts are flared to adjust the wheel for shifts in the wind direction. The wheel could be

connected to a generator by using conventional couplings at the ends of its axle, or it can be modified to serve as a primary generator.
(See page 276.)

Improved Paint Binders

A new family of inorganic paint binders can protect ferrous metals and aluminum alloys in salt environments. The binders are stable, inexpensive, extremely water-resistant, and easy to apply. They are prepared by mixing a starter alkali-metal/silicate solution with silicon dioxide hydrogel, water, and a silicone compound such as methyl trimethoxysilane. The final product contains a high molar ratio of silicon dioxide in the form of a hydrated sol, an alkali-metal oxide, water, and the silicone. Lithium compounds, which are expensive and can degrade the adhesive qualities of the paint, are not used in the formulations.
(See page 231.)

Fire-Retardant Epoxy

A new epoxy resin is made fire-retardant by phosphorus in its molecular structure. In contrast to other adhesives that use phosphate ester fluids, the new polymer does not lose its adhesive strength after it is applied. Moreover, the epoxy is transparent, unlike resins containing arsenic or certain inorganic compounds. The new resin is formed by reacting allylphenols with alkyl or arylphosphonic dichloride; the reaction is followed by epoxidation. The compositions have been used in adhesives to bond polyvinylfluoride and polyether sulfone films onto polyimide glass laminates.
(See page 225.)

Improved X-Ray Exposure Sensor

An improved X-ray sensor is compatible with the short exposure times typical of modern X-ray film. It uses solar cells and scintillator sheets stacked in alternating layers to generate a current proportional to the X-ray radiation level. The time-integrated current is proportional to the exposure. In each layer, the incoming X-rays are converted to longer wavelength photons by the scintillator and then into electricity by the solar cell. The cell outputs are connected in series. Exposure sensitivity is increased by a factor of 15 or more over single-layer sensors.
(See page 250.)

Electronic Components and Circuits

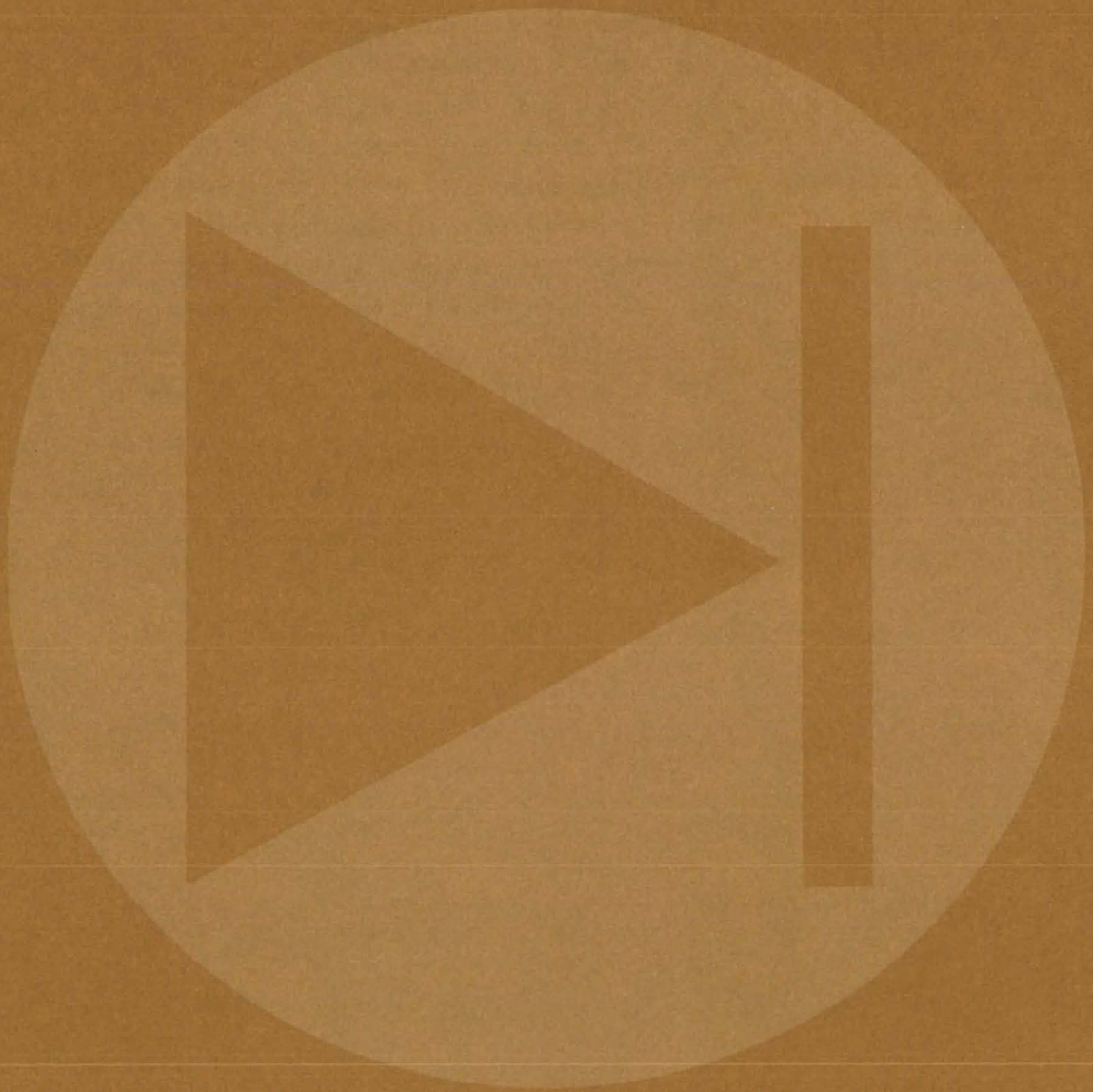

Hardware, Techniques, and Processes

165 Symmetric Voltage-Controlled Variable Resistance
166 Fast Differential Analog-to-Digital Conversion
167 Improved Servocontrol System
168 High-Power RF Switch
169 Temperature Stabilization of Microwave Ferrite Devices
170 IC Implementation of Crossbar Switches
171 Strobe-Margin Test for Plated Memory Systems
171 Safe Venting for Electronic Components
172 Direct-Reading Group-Delay Measurement
173 Synchronous Transfer Circuits for Redundant Systems

Books and Reports

174 Analyzing CMOS/SOS Fabrication for LSI Arrays

Symmetric Voltage-Controlled Variable Resistance

A feedback network makes the resistance of an FET the same for current flowing in either direction.

Lyndon B. Johnson Space Center, Houston, Texas

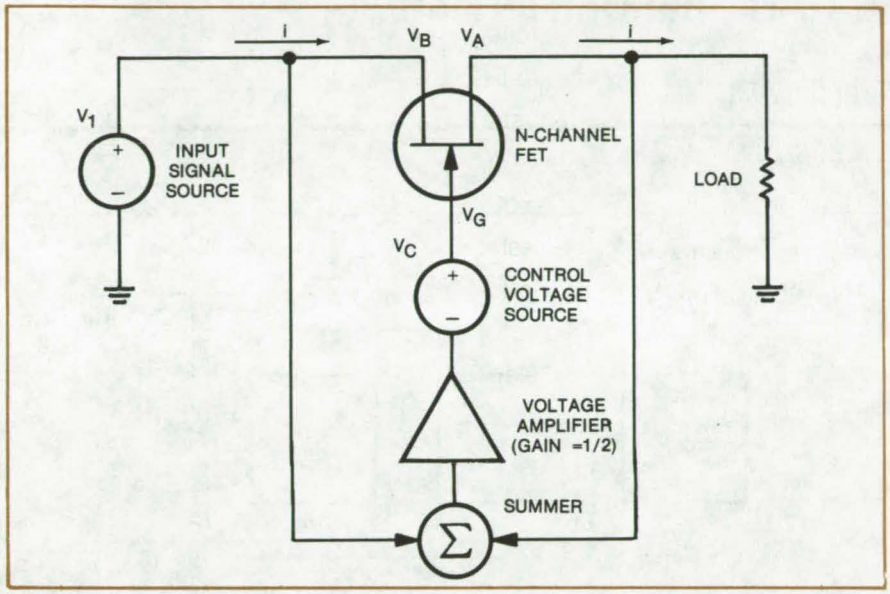

Figure 1. **Control Elements Adjust the Voltage** on the gate of this field-effect transistor so that its resistance is the same for equivalent current flow in either direction. Summer and amplifier circuits can be implemented by using operational amplifiers.

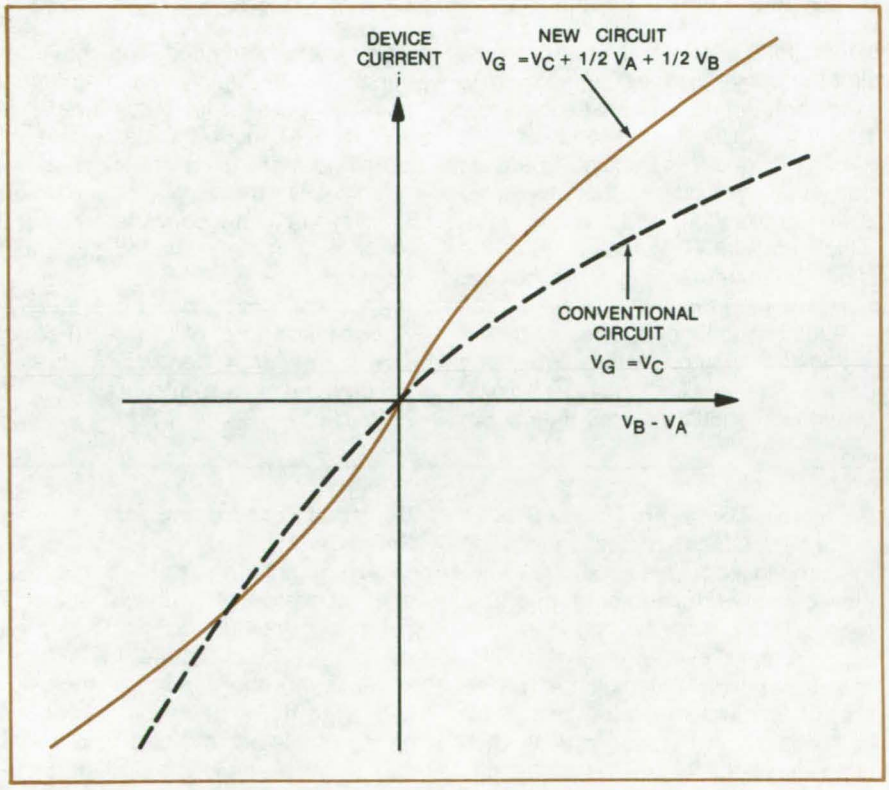

Figure 2. **I-V Characteristic Is Symmetric** about the origin for the circuit of Figure 1. The behavior when the control signal is applied without feedback (dashed line) is quite different in the first and third quadrants.

The main difficulty in using a field-effect transistor (FET) as a voltage-controlled variable resistance (VCVR) is that the device current/voltage characteristic is not symmetric; when the voltage and current go negative, their relationship can be quite different than when they are positive. Symmetry can be imposed by using matched complementary FET's or by keeping signal levels low; however, these methods are only approximately effective and can be overly restrictive for many applications.

A new FET circuit (Figure 1) combines the control voltage with source and load voltages to give a symmetric current/voltage characteristic (Figure 2). Since the circuit produces the same magnitude output voltage for current flowing in either direction, it introduces no offset in the presence of alternating polarity signals. It is therefore ideal for sensor and effector circuits in servocontrol systems.

The new circuit overcomes the inherent asymmetry of the FET by feeding back the input and load voltages to the control circuit through a summer and an amplifier (gain = 1/2). The voltage loop equations show that the I-V curve is the same for current flow in either direction. The various control elements, including the summer and the amplifier, can be implemented with operational amplifiers having adequate frequency response and high input impedance.

The circuit shown in Figure 1 has been built and tested and has performed as predicted. A representative application of the circuit is in a feedback control system in which the VCVR sets the open-loop gain. The input to the system is an analog error signal of alternating polarity. If a device with an asymmetric response were used to set the loop gain, the gain would be different for signals of different polarity. This difference in response would introduce an offset

(continued next page)

voltage in the system output that would seriously degrade performance. With the symmetric VCVR, no such offset is produced.

The circuit concept applies equally well to N-channel and P-channel FET's and to metal-oxide semiconductor devices, as well as to junction FET's.

This work was done by James C. Vanelli of Lockheed Electronics Co., Inc., for **Johnson Space Center.** *For further information, Circle 1 on the TSP Request Card.*
MSC-16685

Fast Differential Analog-to-Digital Conversion

Tracking converters and successive approximations combined in a differential ADC

Lewis Research Center, Cleveland, Ohio

Successive approximation converters are almost universally used for high-speed analog-to-digital conversion (ADC). However, for high accuracy, in the order of 12 to 16 bits, conversion times increase by approximately 2^n, where n is the number of bits. Another comparison must be made for each additional bit, and the settling time is approximately doubled for each doubling of accuracy (bit).

The differential conversion technique shown in the figure is a hybrid achieved by combining tracking converters and successive approximation techniques. An analog-to-digital conversion is performed on the difference between the present input signal and the last converted value, which has been stored in the accumulator. This digitized difference signal is added to the previous digitized value to attain the new value representing the digitized analog input.

Since the ADC used in this technique digitizes only the difference signal, it is not required to digitize as many bits as are required for the complete answer. This converter performs significantly faster than a converter required to digitize the complete answer.

After the difference is digitized, it is added to the previous stored value, and the converter must be allowed to settle before another conversion cycle is started. Conversion time is one settling of the n-bit digital-to-analog conversion, m bits of the analog-to-digital conversion, and the add time, which totals less than n settlings of the n-bit digital-to-analog conversion, normally required.

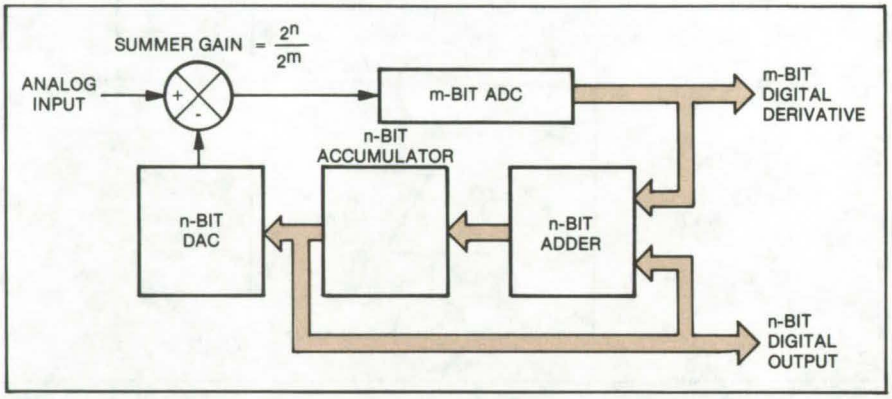

Differential Analog-to-Digital Converter first digitizes the difference between the input and the previous conversion (stored in the accumulator). This digitized difference is added to the previous digitized value to yield a new digital representation of the analog input.

Accuracy is limited primarily by the digital-to-analog converter. Offset and gain errors in the analog-to-digital conversion should be less than 1 bit, which is easily attained. The converter cannot handle rapidly changing inputs because it is slew limited; however, it will recover input transients without overshoot or extra settling time. Additionally, the output of the m-bit (analog-to-digital) converter is useful as a digital derivative of the input signal.

This work was done by Arthur G. Birchenough and William J. Rice of **Lewis Research Center.** *No further documentation is available.*
LEW-12909

Microcircuit-Cleaning Machine

An easily-constructed circuit shaker that removes loose particles from hybrid microcircuit packages before sealing can reduce rejections from noise tests to less than 7 percent. With this workbench-mounted machine, which works like a pendulum, loose particles are removed by shock impact. Clean-room procedures are used in circuit handling.
(See page 299.)

Protective Coating for Laser Diodes

The ideal facet protective coating for GaAs laser diodes should not alter their optical and electrical properties. A borosilicate glass coating is easy to apply, breaks evenly when cleaved, and is abrasion and moisture resistant. Its low index of refraction (1.45) makes its thickness less critical when depositing a half-wavelength coating.
(See page 191.)

Universal Test Fixture for Solar Cells

Coverings for solar cells are evaluated conveniently with an alumina ceramic circuit board holding three pairs of cells and three FET chips, overlaid with the candidate encapsulant. With the fixture, solar cells and encapsulants are exposed to Sunlight and weather, either natural or artificial, to provide pertinent measurement and performance data.
(See page 205.)

Improved Servocontrol System

Circuit compensates for gain variations caused by a changing error signal.

Marshall Space Flight Center, Alabama

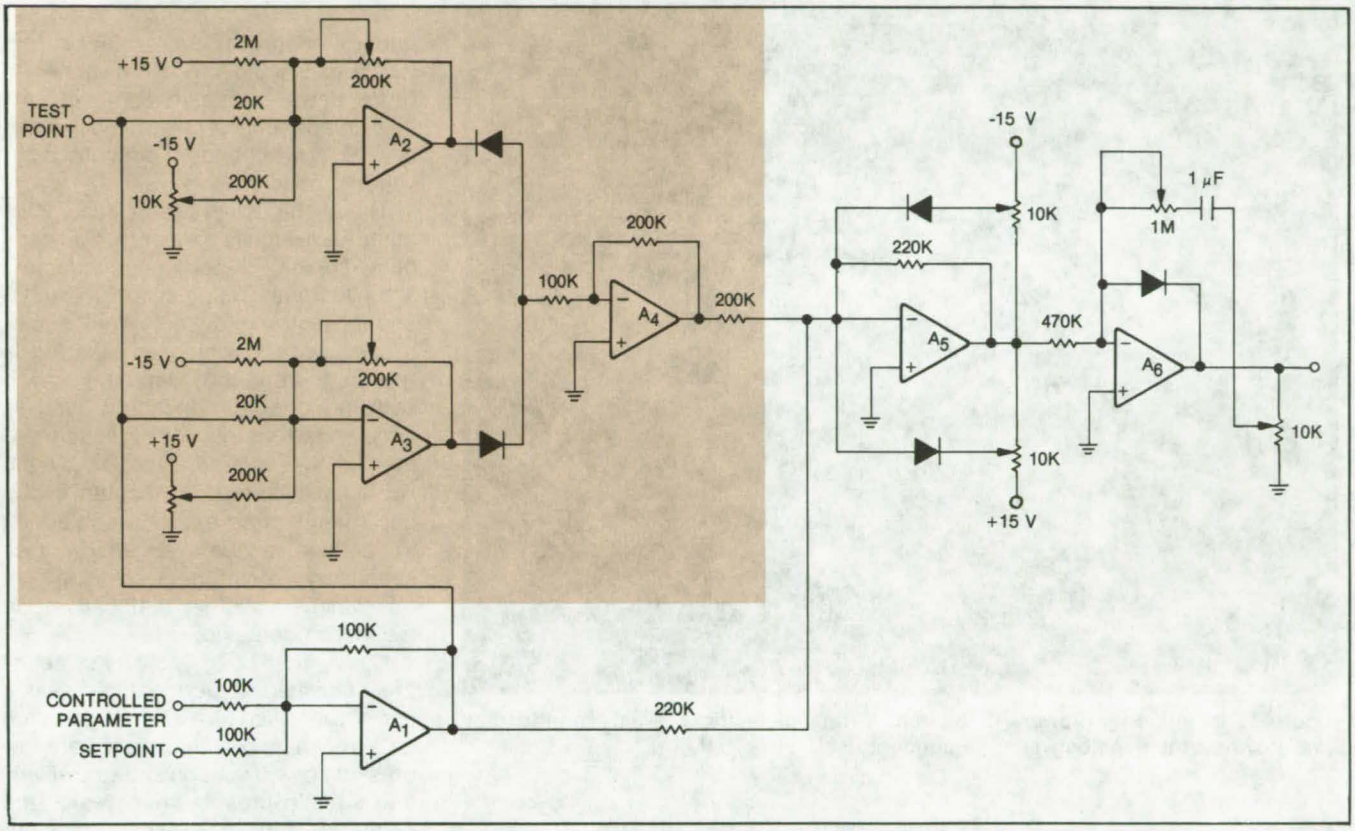

An **Improved Servocontrol System** combines the error signal with the output of a deadband circuit (in color). The deadband output offsets any decrease in the gain of the error circuit for rapid changes in the input signal.

The gain setting of a servosystem is often a compromise between the gain required for good stability and that required for good transient response. In certain closed-loop systems, relatively high gains are necessary to control transient conditions, while lower gains are required for system stability.

The gain of a typical servocontrol system, featuring an integrating circuit with lead compensation, varies with the frequency (or rate of change) of the controlled parameter. By using a circuit that allows the gain to vary as a function of the deviation of the controlled parameter from its setpoint, the system transient response can be improved.

The circuit shown in the figure has this capability. Basically, it consists of two summing amplifiers and a deadband circuit. The input summer (A_1) generates the deviation or error signal from the controlled parameter and the setpoint. The output of this summer connects to a second summing amplifier (A_5) and the deadband circuit (in color). The error signal and the output of the deadband circuit are combined at the input of summer A_5. The output signal from A_5 is integrated by A_6.

Under steady-state conditions, the input to the integrator is the normal error signal. If the rate of change of the error signal exceeds the threshold set by the deadband circuit, the input to the integrator becomes the sum of the error signal plus an additional signal. This added signal from the deadband circuit will increase the output slew rate of the integrator, thereby effectively increasing gain.

This work was done by E. C. Buchanan of Rockwell International Corp. for **Marshall Space Flight Center.** *For further information, Circle 2 on the TSP Request Card.*

Inquiries concerning rights for the commercial use of this invention should be addressed to the Patent Counsel, Marshall Space Flight Center [see page A8]. Refer to MFS-19358.

High-Power RF Switch

Device reliably handles up to
5 kilowatts of radio-frequency power.

NASA's Jet Propulsion Laboratory, Pasadena, California

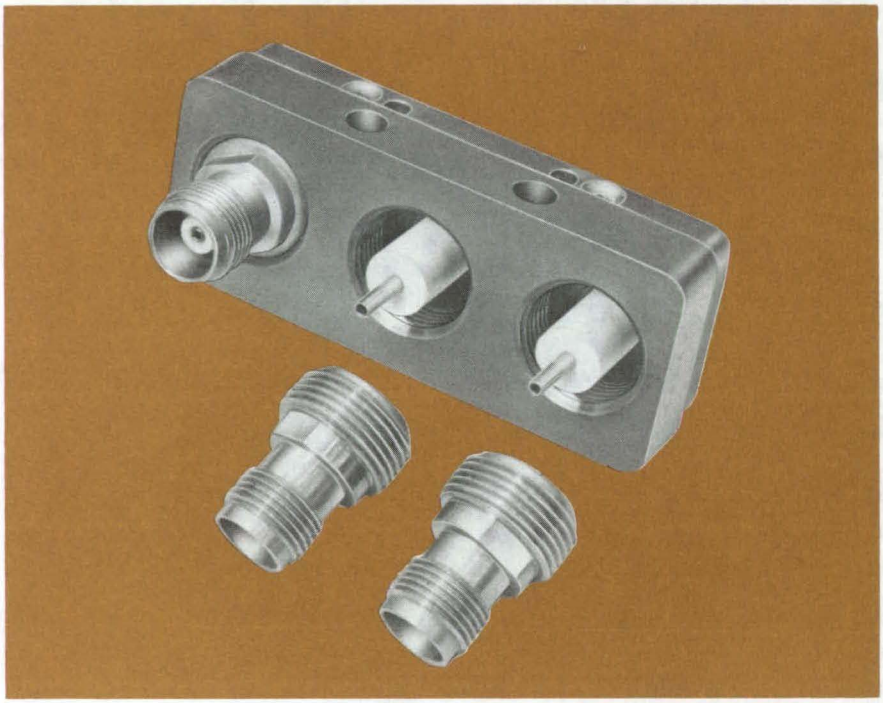

Figure 1. In this **High-Power RF Switch,** Teflon dielectric prevents multipactor breakdown in the gaps between the conductors.

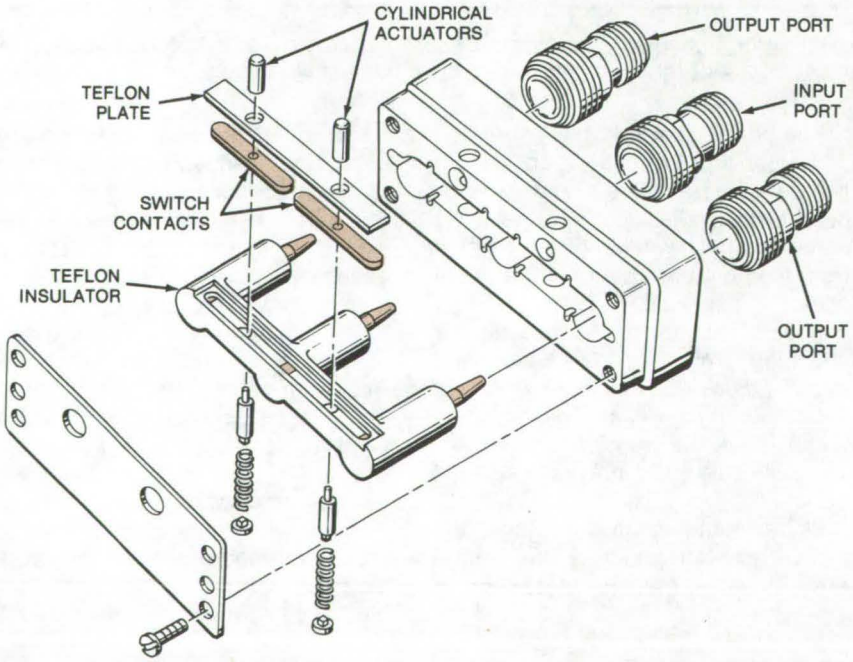

Figure 2. An **Exploded View** of the RF switch shows the assembly of the switch contacts and pins (in color) and dielectric supports.

A new switch handles radio-frequency energy at power levels that would cause ordinary RF switches to break down. Although compact, the new component can switch 5 kilowatts of RF power under difficult high-vacuum conditions.

The high-power switch resembles other RF switches except that all gaps between the RF-carrying conductors are filled with Teflon (see Figure 1). The dielectric prevents "multipactor breakdown," in which an electron is released into the vacuum space between coaxial conductors and is accelerated first in one direction and then in the reverse direction by the RF field. If there is a vacuum in the gap, the electron can be accelerated to a high enough speed to free secondary electrons, creating an "avalanching" effect that can erode the switch contacts.

Conventional RF power switches are contained in hermetically sealed enclosures filled with an inert gas such as nitrogen. When there is a very low pressure or vacuum outside, however, these enclosures tend to leak; and once the inert gas escapes, multipactor breakdown occurs. Because of the inherent unreliability of even the most-elaborately-designed hermetic seals, it was decided to replace the inert gas with the solid dielectric.

The new switch was designed for a synthetic-aperture radar transmitter for spacecraft. It switches the 1.2-GHz outputs of three 400-watt power-amplifier modules so that 400, 800, or 1,200 watts can be transmitted as required. Although RF power-switching requirements as high as 5 kilowatts are not common, a switch of the new design should increase the reliability of systems operating at lower levels. It therefore should find applications in other radar systems and high-frequency radio transmitters.

In the switch (see Figure 2), an E-shaped Teflon dielectric is inserted in a metal body in which the input port and two output ports are mounted. The dielectric surrounds the center con-

ductor for each of the ports. A recessed area in the dielectric holds the switch contact bars. The contacts are moved by spring-mounted cylindrical insulators that slide in holes in the E-shaped dielectric. Each switch bar can make contact with the exposed area of one of the output ports and with the input-port center conductor. A Teflon plate covers the recessed area in the dielectric after the movable switch elements have been inserted. The open end of the switch assembly is covered by a soft-metal plate.

The switch is operated by depressing the spring-mounted insulator to drive one of the contact bars against the center conductors. A lever that is actuated by a relay could be used to move the insulator.

This work was done by Edward R. Caro of Caltech for **NASA's Jet Propulsion Laboratory.** *For further information, Circle 3 on the TSP Request Card.*

Inquiries concerning rights for the commercial use of this invention should be addressed to the Patent Counsel, NASA Resident Legal Counsel-JPL [see page A8]. Refer to NPO-14229.

Temperature Stabilization of Microwave Ferrite Devices

A thin-film heater and copper-clad fiberglass improve a strip-line circulator.

Lyndon B. Johnson Space Center, Houston, Texas

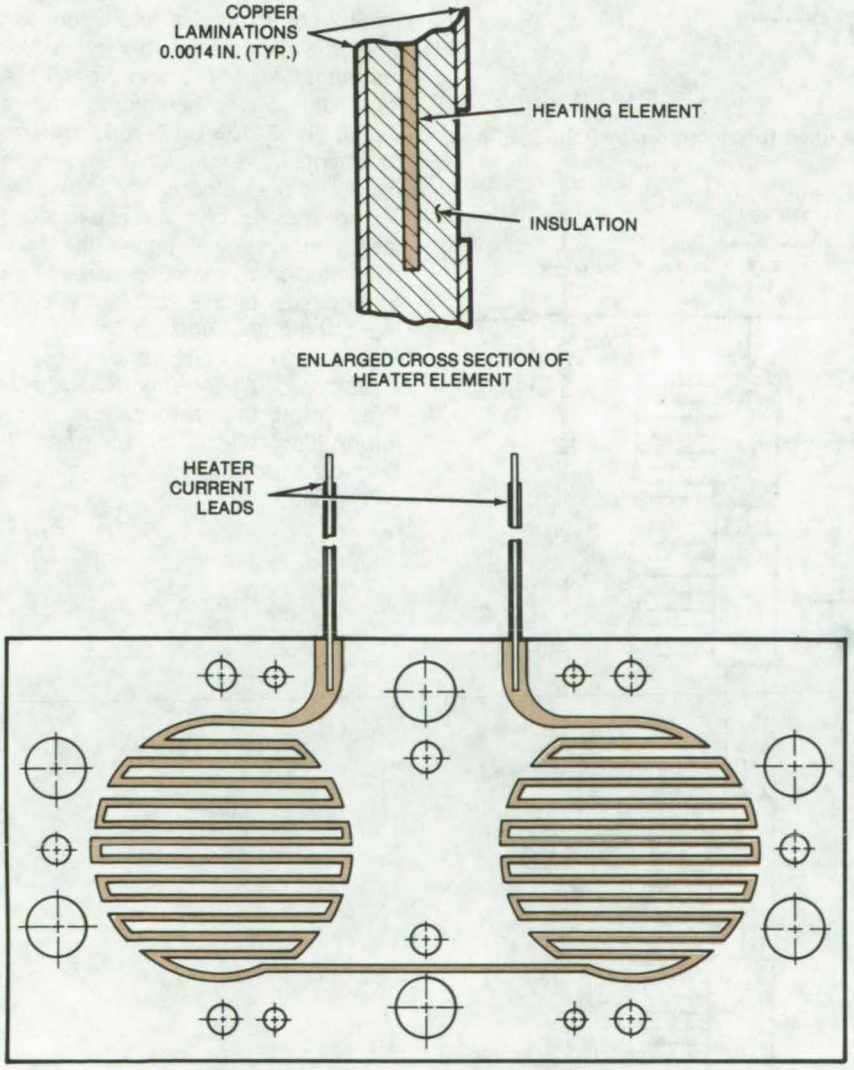

The **Thin-Film Heating Element** for a strip-line circulator is sandwiched between insulation and copper laminations. The disks conform to the shape of the circulator ferrite disks and are installed between copper-clad epoxy ground planes. Mounting holes are shown.

The RF characteristics of a strip-line circulator are directly affected by the temperature of its environment. Ideally, the device should be temperature-stabilized to prevent any variation in its characteristics. External heater cartridges are often used to maintain constant temperature over the entire device; however, since the only components in a strip-line circulator that are sensitive to temperature are the ferrite disks, it is inefficient to expend heater power to warm the entire device.

A new heater design eliminates the need for external cartridges. The heater is made from insulated-copper thin-film elements laminated with a thin copper foil (see figure). The elements take the shape of the ferrite disks to heat the ferrites locally. This arrangement reduces the time to reach the operating temperature and reduces the heater power consumption.

Another improvement involves the use of copper-plated fiberglass and structural foam for the circulator ground planes to decouple the ferrites thermally. The copper-plated fiberglass replaces a heavier aluminum housing, thereby reducing weight by approximately one-third. The thin copper plate provides the metallic surface that is required for microwave transmission.

This work was done by Richard Kaminsky and E. J. Wendt of Cutler-Hammer Inc. for **Johnson Space Center.** *For further information, Circle 4 on the TSP Request Card. MSC-16833*

IC Implementation of Crossbar Switches

A basic switching-element configuration can be expanded to more complex networks.

NASA's Jet Propulsion Laboratory, Pasadena, California

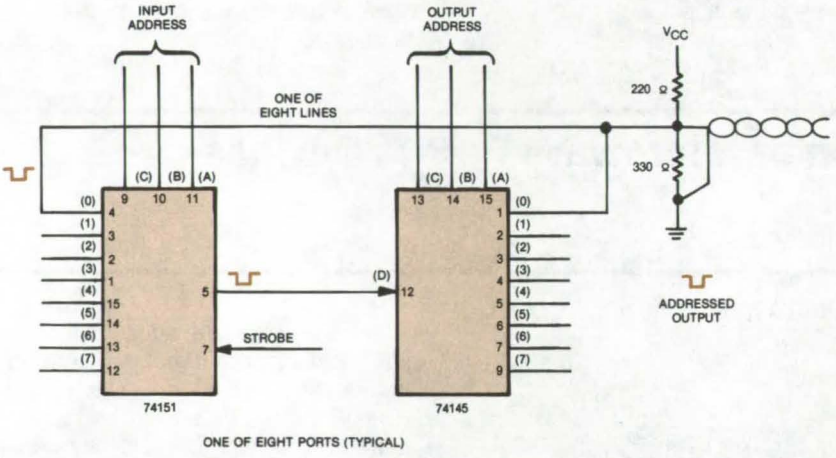

Figure 1. A **Crossbar-Array Building Block** is used for electronic switching of one line to any of the remaining seven lines.

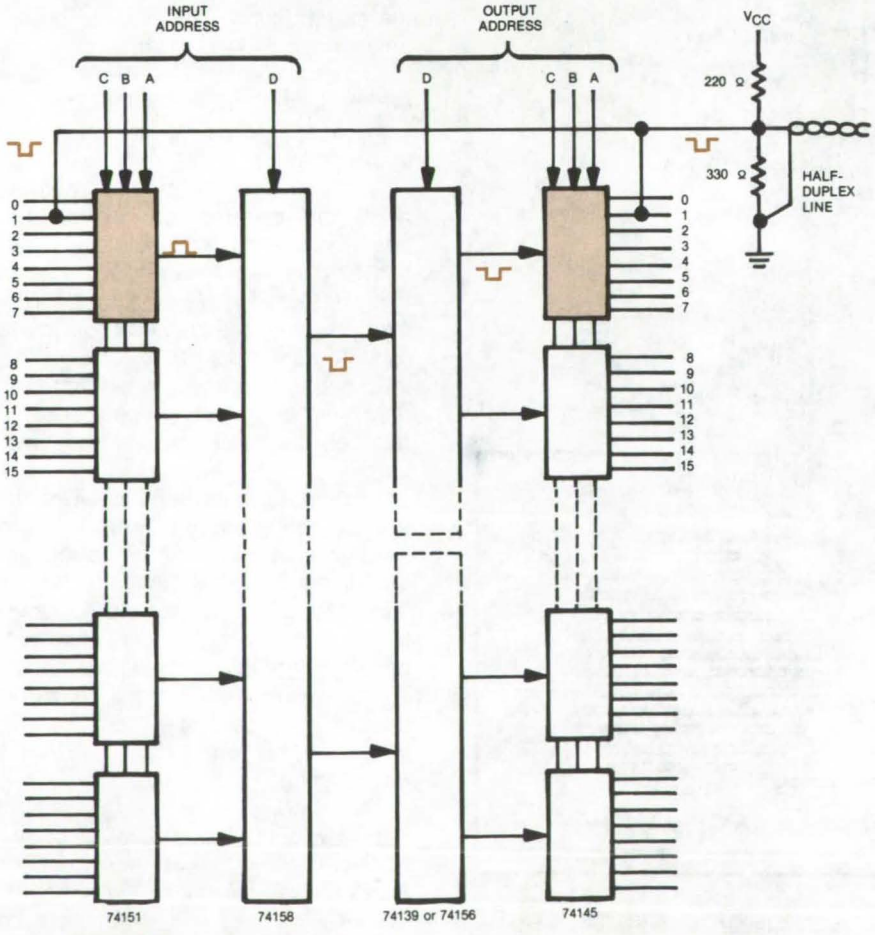

Figure 2. A **Four-Line, 16-Port Array** is configured by combining several circuits of the type shown in Figure 1. The input and output lines are defined by binary addressing.

Standard digital multiplexers and demultiplexers are readily configured into circuits that simulate crossbar arrays of mechanical switches. For example (see Figure 1), a single line switched from any one of eight ports, designated to be the inbound port, to any of the remaining seven, uses 74151 and 74145 (or equivalent) TTL integrated circuits together with a bidirectional-interface line-driver/receiver terminating network.

As shown in Figure 2, the configuration can be expanded into a four-line, 16-port switching network by paralleling eight 74151 IC's and eight 74145 IC's. Digital data selectors, such as 74158 and 74139 or 74156, are used to channel the signals between the input and output ports.

The circuits can be expanded to larger arrays by coupling the basic building blocks in the appropriate way. In all cases, binary addressing of the input and output ports is used.

This work was done by Tage O. Anderson of Caltech for **NASA's Jet Propulsion Laboratory.** *For further information, Circle 5 on the TSP Request Card.*
NPO-13837

Strobe-Margin Test for Plated Memory Systems

A technique for measuring plated-wire-memory performance margins

Marshall Space Flight Center, Alabama

A new technique has been developed for measuring the performance of plated-wire memories. The technique, called the strobe-margin test (SMT), utilizes worst-case testing (i.e., minimum output signal and maximum noise) and automatically gives the exact strobe margin. The test is automatic; and because it is a memory system-level test, under worst-case conditions, it is superior to tests at the component level that use artificial test conditions.

The strobe margin is defined as the difference between the measured strobe window and the calculated worst-case variation of the strobe position. In this definition, the strobe window of a plated-wire memory system is the time, in nanoseconds, that the output of the plated-wire element exceeds the threshold of the sense amplifier and is available for capture by the data register. Primary factors affecting the strobe margin are noise at the sense-amplifier input, the amplitude of the signal from the wire, and the threshold of the sense amplifier.

The hardware and the software required to run the SMT modify an existing memory-interface console (MIC). This MIC had the ability to write data into the memory under test, to read the data back, and to compare the data against those data that should have been read. It was modified by adding a software-controlled variable-delay pulse generator, memory-word-current and digit-current control circuits, and the software to vary these parameters. In addition, the memory-system strobe generator was modified so that it could be varied externally.

Using the developed hardware and software, the test sequence, referred to as a cross-point adjacent-bit-disturb (ABD) test, is as follows:

- First, a hard history of the bits to be tested is written 1,000 times in the opposite polarity.
- Next, a soft write of the desired polarity is written one time into the bit to be tested.
- The bits on either side of the bits to be tested are then written 1,000 times with data of the opposite polarity.
- The bits under test are then iteratively read with a minimum word current while varying the strobe position.

The time between the most-positive strobe position without a read error and the most-negative strobe position without a read error is the strobe window width. This strobe window width can be translated to predicted parity errors per day.

The end result of this test sequence is that each bit in memory is tested after the weakest write of the desired data, the highest self-generated noise, a worst-case disturb condition, and a minimum read excitation. In one application, these conditions were to be met with a minimum strobe window of 28 ns.

The strobe-margin test can be a significant tool in the design and test of plated-wire memory systems. It can rapidly quantify the memory-system margin on each production unit and the impact of any design changes. This can result in better systems at reduced memory-test cost. This concept can be applied to other plated-wire memory systems and, with minor adaptations, to core memory systems.

This work was done by T. E. Anspach, J. W. Clarke, and R. C. Constable of Honeywell Inc. for **Marshall Space Flight Center.** *For further information, Circle 6 on the TSP Request Card.*

Inquiries concerning rights for the commercial use of this invention should be addressed to the Patent Counsel, Marshall Space Flight Center *[see page A8].* *Refer to MFS-23838.*

Safe Venting for Electronic Components

Flames or smoke from malfunctioning circuits are isolated from main cooling system by inexpensive air-cooled enclosure.

Lyndon B. Johnson Space Center, Houston, Texas

Air-cooling systems used in flight cabins and other closed environments must be carefully protected from contamination with flame or smoke. For instance, special care is taken with electronic circuitry because of the toxic gases that would be generated by some components should they burn. Thus electronics are not cooled directly by cabin air in order to prevent any fire or smoke from a malfunctioning circuit from spreading through the entire cooling system.

Presently, the circuits are placed in sealed enclosures, or shelf cooling systems are used. Both of these approaches are expensive and add extra weight, but they are mandatory safety measures.

An alternate but effective technique has been found less expensive. Electronic components are housed in lightweight enclosures that allow air circulation and, at the same time, isolate the components from the cabin airstream. A typical such enclosure has two adjacent compartments, as shown in the figure. The inner compartment encloses the circuit boards,

(continued next page)

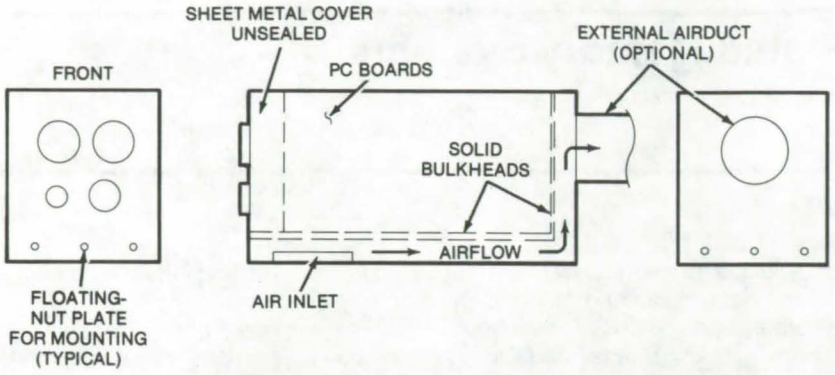

The **Vented Electronic-Circuit Enclosure** is made from lightweight metal. The printed-circuit boards are attached to the bottom and end bulkheads and to the top cover. Airflow cools the components indirectly through the walls of the inner compartment. Flammability and smoke tests have demonstrated the safety of the enclosure.

using two solid bulkheads and a sheet metal cover. Cooling air enters the air inlet of the second or external compartment, which partly surrounds the inner one. In the event of a fire, the inner enclosure safely isolates flame and smoke from the air-cooling system.

This work was done by Randolph Currin, Jr., and Charles W. Fischer of Rockwell International Corp. for **Johnson Space Center.** *For further information, Circle 7 on the TSP Request Card.*
MSC-18007

Direct-Reading Group-Delay Measurement

The retardation of moduation signals by a microwave component is rapidly plotted by an x-y recorder.

NASA's Jet Propulsion Laboratory, Pasadena, California

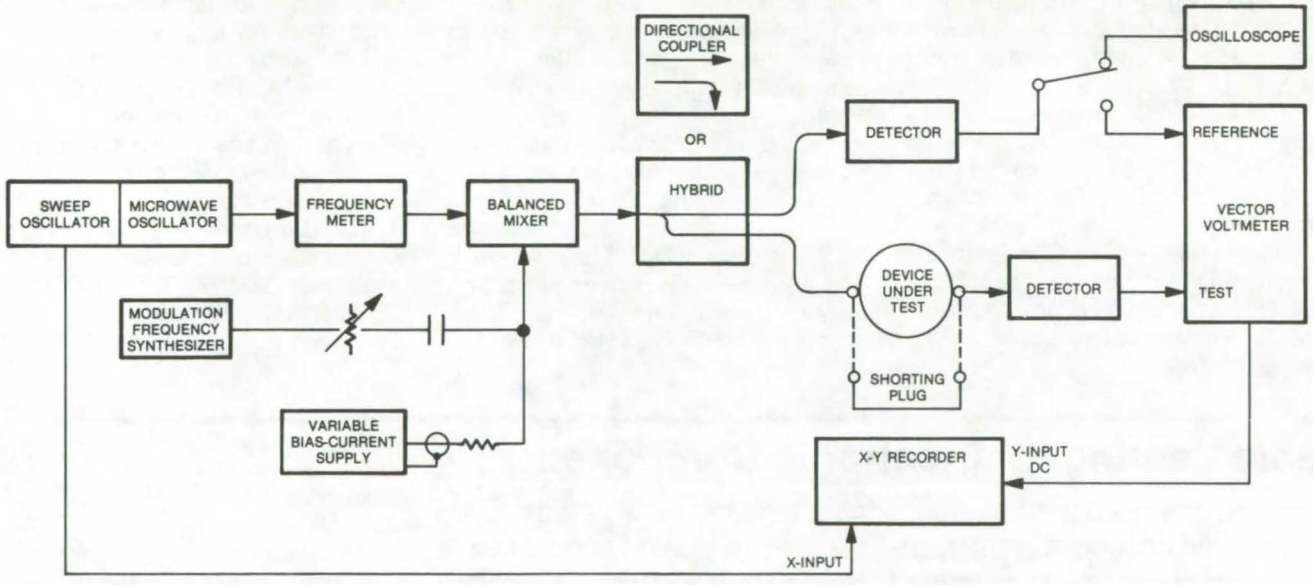

Group-Delay time is plotted directly against carrier frequency, using this setup. The vector-voltmeter phase comparator is initially balanced with the test device out of the circuit; then, the microwave frequency is swept over the band of interest.

A new technique for measuring modulation signal retardation (group delay) in microwave components gives a direct plot of the dependence of the delay time on the carrier frequency. Most previous methods required a laborious reduction of phase and frequency data to calculate the group delay. With the new method, the dependence of the delay time on temperature or mechanical stress is determined easily.

The test arrangement is shown in the accompanying figure. The signal from a microwave oscillator is amplitude-modulated at a constant modulation frequency by the signal from a frequency synthesizer applied at a balanced mixer. This modulated sweep signal is then sent to a reference channel and to a channel containing the device under test. The output signals are detected by a vector voltmeter, which compares the phase

of the test channel with that of the reference. As the carrier frequency is swept, the phase difference, which is proportional to the group delay, is plotted against frequency on an x-y recorder. The recorder sensitivity can be adjusted to give a convenient scale factor for the group delay (e.g., 1 inch = 1 nanosecond). From a family of such recordings, it is possible to observe changes in group delay due to temperature, mechanical stress, and other factors.

This work was done by David L. Trowbridge of Caltech for **NASA's Jet Propulsion Laboratory.** *For further information, Circle 8 on the TSP Request Card.*

This invention has been patented by NASA [U.S. Patent No. 4,084,132]. Inquiries concerning nonexclusive or exclusive license for its commercial development should be addressed to the Patent Counsel, NASA Resident Legal Office-JPL [see page A8]. Refer to NPO-13909.

Synchronous Transfer Circuits for Redundant Systems

Circuits efficiently transfer control to surviving components after a failure.

NASA's Jet Propulsion Laboratory, Pasadena, California

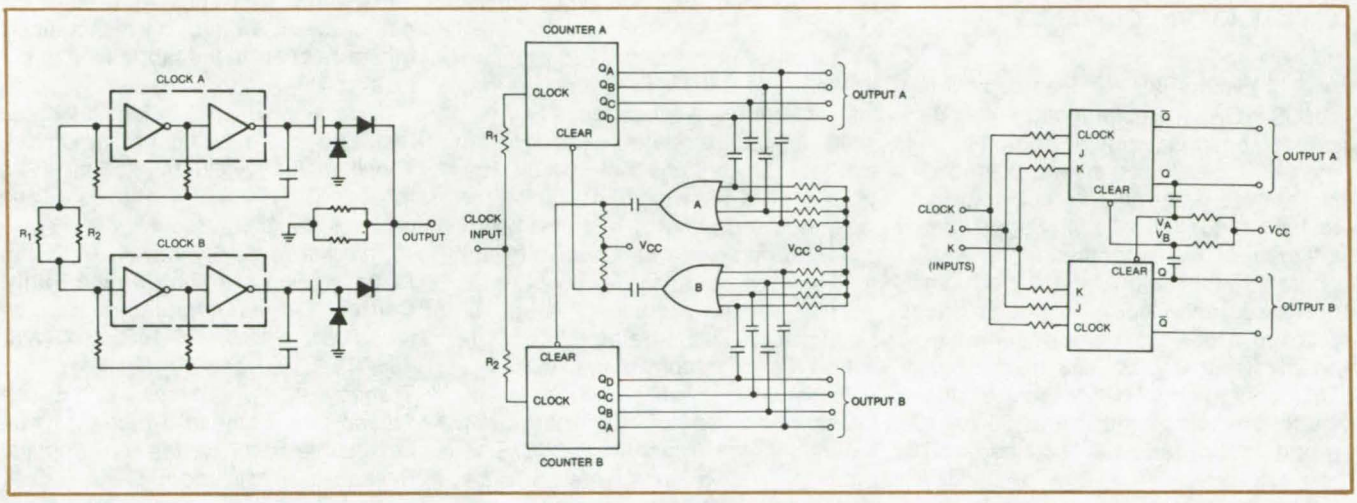

Synchronous Transfer of Control from one element of a redundant pair to another is made possible by circuits that interconnect the elements in the appropriate way. Clock-driver (left), counter (center), and flip-flop (right) circuits are shown. The outputs would be coupled through OR gates (shown only for the clock drivers, which use a diode OR gate).

New circuit arrangements for flip-flops, counters, and clock drivers in redundant systems ensure that control is synchronously transferred to surviving components when a failure occurs. In addition to their original application to spacecraft systems, the redundant circuits should have terrestrial uses in power generators, solar-energy converters, computers, vehicle controllers, and other systems demanding high reliability.

The two clock-driver modules (see figure, left) are synchronized in phase and frequency so that if one of the modules fails, the output signal is virtually unaffected. The arrangement consists of two astable multivibrators, with their outputs in an ac-coupled diode OR function so that only the output signal from the surviving module is transmitted. The synchronization and phase forcing are exerted through the common impedance R_1 and R_2 and will occur provided the frequency difference is not too great (within about 10 percent). Resistors R_1 and R_2 have high values so that if one fails, the effect on the frequency of the surviving module is minimal.

The redundant counters (see figure, middle) are arranged so that they cross-reset each other periodically. A "clear" signal is transmitted through one of the four-input OR gates only when all of the outputs of one counter reach zero. When this happens, the output of the other counter is reset to all zeros, bringing both counters into synchronization. The counter outputs are coupled together by ac-coupled diode OR gates. If one fails, the other takes over without losing count.

The Q output of one redundant flip-flop is coupled to the "clear" input of the other, forcing synchronous operation of both. When flip-flop A is reset (Q = 0), V_A activates the "clear" input of flip-flop B and resets its Q output to zero. Similarly, if flip-flop B is reset before flip-flop A, a signal at V_B resets flip-flop A.

This work was done by Satoshi Nagano of Caltech for **NASA's Jet Propulsion Laboratory.** *For further information, Circle 9 on the TSP Request Card.*

Inquiries concerning rights for the commercial use of this invention should be addressed to the Patent Counsel, NASA Resident Legal Office-JPL [see page A8]. Refer to NPO-14162.

Books and Reports

These reports, studies, and handbooks are available from NASA as Technical Support Packages (TSP's) when a Request Card number is cited; otherwise they are available from one of NASA's Industrial Application Centers or the National Technical Information Service.

Analyzing CMOS/SOS Fabrication for LSI Arrays

A method for optimizing the CMOS/SOS process for the fabrication of LSI semiconductor structures

A silicon-gate deep-depletion CMOS/SOS (complementary metal-oxide semiconductor/silicon-on-sapphire) process has been examined in depth to determine its applicability to the fabrication of LSI (large-scale integration) semiconductor arrays. Three different test arrays have been designed and built to determine problem areas that may occur when adapting the CMOS/SOS process to LSI fabrication. The results of the study are presented in a 56-page report that can be obtained on request.

The three test arrays used in the analysis are the process analysis structure (PAS) test cell, the spacing array (SPAR), and the contact array (CAR). The PAS assists in determining the frequency of defects that arise during the CMOS/SOS process when fabricating an array of a particular size. The PAS array is laid out so that an increasing number of cells of different sizes can be analyzed and a pass-or-fail condition set up as a function of the number of cells.

The SPAR structure tests the ability of a process sequence to define conducting lines spaced a given distance apart. The CAR contains an array of SOS islands that become interconnected with metal; this array is interrogated for continuity of contacts.

The study uncovered three problem areas in the CMOS/SOS process that warrant future investigation. The first, which is process related, concerns the integrity of the channel oxide. The yield curves showing the number of gate-to-island short circuits were widely variable and can dominate the final yield in LSI arrays.

The second problem area is process-dimension related and involves the topography of the structure. A substantial yield reduction is incurred because of the nonplanar nature of the present CMOS/SOS process. The various layers could be patterned with higher reliability on a planar surface.

The third area, also process-dimension related, is concerned with contact openings. At present, fine-line patterns can be defined (at least on a planar surface) with decent yields, but the size of the contact that must be used to connect one layer to another must be larger than either level, to have a relatively high probability of opening. The dimensions of the array and the packing density become dominated by the size of the contact opening.

The report discusses a set of new design rules that have been developed as a result of work with the test arrays. A set of optimum dimensions is given that would maximize the process output and would correspondingly minimize costs in the fabrication of LSI arrays.

Several new applications of these test arrays are being contemplated. These include yield prediction, yield modeling, diffusion studies, and process reliability.

This work was done by A. C. Ipri of RCA Corp. for **Marshall Space Flight Center.** *Further information may be found in NASA CR-150213 [N76-78470], "Design, Processing, and Testing of LSI Arrays for Space Station," a copy of which may be obtained at cost from the New England Research Application Center* *[see page A7]*.

MFS-23788

Electronic Systems

Hardware, Techniques, and Processes

177 Finding Radiant-Energy Sources
178 Noise Tolerant Computer Link
179 Human Arm May Act as Antenna
180 Femtosecond Time-Domain Phase Comparator
181 Chopper-Stabilized Phase Detector
182 Bit-Synchronizer Lock Detector
183 Automatic Radio-Transmission Monitor

Books and Reports

184 Control of Small Phased-Array Antennas

Finding Radiant-Energy Sources

An antenna is scanned in orthogonal directions to pinpoint interfering sources.

Goddard Space Flight Center, Greenbelt, Maryland

A NASA satellite system [see "Satellite-Based Interference Analyzer" (GSC-12150) on page 326 of *NASA Tech Briefs*, Vol. 2, No. 3] pinpoints the locations of radiant-energy sources by scanning the region of interest with a narrow-beam steerable antenna and then plotting the received signal strength on a two-dimensional contour map. Although it was originally developed to protect satellite communications networks against microwave interference, the principle is also applicable to locating sources of sound, infrared, and other forms of radiant energy.

In the satellite system, the RF band between 5.925 and 6.425 GHz is sampled in 10-kHz slots. As the spectrum is sampled, the antenna boresight axis is swept in latitude and longitude or in roll and pitch (under computer control) to generate two orthogonal scans. During a scan, each of the 10-kHz slots is sampled about 10 times. For each slot, the received power is recorded as a function of antenna displacement and is plotted on an x-y recorder. A simple plot, for one frequency slot and one radiation source, would look like that shown in Figure 1. For a more accurate determination of the position of the source, an enclosed contour plot (Figure 2) would be generated by the computer after all the scan data had been received and processed. The intersection of the roll and pitch coordinates of the signal maximums would be converted to geocentric latitude and longitude to locate the radiation source.

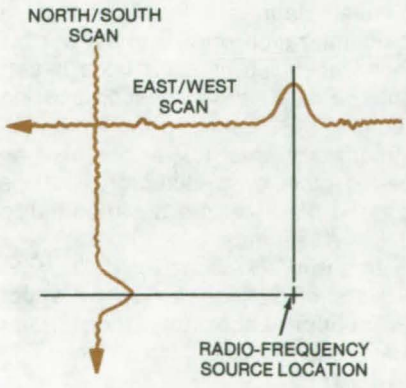

Figure 1. **Orthogonal Scans** of received power versus geographical position can pinpoint the location of a source of radiant energy.

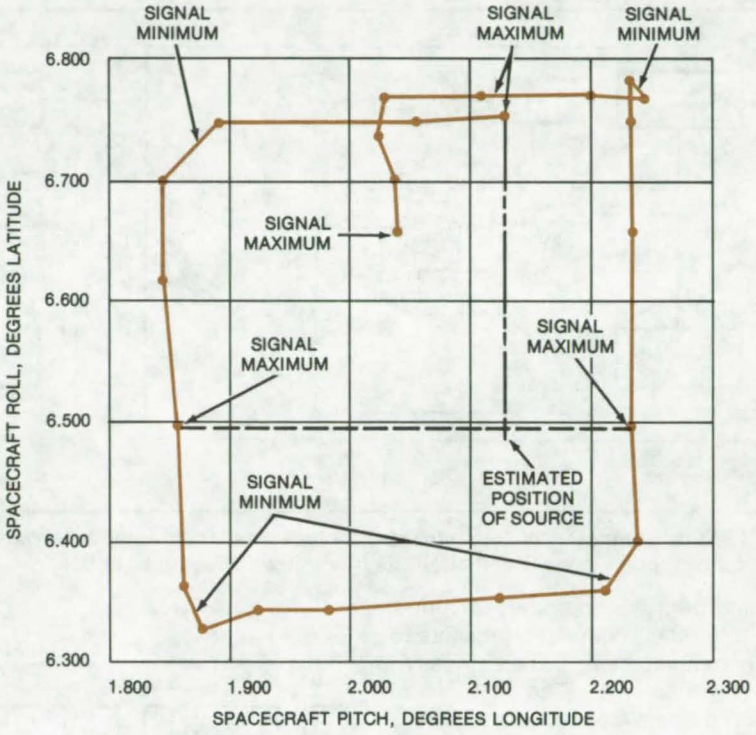

Figure 2. A **Complete Contour Plot** is obtained by varying the antenna roll and pitch angles to form an enclosed two-dimensional area. The location of an interfering source can be determined to better than 100 miles by this method.

The resolution of the method depends on several factors, including the amplitude stability and frequency stability of the source and the receiver threshold detection level. For very weak signals, the scan would be repeated several times and signal averaging methods used. If several sources are present within a geographical region, the coordinates of each could be computed automatically from the scan data. In this case the ability to discriminate between two sources would depend in part on the spatial resolution of the receiver.

In tests, the satellite system could locate a ground-based microwave transmitter to an accuracy of about 100 miles (161 km). When data on the misalinement of the satellite antenna boresight were used to correct the antenna pointing, the accuracy was improved to better than 70 miles (113 km). Other corrective measures are expected to increase the accuracy to below 50 miles (80 km).

This work was done by Gustave J. Schaefer of Hughes Aircraft Co. for **Goddard Space Flight Center.** *For further information, Circle 10 on the TSP Request Card.*

This invention is owned by NASA, and a patent application has been filed. Inquiries concerning nonexclusive or exclusive license for its commercial development should be addressed to the Patent Counsel, Goddard Space Flight Center [see page A8]. Refer to GSC-12147.

Noise Tolerant Computer Link

Bit data are transmitted serially over long distances, using a bidirectional computer-to-computer link.

NASA's Jet Propulsion Laboratory, Pasadena, California

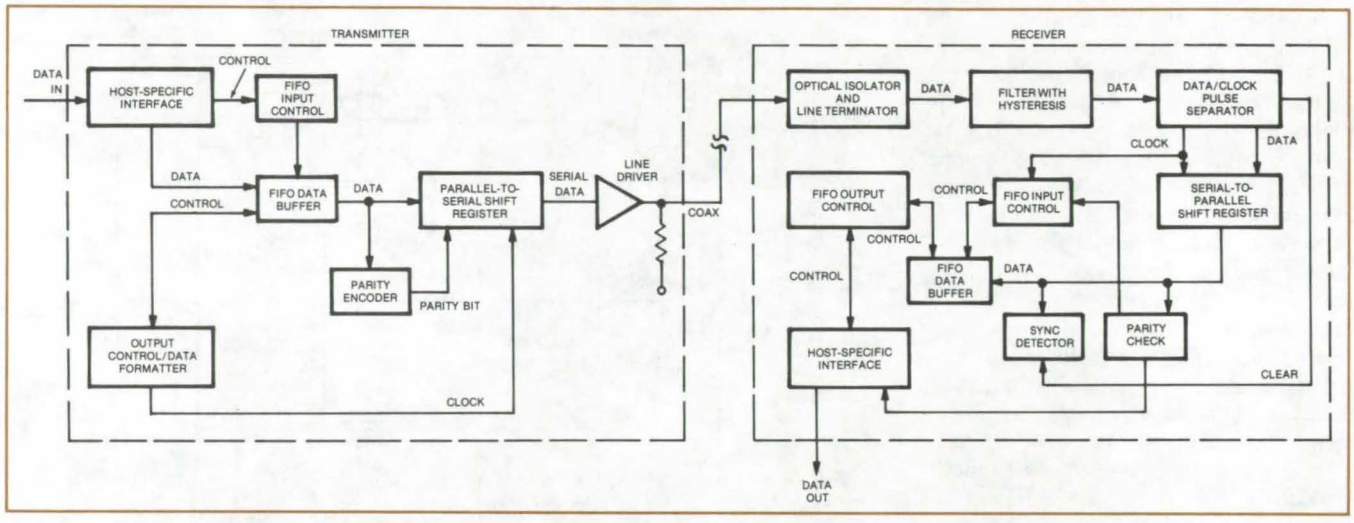

Figure 1. This **Computer-to-Computer Link** includes transmitter and receiver sections that communicate serially over a coaxial line. A form of pulse-code modulation, as illustrated in Figure 2, is used.

An inexpensive computer-to-computer link (see Figure 1) facilitates data communication in electrically noisy environments. The link can connect process-control computers, for example, while reducing errors from the electrical noise of manufacturing operations.

The link has been used to provide simultaneous two-way communication over two coaxial cables, for distances up to 1,000 meters. Data are encoded into a form of pulse-code modulation in which bit values of 1 or zero are coded by either the presence or absence of a data pulse. Each bit period is divided into two subperiods: a clock subperiod that signals the start of the bit period, followed by a data subperiod.

In the example shown in Figure 2, the clock pulse is 400 ns wide, and the data period is 1,200 ns. If a 400-ns pulse is inserted in the data period, it represents a logical 1; if no pulse is inserted, it represents a zero. The width and duty cycle of the pulses are chosen so that transient charge on the coaxial line has enough time to decay after a pulse before the next pulse comes along, and a filter has time to remove transient errors from pulses.

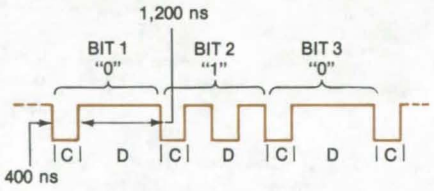

Figure 2. The **Modulation Code** is sent as alternating clock (C) and data (D) periods. A pulse within the data period represents a 1; the absence of a pulse represents a zero.

This modulation scheme is relatively simple to generate and transmit; also, the original signal is easily recovered. Consequently, the parts count can be less than for some other transmission schemes. In addition, the selection of the duty cycle and the pulse repetition rate to permit the coaxial cable to return to a normal state between pulses eliminates the need for a bipolar signal. Optical isolators are used to ensure that common-mode noise is not a problem in transmitting the single-ended signal.

An interface connects the computer to the transmitter section of the link. A first-in, first-out (FIFO) data buffer is filled with data from the computer under the supervision of the FIFO input control.

On receipt of a transmit command, the transmitter output control/data formatter orders data to be read out of the FIFO buffer and sent over the link. (The host computer may enter data into the FIFO while the link removes data.)

At the receiving end, the signal passes through the isolation and filtering circuits and is split back into data and clock pulses. The output clock strobes the data bits into a serial-to-parallel shift register. The parallel data are scanned for a synchronization word, and if a word is found, the sync detector latch is set, and the data word is strobed into the receiver FIFO buffer. If the input data stream vanishes for a preset time period, the sync detector latch is cleared. Parity errors are reported to the host interface.

This work was done by Michael W. Sievers of Caltech for **NASA's Jet Propulsion Laboratory.** *For further information, Circle 11 on the TSP Request Card.*

Inquiries concerning rights for the commercial use of this invention should be addressed to the Patent Counsel, NASA Resident Legal Office-JPL [see page A8]. Refer to NPO-14152.

Human Arm May Act as Antenna

Wrist strap with copper strips can be used as coupler of radio-frequency energy.

Ames Research Center, Moffett Field, California

A human arm may be made to act as an antenna for a communications system. It has been done by using an energy coupler made of two strips of copper foil fastened to a strap and wrapped around the wrist. Apparently, the wrist strap can efficiently transfer radio-frequency energy to or from the arm. A prototype of the antenna coupler was built and found suitable for both sending and receiving very-high-frequency signals. The goal of the developers is to build a body-worn communications system for the deaf blind, and it was with this purpose in mind that the prototype unit was built and tested. Other potential applications for the compact coupler include body-worn two-way local communications systems for police and as part of a portable personal communications system that could communicate via satellite.

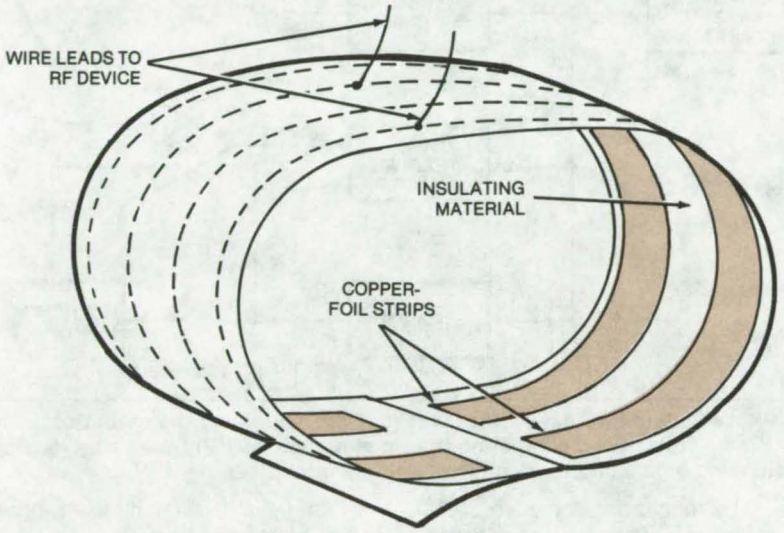

Figure 1. **Wrist-Strap Coupler** of radio-frequency energy consists of two strips of copper fastened to an insulating material. Wires at the midpoints of the strips lead to the radio-frequency device that can act as a transmitter or receiver.

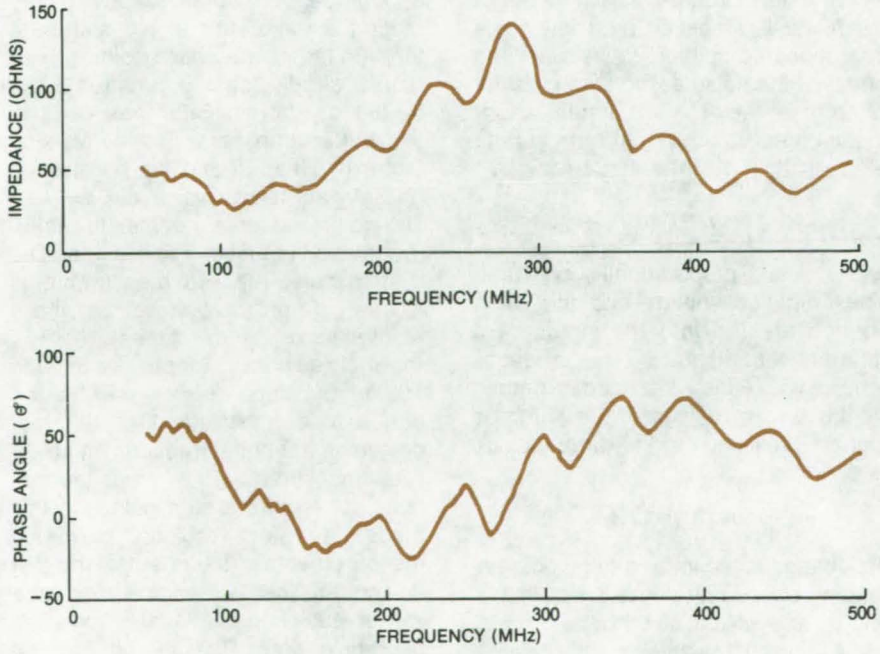

Figure 2. **Electrical Impedance Characteristics** of the wrist-strap antenna coupler were measured with a General Radio 1710 RF Network Analyzer. Varying the widths of the copper strips will produce somewhat different characteristics.

The copper-foil strips of the wrist-strap coupler, shown in Figure 1 are rectangular, 5 in. (13 cm) long, and 1/2 in. (1.3 cm) wide. They are placed 7/16 in. (1.1 cm) apart and are fastened to the underside of a wrist strap made of an electrically insulating material. A thin insulating strip is also placed over the straps as a protective cover. Such an insulator can be added to the wrist strap because the copper strips need not be in direct contact with the skin for the RF signals to be coupled to or from the arm.

For connecting the coupler to a transceiver, or receive- or transmit-only unit, a small wire is attached to the edge of each copper strip at a point equidistant from the ends of the strip. Each wire is then routed through a hole in the insulating material to the upper surface of the strap. In addition, a fastener must be attached to the strap so that it can be pulled snugly against the wrist.

Radio-frequency energy couples to or from the arm through the electrical capacity between the arm and the copper strips. Electrical impedance characteristics of the antenna are shown in Figure 2. The radiated field strength, with the strap driven by a 170-MHz, 10-mW transmitter, was found to be slightly greater than that from a well-designed loop antenna built with a 16- by 11- by 3-mm ferrite core and driven by the same transmitter.

This work was done by James C. Gaddie and Russell T. Wolfram of Stanford Research Institute for **Ames Research Center.** *For further information, Circle 12 on the TSP Request Card.*

ARC-11195

Femtosecond Time-Domain Phase Comparator

Relatively simple circuit makes time-domain phase-stability measurements to 20 fs (at 5 MHz) with a single crystal-oscillator reference.

Goddard Space Flight Center, Greenbelt, Maryland

The simplest method for measuring the phase stability of electronic equipment is to split the signal from a reference oscillator, sending part of it through the device under test and the rest (phase-shifted by 90°) along a reference line. By recombining the signal in a mixer, a voltage that represents the phase shift of the test device is generated, independent of any phase fluctuations in the oscillator. This voltage is analyzed to determine the phase stability of the test device.

While this circuitry is simple, it is generally unsuitable for time-domain stability analysis unless complex noise analyzers or data processors are available. A standard technique for making time-domain stability measurements independent of reference-oscillator noise requires two reference oscillators (offset in frequency), two mixer systems, and multiple buffer amplifiers. In this technique, the oscillators drive the mixers to produce two sets of beats corresponding to the frequency offset in the oscillators. The test device is inserted in one of the lines between an oscillator and a mixer so that the phase of one of the beats is offset by the phase shift of the test device. Buffer amplifiers are also inserted at appropriate places to avoid cross talk between the mixer systems. To make time-domain measurements independent of reference oscillator noise, the two beats are fed into the start and stop inputs of a time interval counter. The time interval between the beats at any given time will then correspond to the phase shift at that time introduced by the test device. Any phase shift introduced by a reference oscillator will affect both beats simultaneously and not affect the time interval measurement.

The complexities of this technique are greatly reduced in the system shown in the figure. Only one oscillator is required; the beat signal is mimicked by summing a low-noise ramp voltage with the output of a single mixer. The phase shift of the test device is converted to a counter reading by monitoring the zero crossings of the mimicked beat with a low-frequency reference used to drive the ramp generator.

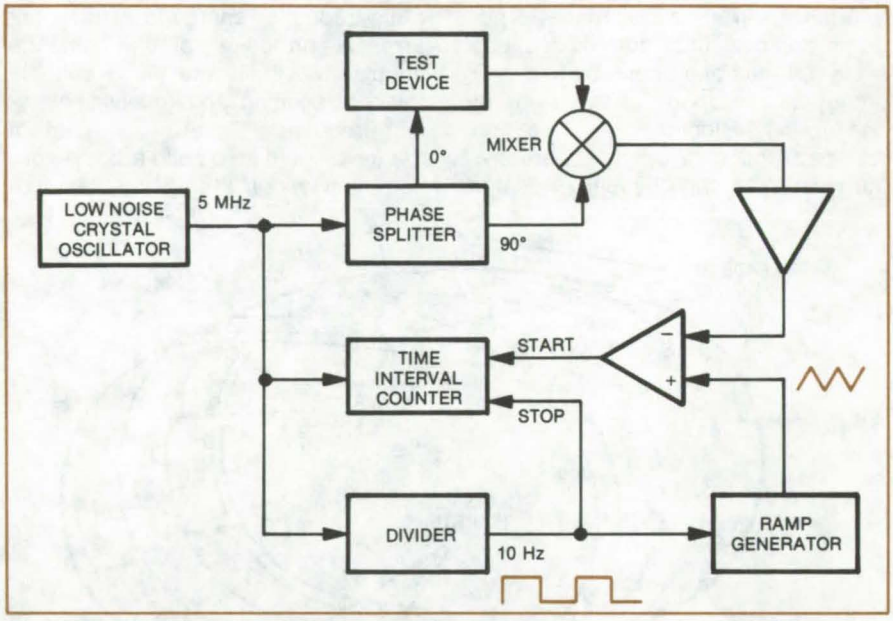

The **Phase Shift in the Test Device** is measured by summing the output of the mixer with a ramp voltage and comparing the time interval between the zero crossings of the summed signal and ramp reference frequency.

In the new circuit, the voltage out of the mixer is amplified by a low-noise operational amplifier to reduce the effect of the noise associated with the ramp generator. After amplification, the voltage (V) is given in terms of the phase shift (φ) of the test device by

$$V = A\varphi$$

where A is a proportionality constant. The amplified voltage and the ramp voltage are fed into the inputs of a differential comparator. This produces a pulse with edges that are determined by the zero crossings of the summed signal. If the slope of the ramp voltage is given by

$$dV/dt = 1/B$$

the change in the time-interval counter reading caused by phase shifts in the test device will be given by

$$dt = 2\pi f_0 BA(\varphi/2\pi f_0)$$

when f_0 is the oscillator frequency. The expression is written in terms of the normalized phase shift ($\varphi/2\pi f_0$). The calibration factor that relates dt and φ can be obtained directly by putting a calibrated phase shifter in the 90° leg of the phase splitter.

In a circuit actually constructed, a 5-MHz crystal oscillator was used to test buffer amplifiers. The conversion factor between dt and the normalized phase was 10^8. This would allow a 100-ns time-interval counter to measure phase fluctuations to 10^{-15} s. The system noise allowed measurements to be made on the test device with a resolution of a few times 10^{-14} s (normalized phase) for periods of up to 100 s. By using the counter in the period mode, the effect of the test device on fractional frequency stability was measured. This measurement does not require a stop pulse. In this mode the system resolution permitted measurements of the effect of the test device on the two-sample variance with a resolution of 2×10^{-14}, for a 1-s averaging time. The circuit can be

used to test devices at other frequencies by changing only the signal source, the phase splitter, and the mixer; the divider and the time-interval counter need not be driven by the RF oscillator.

This work was done by Theresa Donahoe and Victor Reinhardt of **Goddard Space Flight Center.** *For further information, Circle 13 on the TSP Request Card.*

This invention is owned by NASA, and a patent application has been filed. Inquiries concerning nonexclusive or exclusive license for its commercial development should be addressed to the Patent Counsel, Goddard Space Flight Center [see page A8]. Refer to GSC-12228.

Chopper-Stabilized Phase Detector

Offset, drift, and gain imbalance are canceled by synchronized switching.

Lyndon B. Johnson Space Center, Houston, Texas

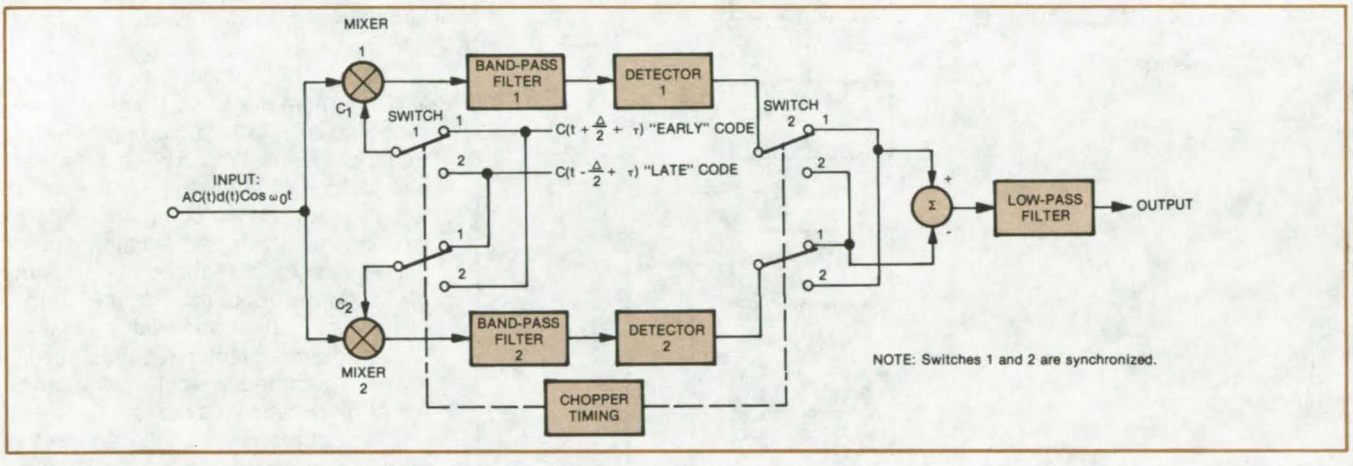

"Early" and "Late" Codes Are Chopped and mixed with the input signal. Switching is synchronized with polarity switching of the detector outputs to cancel the effects of offset and gain imbalance. The chopper can be implemented with standard logic gates.

A phase-detector circuit for binary-tracking loops and other binary-data acquisition systems minimizes the effects of drift, gain imbalance, and voltage offset in the detector circuitry. The input signal is passed simultaneously through two channels where it is mixed with "early" and "late" codes that are alternately switched between the channels. The code switching is synchronized with polarity switching of the detector output of each channel so that each channel uses each detector for half the time. The net result is that dc offset errors are canceled, and the effect of gain imbalance is simply a change in sensitivity.

The new circuit combines the best features of two older circuits. Specifically it uses the two-detector feature of the delay-lock loop for continuous processing and uses the "dither" feature of the tau-dither loop for canceling imbalance and offset.

As seen in the figure, the input to the new detector is a carrier at frequency ω_0, modulated by a data signal d(t) and a pseudorandom code C(t). Both the data and the pseudorandom code are binary signals with possible values of either +1 or -1. When switch 1 is in position 1, the output of mixer 1 is a combination of the input and the "early" code, and the output of mixer 2 is a combination of the input and the "late" code.

The band-pass filters are designed to pass the spectrum of the data d(t), but the bandwidths are small compared with the spectrum of the pseudorandom code C(t). As a result, the outputs of the band-pass filters consist of the carrier, the data, and the cross-correlation functions of the incoming code with the early and late codes, respectively.

With switches 1 and 2 in position 1, the output of detector 2 is subtracted from the output of detector 1, and the result is passed through a low-pass filter. Similarly, when the switches are in position 2, the output of detector 1 is subtracted from that of detector 2 and passed through the low-pass filter. If the switches are operated at a rate that is high compared with the bandwidth of the low-pass filter and if the switches spend exactly half the time in each position, then the filter output is half the average value of its inputs. Thus, the dc offsets cancel in the final output, and the gains of the two channels affect only the amplitude of the output.

This work was done by Phillip M. Hopkins of Lockheed Electronics Co. for **Johnson Space Center.** *For further information, Circle 14 on the TSP Request Card.*

This invention is owned by NASA, and a patent application has been filed. Inquiries concerning nonexclusive or exclusive license for its commercial development should be addressed to the Patent Counsel, Johnson Space Center [see page A8]. Refer to MSC-16461.

Bit-Synchronizer Lock Detector

Simplified circuit indicates the phase error between recorded and reconstructed clock signals.

Lyndon B. Johnson Space Center, Houston, Texas

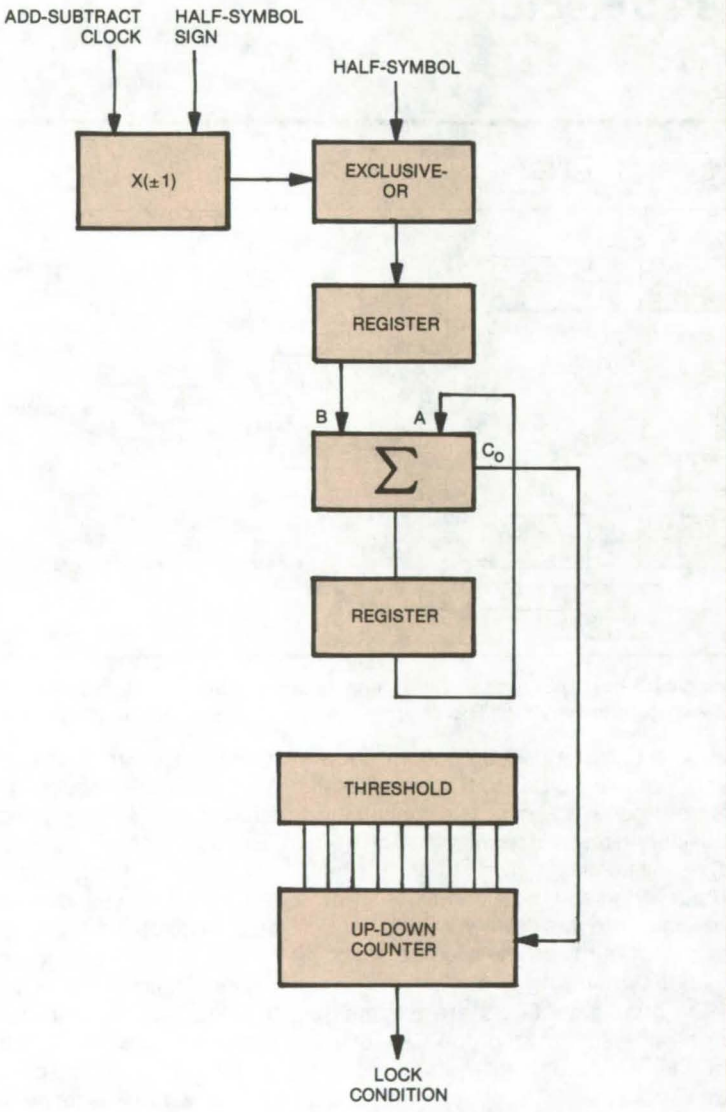

Recorded [Half-Symbol] and Reconstructed Clock Signals are processed to yield a signal that represents their phase-lock relationship. The output (a digital word) can be compared with a specified threshold to provide a 1-bit indication of lock status.

A novel circuit measures the phase error that exists in a phase-locked loop between the clock signal recorded in data on magnetic tape and the reconstructed clock signal. The circuit presents the error as a digital word that can be compared with a predetermined threshold to indicate lock status. With simple alterations, the circuit can also be used as a phase detector.

The lock detector utilizes an early/late algorithm used in a NASA bit-rate synchronizer, but implements it by treating 1/2-bit time as the smallest unit of time of interest (rather than 1 full-bit time). By so doing, it renders part of the algorithm redundant and unnecessary and reduces the amount of hardware required. In the aerospace application for which it was designed, the detector requires seven fewer integrated circuits and two fewer discrete components.

The circuit operates (see figure) by taking the absolute value of two in-phase half-symbol integrations, subtracting the sum of the absolute values of two quadrature half-symbol integrations, and then summing over 2^n symbol times (n being the number of symbols). The output is a maximum for either 0° or 180° phase offset between the recorded and reconstructed clocks. It is zero for ±45° offset and a negative maximum for ±90°. The equality of the output for phase-locked and 180° out-of-phase clocks is a characteristic of any lock detector operating on a Manchester-encoded signal, which uses only half-symbol instead of full-symbol information.

This work was done by Douglas C. Huey and Benedict A. Itri of TRW, Inc., for **Johnson Space Center.** *For further information, Circle 15 on the TSP Request Card.*

Inquiries concerning rights for the commercial use of this invention should be addressed to the Patent Counsel, Johnson Space Center [see page A8]. Refer to MSC-16744.

Automatic Radio-Transmission Monitor

System compares radio emissions to reference levels and stores deviant data for later analysis.

NASA's Jet Propulsion Laboratory, Pasadena, California

An RF-spectrum monitoring system continuously monitors radio transmissions and compares them with a reference stored in memory. If the spectrum deviates beyond preset limits, an alarm is tripped, and the spectrum is transferred to long-term storage for later analysis.

This system was originally developed for analyzing command communications links to spacecraft, where it is important to know when a failure has occurred so that commands can be retransmitted or corrections made. In commercial communications, such as TV and FM broadcasting, the spectrum monitor can be useful in ensuring proper power level and spectral quality and in finding the cause of failure. It might also be used to monitor radio-frequency interference or the power levels of citizen's-band transmitters.

As shown in the figure, the system consists of an RF-spectrum analyzer, an analog-to-digital converter, a timing generator, a comparator, level-detector signal switches, memory units, and a cathode-ray tube (CRT) display.

The spectrum analyzer generates an analog voltage representing the power spectrum across the width of the channel being monitored. This voltage is transformed to a digital signal by the analog-to-digital converter. (The spectrum is sampled and converted at a rate controlled by the timing generator.)

A switch (sequentially operated by the timing generator) routes the digitized spectrum between memory 1, memory 2, and the comparator. One band sweep is stored in memory 1 as a reference, for comparison with subsequent band sweeps. Each subsequent sweep is also temporarily stored in memory 2. If there is no difference between the incoming spectrum stored in memory 1, the comparator produces no output. If there is a difference, the comparator sends the difference to the level detector. When a preset level stored in the detector is exceeded, it sends a signal to an alarm circuit that energizes a warning indicator and prevents the spectrum stored in memory 2 from being erased. The spectrum is also presented on the CRT display. Memory 2 can then send the spectrum to long-terms storage for later analysis. Actually, memory 2 is composed of two buffer memories. If one of these is busy sending an out-of-limits spectrum to long-term storage, the other is free to accept the next batch of data from the spectrum analyzer, and vice versa.

The long-term storage medium may be magnetic tape or, perhaps, photographic film. For the latter, a camera attached to the CRT display can have its shutter opened by the alarm signal. The spectral data then displayed on the screen in analog form are recorded on the film. The next index pulse from the timing generator closes the shutter to complete the recording process.

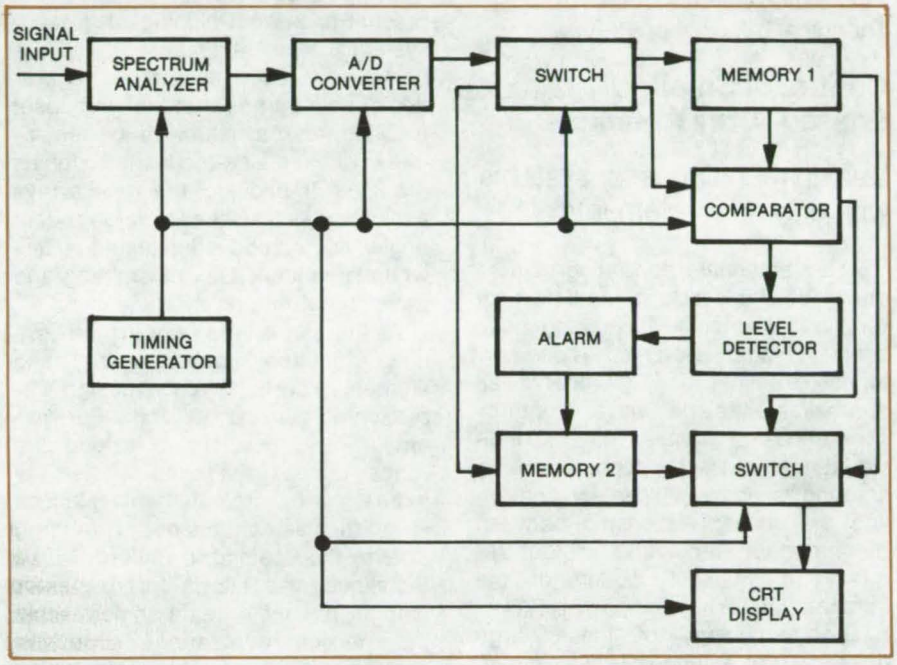

System for **Automatic Monitoring of a Communication Signal** in the RF or IF spectrum uses a superheterodyne spectrum analyzer to select and sweep the frequency band of interest. The memories store one band sweep as a reference for comparison with subsequent band sweeps.

This work was done by Albert J. Bernstein of Caltech for **NASA's Jet Propulsion Laboratory.** *For further information, Circle 16 on the TSP Request Card.*

This invention is owned by NASA, and a patent application has been filed. Inquiries concerning nonexclusive or exclusive license for its commercial development should be addressed to the Patent Counsel, NASA Resident Legal Office-JPL [see page A8]. Refer to NPO-13941.

Books and Reports

These reports, studies, and handbooks are available from NASA as Technical Support Packages (TSP's) when a Request Card number is cited; otherwise they are available from one of NASA's Industrial Application Centers or the National Technical Information Service.

Control of Small Phased-Array Antennas

Design techniques for systems with only a few elements

Array antennas, consisting of hundreds or thousands of radiating or receiving elements, have long been used in radar systems. These antennas transmit and/or receive an approximately-plane wave front by superimposing signals from the individual elements. In addition, beam steering is accomplished by controlling the phase relationship between the radiators (receivers) without requiring mechanical motion of the antenna itself.

The technology of these large phased-array antennas is well developed. Recently, there has been a need for small arrays, containing only a few (less than 20) radiators, for use in spacecraft and other applications; however, considerably-less design information is available for these systems.

A series of reports, patent descriptions, calculator programs, and other literature that describes antenna control and steering apparatus for a seven-element phased array is available and should be useful to designers and operators of small-array systems. Though the series contains information specific to a particular system, it illustrates methods that can be applied to antennas with greater or fewer numbers of elements. Included are programs for calculating beam parameters and design functions and information to interfacing a digital controller to the beam-steering apparatus.

Small arrays are subject to a variety of design problems that are either not present or are not significant in large systems. For example, they are particularly susceptible to the generation of phase transients that can upset tracking and synchronization equipment when phase-modulated signals are used. In addition, the small arrays exhibit power losses at large beam angles and can have tuning difficulties when simultaneously transmitting and receiving at different frequencies.

At the same time, since there are only a limited number of radiating elements, certain unique design approaches can be utilized. For example, it is possible to extend the range of beam-steering angles by increasing the interelement spacings in particular directions. (In large arrays, the spacing is uniform.) This technique also allows for a greater number of usable beam angles within the maximum steering range. In addition, it is possible to provide independent phase control of each radiating element, rather than row or block-area steering as with large arrays. This finer control gives improved antenna patterns and a reduction in power losses and increases the number of beam-steering positions. Phase transients are reduced by using pairs of elements equidistant from the center of the antenna and imposing phase increments of equal magnitudes but opposite signs.

A digital steering controller has been developed that allows the beam direction to be selected automatically by the operator. The X and Y angular displacements are provided as input, and the controller sets the phase of each element. It is also designed to accept input from a computer or desk calculator. Since there is no simple relationship between the beam angle and the phases of individual radiators, the phase settings are stored in preprogramed read-only memories (ROM's). Three memories are required: one for vertical control, one for horizontal control, and one to "sum" the outputs of these devices to provide signals to the phase-shift networks.

A calculator program has been developed that determines the beam angle for all possible control-signal phase angles. The program can be used to find the optimum element spacings.

For communications applications, phased-array antennas can be simultaneously operated at different transmitting and receiving frequencies. However, since the element spacings are frequency dependent, the beam direction may be significantly different for transmit and for receive. By making the control-signal phase angles also frequency dependent (using delay lines), the same pointing angle can be set for both modes. Separate transmit and receive phase-shift networks can be used to permit transmission and reception at different phase angles.

This work was done by George D. Doland of Lockheed Electronics Co., Inc., for **Johnson Space Center.** *For further information, Circle 17 on the TSP Request Card.*

This invention is owned by NASA, and a patent application has been filed. Inquiries concerning nonexclusive or exclusive license for its commercial development should be addressed to the Patent Counsel, Johnson Space Center [see page A8]. *Refer to MSC-14938.*

Physical Sciences

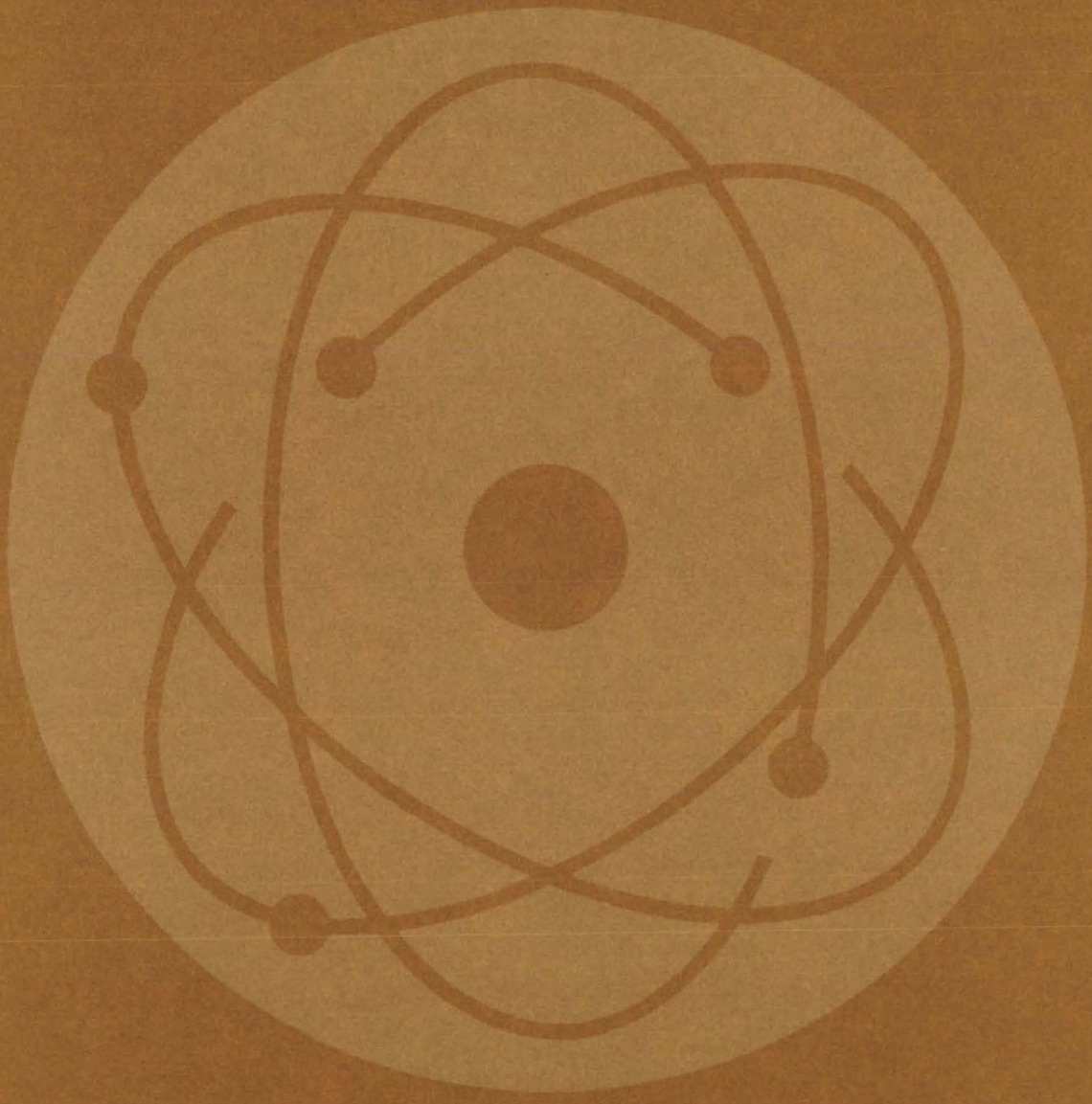

Hardware, Techniques, and Processes

187 Improved "Spectrophone"
188 Low-Background Trace-Gas Detector
188 Vibration-Free Thermal Link
190 Practical and Efficient Magnetic Heat Pump
191 Protective Coating for Laser Diodes
191 Infrared-Enhanced TV for Fire Detection
192 Wide-Angle Pinhole Camera
193 Laser Beam Color Separator
194 Pulsed NMR Spectroscopy
195 Optical Gyroscope
196 Improved Double-Pass Michelson Interferometer

Books and Reports

197 Energy Conservation, Using Remote Thermal Scanning

Computer Programs

198 Electrolysis Cell Simulation

Improved "Spectrophone"

The sensitivity of an optoacoustic gas analyzer can be improved by using a Stark modulation technique.

NASA's Jet Propulsion Laboratory, Pasadena, California

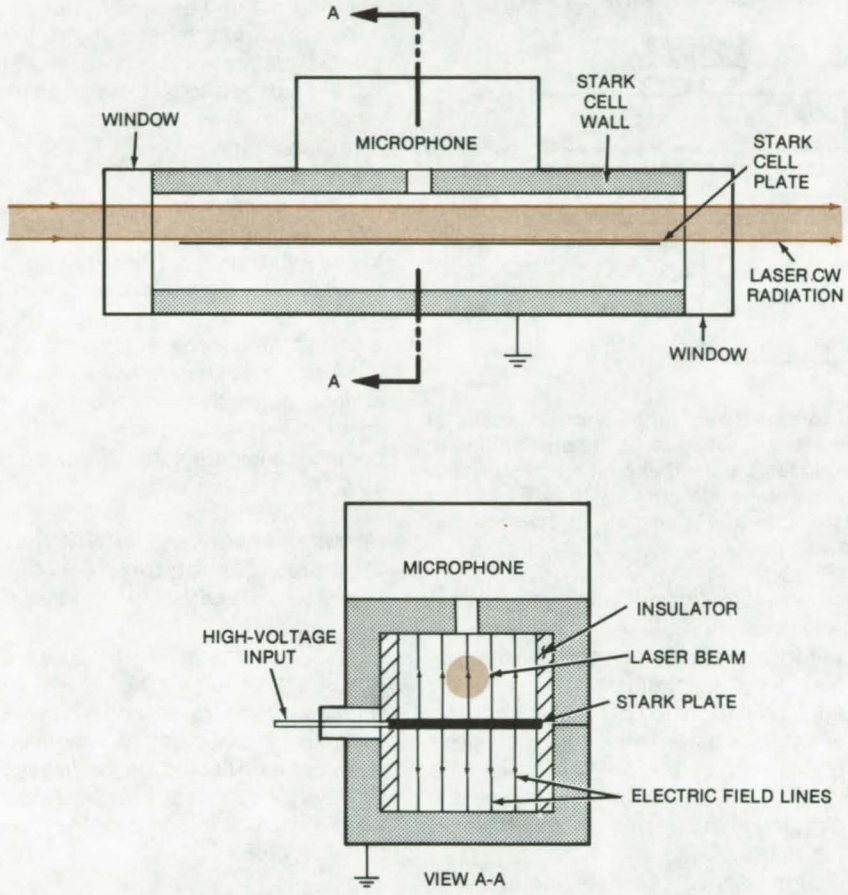

The **Spectral Lines of a Gas Sample** are modulated by an electric field in this proposed optoacoustic gas analyzer. Pressure fluctuations caused by local heating of the absorbing gas are picked up by the microphone. Since the laser is operated in the CW mode, background noise due to heating of the windows is eliminated.

A conventional laser optoacoustic gas analyzer, or "spectrophone," operates by sensing pressure changes in an unknown gas as chopped laser radiation passes through it. If the laser frequency coincides with a spectral line of the gas, absorption and local heating occur and create pressure changes that are detected by a transducer. The magnitude of these changes, which occur at the chopper frequency, is proportional to the absorption coefficient of the gas sample.

In conventional spectrophone designs, the windows at each end of the sample chamber can absorb significant amounts of laser energy and cause local heating and pressure changes at the chopper frequency. This shows up as a type of background noise that limits the sensitivity of the analyzer.

A new proposal for spectrophone design eliminates the effects of window heating by using CW rather than chopped laser light while the gas spectral line is modulated with an electric field (Stark modulation). Since the laser energy that passes through the end windows remains constant throughout the measurement, the heating of the windows is uniform and does not contribute to the absorption signal.

As shown in the figure, the proposed spectrophone has a central high-voltage plate and parallel plates at ground potential along the longitudinal walls of the gas cell. This arrangement, besides providing a uniform electric field, also gives rigidity and mechanical stability. A high-voltage dc power supply and square-wave generator could be used to apply the bias and modulation voltages that move the spectral line into and out of coincidence with the laser line. A microphone and conventional phase-detection circuitry would detect the resulting pressure fluctuations and convert them to a meter reading or CRT display.

The Stark effect is most effective in modulating the absorption lines of gas molecules when the lines are narrow. This requires low pressures; however, the pressures should not be too low, to prevent the possibility of electrical breakdown. Many molecular gas lines can be brought into resonance with a CO_2 laser line in electric fields of the order of a few thousand volts/cm. For example, there are lines in NH_3 that will resonate in fields of less than 3,000 V/cm and many lines of CH_3F* are within 5,000 V/cm of resonating with CO_2 laser lines.

This work was done by Jack S. Margolis and Michael S. Shumate of Caltech for **NASA's Jet Propulsion Laboratory.** *For further information, Circle 18 on the TSP Request Card.*

Inquiries concerning rights for the commercial use of this invention should be addressed to the Patent Counsel, NASA Resident Legal Office-JPL [see page A8]. Refer to NPO-14143.

Low-Background Trace-Gas Detector

Reduced background signal in optoacoustic detector may allow pollutant gases to be detected at 0.01 parts per billion.

NASA's Jet Propulsion Laboratory, Pasadena, California

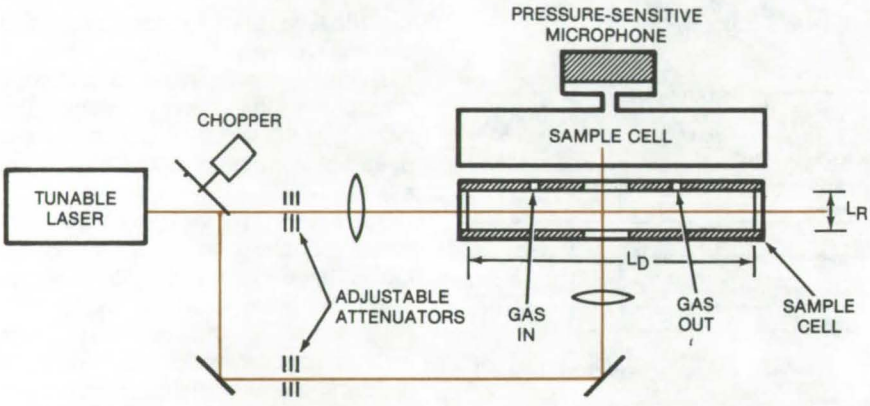

Low-Background Spectrophone can be used to detect very small concentrations of trace gases. With a gas in the sample cell, the laser is tuned to an absorption line of interest. Molecular absorption in the cell produces a pulsed acoustical pressure at the chopper frequency. As described in the text, two optical paths with very different absorption lengths, L_D and L_R, are used to "pretune" the cell to balance out background absorption by the cell windows.

Spectrophones are gas detectors that measure the acoustical pressure when gas in a sample cell is being "absorption-excited" by a tunable laser. These potentially compact and rugged analyzers have suffered from limited sensitivity due to high background signals caused by absorption losses in the window of the spectrophone cells.

It has been suggested that these residual pressures can be balanced out automatically with an optical reference path. A second pair of cell windows is placed in a path perpendicular to the original pair, and an additional radiation path through these windows is established with a chopper and a pair of mirrors that pulse the laser beam. One-half of the pulses are directed along each path, as shown in the figure.

The laser is set at a frequency at which no absorption occurs (preferably the major absorption line of the windows), and the beam intensities in the two paths are adjusted to flatten out the pulsed acoustic signal as much as possible. Then the laser is retuned to an absorption line for a measurement.

The microphone will output a pulsed signal due to pressure differences in the unequal paths. (Because absorption pressure depends directly on the optical path length, a pulsed acoustic signal at the chopper frequency will be produced.) This differential signal is almost perfectly dependent on the specific gas absorption and is expected to indicate constituents as rare as 0.01 parts per billion.

This work was done by Lars-Goran Rosengren of Caltech for **NASA's Jet Propulsion Laboratory.** *For further information, Circle 19 on the TSP Request Card.*

This invention has been patented by NASA [U.S. Patent No. 3,995,960]. Inquiries concerning nonexclusive or exclusive license for its commercial development should be addressed to the Patent Counsel, NASA Resident Legal Office-JPL [see page A8]. Refer to NPO-13683.

Vibration-Free Thermal Link

A diode laser is temperature stabilized by a helium refrigerator, but isolated from its vibrations.

Goddard Space Flight Center, Greenbelt, Maryland

In many structures, the physical requirements of mechanical stability and good thermal contact are very often incompatible since the supports and materials that isolate an object from vibration and shock will usually also isolate it from heat exchange with its surroundings.

When both stability and thermal conductivity are required, as in a temperature-stabilized diode-laser system, a support of the kind shown in Figure 1 may be used. This system, which was designed to hold a diode laser at the temperature of the cold tip of a helium refrigerator (10.5 K), uses thermally-conducting flexible straps and a special layered support structure.

As shown in Figure 1, a braided copper strap is firmly attached (by soldering, for example) to the copper diode-mounting block. It is thermally anchored to a copper block on the cold tip by an indium gasket and is secured by a bolt through its center. The lead/indium wafer in the cold-tip assembly acts as a thermal damper that smooths out temperature oscillations that occur during the refrigeration cycle.

The diode and its mounting block are rigidly fastened to the optical

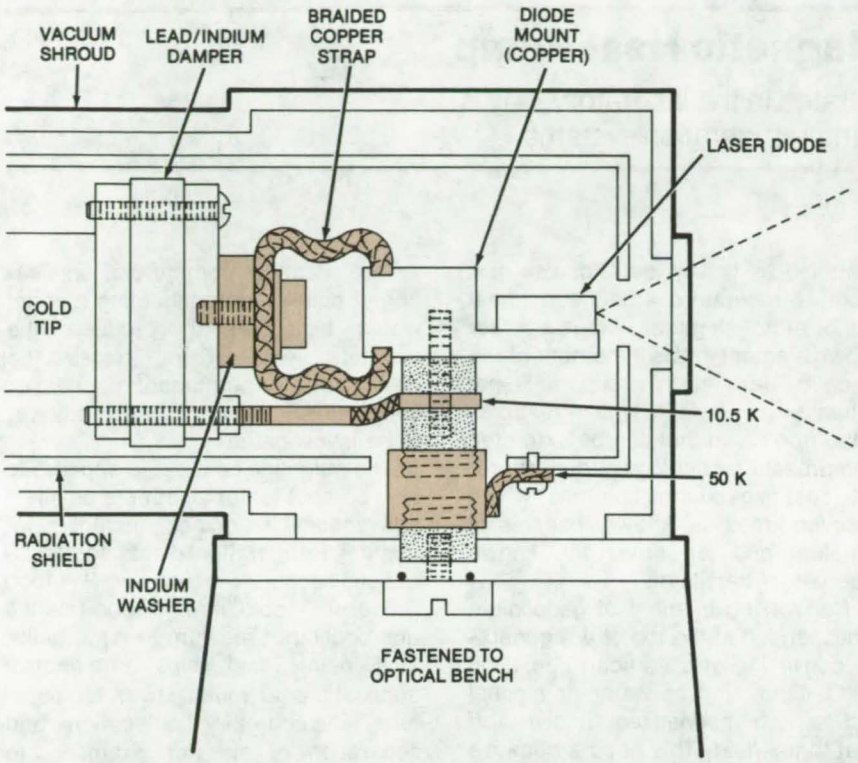

Figure 1. This **Shock Isolator Provides Good Thermal Conductivity** through its braided copper strap. Alternating layers of nylon and copper buffer the diode mounting block against heat loss to the "outside world."

bench by the sandwich support structure shown. This support consists of two layers of copper and three layers of nylon. The copper layer closest to the diode is held at the temperature of the cold tip by a braided copper strap. The other copper layer is tied to the radiation shield of the refrigerator (at about 50 K). A threaded nylon insert and a stainless-steel screw firmly anchor the assembly to the vacuum shroud, which is attached to the optical bench. The shroud is isolated from the refrigerator by a short length of vacuum hose (not shown).

The improved performance that can be obtained with this system is seen in Figure 2, which shows three scans of a line in NH_3 (obtained by sweeping the diode laser current). The scan at the top was recorded before the shock isolator was installed; in the center scan, the isolator was in place, but without the lead/indium damper; and for the lower scan, both the shock isolator and the damper were installed. In tests to observe CCl_2F_2 lines near 920 cm^{-1}, the diode appeared to be frequency stable to better than 5 MHz.

This work was done by Donald E. Jennings of **Goddard Space Flight Center.** *For further information, Circle 20 on the TSP Request Card.*

This invention is owned by NASA, and a patent application has been filed. Inquiries concerning nonexclusive or exclusive license for its commercial development should be addressed to the Patent Counsel, Goddard Space Flight Center [see page A8]. *Refer to GSC-12297.*

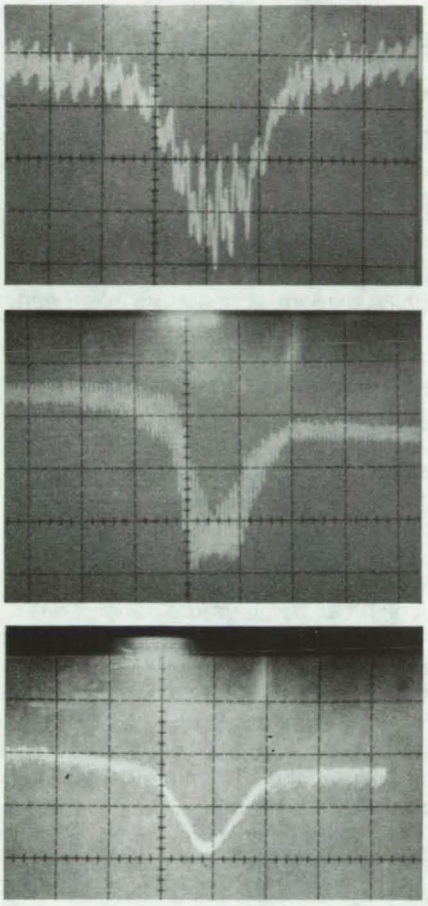

Figure 2. **Three Scans** of a line in NH_3 show improvements in the signal-to-noise ratio obtained when the shock isolator was used. The signal at the top was obtained on the unmodified system; the sweep in the center was obtained with the shock isolator in place, but no lead/indium damper; and the lower scan was taken after both the isolator and the damper were installed.

Practical and Efficient Magnetic Heat Pump

Magnetothermal heat pump demonstrated in the laboratory may be more economical than most existing refrigeration systems.

Lewis Research Center, Cleveland, Ohio

A method for pumping heat magnetically at room temperature has been developed and demonstrated experimentally. The method offers a more efficient alternative to existing heat pumping techniques. Its utilization promises potential savings in both energy and operating costs for many commercial and industrial heating and cooling applications.

The apparatus developed has demonstrated magnetic heat pumping over very broad temperature ranges near room temperature. In one experiment, heat was pumped over a temperature span from -13° F (-25° C) at the cold, or heat absorbing, end to 131° F (55° C) at the hot, or heat dissipating, end. In another experiment, the cold end reached a temperature of -21° F (-29° C). Calculations predict that even larger temperature spans will be possible with modified design. The span already achieved is more than enough for standard applications of air conditioning, heat pumping, and food processing.

Magnetic heat pumping is based on the fact that many magnetic materials are warmed by the application of a magnetic field and cooled when the field is removed. This magnetothermal effect is a well-established method for reaching ultra-low temperatures in research. However, near room temperature the magnetothermal effect is very weak in all the magnetic materials previously investigated and heretofore has produced temperature changes of only one or two degrees. Consequently, room temperature magnetic heat pumping has been impractical. The present advance results from the identification of materials that change temperature by 18 to 36° F (10 to 20° C) when a magnetic field is applied and from the use of a simple regenerative thermodynamic cycle that cumulates the one-time temperature changes into a much larger total temperature span.

The ferromagnetic material gadolinium, a rare-earth element with a Curie point of 68° F (20° C), has been identified as nearly ideal for use in a room temperature magnetic heat pump. Although gadolinium is a lesser known element and is a member of the so-called rare earth group, it is not actually rare. In fact, known reserves in the free world that can be extracted with present technology and at affordable cost exceed a million tons; which is seven times the known reserves of tantalum and ten times the known reserves of beryllium.

If a working element of gadolinium is suspended at the top of a regenerator consisting of a vertical tube filled with a fluid such as water or alcohol and is then magnetized, it gives off heat to the fluid. This occurs because of the magnetothermal temperature increase of the gadolinium. If the working element is then lowered to the bottom of the regenerator tube and demagnetized, its temperature decreases, causing it to absorb heat from the fluid. Repeating this process establishes a temperature gradient in the regenerator tube, and the working element functions as a heat pump over a large temperature range.

The way and the efficiency with which regeneration is accomplished determine the temperature span that can be achieved. Although several different regenerative thermodynamic cycles could be used, regeneration performed at constant (or nearly constant) magnetic field strength appears best.

This cycle can be considered a magnetic Stirling cycle because of its similarity to the gas Stirling cycle. In principle, the efficiency of this cycle can approach the maximum theoretical (or Carnot) efficiency because the basic cycle contains no irreversible processes. Also, this Stirling-like regeneration expands the temperature range of the magnetic cycle substantially; existing data do not yet suggest any clear practical temperature limit.

It is also noted that for applications at temperatures far below room temperature, there are magnetic materials that have Curie points in the desired operating range.

In a practical commercial application, a small superconducting magnet would be used to produce the magnetic field — 6 to 7 teslas. The possible use of permanent magnets or conventional electromagnets has yet to be investigated.

The magnetic heat pump appears to be a competitor for all but the smallest conventional machines, including industrial refrigeration plants for applications such as freeze drying and food processing, cold storage, and heating and cooling of medium to large buildings, plants, and ships. Prospective applications at much lower temperatures include the liquification and separation of air (for example, to supply oxygen for steel mills), the liquification of natural gas, and the liquification of lower-boiling gases such as hydrogen and helium. The production of refrigeration near the boiling point of helium is important for the growing applications of superconductivity, which is already important in high energy physics and is being tested for ship propulsion and for electric utility applications such as transmission lines. For these very low temperature applications, the expected efficiency of the magnetic cycle is much higher than that of conventional systems.

In all the above applications, the magnetic system is projected to provide higher efficiency and, thus, would yield lower operating costs than conventional refrigerators. Based on the materials and design features of a magnetic refrigerator, its cost in production is expected to be less than that of a conventional refrigerator.

This work was done by Gerald V. Brown of **Lewis Research Center.** *Further detailed information is given in "Magnetic Heat Pumping Near Room Temperature," Journal of Applied Physics, Vol. 47, No. 8, August 1976, pp. 3673-3680 and in "Magnetic Stirling Cycles — A New Application for Magnetic Materials," IEEE Transactions on Magnetics, Vol. MAG-13, No. 5, September 1977, pp. 1146-1148. This latter reference is also*

available as NASA TM-X-73676 [N77-26616], "Magnetic Stirling Cycles: A New Application for Magnetic Materials," a copy of which may be obtained at cost from the New England Research Application Center [see page A7].

This invention has been patented by NASA [U.S. Patent No. 4,069,028]. Inquiries concerning nonexclusive or exclusive license for its commercial development should be addressed to the Patent Counsel, Lewis Research Center [see page A8]. Refer to LEW-12508.

Protective Coating for Laser Diodes

New facet coating for GaAs injection lasers does not alter laser properties

Langley Research Center, Hampton, Virginia

Continuous-wave (CW) GaAs laser diodes use a special coating to protect their facets. Ideally, the coating should not alter the optical and electrical properties of the diodes. This objective is more easily met if the coating material has a relatively low index of refraction.

Results from recent work indicate that borosilicate glass applied to the injection lasers serves as a very effective coating. A half-wave glass coating with a relatively low, 1.45, index of refraction does not affect laser properties in any way and is relatively easy to apply. It is more effective than the Al_2O_3 or SiO coatings that have relatively high, 1.7 or more, indices of refraction and, therefore, are more likely to change laser characteristics.

Borosilicate glass was chosen because it adheres well to GaAs and AlGaAs; it is readily deposited at relatively low temperatures; it breaks evenly when cleaved; and it is abrasion and moisture resistant. The key property, however, is its low index of refraction, which makes the thickness deposited less critical to obtaining a half-wave coating. (A half-wave coating is used in order not to alter the reflectivity and therefore the threshold current.)

Tests were run with borosilicate glass deposited by RF sputtering under the following conditions:

- argon pressure: 40 millitorr
- target potential: -700 V
- axial magnetic flux density: 25 gauss
- target-to-substrate separation: 2.5 cm
- deposition rate: 41 Å/min
- deposition time: 75 min
- film thickness: 3,100 Å

Film adhesion was tested by cleaving the coated wafer; no measurable film-substrate separation was observed. Abrasion resistance was tested by scraping the film with pointed tweezers, which left no visible mark.

This work was done by Ivan Ladany and John L. Vossen, Jr., of RCA Corp. for **Langley Research Center.** *No further documentation is available.*

Inquiries concerning rights for the commercial use of this invention should be addressed to the Patent Counsel, Langley Research Center [see page A8]. Refer to LAR-11746.

Infrared-Enhanced TV for Fire Detection

Silicon target and visible-light filter adapt a vidicon for fire detection in large areas.

Marshall Space Flight Center, Alabama

Closed-circuit television is potentially superior to conventional smoke or heat sensors for detecting fires in large open spaces (for example, in warehouses). A single TV camera would be able to scan the entire area, whereas many conventional sensors and a maze of interconnecting wiring might be required to get the same coverage.

By adding lens filters and substituting an infrared-sensitive silicon target for the usual antimony trisulfide target found in most vidicons, the ability of a standard TV camera to detect hard-to-see chemical fires (such as those involving hydrogen, or liquid oxygen and hydrogen) can be significantly enhanced. Such a camera could be monitored by a person who would trip an alarm if a fire were detected; or, electronic circuitry could process the camera signal for a fully-automatic alarm system.

In tests of an IR-enhanced camera, a commercially-available silicon target extended the infrared sensitivity to 12 nanometers. The same target also gave 30X sensitivity in the visible region. To restore the baseline sensitivity of the camera in the visible region, it was also fitted with a lens filter that had roughly 3 percent transmission of visible light. (The enhanced sensitivity would have caused overloading problems in bright light.) Initial tests to detect the flame of a butane torch showed a nearly 10-percent increase in flame area, as compared to the image projected by an unmodified visicon. The modified camera was also less susceptible to blooming and highlight smearing.

This work was done by James R. Hall of Rockwell International Corp. for **Marshall Space Flight Center.** *For further information, Circle 21 on the TSP Request Card.*

Inquiries concerning rights for the commercial use of this invention should be addressed to the Patent Counsel, Marshall Space Flight Center [see page A8]. Refer to MFS-19380.

Wide-Angle Pinhole Camera

Refracting elements give a pinhole camera a 180° field-of-view without compromising its depth-of-field or simplicity.

Langley Research Center, Hampton, Virginia

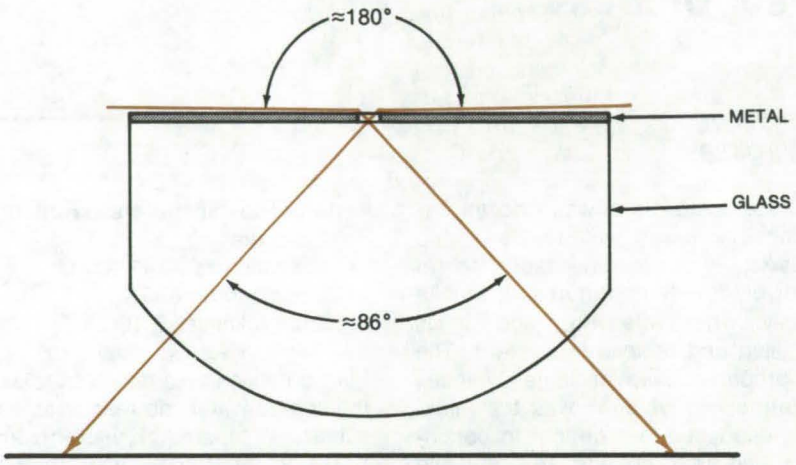

Figure 1. **Field-Widened Pinhole Camera** captures a 180° viewing field on an 86° field at the film plane. It thus combines the advantages of extreme depth-of-field with wide-angle field-of-view.

Figure 2. **The Photograph** above is a typical result using the wide-angle pinhole camera.

A conventional pinhole camera has been modified to extend the field of view to 180°. The camera incorporates a glass hemisphere behind the pinhole. No water or other transparent fluids are used as were in earlier wide-angle models, eliminating leaks and making it easier to handle the film. The depth-of-field of a conventional pinhole camera is maintained.

A cross section of the components used in the camera is shown in the illustration. These include a thin metallic or other opaque plate with a pinhole, and a glass hemisphere.

The glass selected for this model reduces the 180° field-of-view to an 86° field projected onto the film plane. This reduction may be changed by selecting glass with a different index of refraction. The glass hemisphere allows the light rays to emerge undeflected from the glass on the film side of the interface.

This work was done by John M. Franke of **Langley Research Center.** *For further information, Circle 22 on the TSP Request Card.*
LAR-11905

Laser Beam Color Separator

A multiwavelength laser beam is separated into a series of parallel color beams, using a prism and a retroreflector.

Langley Research Center, Hampton, Virginia

Three conventional methods of separating a multiwavelength-output laser beam into separate parallel color beams involve the following:

1. A complex system of mirrors and filters that have to be tuned to each wavelength;
2. A simple prism to disperse the multiwavelength laser beam into separate diverging color components (separate mirrors are used for each color beam to form a parallel output); and
3. Two prisms, the first of which disperses the multiwavelength beam, and the second beam is used in reverse, removing the divergence to form a parallel output.

Each of these methods requires either complex adjustments, a large working space, or expensive filters that can only be used for one wavelength.

A newly proposed setup simplifies the procedure. As shown in Figure 1, a conventional prism disperses the incident multiwavelength laser beam into its color components. The dispersed beams then are returned to the prism in a mutually parallel pattern by a 90° retroreflector. Because of the reciprocity of the dispersing prism, the beams then exit the prism parallel to the incident beam. The beam-to-beam separation is easily varied by moving the retroreflector closer or farther from the prism. The incident and exiting beams can be easily separated without disturbing the parallelism of output beams with a simple mirror as shown in Figure 2.

This setup is inexpensive and needs no critical adjustments. It can incorporate several prisms to increase the dispersion and reduce the overall size. In addition, a transmission grating can be used instead of the prism with some sacrifice in efficiency. Finally, a spatial filter can be employed to remove unwanted beams.

This work was done by John M. Franke of **Langley Research Center.** *For further information, Circle 23 on the TSP Request Card.*

Inquiries concerning rights for the commercial use of this invention should be addressed to the Patent Counsel, Langley Research Center [see page A8]. Refer to LAR-11806.

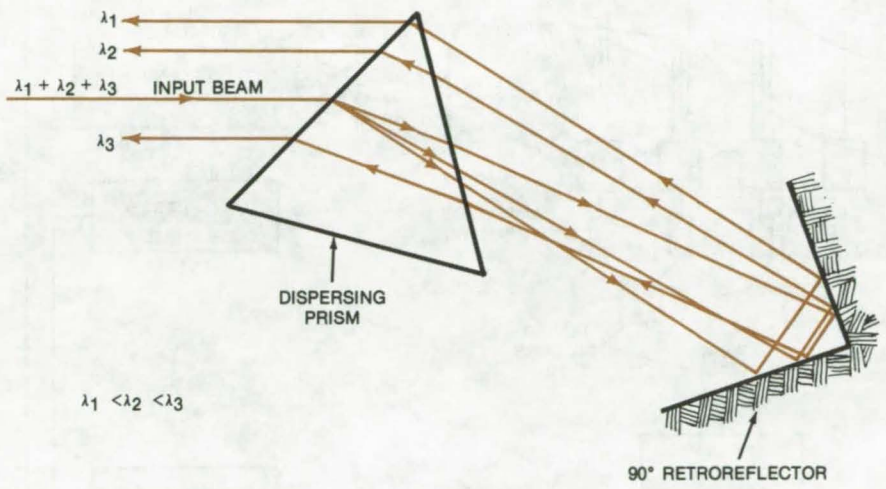

Figure 1. Simple **Laser Beam Color Separator** incorporates a prism and a 90° retroreflector. A multicolor laser beam is separated into its color components, which exit as parallel color beams.

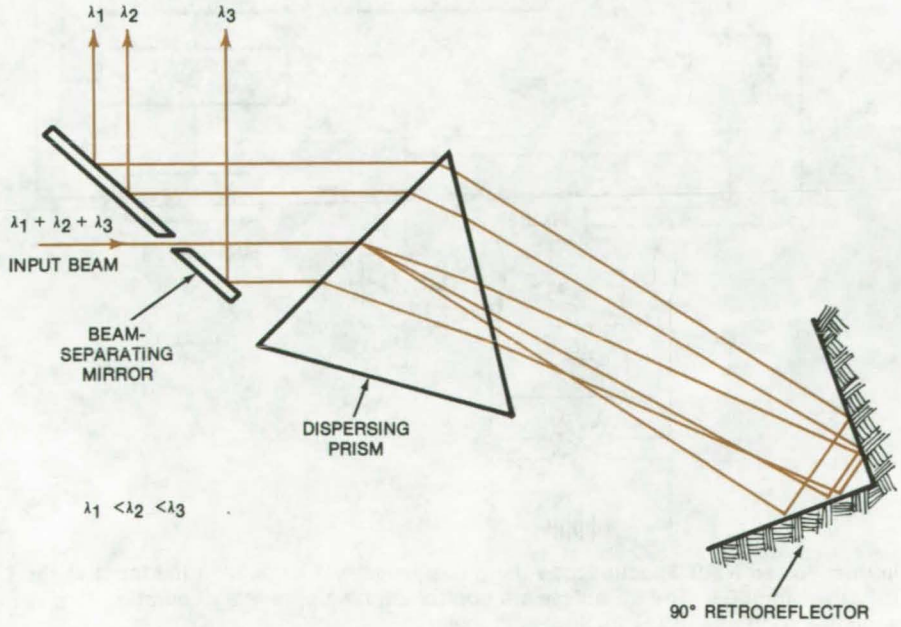

Figure 2. A **Mirror Added to the Color Separator** aims the exiting beams away from the incident.

Pulsed NMR Spectroscopy

Controlled pulses generate quickly- and easily-accessible nuclear magnetic resonance data.

NASA's Jet Propulsion Laboratory, Pasadena, California

A pulsed method for nuclear magnetic resonance (NMR) spectroscopy can give results approximating those of the classical continuous-irradiation method, but in much less time. The new method also makes it possible to measure chemical shifts and spin-lattice relaxation times with improved sensitivity.

In one form of continuous-wave NMR, a strong radio-frequency (RF) field of considerable duration is applied after a prepulse rotates the nuclear spin axes by 90° from the orientation produced by a large magnet. When the RF field is turned off, the initial amplitude of the fast-decaying signal is recorded. The cycle is then repeated with different durations, and a relaxation curve is plotted from the many signal responses. This procedure, which is often used in NMR investigations of solid samples, is tedious and can be very time consuming.

In the new method, a string of RF pulses is applied to a test specimen, and the relaxation response is recorded between the pulses. Each pulse in the series is controlled so that it produces a preset rotation of 90° or less of the nuclear spin axes. The rotation is adjusted by controlling the amplitudes and durations of the pulses. In NMR measurements on a CaF_2 crystal, the RF pulses produced rotations between 60° and 20° from the normalized spin axes defined by the magnetic field.

It can be shown that with proper coordinate transformations, this discrete excitation scheme approaches the continuous-wave scheme. However, besides giving better sensitivity and higher speed, the discrete method also gives results that are simpler to interpret. Moreover, the spin temperature hypothesis, applicable to continuous-wave experiments, applies equally as well in this approach.

An experimental system for making pulsed measurements is shown in the figure. A crystal oscillator is the

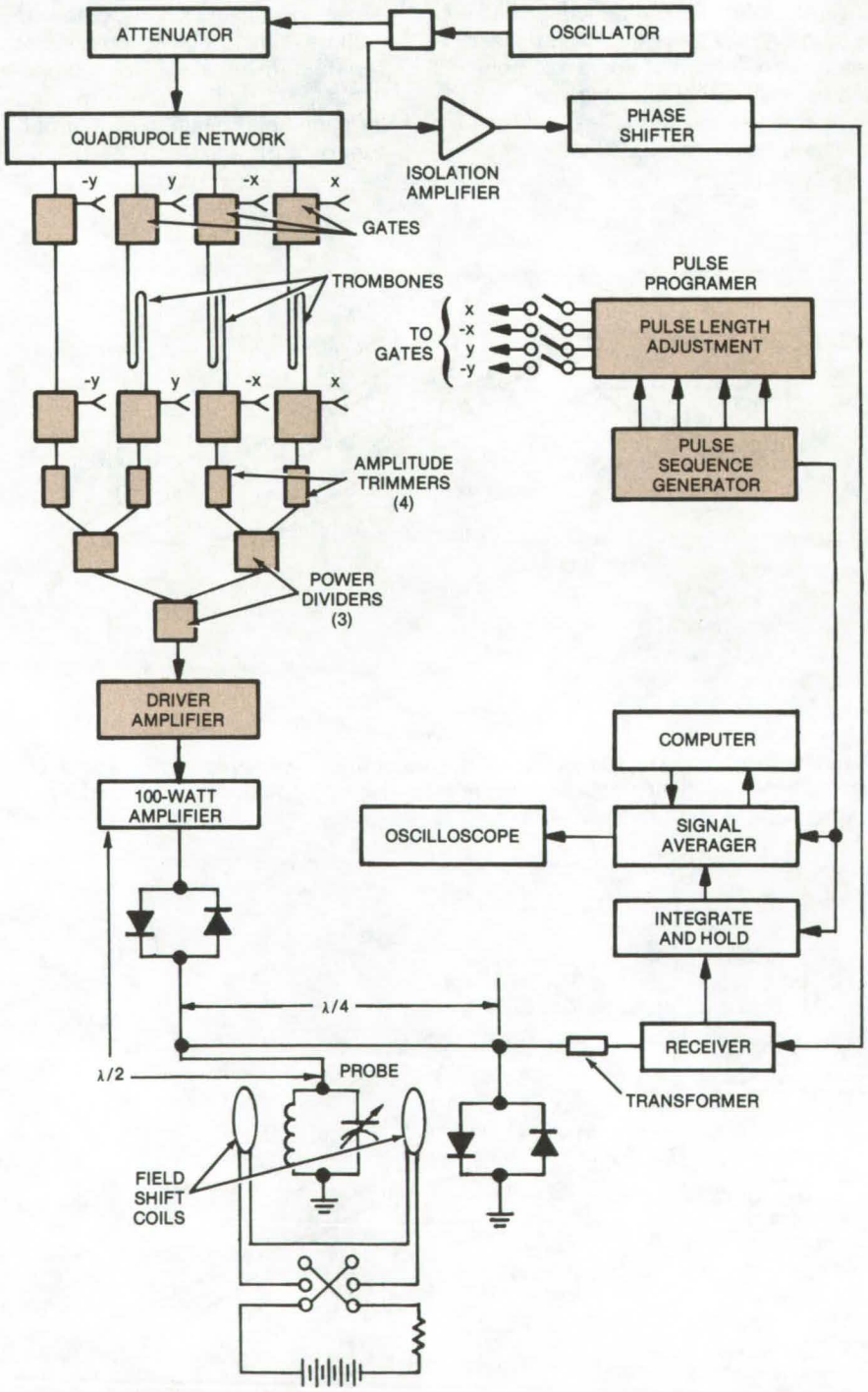

In this **Pulsed NMR Spectroscope** the pulse programer modulates the input to the RF driver amplifier. The RF pulses are controlled in amplitude and duration to give specified rotations of the nuclear spin axes.

frequency source, although a frequency synthesizer can be substituted. The oscillator signal is split to furnish a reference signal for the receiver. The transmitter signal is further divided into four separate channels so that phase-shifted pulses can be produced. Three of the channels use "trombone slides" for fine adjustment of their phases relative to the fourth channel. The four signals are recombined, amplified, and fed to a 100-watt RF amplifier. The sample coil is large enough to hold a standard 5-millimeter, high-resolution NMR tube.

The equipment can be used for adiabatic demagnetization experiments, measurements of rotating-frame spin/lattice relaxation times, and accurate measurements of exact resonance points. When measuring relaxation times, the pulse technique can be very effective since the pulses may be limited in amplitude and length to prevent the spin system from being driven into saturation.

This work was done by Douglas P. Burum, Daniel D. Elleman, and Won-Kyu Rhim of Caltech for **NASA's Jet Propulsion Laboratory.** *For further information, Circle 24 on the TSP Request Card.*
NPO-14023

Optical Gyroscope

Laser interferometric system could surpass conventional spinning-mass gyroscopes in reliability and accuracy.

NASA's Jet Propulsion Laboratory, Pasadena, California

A proposed gyroscope uses the phase difference between two beams of light to measure rotation. The optical gyroscope, which is in the development stage, would be considerably simpler and more reliable than the conventional spinning-mass gyroscopes used for inertial guidance and would be more compact, lighter, and potentially less expensive. Moreover, the optical gyroscope would require no warmup period. Although it was originally conceived for spacecraft and satellite stabilization, the gyroscope should also find applications in flight instruments for private, commercial, and military aircraft.

Although the concept of an interferometer gyroscope is not new, the development of a working model has been hampered by practical difficulties, such as the need for a very long optical path (to obtain a measurable signal) and the sensitivity of the optics to drift errors and instability. The new proposal would use modern laser, fiber-optic, optical waveguide, and electronics technology to overcome these problems in implementing a working system.

In a "breadboard" version of the new system (see Figure 1), a long, low-loss optical fiber is wound into a coil. Two laser beams (derived by splitting a single beam) are passed through the fiber in opposite directions. Rotation of the coil about its axis can be detected because the propagation time of each beam through the coil depends on whether the beam

(continued next page)

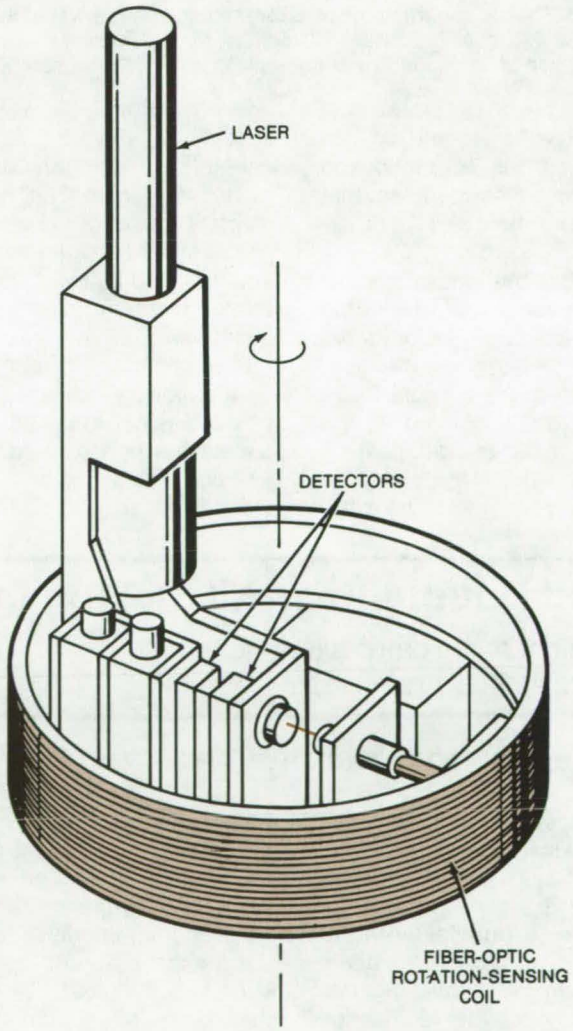

Figure 1. This proposed **Optical Gyroscope** operates by laser interferometry. Rotation about a vertical axis causes a phase difference to arise between two beams transmitted in opposite directions through the coil. The phase difference is sensed by the detectors (e.g., silicon photodiodes).

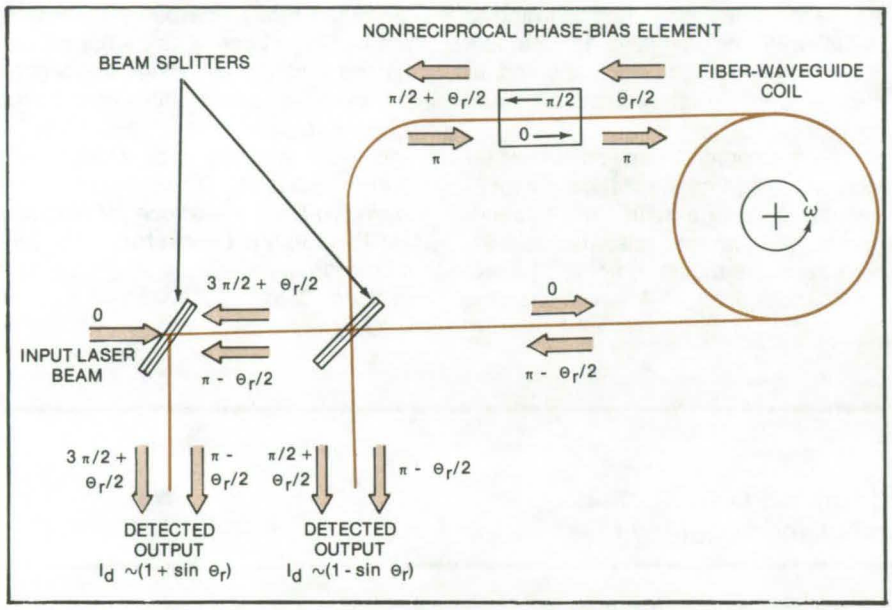

Figure 2. **Phase Shifts Are Introduced** at several points along the optical path. In addition to the shift that occurs in the rotation-sensing coil, a waveguide phase-bias cell maintains a 90° baseline phase difference to maximize sensitivity. There is another 180° phase shift caused by reflection off the second beam splitter.

travels with or against the direction of coil rotation. As a result of the rotation, one beam is advanced and the other beam is retarded, so that they emerge from the coil with different phases.

To ensure that the phase shift is detected with adequate sensitivity, the optical-fiber-gyroscope includes a nonreciprocal phase-bias element. This element could be a single-mode optical waveguide implanted in an electro-optical material and passing under an electrode. The electrode would be switched alternately "high" and "low" during the passage of laser light pulses traveling clock-wise and counterclockwise through the instrument (see Figure 2). The phase-bias element introduces a $\pi/2$ differential phase offset between the two beams. The detected outputs are then simply related to the rotation-induced phase offset and have maximum signal rate-of-change with rotation rate.

Alternatively, voltage applied to the phase-bias cell could be controlled by a feedback loop to maintain a constant $\pi/2$ phase offset to buck out rotation-induced phase offsets. The differential voltage applied to the bias cell would then become the signal that would be linear with rotation rate.

To minimize long-term drift, the optical-fiber gyroscope employs synchronous modulation and demodulation. A double-pole, double-throw optical waveguide switch transposes the two split beams as they enter the rotation-sensing coil. This converts the detected signal to an ac mode that cancels the effect of a drifting zero level. Also, the outputs of the two detectors are combined electronically to cancel drifts due to fluctuations of the laser output.

The source of the light beams could be a pulsed gallium/aluminum arsenide diode laser emitting at a wavelength of 0.82 micron. Laser diodes are currently available with power-output levels of tens of milliwatts, which are more than adequate for this application. The laser is bonded to fiber, coupling the light directly without focusing lenses. In another possible implementation, the optical fiber could itself be a lasing material.

This work was done by Raymond Goldstein and Willis C. Goss of Caltech for **NASA's Jet Propulsion Laboratory.** *For further information, Circle 25 on the TSP Request Card.*

Inquiries concerning rights for the commercial use of this invention should be addressed to the Patent Counsel, NASA Resident Legal Office-JPL [see page A8]. Refer to NPO-14258.

Improved Double-Pass Michelson Interferometer

Rearrangement of ray paths allows a thinner beam splitter to be used.

NASA's Jet Propulsion Laboratory, Pasadena, California

In an application of a modified double-pass Michelson interferometer that uses cat's-eye retroreflectors in the fixed and traveling arms, the centerlines of the retroreflectors were offset horizontally to prevent the beam in one arm from cross-coupling into the other. This geometry demanded that the beam splitter have minimum thickness of about 2 inches (5.1 cm); however, a beam splitter of this thickness, with good optical properties, is an expensive optical component, particularly when made of infrared-transmitting materials.

An improved interferometer design separates the beams by offsetting the centerlines of the cat's-eye retroreflectors vertically, rather than horizontally. Since the beam splitter is insensitive to the minimum-thickness condition in this geometry, a relatively-low-cost, optically flat plate, about 1/2 in. (1.3 cm) in thickness, can be used.

In the new design (see figure), light rays enter the interferometer through the center of the beam-splitter flat. Rays transmitted through the flat enter the fixed cat's-eye retroreflector,

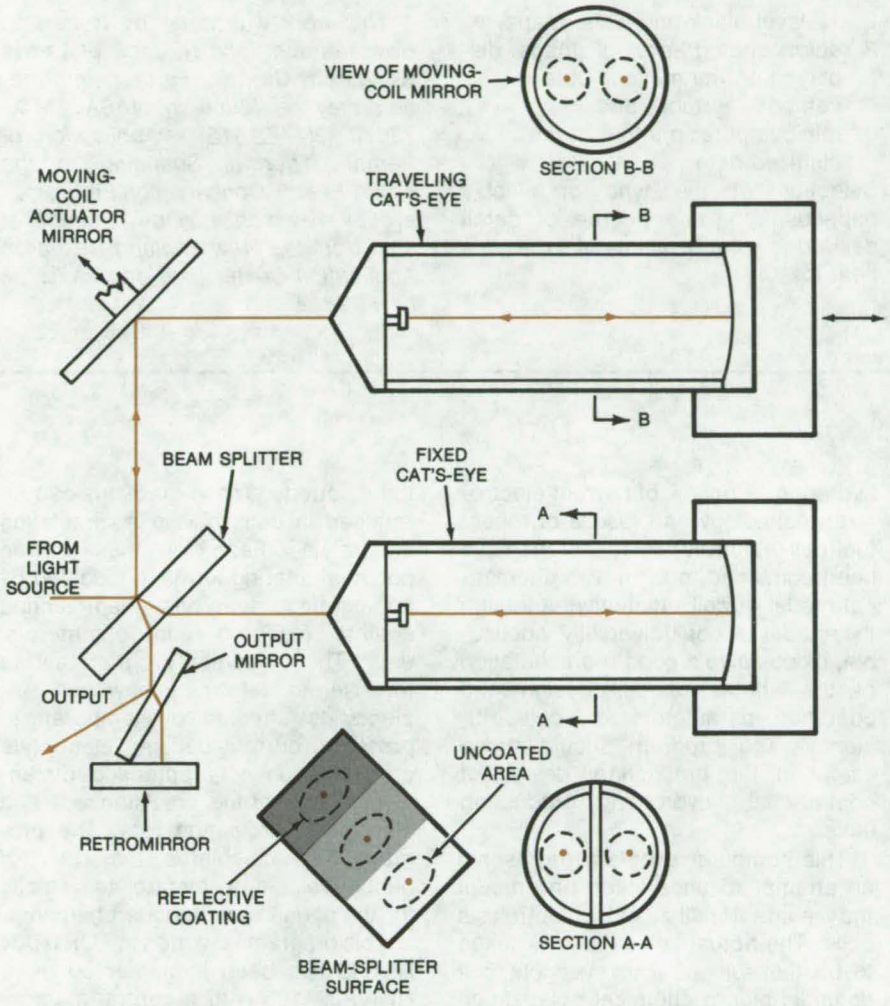

Cat's-Eyes Are Displaced vertically (perpendicular to the page) in this improved Michelson interferometer. This geometry separates the beams in the fixed and traveling arms without requiring that the beam splitter satisfy a minimum-thickness criterion. A thin, relatively-low-cost, flat-plate beam splitter may be used.

which reflects them back under the entering rays. The retroreflected rays are then reflected by the reflective coating on the beam-splitter flat onto the retromirror, back to the reflective coating on the beam-splitter flat, to the fixed cat's-eye, and finally to the beam-splitting surface on the beam-splitter flat.

The rays initially reflected by the beam splitter, on the other hand, are reflected by a plane mirror on a moving-coil actuator and then into the traveling cat's-eye retroreflector. The rays are reflected out of the traveling cat's-eye above the entering rays, are reflected to the beam splitter, and are transmitted through an uncoated part of the beam splitter to the retromirror, which reflects the rays back through the system. This set of rays then recombines to form the interference pattern that is sensed by the detector.

This work was done by Rudolf A. Schindler of Caltech for **NASA's Jet Propulsion Laboratory.** *For further information, Circle 26 on the TSP Request Card.*

This invention is owned by NASA, and a patent application has been filed. Inquiries concerning nonexclusive or exclusive license for its commercial development should be addressed to the Patent Counsel, NASA Resident Legal Office-JPL [see page A8]. Refer to NPO-13999.

Books and Reports

These reports, studies, and handbooks are available from NASA as Technical Support Packages (TSP's) when a Request Card number is cited; otherwise they are available from one of NASA's Industrial Application Centers or the National Technical Information Service.

Energy Conservation, Using Remote Thermal Scanning

Readily available equipment is used to spot heat losses in several facilities.

Airborne thermal infrared scans and thermal maps utilized in NASA's energy conservation program have proved to be an efficient cost-effective method for identifying heat losses from building roofs and heating-system distribution lines. The use of thermal scanning to locate excessive energy losses at all NASA facilities has resulted in first-year cost savings of $480,000. Accounting for the cost of the program produces a net savings of $386,000 for the first year.

For example, at the National Space Technology Laboratory in Bay St. Louis, Mississippi, a primary concern was the location of heat losses from leaks and insulation deterioration in a 13-mile-long (21 km) system of underground high-temperature hot-water lines buried at an average depth of 1.8 meters. An airborne thermal scan, verified by spot excavation, effectively located all of the heat losses with a cost saving of $93,000.

The method employs commercially available equipment in a highly developed way. A thermal infrared optical detector and scanning system coupled to a magnetic-tape data recorder have been installed in a NASA C-47 aircraft. As the aircraft flies over the ground facilities, the system scans the area. Flights are usually made at night to minimize the effects of solar heating, and typically at altitudes of 1,000 or 1,500 ft (305 or 455 meters). The signals from the thermal-energy detector are digitized and recorded on

(continued next page)

high-density magnetic tape. The data are subsequently processed in a ground-based minicomputer system to reconstruct a thermal map.

The minicomputer is programed to divide the recorded data into 24 signal levels for display and analysis. The data are then processed and displayed in one, or more, of four different ways:

1. 24-level color maps of the area scanned.
2. 12-level black-and-white maps,
3. color photographs of maps displayed on the minicomputer cathode-ray tube, and
4. minicomputer printout of the digitized data.

Selection of the type of display depends upon the degree of detail desired to identify places of excessive heat loss.

This work was done by Robert L. Bowman and John R. Jack of **Lewis Research Center.** *Further information may be found in NASA TM-X-73570 [N77-21518], "Application of Remote Thermal Scanning to the NASA Energy Conservation Program," a copy of which may be obtained at cost from the New England Research Application Center* *[see page A7]*. *Lew-12812*

Computer Programs

These programs may be obtained at very reasonable cost from COSMIC, a facility sponsored by NASA to make new programs available to the public. For information on program price, size, and availability, circle the reference letter on the COSMIC Request Card in this issue.

Electrolysis Cell Simulation

Mathematical model of cell efficiency

The potential advantages of hydrogen-fueled energy systems for electrical power generation are currently being assessed and recognized by many independent utilities, institutions, and agencies. These energy systems consist of three major subsystems: production, storage/transmission, and utilization. A thorough understanding of a high-efficiency, low-cost hydrogen production subsystem is considered the first priority for development of this type of energy system. The favored near-term approach is the electrolytic production of hydrogen. A review of current electrolyzer technology and results of recent fuel-cell/electrolyzer research have been combined to form a mathematical model of cell efficiency. Although the model is not universally applicable, it does give a good representation of the effects of cell design and operation parameters on cell efficiency. The program should prove useful in the preliminary design of commercial hydrogen production units.

This computer program represents an attempt to understand and model the characteristics of electrolysis cells. The actual cell voltage is taken to be the sum of the reversible cell potential plus a chemical polarization term, an ohmic loss term, and a concentration polarization term. Chemical polarization results from charge-transfer inhibition at the electrode and is determined by the catalytic activity of the electrodes and the surface roughness. Ohmic loss is taken to be the sum of the internal resistance terms due to the anolyte, membrane, and catholyte. Concentration polarization results from concentration gradients that exist in the neighborhood of the electrode. These gradients can be reduced in cells having a circulating electrolyte. Each of these three potential-altering terms is modeled by an algorithm that has been verified against research and commercial data. The computer program allows the user to determine how cell efficiency is affected by temperature, pressure, current density, electrolyte concentration, characteristic dimensions, membrane resistance, and electrolyte circulation rate. The program also calculates the ratio of bubble velocity to electrolyte velocity for the anode and cathode chambers.

This program is written in FORTRAN IV and has been implemented on a UNIVAC 1106 with a central memory requirement of approximately 9K of 36-bit words.

This program was written by Larry H. Gordon and Bert R. Phillips of **Lewis Research Center** *and John Evangelista of Wyandotte Corp. For further information, Circle R on the COSMIC Request Card.*
LEW-12740

Solar Energy

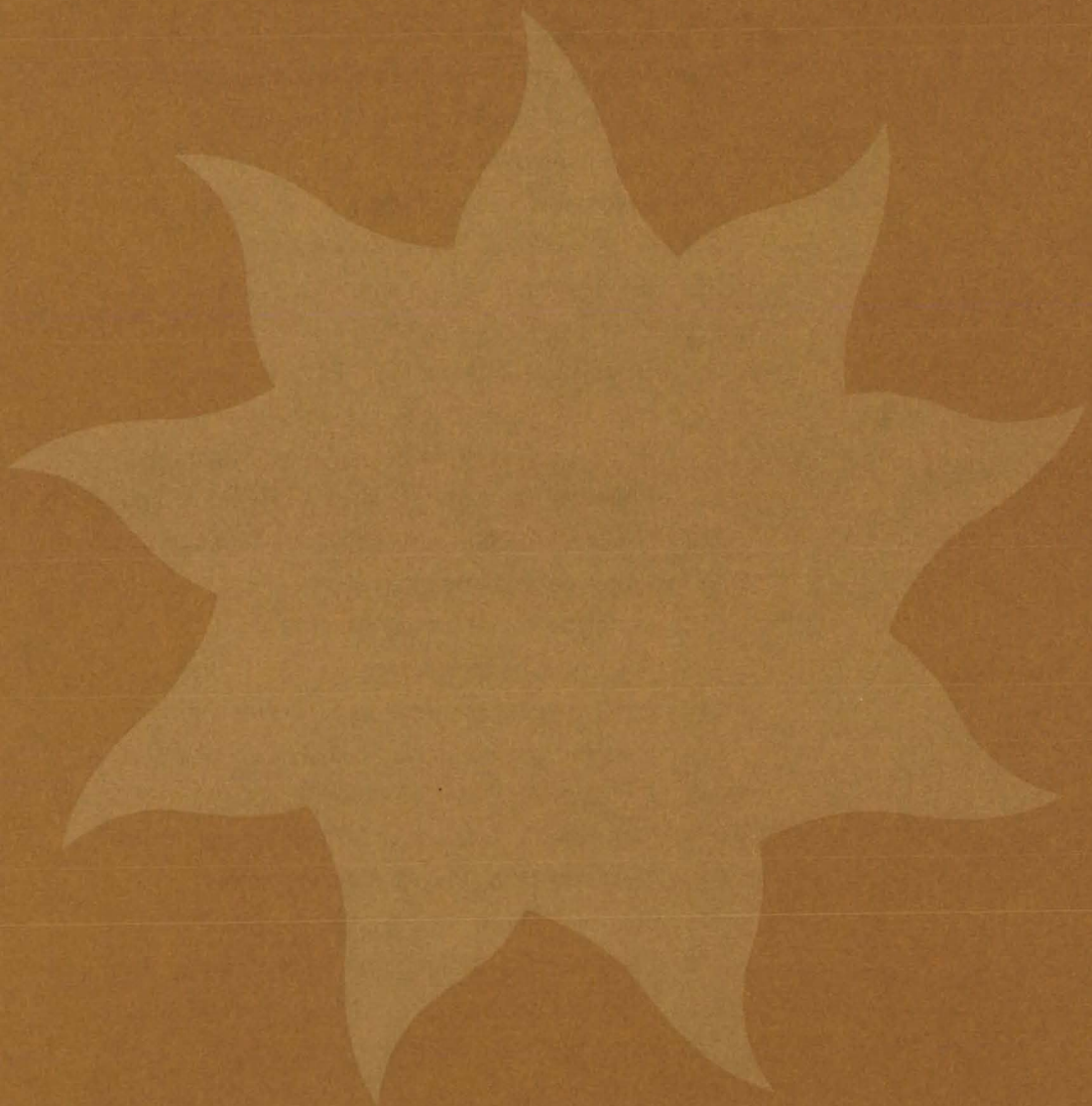

Hardware, Techniques, and Processes

201 Prototype Solar-Heating System
202 Residential Solar-Heating System
203 Multichannel Temperature Controller for Solar Heating
204 Programable Controller for Solar Heating
205 Universal Test Fixture for Solar Cells
205 Accelerated-Weathering Test-System for Solar Cells
206 Automated Solar-Cell-Array Assembly Machine
207 Improved Conical Solar Concentrator
208 Inexpensive, Portable, Integrating Solar Energy Meter
209 Optics for Natural Lighting
211 Selection Standard for FEP Films for Solar Energy

Books and Reports

211 Prototype Residential Solar-Energy System
212 Prototype Residential Solar-Energy System-Engineering Analysis
212 Residential Solar-Heating System — Design Brochure
213 Prototype Solar-Heating System — Engineering Analysis
213 Prototype Solar-Heating System — Installation Manual
213 Solar-Heating Module
214 Passive Heat Exchanger for Solar Heating
214 Passive Heat Exchanger — Installation Package
214 Prototype Air Flat-Plate Solar Collector
214 Flat-Plate Solar Collector — Installation Package
215 Testing of Three Hot-Air Solar Collectors
215 Thermal Performance of a Hot-Air Solar Collector
215 Performance and Structural Tests of Hot-Air Solar Collectors
216 Thermal Performance of a Hot-Air Solar Collector
216 Flat-Plate Liquid Solar Collector
216 Performance Evaluation of a Liquid Solar Collector
217 Indoor and Outdoor Tests of a Liquid Solar Collector
217 Thermal Performance of a Flat-Plate Liquid Solar Collector
217 Corrosion Inhibitors for Solar Heating and Cooling Systems
218 Performance of Black-Nickel and Black-Chrome Solar Collectors
218 Measuring Metallic Concentrators in Glycol Solutions
218 Glass Solar Collector — Materials Assessment
219 Pump Efficiency in Solar-Energy Systems
219 The Economics of Solar-Powered Absorption Cooling
220 Application of Solar Energy to Air-Conditioning

Prototype Solar-Heating System

Complete air-collector system to meet the needs of a single-family dwelling

Marshall Space Flight Center, Alabama

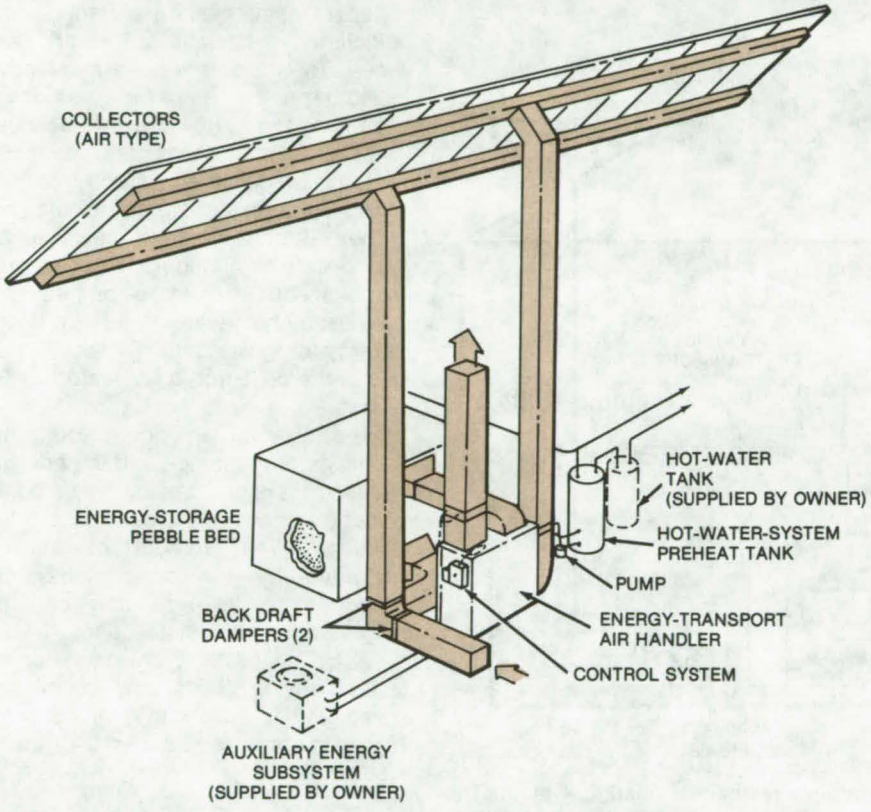

A complete Solar-Heating and Hot-Water System is designed for a single-family dwelling. A system prototype can meet the requirements of a dwelling in the range from 1,500 to 2,500 square feet; it can be scaled up or down to accommodate other buildings.

A prototype solar-heating and hot-water-preheat system has been designed for a single-family dwelling in the range 1,500 to 2,500 ft^2 (139 to 232 m^2). The system, shown in the figure, uses air collectors and pebble-bed storage. Domestic water is preheated with a heat exchanger in the hot-air duct. The design can be scaled up or down to accommodate a wide range of heating and hot-water requirements for single-family, multi-family, or commercial buildings without significantly changing the design concept.

Principal elements of the system are:

- flat-plate air-type solar collectors,
- a pebble bed for thermal storage of collected solar energy,
- an air-handling unit to move and direct the air through the energy-transport system,
- an air-to-water heat exchanger and circulating pump to allow for transfer of heat from the collector/storage circuit to the domestic hot-water circuit,
- a domestic hot-water preheat tank for storage and transfer of collected energy into the conventional domestic water heater,
- an air-to-air heat pump and electric strip heaters to supply auxiliary energy during periods of insufficient insolation, and
- a ducting system to convey the solar-heated air betwen system components and into the heated space.

The system is designed to operate in any region of the United States except in the extreme north and south. At a location for which the mean daily winter insolation is 770 Btu/ft^2 (7.54×10^4 J/m^2) and the yearly-heating degree-days is 3,300, the solar-heating portion of the system can provide 58 percent of a total annual heating load of 65×10^6 Btu (6.86×10^{10} J). For this system, the minimum temperature of the 74-gallon (0.32-m^3) domestic-hot-water supply tank is 140° F (60° C). The maximum average electrical energy consumption for the entire system, including an auxiliary 4-ton (3.6×10^3-kg) heat pump and a 20-kW strip heater, is 6,700 kWh (electrical input for the solar system is 1 kW).

[See related articles: "Prototype Solar-Heating System — Engineering Analysis" (MFS-23910) on page 213 of this issue and "Prototype Solar-Heating System — Installation Manual" (MFS-23907) on page 213 of this issue.]

This work was done by the Federal Systems Division of IBM Corp. for **Marshall Space Flight Center.** *Further information may be found in NASA CR-150534, "SIMS Prototype System 1 — Design Data Brochure," a copy of which may be obtained at cost from the New England Research Application Center.* *[see page A7].*

MFS-23916

Residential Solar-Heating System

A complete system that can be scaled to meet site and heat-load requirements

Marshall Space Flight Center, Alabama

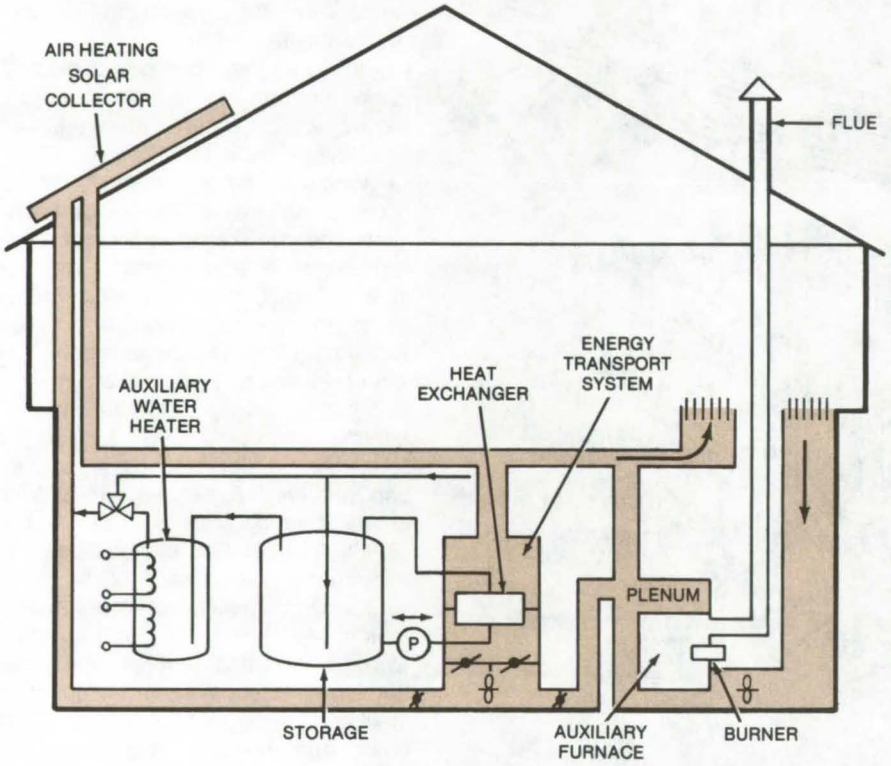

Solar Energy Is Converted to Heat in this complete residential heating system. The auxiliary furnace, for use on cloudy days, can be a conventional warm-air heater.

A complete residential solar-heating and hot-water system, when installed in a highly-insulated energy-saver home, can supply a large percentage of the total energy demand for space heating and domestic hot water. The system, which uses water-heating energy storage, can be scaled to meet the requirements of the building in which it is installed.

The system (see figure) consists of six modular subsystems, including:

- an air-heating solar-collector subsystem,
- a solar-energy transport subsystem,
- water-heating energy storage,
- a control subsystem,
- an auxiliary warm-air furnace, and
- an auxiliary domestic hot-water heater.

Low maintenance, durable, and efficient air-heating collectors are used. The collectors have a selective absorber and a tempered-glass cover nearly 1/4 in. (0.64 cm) in thickness with an aluminum frame. The solar energy is delivered directly to the living area or is stored in the hot water. The hot-water storage uses an air-to-water exchanger. This system is simultaneously used to preheat the domestic hot water and to store energy for space heating. The service life of the collector is estimated as 30 years.

The size of the collectors, the energy storage tanks, and the energy-transport system can be adjusted to meet the needs of the building and the location. The amount of heating provided by the solar subsystem depends on its size and can be adjusted for each installation.

A typical system, designed for an East Lansing, Michigan, installation used 240 ft^2 (22.3 m^2) of collector area to provide 53.38×10^6 Btu/yr (56.31×10^9 J/yr) of heat, of which 56 percent was furnished by solar energy. This system included an 80-gallon (0.3-m^3) domestic-water storage unit, at a minimum supply temperature of 140° F (60° C). Average daily winter insolation at this location was between 703 and 1,346 Btu/ft^2 (8.05 and 15.4×10^6 J/m^2).

This work was done by Solafern, Ltd., for **Marshall Space Flight Center.** *Further information may be found in NASA CR-150515, "Solafern Solar System Desigh Brochure," a copy of which may be obtained at cost from the New England Research Application Center* [see page A7].

MFS-23909

Multichannel Temperature Controller for Solar Heating

Multiplexer/amplifier circuit monitors temperatures and temperature differences.

Marshall Space Flight Center, Alabama

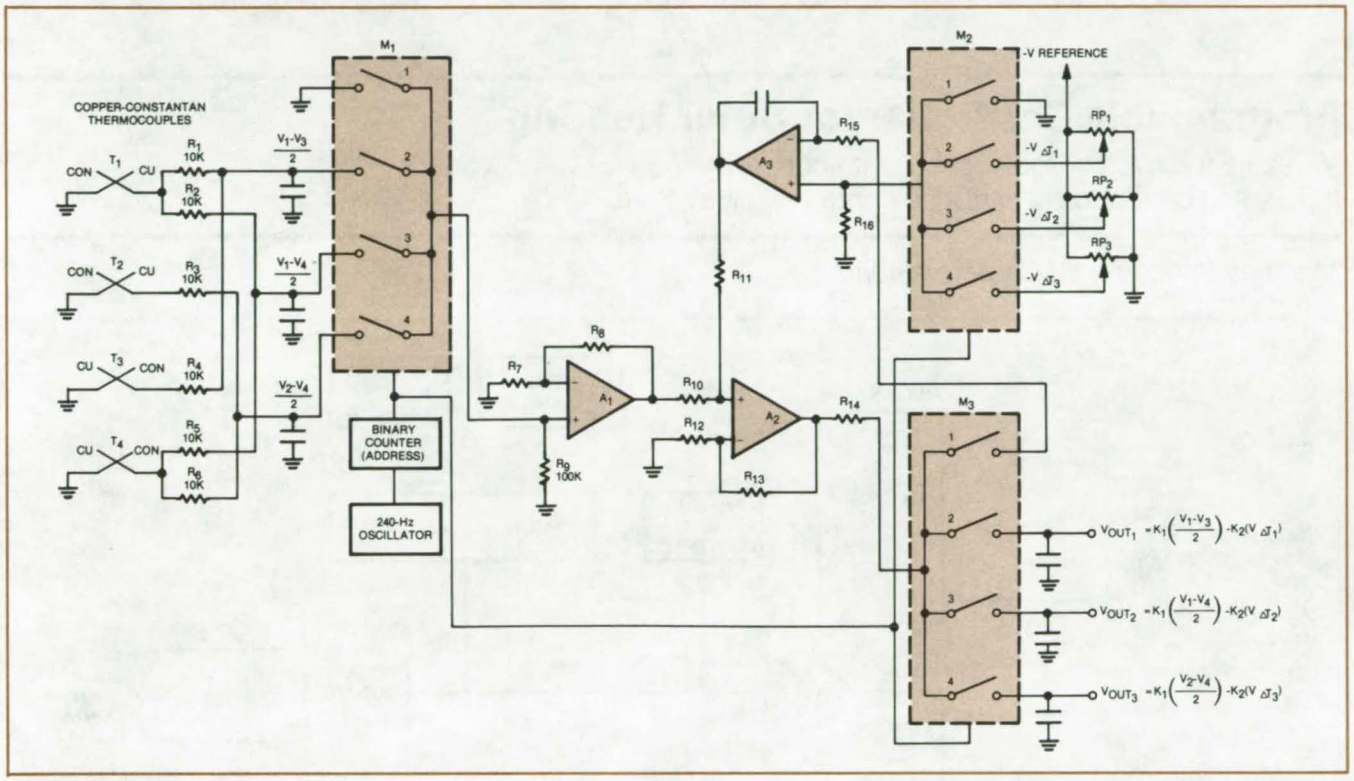

Temperature-Monitoring Circuit amplifies thermocouple outputs in sequence. Temperature differences [e.g., $(T_1 - T_3)/2$] are supplied as inputs to A_1. When the switches are in position 1, the offset voltages of A_1 and A_2 are canceled by feedback through A_3.

Control circuits in solar-heating systems typically follow an equation of the form

$$T_2 = T_1 + \Delta T$$

where T_2 and T_1 might be the temperatures of the collectors and the storage tank, respectively, and ΔT is a user-designated temperature differential. If the controller finds that this equation is satisfied (or exceeded), it could turn on a pump or blower to activate the heating system. In a typical setup, several pairs of temperature sensors might have to be monitored simultaneously.

A new temperature-sensor control circuit, shown in the figure, has been configured for this type of application. Although primarily designed for cycle control in solar-heating systems, it can also be used to measure temperatures in motors, ovens, electronic hardware, and other equipment.

In previous circuits, a separate amplifier was required for each temperature sensor. For differential measurements, the outputs of two amplifiers had to be fed to yet another amplifier.

In the new circuit, a two-stage amplifier and multiplexers handle the signals from many temperature sensors. Temperature differences and minimum temperature offsets are included automatically. The circuit eliminates errors resulting from gain variation among separate amplifiers and is wired to null voltage offsets automatically.

The circuit uses three electronic-switch arrays, synchronized by a common oscillator and logic circuit, to multiplex the signals from the temperature sensors. In a typical application, the sensors would be thermocouples or thermistors. The switches connect the channels in the same numerical order so that at any instant the same channel is routed through all the multiplexers.

The circuit provides two stages of amplification, indicated by the gain factors K_1 and K_2 in the expressions for the output signals. Resistors R_7 through R_{13} control amplifier gain. Amplifier A_3 is a sample-and-hold device that is wired to nullify the offset signals of A_1 and A_2. A calibrated bias voltage that represents a specific temperature differential is added to the output signal through A_3.

Multiplexer M_1 furnishes an output consisting of temperature-difference

(continued next page)

signals $(T_1 - T_3)/2$, $(T_1 - T_4)/2$, and $(T_2 - T_4)/2$, in sequence, to the input of A_1. Multiplexer M_2 furnishes a sequence of bias signals to the input of A_3. The output signals from A_2 are multiplexed by M_2.

The circuitry runs through the multiplex cycle 60 times a second if the control oscillator runs at 240 Hz. The system can be expanded or compressed to handle a greater or fewer number of channels. Unlike other circuits in which a reference temperature is measured for each thermocouple, the new circuit does not require precision components or precise calibration against a standard reference curve.

This work was done by James R. Currie of **Marshall Space Flight Center.** *For further information, Circle 28 on the TSP Request Card.*

Inquiries concerning rights for the commercial use of this invention should be addressed to the Patent Counsel, Marshall Space Flight Center [see page A8]. Refer to MFS-23775.

Programable Controller for Solar Heating

Versatile microprocessor-based unit accepts sensor inputs and generates programed control signals.

Marshall Space Flight Center, Alabama

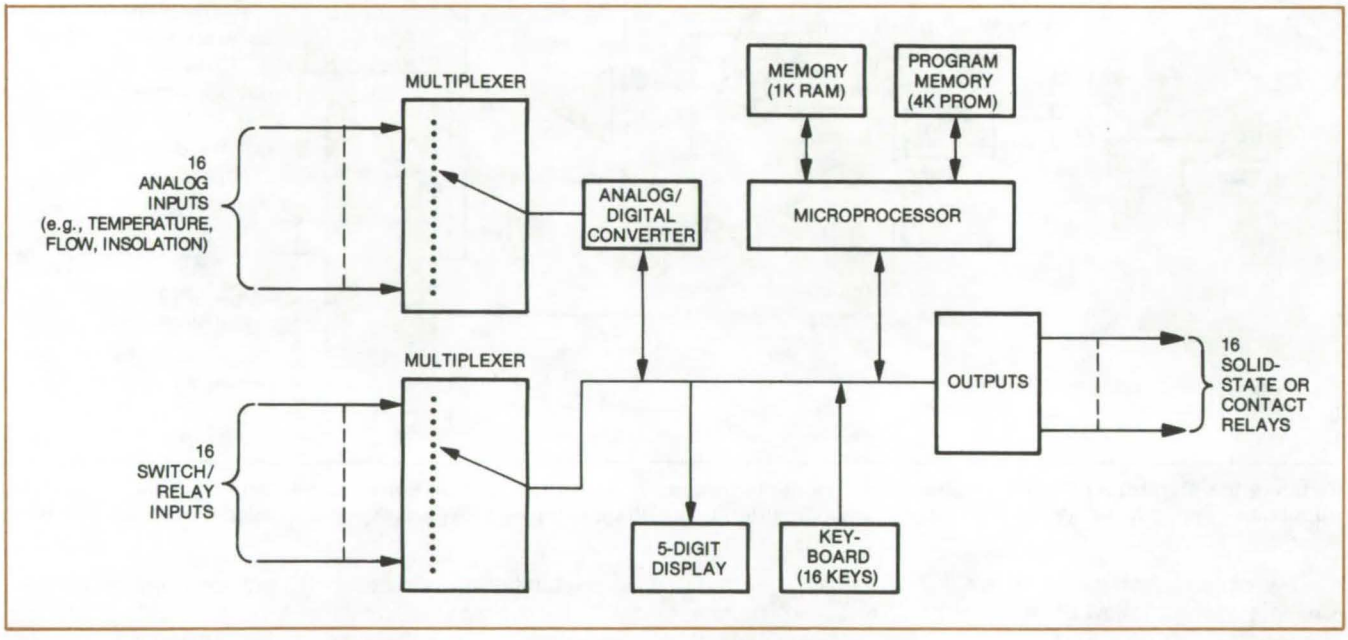

Programable Controller has been designed to supervise solar-heating systems, but can be programed for other applications in which there are multiple sensor inputs and control outputs.

A new programable controller accepts inputs from many types of sensors and converts them to engineering units. User-designated control equations are then solved to command the system outputs. Typical of possible applications would be to monitor differential temperature measurements in solar-heating systems, to turn on pumps and backup systems, and off-peak control for backup systems.

As seen in the figure, the programable controller utilizes a microprocessor to perform all timing, control, and calculation functions. An internal clock/calender is included. The microprocessor follows a program that is stored on plug-in, ultraviolet-erasable, programable read-only memories. These are changed to customize the system for particular requirements. Analog inputs include those for thermistors, pyranometers, flowmeters, and switched signals. Eight TTL-compatible logic inputs are also included. The 16 outputs are optically-coupled solid-state relays and contact relays that can be used to run pumps, fans, and control valves. An optical five-digit LED display will automatically display the input channels, or it can be set to monitor one channel. The display will also show the date and time. Fifty-two constants in the programed equations can be set through the 16-key keyboard.

This work was done by Rho Sigma, Inc., for **Marshall Space Flight Center.** *Further information may be found in NASA CR-150535, "System Design and Installation for RS600 Programmable Control System for Solar Heating and Cooling," a copy of which may be obtained at cost from the New England Research Application Center [see page A7].*

MFS-23915

Universal Test Fixture for Solar Cells

Circuit card holds cells so that properties of encapsulating materials can be measured.

NASA's Jet Propulsion Laboratory, Pasadena, California

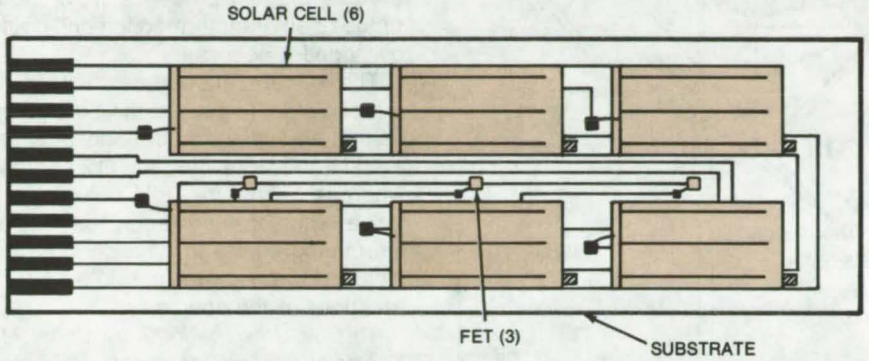

Active area of **Universal Test Fixture** measures 4 by 1-1/4 inches (10.2 by 3.2 cm). It contains three pairs of solar cells and three field-effect transistor (FET) chips, overlaid with the encapsulation material to be evaluated.

Protective coverings for solar cells can be evaluated conveniently by using the test fixture shown in the figure. With the fixture, solar cells and their encapsulants can be exposed to both natural and artificial (accelerated) weathering. Since solar cells are potentially an important source of electric power, the fixture should find wide use as an aid in selecting materials to protect cells from the environment. It is able to provide data on moisture penetration, ionic contamination, solar-cell performance, adhesion of the encapsulant layers, and properties of the encapsulant, such as haze, opacity, spectral response, and mechanical strength.

Designed essentially as a circuit board, the fixture holds three pairs of solar cells. The board and its solar cells are coated with the candidate encapsulant material and are exposed to Sunlight and weather, either natural or artificial.

The board itself is made of alumina ceramic, chosen instead of the usual epoxy because it will not decompose and contaminate the solar cells. Mounted on the board, between each pair of cells, are field-effect transistor (FET) chips; these are sensitive to moisture and ionic contamination and thus indicate whether the encapsulant is permeable to these substances. Circuit interconnections from the chips and solar cells to external contacts consist of molybdenum/manganese films overplated with 100 microinches (2.5 microns) of nickel and 60 microinches (1.5 microns) of gold for solderability and corrosion resistance.

The test fixture comes in two versions: one for field tests and one for accelerated tests. The field-test version can be inserted directly into an edge connector mounted on a test box. The accelerated-test version is connected by a cable to a plug-in circuit card that is inserted in the edge connector; thus the accelerated-test board does not have to be removed from the test chamber for measurements. Typical measurements include the leakage currents of the field-effect transistors and current-vs.-voltage characteristics of the solar cells.

[See following article "Accelerated-Weathering Test System for Solar Cells" (NPO-14061).]

This work was done by John M. Kolyer of Rockwell International Corp. for **NASA's Jet Propulsion Laboratory.** *For further information, Circle 29 on the TSP Request Card. NPO-14062*

Accelerated-Weathering Test-System for Solar Cells

New test system rapidly evaluates the effects of Sunlight, humidity, and temperature.

NASA's Jet Propulsion Laboratory, Pasadena, California

A compact system exposes encapsulated solar-cell arrays to Sunlight, temperature, and humidity for accelerated-weathering. The apparatus, as shown in the illustration, includes two troughs of water, one kept at 5° C and the other at 50° C, and a xenon-arc lamp.

A set of tubes designed to hold solar-cell-array test fixtures [see preceding article "Universal Test Fixture for Solar Cells" (NPO-14062)] is placed in each trough. The tubes receive different amounts of Sunlight, simulated by the arc lamp. Three tubes in each trough (not shown) are kept in total darkness, while 12 others (6 in each trough) are subjected to an intensity equivalent to noon Sunlight exposure. There are also three tubes at each temperature that are positioned to receive half this intensity. In addition, tubes within each set subjected to a given temperature and

(continued next page)

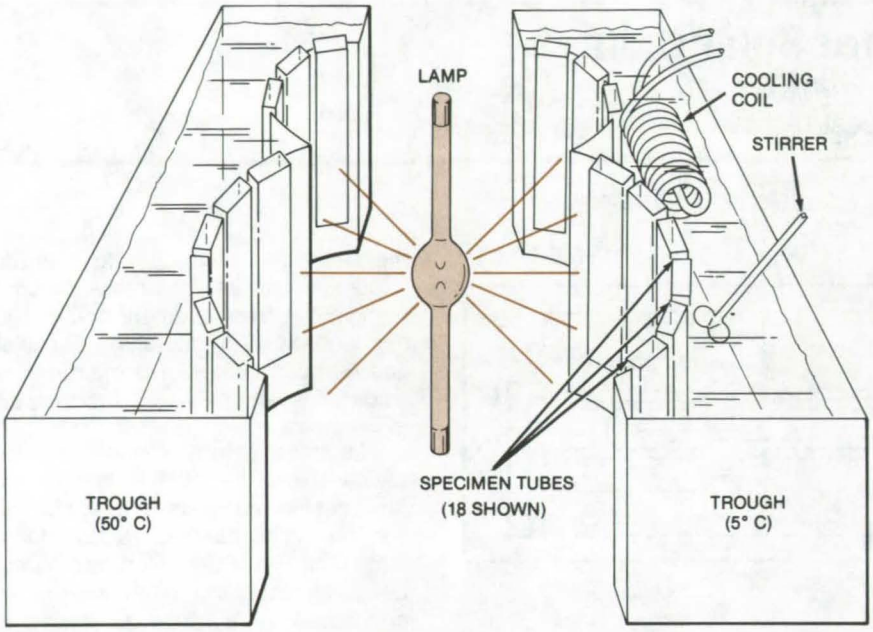

An **Apparatus for Accelerated Weathering** includes two troughs filled with water. A refrigeration coil in the one on the right cools the water to a temperature of 5° C; the left one is warmed to 50° C. Tubes containing solar-cell test specimens are immersed in the troughs. A 2,500-watt xenon-arc lamp simulates the Sun.

solar exposure contain different levels of relative humidity: either zero, 50 percent, or 100 percent. The tubes receiving Sunlight are alternately exposed for 12 hours and shaded for the same period. Electrical feedthrough in the covers of the specimen tubes allow the cell properties to be measured as the test proceeds. A broader range of environment conditions could be added if necessary.

The system accelerates the environmental testing since the Sunlight is held at equivalent noon exposure (for a selected locality) for 12 hours, whereas, in nature, this only occurs for a short period each day. The alternating light and dark periods are included to check for possible "dark" reactions in the specimens.

This work was done by John M. Kolyer of Rockwell International Corp. for **NASA's Jet Propulsion Laboratory.** *For further information, Circle 30 on the TSP Request Card.*
NPO-14061

Automated Solar-Cell-Array Assembly Machine

Continuous-feeding machine automatically bonds solar cells to a printed-circuit substrate.

NASA's Jet Propulsion Laboratory, Pasadena, California

The possibility of using solar cells for the generation of electricity on a large scale has been limited partly by the high cost of producing large arrays of solar cells. Engineers at NASA's Jet Propulsion Laboratory have produced a prototype continuous-feeding machine that automatically assembles the cells on a lightweight flexible substrate. It may help to lower costs in future solar-cell production.

The solar-cell assembly machine (see figure) will carry out a controlled five-step synchronous process. The flexible printed-circuit substrate is stored on a drum and is advanced in steps through the machine. Solder is applied to the substrate before it is wound on the drum.

As the substrate passes through the soldering station, a pair of solar cells is automatically fed from a storage cartridge and is alined against the printed-circuit pattern. An infrared

This prototype of a **Solar-Cell-Array Assembly Machine** automatically bonds solar cells to a flexible printed-circuit substrate. The prototype has been used to attach wraparound-contact n-on-p solar cells to a polyimide-film-coated substrate. The polyimide has holes in it at the solder attachment points. Work on the prototype is continuing; an electrical-test station, and a station at which the completed cell is encapsulated in a protective coating are being developed.

lamp heats the assembly and melts the solder, bonding the cells to the printed circuit. A work station cleans excess flux from the cells.

In the completed machine, the cells would move to a test station where the electrical characteristics could be checked. If the performance of a cell were below specifications, that cell would be marked and removed. The soldered and tested units would then be encapsulated in a protective coating, and another electrical performance check made. Finally, as shown in the figure, the completed cells are stored on a takeup reel. All machine functions are synchronized by electronics located within the unit.

This work was done by Ernest N. Costogue, Robert L. Mueller, Jerry K. Person, and Robert K. Yasui of Caltech for **NASA's Jet Propulsion Laboratory.** *For further information, Circle 31 on the TSP Request Card.*

This invention is owned by NASA and a patent application has been filed. Inquiries concerning nonexclusive or exclusive license for its commercial development should be addressed to the Patent Counsel, NASA Resident Legal Office-JPL [see page A8]. Refer to NPO-13652.

Improved Conical Solar Concentrator

Varied shapes give more uniform concentration, without significantly increasing fabrication costs.

NASA's Jet Propulsion Laboratory, Pasadena, California

Considerable work is currently underway to utilize solar radiation through photochemical, photovoltaic, or thermal-energy conversion processes. At present, these methods are limited by the high cost of producing a converter that is large enough to be of use in a practical application. Until the costs are lowered, solar concentrators appear to be the best way of increasing the output of these systems.

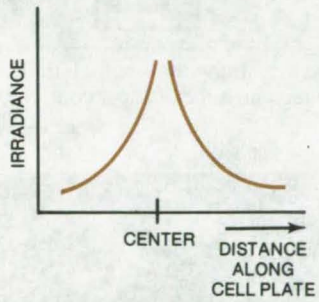

Whereas the cost of fabricating a good parabolic concentrator is relatively high, simple conical concentrators are comparatively inexpensive and are also more tolerant of aiming inaccuracies. While the concentration ratio is not as high as for parabolic shapes, they can give an effective concentration ratio of about 4 or more (after reflectance and temperature loses have been deducted), which is good enough for many purposes.

Conical reflectors have the drawback of not reflecting Sunlight uniformly over the entire cell area (see figure, left). Instead, there is a high concentration of light near the center and less near the cell perimeter. This causes local heating at the center, which degrades efficiency.

An improved conical configuration, in which a cone at the bottom of the reflector supports a second conical shape that has a slightly larger included angle (see figure, center), reflects light more uniformly yet is not much more expensive to manufacture. In this design, a ray of Sunlight that strikes the cone near its top edge will be reflected to the far side of the cell

(continued next page)

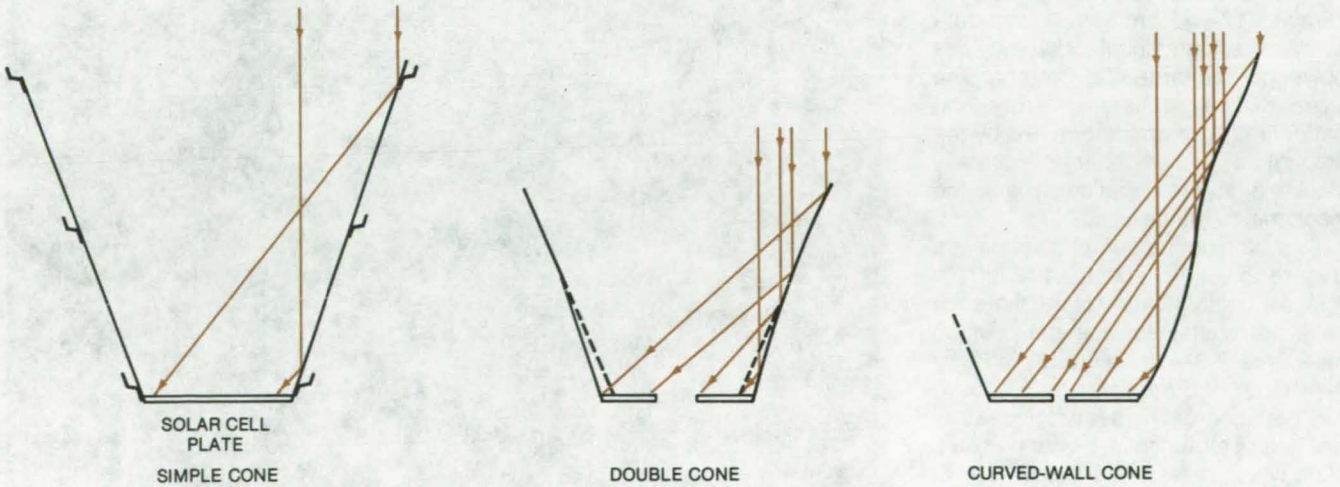

Radiation Pattern Is More Uniform if the simple conical solar concentrator at the left is modified to a double-cone (center) or curved-wall (right) configuration.

plate, whereas an incoming ray that strikes the bottom will be reflected to the near side of the plate. A dark spot occurs at the center, which is devoid of cells. Standard sheet-metal fabrication methods could be used to produce this type of concentrator.

More complex shapes can be developed to make the reflection pattern even more uniform, without going over to parabolic surfaces. Various simple curves and S-shapes (see figure, right) could be constructed by spinning or hydroforming methods.

This work was done by John S. Griffith of Caltech for **NASA's Jet Propulsion Laboratory.** *For further information, Circle 32 on the TSP Request Card.*
NPO-13825

Inexpensive, Portable, Integrating Solar Energy Meter

Silicon-cell insolometer measures accumulated solar energy over a selected period.

Lewis Research Center, Cleveland, Ohio

An inexpensive, portable, integrating solar-energy meter automatically measures and totals the amount of energy available in Sunlight falling on the Earth at a specific location over a selected period of time. The device incorporates a single silicon solar cell as the sensing element and relies on the principle that the short-circuit current from a solar cell is directly proportional to the amount of light that shines on the cell. This principle is also the basis for an "instantaneous" insolometer described in NASA Tech Brief B75-10283 "Inexpensive Pocket-Sized Solar Energy Meter".

The signal from the sensing solar cell is applied to an electronic circuit which performs the integration. Primary circuit components are shown in Figure 1. Power for the electronic components is supplied by self-contained, rechargeable nickel-cadmium cells connected in series to form a nominal 12-volt battery. A separate array of silicon solar cells provides power to recharge the battery. The sizes of the recharging array and battery required are determined by the amount of solar energy normally available at the location where the insolometer will be used.

A prototype model of the device (Figure 2) weighs about 2-1/2 lb (1.1 kg). All components except the solar cells are contained in a case which measures 2-3/4 in. (7 cm) wide by 4-1/8 in. (10.5 cm) high by 6-1/4 in. (16 cm) deep. The recharging array and solar cell sensor are mounted on a plate which is fastened to the case at an angle and increases the overall height of the entire unit to 7-in. (18 cm) maximum.

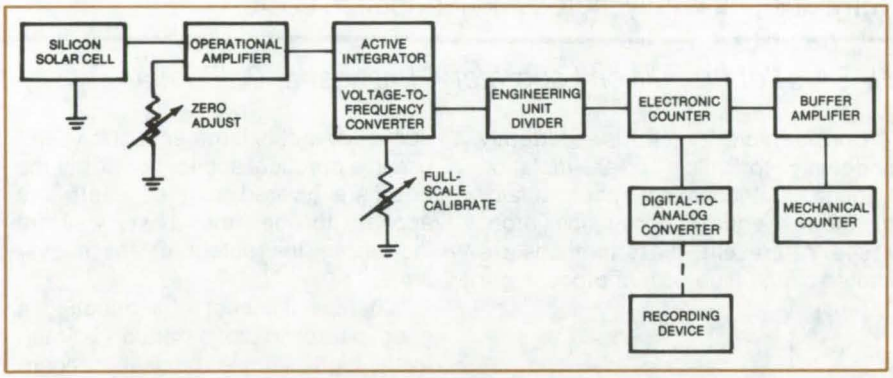

Figure 1. **Integrating Insolometer Circuit** amplifies and integrates output from a silicon solar-cell used as a sensor. Results may be read on a mechanical counter or input to a graphic recorder.

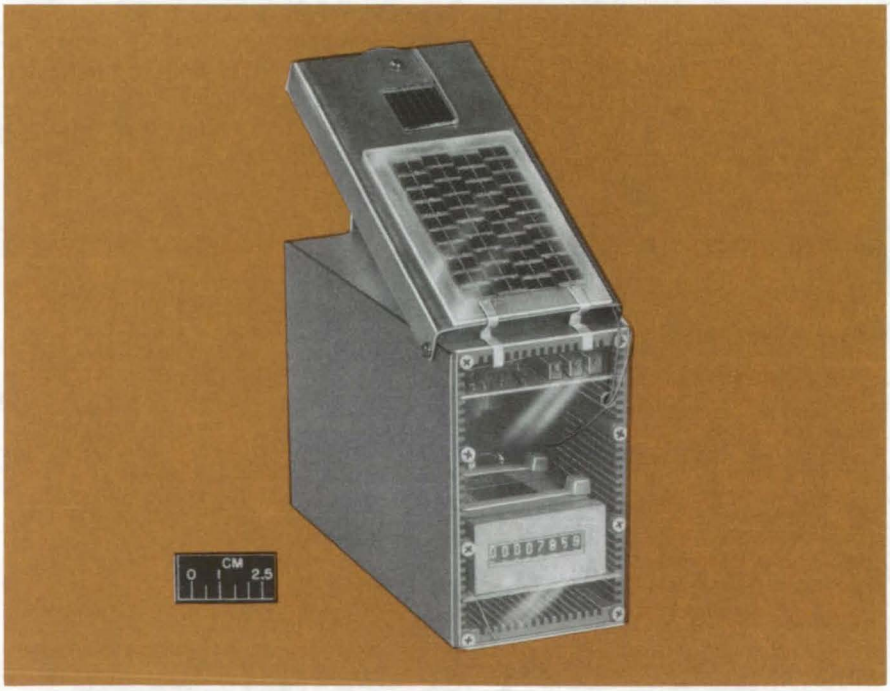

Figure 2. **Prototype of the Integrating Insolometer** is a compact instrument suitable for field use. It is battery powered, and the batteries are recharged via a solar cell array.

The integrating insolometer is installed at a given location, switched on, and left to automatically measure and total the amount of solar energy available at that location. Measurement units (e.g., watt-hours per square meter) are set during calibration and are displayed on a digital mechanical counter. An analog electronic output signal is also available from a jack adjacent to the on/off switch at the back of the instrument. This signal can be provided to a strip chart recorder, for example, to obtain a solar energy time history.

A potential product which might be developed based on this technology is a "solar dosimeter" for use by Sun bathers or for other purposes where information concerning total exposure to solar energy over a period of time is desired.

This work was done by Robert M. Masters of **Lewis Research Center.** *Further informaton may be found in NASA TM-73791 [N78-14630], "Solar Energy Meter," copies of which may be obtained at cost from the Technology Application Center [see page A7].*

LEW-12804

Optics for Natural Lighting

Energy-saving optics utilize sky and Sun for lighting.

Langley Research Center, Hampton, Virginia

Incandescent lighting is about 13 percent efficient; fluorescent, about 22 percent; solar, about 35 percent or more; and blue sky, 80 percent or more. These efficiencies become very critical in summer when every 100 watts of lighting put into a building requires 20 to 40 watts of airconditioning to remove the heat generated. Some innovative optical arrangements for transmitting outdoor light into building interiors are described here.

In the classic light shaft or courtyard extending from ground level to the top of the building, the brick often used is not effective for lighting because it absorbs much of the light. The increased, but diffuse, reflection of a flat white surface or of white brick is a considerable improvement, and a glossy white surface reflects even more of the light down the shaft. With the use of mirror surfaces, almost none of the light is reflected out.

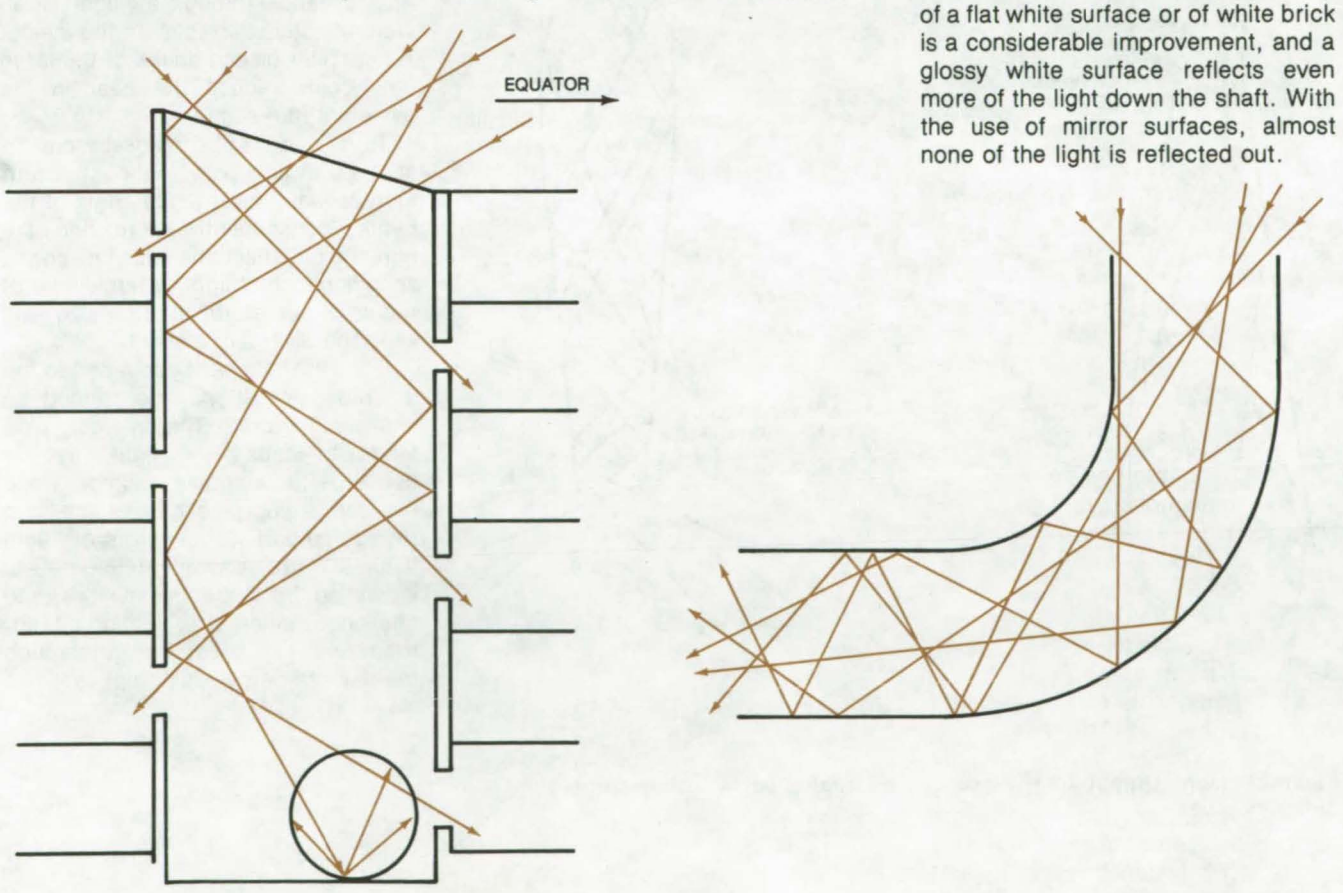

Figure 1. **Two Light Shafts** for efficient illumination with Sunlight are shown. On the left, a vertical shaft for a six story building incorporates sized windows; on the right, a curved shaft directs light around a corner.

(continued next page)

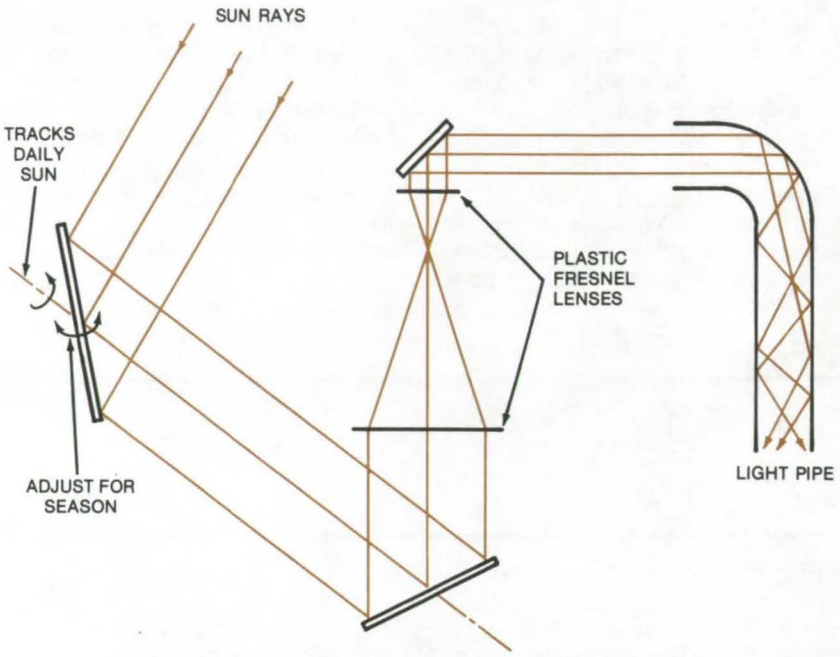

Figure 2. **A Sun Tracker** concentrates light that can be "piped" a considerable distance to an interior room.

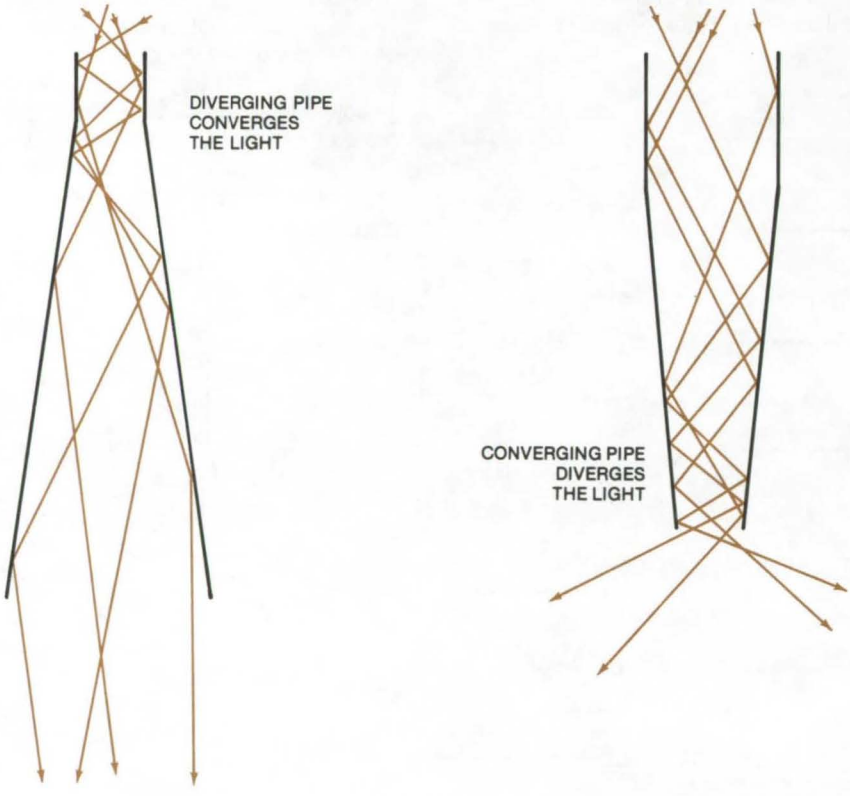

Figure 3. **Light Output from Pipes** can be controlled by using converging and diverging pipes.

Any light entering the upper windows, however, is lost to the lower windows. This suggests, as shown in left half of Figure 1, that the number, size, and location of windows be considered carefully, with "minimum" window area at the top and maximum at the bottom. A sloping window at the top of the shaft, facing south, will protect the mirror surfaces from rain and dirt. This window may be treated to reflect the Sun's heat in summer.

A variation of the mirrored shaft is to run it horizontally from an outside window to an interior room. Skylight can also be reflected around a corner by curved reflecting surfaces (right half of Figure 1).

If space is not available for light shafts, solar light can be piped into interior rooms as shown in Figure 2. The Sun tracker shown is similar to one developed at Sandia Laboratories. The large mirror is driven to track the Sun and reflect its light into the concentrating lens. The concentrated beam can be piped over a considerable distance through a "light pipe" with reflecting surfaces on the inside. A heat filter placed ahead of the large lens could reduce the heat in the system in the summertime.

Turns can also be made by curved sections of light pipe. Although a turn increases the divergence angle of the beam, consequently increasing the number of reflections with the corresponding loss of light, a large ratio of radius-of-curvature to pipe-size will keep the divergence small.

Once the light has been piped to the desired point, it may be treated as shown in Figure 3. The diverging pipe tends to cause the light rays to converge for a spotlight effect, while the converging pipe causes the light rays to spread. Other forms of "light fixtures" are shown in Figure 4, indicating both the possibilities and challenges inherent to lighting interior rooms with skylight or Sunlight through the use of energy-saving optics.

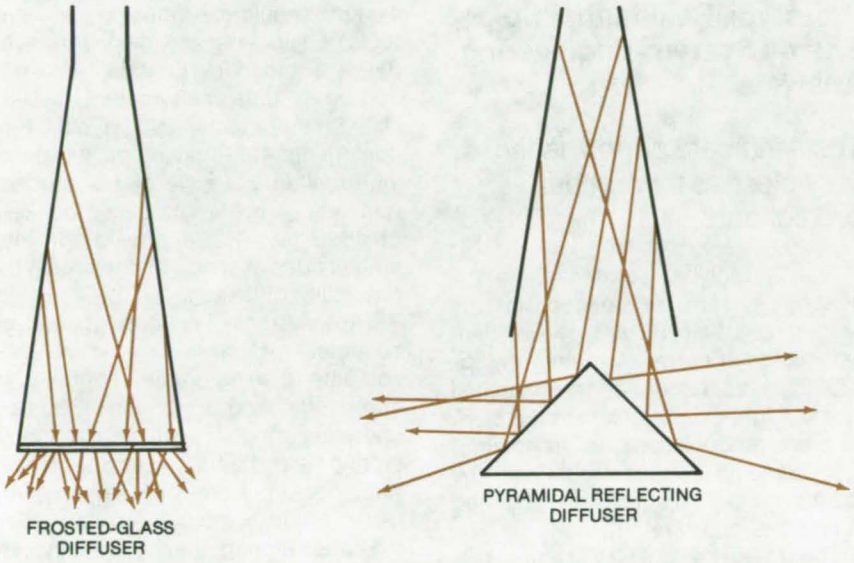

Figure 4. **Two Types of Diffusers** illustrate alternate ways of lighting rooms with solar light.

This work was done by Howard B. Edwards of **Langley Research Center.** *No further documentation is available.*
LAR-12333

Selection Standard for FEP Films for Solar Energy

"Purple" FEP films are more efficient due to low absorptance.

Lyndon B. Johnson Space Center, Houston, Texas

For highest efficiency, Teflon films used as thermal-control coatings in solar-energy conversion systems should have low absorptance in the solar spectrum. Because the levels of various brown/purple tints in a typical production batch are unpredictable, however, absorptance values in Teflon can vary by 30 percent or more. In a recent measurement on fluorocarbon ethylene propylene (FEP) Teflon films obtained for the Space Shuttle program, for example, the solar absorptance values varied between 0.062 and 0.095.

Designers seeking to improve the coatings were able to quantify this effect and to devise a simple screening test based on the transmittance of the films. Samples that passed the test had absorptances as low as 0.059, or lower than the best coatings previously obtained.

The transmittance of films with brown tints was found to be lower than that of the more purple films, with the effect being most pronounced at shorter wavelengths (i.e., in the ultraviolet). Thus, the transmittance at 0.33 micron was chosen as the test wavelength, and the film-selection criterion was set at a transmission of at least 83 percent (that measured for the clearer purple samples). Brown films, in comparison, gave typical transmittances around 68 percent.

By selecting only the purple films with transmittances exceeding 83 percent at 0.33 micron, coatings with more uniform and lower absorptance values were consistently obtained.

This work was done by Madison W. Reed of Vought Corp. for **Johnson Space Center.** *No further documentation is available.*
MSC-16999

Books and Reports

These reports, studies, and handbooks are available from NASA as Technical Support Packages (TSP's) when a Request Card number is cited; otherwise they are available from one of NASA's Industrial Application Centers or the National Technical Information Service.

Prototype Residential Solar-Energy System

A solar-powered domestic-hot-water system for residences and light commercial buildings

A complete solar-energy domestic-hot-water system for single-family residences, one of several systems designed under contracts to Marshall Space Flight Center, is described in a brochure that can be obtained on request. The brochure contains data on procurement, installation, operation, and maintenance of the system in residential or light commercial buildings.

(continued next page)

The solar-powered system consists of energy collectors, a storage tank, pumps, a heat exchanger, and associated plumbing and controls. A silicone fluid circulated through the collector absorbs energy, which is transferred by a heat exchanger to potable water in a preheat tank. The preheat tank, which stores solar energy, services a standard domestic-hot-water heater tank that maintains the supply water at a preset temperature, typically 140° F (60° C). City water replenishes the water flowing from the preheat tank. The standard domestic-hot-water system is the auxiliary-energy source and can supply the hot water in inclement weather.

General features of the system include:

- single-family residence application,
- locatability throughout the continental United States,
- liquid flat-plate collectors,
- silicone heat-transfer fluid (nontoxic),
- fail-safe double-wall heat exchanger,
- automatic operation,
- conventional auxiliary-energy domestic-hot-water system, overtemperature protection, and
- freeze protection.

The system accommodates nominal domestic-hot-water requirements of 50 to 120 gallons per day at 140° F. It can be scaled up or down, however, for a wide range of hot-water requirements for single-family, multifamily, or light commercial applications without significant changes in the design.

The elements of the system are arranged into subsystems, which are described in detail. System performance and sizing are discussed and illustrated by an example of an installation in Bangor, Maine. An appendix includes vendor brochures for the major system components. Drawings, tables, and graphs complement the text.

This work was done by IBM Corp. for **Marshall Space Flight Center.** *Further information may be found in NASA CR-150558, "Design Data Brochure SIMS Prototype System 2," a copy of which may be obtained at cost from the New England Research Application Center* [see page A7].
MFS-23932

Prototype Residential Solar-Energy System-Engineering Analysis

Tests indicate performance very close to theoretical predictions.

The prototype residential solar-heating system referenced in the preceding article [Prototype Residential Solar Energy System (MFS-23932)] was tested at the Marshall Space Flight Center solar simulator. A 43-page report describes the testing, the problems encountered, and the results and conclusions obtained during this program.

The major objectives of the test program were:

- to verify the system installation techniques, operation, and performance;
- to verify the performance of the individual subsystems; and
- to provide a general test data base for comparison with field data.

The system, which was turned on for the first time in late August 1977, gave no operational problems. Overall system performance was very close to predictions, leading to the conclusion that it would perform satisfactorily in most areas of the United States without any problems of freezing, boiling, corrosion, or collector-fluid breakdown. Approximately 60 percent of the building heating load should be supplied by solar energy. This is better than the 56 percent originally predicted during system design.

This work was done by IBM Corp. for **Marshall Space Flight Center.** *Further information may be found in NASA CR-150544, "SIMS Prototype System 2 Test Results — Engineering Analysis," a copy of which may be obtained at cost from the New England Research Application Center* [see page A7].
MFS-23929

Residential Solar-Heating System — Design Brochure

Includes instructions on sizing and layout for a single-family residence

A new design brochure for a commercially-available solar-heating system should be valuable to architects, engineers, and designers. The 31-page brochure contains information on system configuration, system sizing, and mechanical layout. Few constraints are imposed on the building architectural style or construction methods. A full-length collector fabricated to the job size is used, allowing efficient use of space and reducing the possibility of leakage.

The system includes a hot-air collector, rock storage, air-circulating equipment, an automated control unit, and overheating protection. It has six operating modes, including standby, storing heat, heating from the collectors, heating from storage, auxiliary heating, and combined auxiliary heating and storing heat. The system controller switches between the modes as required. It compares temperature-sensor and thermostat inputs and optimizes the use of solar energy while minimizing the use of the auxiliary heaters.

The report discusses the importance of proper sizing of the collector array, and a size-estimating technique is presented. A complete computerized analysis is offered by the manufacturer. Details of the storage and the transport subsystems are provided, with guidelines for specifying the size and layout of each.

Drawings and specifications of all components and typical installation details are included in an appendix. The entire system has been designed to facilitate quick installation, with a minimum of onsite labor. The installation techniques have been thoroughly field-tested and require no special knowledge other than the information provided in the installation manual.

This work was done by Contemporary Systems, Inc., for **Marshall Space Flight Center.** *Further information may be found in NASA CR-150600, "Design Data Brochure for CSI Series V Solar Heating System," a copy of which may be obtained at cost from the New England Research Application Center* [see page A7].
MFS-23933

Prototype Solar-Heating System — Engineering Analysis

Evaluation tests prior to field installation

The space and domestic-water solar-heating prototype described in "Prototype Solar-Heating System" (MFS-23916) on page 201 of this issue has been evaluated at the Marshall Space Flight Center solar-heating and cooling test facility. The test system utilized 720 ft^2 (66.9 m^2) of air collectors (gross), a commercial air handler with a control unit, a storage tank with controller, and 20 tons (8.83×10^4 kg) of rock storage. The procedures and results are summarized in a report that can be obtained on request.

Testing was conducted in three phases, including: (1) simulated energy function, (2) winter normal operation, and (3) summer normal operation.

The simulated energy phase consisted of controlled temperature inputs and loads on the pebble-bed storage and domestic hot-water subsystem. Operation during phases (2) and (3) duplicated "as installed" operation for the winter and for the summer seasons. In addition to the three phases, the collector, the air-handler unit, the control, and the domestic hot-water subsystems were each tested at the subsystem level.

In the tests, an operating sequence begins when insolation striking the absorbers raises the collector control sensor above the rock-storage temperature by 45° F (25° C); collector flow begins at this point. The control unit maintains collector flow only while a minimum temperature difference of 28° F (15.5° C) is maintained between the collector exit and the storage tank.

The heat delivery subsystem is activated by a room-thermostat first-stage heat request if the rock-storage temperature is above the minimum set point of 90° F (32.2° C). (If the minimum-storage-temperature test fails, the heat request is routed to the auxiliary heat equipment.) Room-thermostat second-stage heat requests always initiate electric heat strips. Solar heat and auxiliary heat may not operate concurrently.

The heating of domestic water is restricted to collector operating periods. Heat will be transferred from the collector airstream to the domestic hot-water tank anytime the collection temperature satisfies the 20° F/3° F (11.1° C/1.7° C) on/off differential thermostat parameters.

The performance testing showed:

- The prototype will provide 46 percent of the 65×10^6 Btu (6.8×10^{10} J) design heating load (based on test data projected to Nashville, Tennessee, weather data).
- The electrical energy required to drive the solar portion of the system was 1.3 kW with short-term operation near 1.4 kW.
- Collector flow of 1.7 ft^3/min per collector-ft^2 (8.5×10^{-3} m^3/s per collector-m^2) was less than the 2.5-ft^3/min (12.5-m^3/s) design value. The 3/4-hp (559-watt) air-handler motor was inadequate for 720-ft^2 collectors. This motor would be suitable, however, for a system with a smaller collector array.
- Air-handler control-relay failures occurred that can be prevented by modifying the circuit of the controller.
- The prototype was judged suitable for field installation.

[See following article "Prototype Solar-Heating System — Installation Manual" (MFS-23907).]

This work was done by IBM Corp. for **Marshall Space Flight Center.** *Further information may be found in NASA CR-150522, "SIMS Prototype System 1 Test Results — Engineering Analysis," a copy of which may be obtained at cost from the New England Research Application Center [see page A7].*
MFS-23910

Prototype Solar-Heating System — Installation Manual

Installation instructions for a complete solar-heating system for residential or commercial application.

The installation manual for the prototype solar-heating system referenced in the preceding article is available and can be obtained on request. The manual gives detailed installation procedures for each of the seven subsystems that comprise the prototype. Procedures for operation and maintenance are also included.

The manual discusses architectural considerations, such as the orientation of the collectors, shading, and the influence of the surrounding environment; building construction considerations are also discussed. The manual also describes checkout-test procedures. The test is complemented by drawings and tables that clarify the discussions.

This work was done by IBM Corp. for **Marshall Space Flight Center.** *Further information may be found in NASA CR-150524, "Installation Package — SIMS Prototype System 1A," a copy of which may be obtained at cost from the New England Research Application Center [see page A7].*
MFS-23907

Solar-Heating Module

Module provides the hot-air or hot-water needs for a residence or a commercial building.

A comprehensive set of engineering drawings and instructions for the installation, operation, repair, and maintenance of a solar-energy heating module can be obtained by requesting the Technical Support Package (TSP) referenced at the end of this article. The module, which is housed in a small building with the collectors mounted on the roof, can provide hot water or hot air for residential or commercial applications. A prototype is now operating at the Alabama Space and Rocket Center in Huntsville to heat the "Space Odyssey," a simulated space ride. In the prototype, 500 gallons (1.89 m^3) of hot-water storage provide a year-round source of wash water for tour buses and mobile exhibit vans, in addition to meeting the heating requirements for the space ride.

The module uses water as a transfer medium. The heated water is pumped to a storage tank and can be transferred from the tank through an air handler to provide heated air.

(continued next page)

The module can accommodate solar collectors of various sizes and types. It can provide utility, workshop, or storage space, in addition to providing hot water or hot air. Extensive insulation minimizes heat losses in the structure and in the storage and the fluid-handling subsystems.

This work was done by David L. Christensen of The University Of Alabama In Huntsville for **Marshall Space Flight Center.** *For further information, Circle 33 on the TSP Request Card.*
MFS-23925

Passive Heat Exchanger for Solar Heating

Complete design, manufacturing, and installation specifications

The requirements for design, manufacture, installation, and performance of a passive heat-exchanger module with auxiliary heaters for use with solar-heating systems are described in a report that is now available.

The performance specification is for (1) a thermosyphon liquid-to-air heat exchanger for heating systems in single-family dwellings and (2) electric resistance-heating element(s) to provide backup heat.

The pumpless heating module, when attached to a water storage tank, comprises a self-contained heating unit. The architect, engineer, or consumer is required to supply the storage tank and two pipes welded to the tank for coupling to the thermosyphon inlet and outlet tubes. Natural convective circulation between the storage tank and the heat exchanger replaces the conventional pumped loop.

The heat exchanger is designed to supply more than 54,000 Btu/h (1.37×10^7 cal/h) air-heating capacity at a temperature differential of 70° F (38.8° C) between the inlet fluid and the inlet air (with water as the fluid).

The manufacturing specifications include a parts list, suggested suppliers, and instructions for assembly fit-up, mounting, painting, module assembly, and packaging for shipment. Drawings complement the text discussions.

This work was done by Sigma Research, Inc., for **Marshall Space Flight Center.** *Further information may be found in NASA CR-150516, "System Design Package — Maxi-Therm S-101 Heating Module, Passive Heat Exchanger," a copy of which may be obtained at cost from the New England Research Application Center* [see page A7].
MFS-23914

Passive Heat Exchanger — Installation Package

Includes installation, operation, and maintenance procedures

The installation package for the heating module referenced in the preceding article is now available. The package covers installation, operation, and maintenance of the heat exchanger, which has auxiliary heaters that provide backup heat in inclement weather.

Drawings, including schematics, complement the text material, which is organized as step-by-step instructions. A troubleshooting section discusses probable causes and repairs for the most common difficulties that might be experienced.

This work was done by Sigma Research, Inc., for **Marshall Space Flight Center.** *Further information may be found in NASA CR-150512, "Installation Package Maxi-Therm S-101 Heating Module," a copy of which may be obtained at cost from the New England Research Application Center* [see page A7].
MFS-23930

Prototype Air Flat-Plate Solar Collector

Four reports trace its development from preliminary design through delivery of hardware.

A collection of quarterly reports describes development and fabrication of a prototype air flat-plate solar collector subsystem having 320 ft^2 (29.4 m^2) of collector area [ten panels, each 4 by 8 ft (1.22 by 2.44 m)]. Three (instrumented) panels were completely assembled with glazing and insulation. Manufacturing of seven prototype collectors for delivery was completed in October 1977.

The reports trace the program from the preliminary design stages through delivery of the hardware. Developmental tests, including airflow, air temperature, and efficiency, are discussed in the reports, as are qualification tests on prototypes and final acceptance tests.

The qualification test program included measurements on the absorber coatings, comparison of glazings, stagnation tests, environmental tests, and structural analysis.

This work was done by Life Sciences Engineering for **Marshall Space Flight Center.** *Further information may be found in NASA CR-150514, "Collation of Quarterly Reports on Air Flat Plate Collectors," a copy of which may be obtained at cost from the New England Research Application Center* [see page A7].
MFS-23893

Flat-Plate Solar Collector — Installation Package

Includes installation, operation and maintenance, and repair procedures

The installation package for the air flat-plate solar collector described in the preceding article can be obtained by requesting the report referenced below. The package includes the installation, operation, and maintenance manual for the collector, an analysis of safety hazards, special handling instructions, a materials list, installation drawings, and the warranty and certification statement.

The installation, operation, and maintenance manual includes instructions for roof preparation and for preparing the collector for installation. Checkout procedures are also given. Several pages in the maintenance section are devoted to procedures for major and minor repairs.

This work was done by Life Sciences Engineering for **Marshall Space Flight Center.** *Further information may be found in NASA*

CR-150536, "Installation Package for Air Flat Plate Collector," a copy of which may be obtained at cost from the New England Research Application Center [see page A7].
MFS-23921

Testing of Three Hot-Air Solar Collectors

Tests to determine the dependence of pressure on air velocity and temperature

A report that presents the procedures used and the results obtained during a program to determine the pressure drops across three prototype hot-air solar collectors as a function of air velocity and operating temperature is now available.

During the tests, the three hot-air collectors, manufactured by Marshall Space Flight Center, were manifolded in series. Each collector had a surface area of 17.5 ft^2 (1.62 m^2) with air transfer ducts of 0.65 ft^2 (0.06 m^2). Each was 3 ft (0.91 m) wide, 6 ft (1.8 m) long, and 0.6 ft (0.18 m) deep and weighed approximately 35 lb (15.9 kg). The collector surface was a 2024-T3 aluminum plate 0.012 in. (0.030 cm) in thickness, coated dark on the top surface. The collector was covered with a single standard plate glass 0.125 in. (0.318 cm) in thickness. In most cases, the tests were performed at an atmospheric pressure of 29.38±0.05 inches (74.6±1.3 cm) of mercury (absolute), a temperature of 23° ±2° C, and a relative humidity of approximately 50 percent.

The pressure-drop versus flow-rate characteristics for these collectors were determined under 14 different test conditions, each of which was characterized by a unique combination of inlet air temperature and airflow rate. The characteristics of inlet, exit, and transfer ducts of these collectors were also determined during this testing.

The test results indicate:

1. Significant pressure drop occurs at airflow rates greater than 150 $stdft^3/min$ (70.7 l/s), and this drop does not depend heavily on inlet air temperature; and
2. Inlet, exit, and transfer duct characteristics differ sufficiently to suggest that system performance may be enhanced through careful design of each type of duct.

This work was done by R. Losey of Wyle Laboratories for **Marshall Space Flight Center.** *Further information may be found in NASA CR-150495, "MSFC Hot Air Collectors — Phase I Test Report," a copy of which may be obtained at cost from the New England Research Application Center [see page A7].*
MFS-23887

Thermal Performance of a Hot-Air Solar Collector

The results of a comprehensive outdoor test program

A series of tests has been conducted to evaluate the thermal performance of a hot-air solar collector.

The collector is single glazed with a nonselective absorber plate and uses flowing air as the heat-transfer medium. The absorber plate and box frame are aluminum, and the insulation is isocyanurate foam board 1 in. (2.54 cm) thick, with a thermal conductivity of 0.11 Btu/ft-h-°F (0.0075 cal/m-s-°C). The collector measures 25-1/8 by 146-3/4 by 3-5/16 in. (63.8 by 372.7 by 8.4 cm), provides 25.6 ft^2 (2.38 m^2) of collector surface area, and weighs 65 pounds (29.4 kg).

The performance evaluation included:

- time-constant test,
- collector-efficiency test,
- collector-stagnation test,
- incident-angle-modifier test,
- load test,
- weathering test, and
- absorber-plate optical-properties test.

Data sheets, graphs, and tables for all tests are included in the report.

The time constant of the collector was 4 minutes and 30 seconds. It sustained loads of up to 120 lb/ft^2 (5.05 kg/m^2) with no apparent damage or leakage.

The weathering test was conducted from December 1976 through April 1977. The only deficiency noted during this test was a shrinking and separation of the trim from the frame.

This work was done by J. Chiou of Wyle Laboratories for **Marshall Space Flight Center.** *Further information may be found in NASA CR-150509, 'Thermal Performance Evaluation of Solar Energy Products Company [SEPCO] "Solaron" Collector Tested Outdoors,' a copy of which may be obtained at cost from the New England Research Application Center [see page A7].*
MFS-23891

Performance and Structural Tests of Hot-Air Solar Collectors

Five collectors were tested in a three-phase program.

A 36-page report describes a program to determine the thermal performance and structural characteristics of selected hot-air collectors in both real and simulated environmental conditions. Five collectors designed at Marshall Space Flight Center were tested in the three-phase program.

The five collectors were identical except that a different foam was used to form the bodies of two of the collectors. Absorber plates were made of sheet metal, 0.02 in. (0.051 cm) in thickness, and were coated with black paint. Each collector had a single cover made of standard glass. Each weighed approximately 21 pounds (9.5 kg). The dimensions were: width, 38-1/8 in. (96.8 cm); length, 74 in. (187.9 cm); depth, 7 in. (17.8 cm); inlet and outlet ducts, 3-5/8 by 15 in. (9.21 by 38.1 cm).

Phase one of the program was a series of outdoor tests to determine stagnation temperatures on a typical bright day and to determine the ability of each collector to withstand these temperatures. The two collectors fabricated of the alternate foam material failed structurally and were eliminated from the rest of the program. Of the three remaining collectors, one was chosen as the test article for the last two phases.

Phase two was a series of outdoor tests to evaluate the thermal performance of the selected collector at different combinations of inlet temperature, flow rate, and solar flux. The final phase of the program was a series of indoor tests to evaluate the thermal performance of the collector

(continued next page)

under closely-controlled simulated conditions.

This work was done by K. Shih, Sr., of Wyle Laboratories for **Marshall Space Flight Center.** *Further information may be found in NASA CR-150506, "Thermal Performance of MSFC Hot Air Collectors Under Natural And Simulated Conditions," a copy of which may be obtained at cost from the New England Research Application Center* [see page A7].
MFS-23911

Thermal Performance of a Hot-Air Solar Collector

Tests of a double-glazed collector, using a solar simulator

A new report contains the procedures and results of thermal-performance tests on a double-glazed air solar collector. The Marshall Space Flight Center solar simulator was used for the tests.

The collector is a commercially-available double-glazed flat-plate type. Gross area is 19.00 square feet (1.77 m^2) with an aperture area of 16.91 square feet (1.57 m^2). The approximate weight is 160 pounds (72.5 kg).

Four types of tests were carried out, including thermal-efficiency and stagnation tests, collector time-constant tests to assess the effect of transients, and incident-angle modifier tests. The thermal-performance data were taken for a range of inlet and ambient temperatures and incident flux values.

The data are presented in tables and as graphs and are discussed and analyzed.

This work was done by Wyle Laboratories for **Marshall Space Flight Center.** *Further information may be found in NASA CR-150572, "Indoor Test for Thermal Performance Evaluation of The Solaron [Air] Solar Collector," a copy of which may be obtained at cost from the New England Research Application Center* [see page A7].
MFS-23924

Flat-Plate Liquid Solar Collector

A comprehensive series of performance tests on a 24.95-ft^2 solar collector

A 47-page report presents the test procedures and results of a program to obtain thermal performance data on a liquid solar collector. The tests employed the Marshall Space Flight Center solar simulator.

The test article for the program is a flat-plate solar collector with a liquid heat-transfer medium. The absorber plate is copper coated with black paint. Between the tempered low-iron glass and absorber plate, a polycarbonate trap suppresses convective heat loss.

The collector incorporates a convector heat-dump panel to limit temperature excursions during stagnation. The absorber plate has an absorption coefficient of 0.985, the glass cover has a transmission coefficient of 0.90, and the effective transmission coefficient of the heat trap is 0.935. The product of transmissivity and absorptivity is 0.829. The dimensions of the collector are 44-1/2 by 80-3/4 by 5-1/4 in. (113 by 205 by 13.3 cm). The gross surface area is 24.95 ft^2 (2.29 m^2) with an aperture area of 21 ft^2 (1.93 m^2). The collector weighs approximately 145 pounds (65.7 kg).

The tests conducted included:

- thermal-efficiency test,
- time-constant test,
- incident-angle-modifier test,
- heat-loss-coefficient test, and
- stagnation test.

Complete descriptions of the test procedures, analyses, and results are contained in the report.

This work was done by Ken Shih of Wyle Laboratories for **Marshall Space Flight Center.** *Further information may be found in NASA CR-150511, "Indoor Thermal Performance Evaluation of Daystar Solar Collector," a copy of which may be obtained at cost from the New England Research Application Center* [see page A7].
MFS-23912

Performance Evaluation of a Liquid Solar Collector

Test procedures and data are given for a single-covered collector.

A new report presents the procedures and results of thermal performance tests on a single-covered liquid solar collector under simulated conditions. The Marshall Space Flight Center solar simulator was used for the tests.

The collector tested is a flat-plate type that uses water as the heat-transfer medium. The absorber plate is copper and is selective-black coated with an absorptivity of 0.87 to 0.92 and an emissivity of 0.10 to 0.20. Copper tubes with inside diameters of 1/4 in. (0.64 cm) are bonded to the absorber plate by soft solder, with a center-to-center tube spacing of 6 in. (15.2 cm). The collector has a single cover of tempered glass with transmissivity of 0.92. The overall dimensions are 36 by 84 by 4 in. (91 by 213 by 10 cm). It weighs approximately 115 pounds (51 kg) when filled.

The test conditions and data are given in tables and graphs for stagnation tests and thermal performance tests. In addition, a time-constant test and an incident-angle modifier test were conducted to determine the transient effect and the incident-angle effect. The results of collector load tests are also given.

This work was done by Ken Shih of Wyle Laboratories for **Marshall Space Flight Center.** *Further information may be found in NASA CR-150573, "Indoor Test for Thermal Performance Evaluation of Sunworks [Liquid] Solar Collector," a copy of which may be obtained at cost from the New England Research Application Center* [see page A7].
MFS-23931

Indoor and Outdoor Tests of a Liquid Solar Collector

A comparative thermal-performance study

Two new reports describe thermal-performance data obtained on a double-covered liquid solar collector. One report describes data obtained during outdoor testing, and the other describes indoor test data obtained by using the Marshall Space Flight Center solar simulator. The indoor data were taken to verify the performance of the solar simulator.

The solar collector has a double-glass cover with dimensions 3 by 4 by 0.5 ft (0.91 by 1.2 by 0.152 m); its dry weight is 65 lb (29.4 kg). The iron oxide absorber has an absorbtivity of 0.91, an emissivity of 0.37, and a surface area of 10.23 ft^2 (3.12 m^2).

The outdoor tests checked the thermal performance of the collector at 100°, 150°, and 200° F (37.7°, 65.5°, and 93.3° C) inlet temperature with the flow rate controlled at 120 lb/h (0.015 kg/s). The solar flux was between 190 and 360 Btu/h-ft^2 (0.014 and 0.027 cal/s-cm^2). Parameters such as absorber temperature, flow rate, and wind velocity and direction were recorded and are presented in tables.

The indoor test program obtained thermal performance data under similar conditions for comparison with the data obtained outdoors. The comparison is presented as a graph of collector efficiency versus a normalization parameter that includes the effects of ambient and inlet temperatures and of the incident flux.

This work was done by R. Losey and K. Shih of Wyle Laboratories for **Marshall Space Flight Center.** *Further information may be found in:*

NASA CR-150505, "Thermal Performance of Honeywell Double Covered Solar Collector," and NASA CR-150507, "Verification Test of the MSFC Solar Simulator Using a Honeywell Double-Covered Liquid Solar Collector."

Copies of these reports may be obtained at cost from the New England Research Application Center [see page A7].

MFS-23886

Thermal Performance of a Flat-Plate Liquid Solar Collector

Comprehensive tests were carried out in a solar simulator.

A report is available that presents the procedures and results of a program to obtain thermal performance data on a double-covered liquid solar collector. The Marshall Space Flight Center solar simulator was used for the tests.

The device tested is a flat-plate solar collector that uses a liquid heat-transfer medium. The copper absorber plate is 0.021 in. (0.053 cm) in thickness; the absorber surface is 19.74 ft^2 (1.82 m^2); and the overall dimensions of the collector are 3 by 4 ft by 3/4 in. (0.91 by 1.22 m by 1.9 cm). It has a double cover made of tempered glass 1/8 in. (0.318 cm) in thickness. The weight is approximately 130 pounds (58.9 kg).

The thermal performance tests were conducted at inlet temperatures of 100°, 120°, 150°, and 200° F (38°, 49°, 66°, and 93° C) with a controlled liquid-flow rate of 290 pounds per hour (0.036 kg/s) at solar flux levels of 230 and 270 Btu/h-ft^2 (0.017 and 0.020 cal/s-cm^2) with simulated wind conditions of 0, 10, and 13 mi/h (0, 16, and 21 km/h). The test conditions and the thermal performance data obtained during the tests conducted on the simulator are contained in the report.

In addition, a test was carried out to obtain the time constant for the collector with the inlet held at ambient air temperature, the solar flux level at 230 Btu/h-ft^2, and the liquid flow rate at 290 lb/h.

The effect of incident angle on the collector was also tested with a liquid flow rate of 290 lb/h, the inlet temperature controlled to ambient air temperature, and with the collector tilted at 45°, 60°, and 75° with respect to the solar simulator surface.

This work was done by K. Shih of Wyle Laboratories for **Marshall Space Flight Center.** *Further information may be found in NASA CR-150508, "Indoor Test for Thermal Performance Evaluation of Libby-Owens-Ford Solar Collector," a copy of which may be obtained at cost from the New England Research Application Center* [see page A7].

MFS-23890

Corrosion Inhibitors for Solar Heating and Cooling Systems

Tests of several inhibitors under simulated conditions

Several forms of corrosion, including uniform, galvanic, and pitting, can degrade performance and increase the maintenance costs of solar heating and cooling systems. In a recent study carried out for Marshall Space Flight Center, several candidate materials were tested for their ability to limit corrosion under conditions that approximate those found in a typical solar-energy system. The results of the study are available in a new report.

In the test system, a cartridge heater was enclosed in an aluminum test coupon, and the assembly was seated in a glass jacket. During the tests, the cartridge heated the aluminum (which simulates a solar panel), and the aluminum heated a fluid flowing through the glass jacket. A mild-steel coupon in the fluid reservoir represented the steel that is often used for the storage basin in solar heating systems. A copper wire connected the aluminum coupon to the steel to simulate galvanic coupling and copper joints in the plumbing of a solar system. The various inhibitors were added in controlled amounts, and the weights of the test coupons were checked at the end of each test; any loss of weight was attributed to corrosion.

The study included both short- (7-day) and long-term (60-day) tests and an economic analysis of each inhibitor. Several promising additives were found. Of these, sodium chromate at 1,000 parts per million gave the best corrosion protection in both the short- and long-term tests. In the test system, for which the corrosion rate was 6.3 mil/yr (0.16 mm/yr) for aluminum and 22.7 mil/yr (0.58 mm/yr) for steel without the inhibitor, long-term corrosion was only 0.12

(continued next page)

mil/yr (0.003 mm/yr) for aluminum and 1.77 mil/yr (0.04 mm/yr) for steel if sodium chromate was added.

In addition to a presentation of the data, the report also includes a discussion of the different forms of corrosion and recommendations for future work.

This work was done by John H. Tabony of Southern University for **Marshall Space Flight Center.** *Further information may be found in NASA CR-150513, "Inhibitor Analysis for A Solar Heating and Cooling System," a copy of which may be obtained at cost from the New England Research Application Center* [see page A7].
MFS-23892

Performance of Black-Nickel and Black-Chrome Solar Collectors

A comparative study

A new report presents the procedures used and results obtained during tests to determine the comparative efficiency of black-nickel and black-chrome solar-collecting surfaces.

The program evaluated four unique solar collectors, including:
- a black-nickel collector surface with a desiccant drying bed,
- a black-nickel collector surface without a desiccant drying bed,
- a black-chrome collector surface with a desiccant drying bed, and
- a black-chrome collector surface without a desiccant drying bed.

The test program included three distinct phases:
- phase I — initial performance evaluation,
- phase II — natural environmental aging, and
- phase III — post-aging performance evaluation.

The test conditions included seasonal ambient conditions. Phase I testing occurred during the winter months, while phase III occurred during the summer months. Performance evaluation testing occurred only during daylight hours with the solar flux greater than 250 Btu/h-ft^2 (0.019 cal/s-cm^2) for an extended period of time. Results of phase III testing indicated a higher normalized efficiency for black-chrome collector surfaces than for black nickel.

This work was done by R. Losey of Wyle Laboratories for **Marshall Space Flight Center.** *Further information may be found in NASA CR-150497, "Performance Evaluation of Two Black Nickel and Two Black Chrome Solar Collectors," a copy of which may be obtained at cost from the New England Research Application Center* [see page A7].
MFS-23888

Measuring Metallic Concentrations in Glycol Solutions

A study of a possible corrosion indicator for solar-energy systems

A new report describes a study to develop procedures for determining low levels of aluminum, copper, iron, and lead in aqueous glycol formulations. At the outset of the study, it was hoped that the procedures could be used to monitor the extent of corrosion of solar panels without requiring that the panels be dismantled.

Atomic absorption spectroscopy was selected for Cu, Fe, and Pb. After comparison with emission spectroscopy, this technology was selected for Al also. Prior to the analysis, Cu, Fe, and Pb are extracted with diethyldithiocarbamate into methyl isobutyl ketone (MIBK). Aluminum was also extracted into MIBK by using 8-hydroxyquinoline as a chelating agent. As little as 0.02 mg/l of Cu, 0.06 mg/l of Pb or Fe, and as little as 0.3 mg/l of Al in glycol formulations can be measured by these techniques.

The test results were compared with the actual weight losses of metal samples that had been immersed in the solutions. However, very little correlation was found, indicating that this is not a promising approach for monitoring corrosion. Instead of going into solution, it appears that the corrosion products adhere to the base metal. They are removed by scrubbing prior to weighing the sample.

The study recomends that other methods for determining the extent of corrosion during testing be considered. For example, test samples could be installed in the system and removed periodically for examination.

This work was done by the Houston Chemical Co. Division of PPG Industries, Inc., for **Marshall Space Flight Center.** *Further information may be found in NASA CR-150520, "The Determination of Aluminum, Copper, Iron and Lead in Glycol Formulations by Atomic Absorption Spectroscopy," a copy of which may be obtained at cost from the New England Research Application Center* [see page A7].
MFS-23894

Glass Solar Collector — Materials Assessment

Tests to prevent explosive failure under boilout conditions

A comprehensive series of tests has been carried out to evaluate the design, materials, and failure modes of a commercially-available glass solar-collector system. The results of the materials analysis segment of the program are presented in a report that is now available.

The collector has 24 glass tubes manifolded together so that fluid flow is channeled sequentially through each tube. Individual tubes consist of two concentric glass tubes with a hard vacuum in the annular space between them. There is a selective absorber coating, with high solar absorptivity and low emittance, on the outer surface of the inner tube. The vacuum protects the coating from atmospheric degradation and suppresses conductive heat loss. This construction allows the temperature of the inner tube to rise to approximately 650° F (340° C) when the collector is stagnated.

The primary problem investigated in the test program was explosive failure of the collector during boilout. Boilout occurs when the system is collecting solar energy but no fluid is flowing through the tubes. Under these conditions, the pressure can rise above that of the pressure relief valve [approximately 35 psig (2.4×10^5 N/m^2)], venting steam and hot water to the outside.

The report presents data obtained during pressure-testing of the individual tubes and during performance-testing of a complete array of tubes on the Marshall Space Flight Center solar simulator. Other parts of the study investigated the effects of thermal shock, fracture initiation, and residual stresses near seals on the glass tubes.

The tube absorber coating, the manifold components, the insulation, and various plastic and rubber components were also evaluated.

It is concluded that proof-testing of the collector tubes prior to their use helps to predict their performance for limited service life. Fracture-mechanics data are desirable for predicting extended service life and establishing a minimum pressure-level requirement.

This work was done by R. L. Nichols of **Marshall Space Flight Center.** *Further information may be found in NASA TM-78163, "Owens-Illinois Liquid Solar Collector Materials Assessment," a copy of which may be obtained at cost from the New England Research Application Center* [see page A7].
MFS-23926

Pump Efficiency in Solar-Energy Systems

An experimental and theoretical study

In systems utilizing fluid-handling pumps, significant energy can be wasted by improperly selected pumps or from inefficiencies in the pump and pump/drive-train combination. Since solar-energy systems may be required to operate for 15 to 20 years or more, an efficient pumping system that is matched to the needs of the solar elements can provide significant savings in operating costs.

A new study has investigated the characteristics of typical "off-the-shelf" pumping systems that might be used in solar systems. The pumps were of the types and sizes that could meet the requirements of solar-collector or solar-load flow loops in residential solar-heating and solar-cooling systems. Establishing the variation of the pump-system overall efficiency with the size and type of pump was a primary goal. Overall pumping-system efficiency, which includes contributions from the pump, the coupler, and the motor, was also examined. Each of these contributions was determined in some cases.

The report includes a discussion of the difficulties in predicting pump efficiency from manufacturers' data. Sample calculations are given. Efficiency data are primarily available for pumps that are larger than those usually found in residential solar-heating systems (1/12 to 1 hp). The available data can be scaled, but the scaling laws can introduce significant errors. Also, the effect of cavitation is not given in the manufacturers' data.

The experimental program included comprehensive tests on representative, commercially available pumps. Peak efficiencies, flow-rate control, and noise levels were investigated. No effort at ranking or recommending specific pumps was attempted. Instead, the primary goal was to assess the factors affecting energy usage.

Design guidelines for selecting a pump and for locating it within the system are given in the concluding section of the report. A review of the theory of pump types and operating characteristics is presented in an appendix, along with brief discussions of noise and cavitation.

This work was done by Tennessee Technological University for **Marshall Space Flight Center.** *Further information may be found in NASA CR-150604, "Pump/Control System Minimum Operating Cost Testing," a copy of which may be obtained at cost from the New England Research Application Center* [see page A7].
MFS-23934

The Economics of Solar-Powered Absorption Cooling

An analytical procedure that considers site-dependent factors

An analytic procedure can evaluate the cost of combining an absorption-cycle chiller with a solar-energy system in a residential or commercial application. The procedure, described in a report that is now available, assumes that a solar-energy system already exists to heat the building and that a cooling system must be added. The decision to be made is whether to cool the building with a conventional vapor-compression-cycle chiller or to use the solar-energy system to provide heat input to the absorption chiller.

Two methods were considered for meeting the cooling load not supplied by solar energy. In the first method, heat is supplied to the absorption chiller by a boiler, using fossil fuel. In the second method, the load not met by solar energy is handled by a conventional vapor-compression chiller. The procedure can also consider waste heat as a form of auxiliary energy.

The analysis has three steps. The first involves determining the percent of the cooling load that must be provided by the solar-energy system in order that the system energy requirement will not be increased. (It is possible, using a solar-powered absorption-cycle chiller, to use more conventional energy than by cooling with conventional means.)

The second step determines the percent of the cooling load that can be supplied by the solar-energy system. Comparison with the minimum solar-cooling fraction from the first step then determines if energy will be saved. If energy savings are possible, the last step is to determine if the system will also give capital savings, using a life-cycle cost analysis.

The process requires several input parameters, including site-dependent building heating and cooling loads, the available insolation for both heating and cooling, and the cost of utilities. Other inputs needed are the fuel-cost escalation rate, discount rate, mortgage interest rate, life of the system, and repair and maintenance costs.

The method has been used to determine sites that are attractive for solar cooling with an absorption chiller. During the analysis the site-independent parameters were held constant (at typical values) so that the influence of the site-dependent parameters could be determined.

The results of the analysis indicate that residential applications of solar-powered absorption cooling are not currently attractive economically. Of the sites considered, Washington and Kansas City are the most favored (although not cost-effective).

Commercial applications of solar cooling with an absorption chiller were found to be more cost-effective than residential applications. Because of the variations in the internally generated energy in a commercial installation, any proposed application should be reviewed on its own merits to determine if it saves energy and is also cost-effective. In general, it was found that the larger the chiller, the more economically feasible it would be.

(continued next page)

Also, it was found that a conventional vapor-compression chiller is a viable alternative for the auxiliary cooling source, especially for larger chillers.

This work was done by J. C. Bartlett of IBM Corp. for **Marshall Space Flight Center.** *Further information may be found in NASA CR-150533, "Site Dependent Factors Affecting The Economic Feasibility of Solar Powered Absorption Cooling," a copy of which may be obtained at cost from the New England Research Application Center* [see page A7].
MFS-23908

Application of Solar Energy to Air-Conditioning

A survey of approaches that could find residential applications

The results of a survey of the application of solar energy to air-conditioning systems are summarized in a new report. This survey reviewed air-conditioning techniques that are most likely to find residential application in the near future (within about 5 years) and that are compatible with solar-energy systems being developed at Marshall Space Flight Center. Solar-powered (absorption-cycle and heat-engine/Rankine cycle) and solar-related (heat-pump) air-conditioning systems are discussed.

The 77-page report includes brief descriptions of the physical and technical implications of the different techniques, discussions of current status, proposed technological improvements, and methods of utilization and simulation. The potential advantages and disadvantages of applying solar energy to air-conditioning are analyzed in the final section of the report. There is also an appendix that contains an extensive bibliography of related literature.

This work was done by Andrew J. Harstad and Jonathon M. Nash of IBM Corp. for **Marshall Space Flight Center.** *Further information may be found in NASA CR-150532, "Application of Solar Energy to Air Conditioning Systems," a copy of which may be obtained at cost from the New England Research Application Center* [see page A7].
MFS-23913

Materials

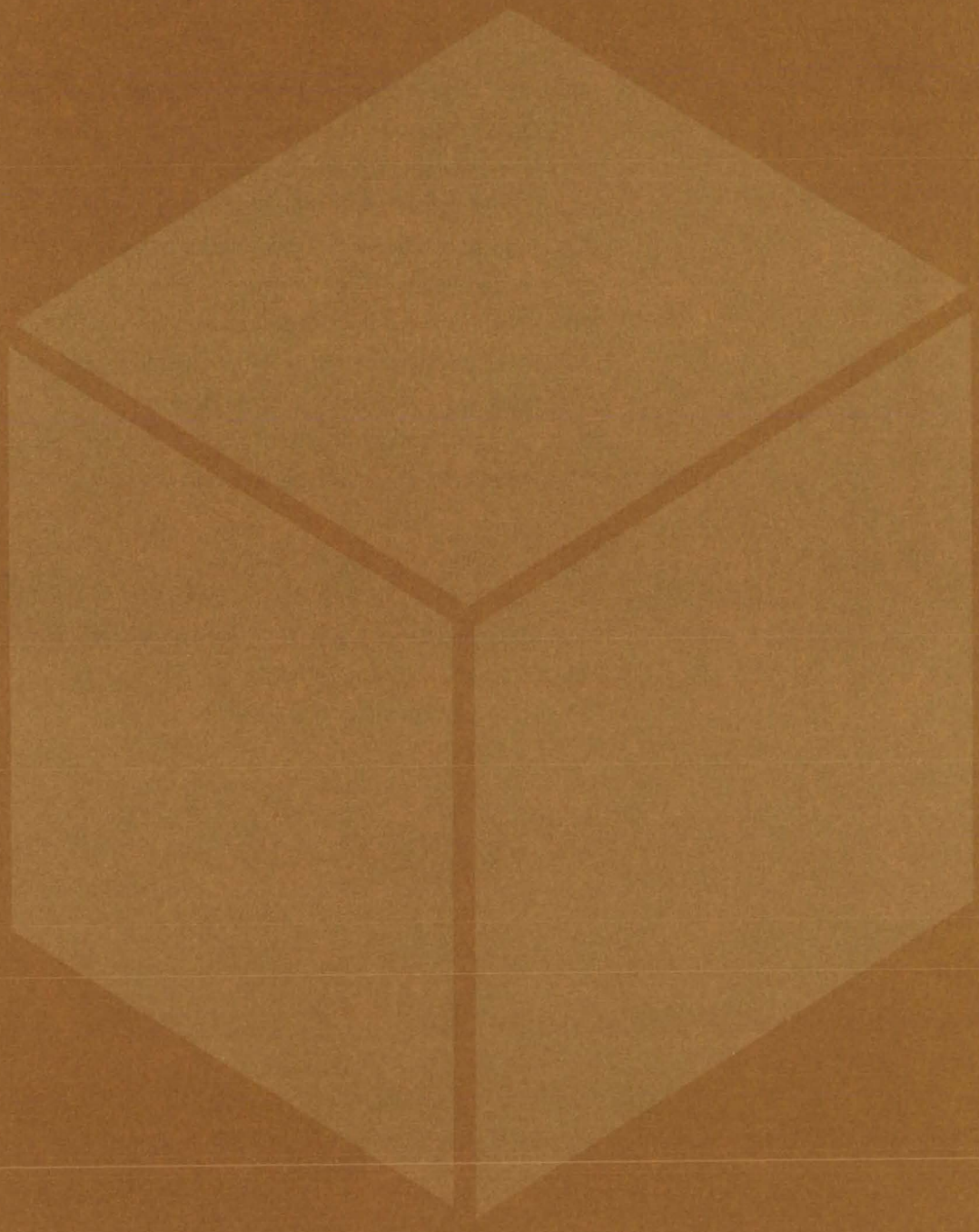

Hardware, Techniques, and Processes

223 High-Yield Process for Preparing Calcium Superoxide
224 Interactive Data-Processing System for Metallurgy
225 Fire-Retardant Epoxy Polymers
226 Compatibility of Au-Cu-Ni Braze Alloy With NH_3
227 Antistatic Additive for Polyimide Films
228 Brazed Boron-Silicon Carbide/Aluminum Structural Panels
229 Pulse-Echo Probe of Rock Permeability Near Oil Wells
230 Pressure-Sensitive Glass Reaction Cell
231 Improved Alkali-Metal/Silicate Binders
231 Improved Epoxy Adhesive With Radiographic Tracer
232 Repairing Silicon Carbide Coatings

Books and Reports

232 Corrosion Detection and Evaluation
233 Response of Graphite/Epoxy Composites to Moisture
233 Mechanical Properties of 18-2 Mn Stainless Steel
233 Nitronic 60: A New Alloy
234 Hydrogen Embrittlement of Nickel

High-Yield Process for Preparing Calcium Superoxide

Pressure and temperature are controlled precisely, and water is rapidly removed to inhibit back reaction.

Ames Research Center, Moffett Field, California

There is a present need for materials that can liberate large quantities of molecular oxygen upon their decomposition. These materials can be used as oxygen sources in self-contained or closed breathing systems.

Potential sources of oxygen include the alkaline earth-metal superoxides such as calcium superoxide; however, demonstrated yields for producing calcium superoxide range only from about 35 to 55 percent. Although higher yields have been reported, they have not been reproducible on a routine basis.

Calcium superoxide is generally prepared from calcium peroxide diperoxyhydrate, a compound that spontaneously undergoes a disproportionation reaction at temperatures between zero and 40° C:

$$2CaO_2 \cdot 2H_2O_2 \rightarrow Ca(OH)_2 + Ca(O_2)_2 + 3/2\ O_2 + 3H_2O$$

The low yield of the superoxide $Ca(O_2)_2$ is due to the tendency of the superoxide to react with water:

$$Ca(O_2)_2 + nH_2O \rightarrow CaO_2 \cdot xH_2O + (n - x)H_2O + O_2$$

The net yield depends upon variables including temperature, pressure, and the time allowed for the reaction to occur.

An improved apparatus for obtaining the superoxide in high yields removes the evolved water before it can react with the superoxide. This is done by condensing the water on a cold surface or sweeping the water away from the reaction site, and by controlling the pressure to increase the mean free path of the water molecules.

One form of the apparatus that has been successful in producing yields in excess of 70 percent is shown in the figure. The cross-shaped vacuum chamber contains the starting material and has a relatively large surface area to enhance evaporation of the evolved water. The calcium peroxide diperoxyhydrate is heated by an infrared lamp (or other heating element). The lamp and the controlled coolant keep the superoxide within 1° C of the optimum temperature. A cold surface, such as a cold "finger" cooled by liquid nitrogen, condenses the evolved water. In a variation of the apparatus, dry nitrogen gas is passed through the reacting material to sweep away the water as it is formed.

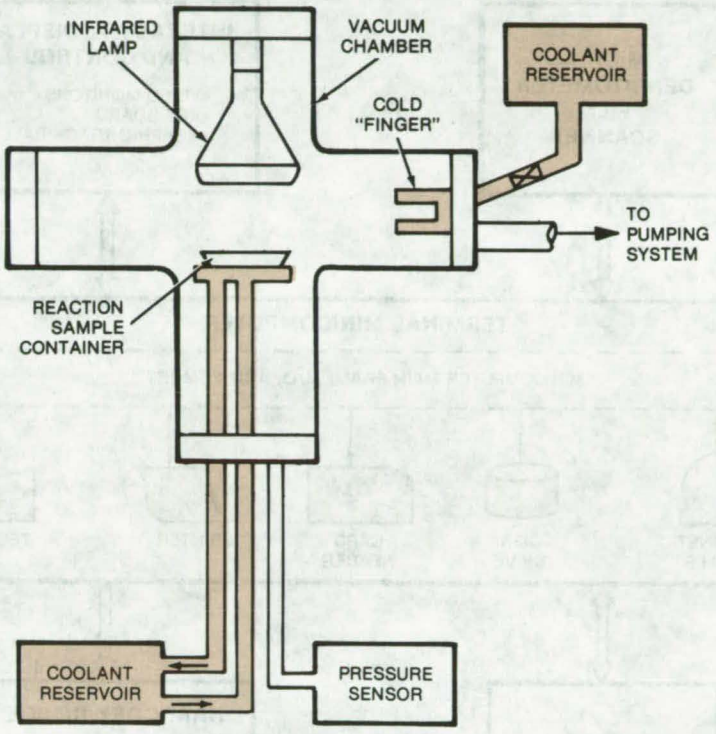

The Efficient Production of Calcium Superoxide is possible by using this apparatus. A temperature-control feedback loop (not shown) is included between a thermocouple in the reaction container and the infrared-lamp power supply; the pumping system would typically include a roughing pump and a cryopump capable of at least 4.0×10^{-3} m^3/s pumping speed at 11 microns pressure.

This work was done by Theodore J. Wydeven of **Ames Research Center** *and E. Vernon Ballou, LeRoy A. Spitze, and Peter C. Wood of San Jose State University. For further information, Circle 34 on the TSP Request Card.*

This invention is owned by NASA, and a patent application has been filed. Inquiries concerning nonexclusive or exclusive license for its commercial development should be addressed to the Patent Counsel, Ames Research Center *[see page A8].* *Refer to ARC-11053.*

Interactive Data-Processing System for Metallurgy

Image data can be rapidly analyzed for materials processing.

Marshall Space Flight Center, Alabama

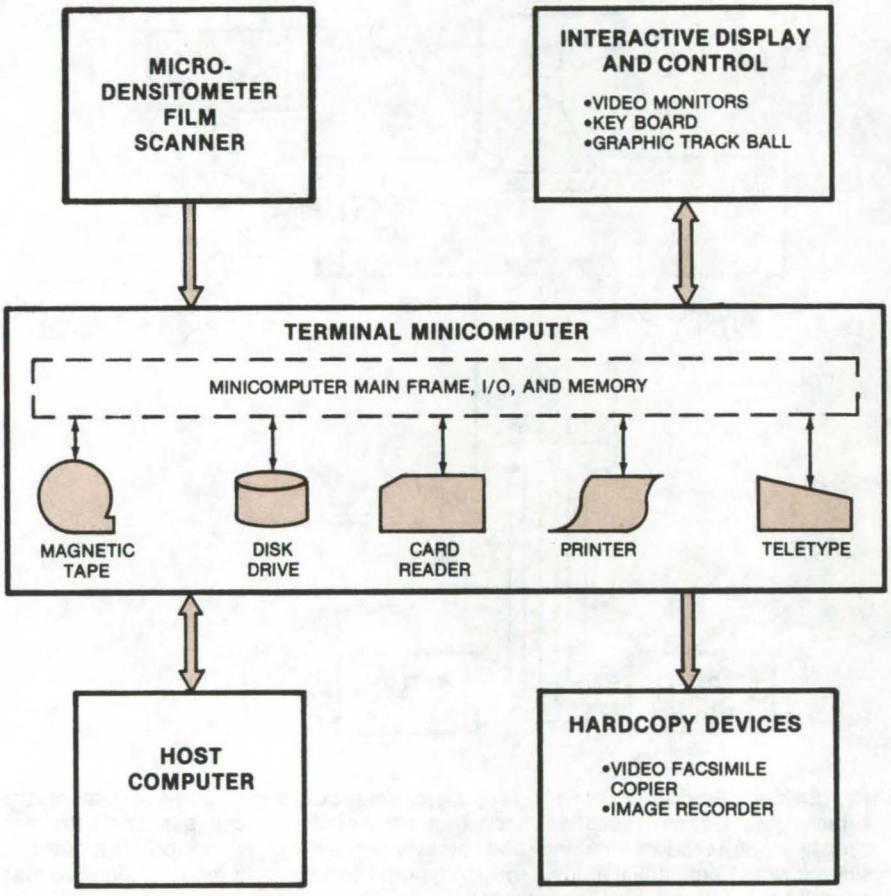

Interactive Data-Processing System can rapidly process image data for metallurgical experiments.

The Marshall Space Flight Center Image-Data Processing System (IDAPS), originally designed for the analysis of Skylab X-ray telescope data, has been used effectively to process and analyze the image data from several metallurgical experiments. These experiments, involving the properties of liquid metals in microgravity, indicate that a system like IDAPS can rapidly and accurately process metallurgical and materials-procesing data for a wide range of applications.

IDAPS (see figure) includes a host computer that is interfaced to the rest of the system via a terminal minicomputer. Data are acquired from photographic film by a microdensitometer. Some items on the "menu" of analytical subprograms contained in the system include linear and nonlinear image-scale adjustments, extractions, and insertions of parts of an image, gray-scale calibration, and image alterations and magnifications. Also included is a Fast Fourier Transform routine with associated filters (e.g., convolution, high- and low-pass). When the image analysis is complete, the results can be retrieved on a film recorder, "dumped" on magnetic tape, printed, or copied on a low-resolution video-facsimile machine. The user can select and combine the subprograms or, if necessary, develop his own programs.

Some of the advantages realized by using IDAPS in specific metallurgical experiments were as follows:

- **Study of Flow Between Liquid Metals in Low Gravity**
  IDAPS gave clear, qualitative images of the flow within each sample and allowed an easy comparison between samples. Details not seen in the original image were made visible by pseudocoloring. Three-dimensional qualitative information was extracted, and the extraction of three-dimensional quantitative data is possible.
- **Study of Surface Tension on Liquid Metals in Microgravity**
  Quick and accurate quantitative information was obtained on microscopic processes occurring within a large surface image. The extent of diffusion between and within samples was easily observed and quantified, allowing an accurate description of surface tension effects. A calibration curve was used to convert the image into units other than gray-scale values. When this can be done, many avenues are opened for extracting excellent information from the converted image (e.g., pseudocoloring, isograming, slicing, and histograming).
- **Microstructural Study of AlSb**
  IDAPS accurately and immediately retrieves quantitative information on the macroscopic processes occurring within a large surface image. The sample homogeneity, as determined by the area fraction of different phases present in the material, could be found simply by using the histogram operator on part or all of a microphotograph. Pseudocoloring of the photomicrographs gave improved contrast and eliminated unwanted surface artifacts. It is recognized that other specialized surface-analysis

machines can perform this type of analysis efficiently and accurately. Possible advantages of IDAPS over these machines could include the increase in contrast between areas on an image, the ability to analyze images via operator-written programs, and the space available for storing images. Perhaps by combining the strong features of several types of machines, a better way of analyzing surface images of metals could be found.

This work was done by Thomas J. Rathz of **Marshall Space Flight Center.** *Further information may be found in NASA TM-X-73379 [N77-23279], "The Application of Digital Techniques to the Analysis of Metallurgical Experiments," a copy of which may be obtained at cost from the New England Research Application Center* [see page A7].

MFS-23774

Fire-Retardant Epoxy Polymers

A phosphonate group in the polymer backbone improves the fire-retardant quality of epoxy compounds.

Ames Research Center, Moffett Field, California

A new type of epoxy resin for adhesives is fire retardant and will not support combustion. The fire-retardant property is attributed to the presence of phosphorus in the molecular structure.

The new polymer retains its adhesive strength, as opposed to fire-retardant polymers that use phosphate ester fluids. Phosphate ester is known to migrate to the adhesive interface and gradually reduce the adhesive bond strength. Also the new epoxy is transparent unlike the compounds using arsenic or certain inorganic compounds that retain bond strength but are opaque.

The general structure and preparation of the new class of compounds are shown in the figure. The products are produced by the reaction of allylphenols with alkyl or arylphosphonic dichloride, and this is followed by epoxidation which results in the general structure shown in the figure.

Other methods of preparation can be used provided that the products are of the type illustrated. The R and R′ groups in this molecule can be aklyl, aryl, alkaryl, aralkyl, and the like. In addition, R′ can be alkoxy or hydrogen.

Stoichiometric blends of adhesive prepolymers, used in this work, with curing agents such as m-phenylenediamine, aminoethylpiperazine, and the like provide cured products useful as adhesives or resins. Such compositions, for example, have been used here to bond polyvinylfluoride and polyether sulfone films onto polyimide glass laminates.

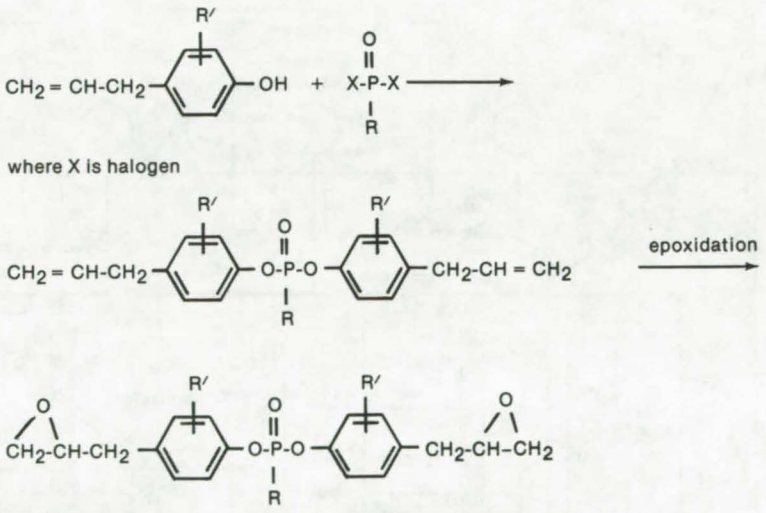

Phosphorylated Epoxy Resin is produced by the reaction of an allylphenol with an arylphosphonic dichloride, followed by epoxidation.

This work was done by Richard I. Akawie, Norman Bilow, and Thomas W. Giants of Hughes Aircraft Co. for **Ames Research Center.** *For further information, Circle 35 on the TSP Request Card.*

Inquiries concerning rights for the commercial use of this invention should be addressed to the Patent Counsel, Ames Research Center [see page A8]. *Refer to ARC-11182.*

Compatibility of Au-Cu-Ni Braze Alloy With NH_3

Tests show that Au-Cu-Ni braze alloy is compatible with ammonia systems.

Lyndon B. Johnson Space Center, Houston, Texas

The Au-Cu-Ni braze alloy is used in joining corrosion-resistant (e.g., 21-6-9 CRES) steel tubes that are used in various fluid systems. The alloy has relatively low brazing temperatures. This reduces the chances of excessive grain growth in the base metal as compared with higher temperature alloys. Joining the tubes by brazing has other advantages such as saving weight, as compared to mechanical joints, and cleanliness, because there are no chips or burrs as with mechanical connectors that may get into the fluid system.

With all these advantages, a major question had to be resolved whether this alloy would be compatible with ammonia, a common working fluid in refrigerators and other cooling systems. The question was focused on copper, which serves to promote wetting of the base metal but which also tends to react with NH_3 to form a soluble complex.

Tests were conducted on brazed CRES tubing (see figure) in liquid ammonia and ammonia diluted with water at a temperature of 71° C and a pressure of 2,200 psig (15.2×10^6

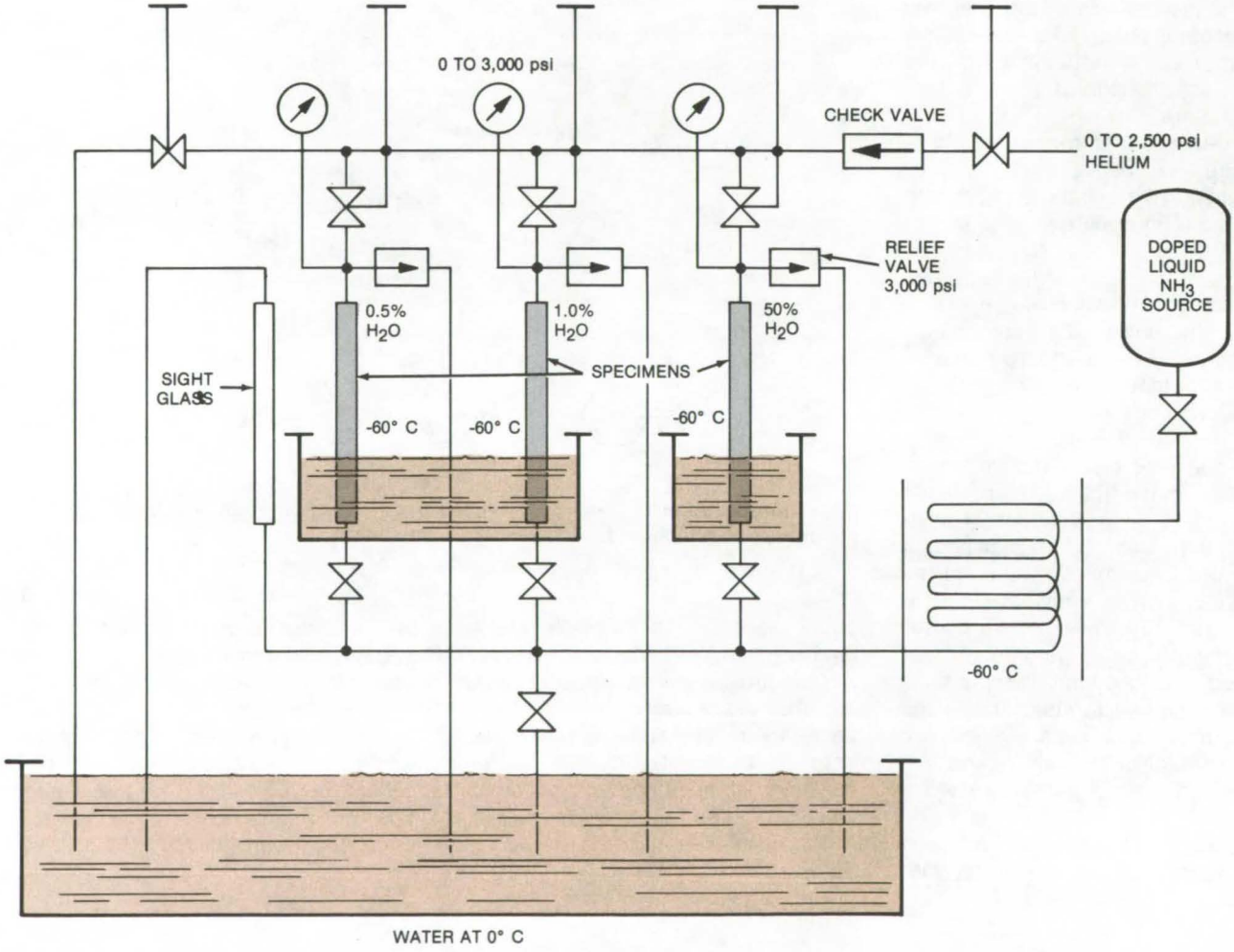

Test Setup for examining Au-Cu-Ni braze compatibility with ammonia is shown. The three brazed tubes were wrapped with heating tapes and insulated. Three separate proportional temperature controllers were used to maintain 71° C for the test duration. The tubes were filled with liquid ammonia at dry-ice temperature. The system was allowed to equilibrate before being pressurized to 2,200 psi with helium. During the test, the pressure was maintained to stress the sample tubes, and the temperature was monitored, using thermocouples attached to the sample tubes.

MECHANICAL PROPERTIES DATA		
Specimen	Ultimate Load (lb)	Ultimate Stress* (ksi)
Control -1	2,200	122.2
Control -2	2,230	123.9
0.5% H_2O - NH_3	2,230	123.9
1.0% H_2O - NH_3	2,250	125.0
50% H_2O - NH_3	2,240	124.4

*Stress data are based on tubing section (0.375-in. O.D., 0.343-in. I.D.). The dimensions are identical.

COPPER CONTENT OF AMMONIA AND RINSE WATER EFFLUENTS			
Specimen*	Copper Content (μg)		
	Rinse Water	Ammonia	Total
0.5%	31.6	25.0	56.6
1.0%	18.3	15.0	33.3
50%	54.3	175.0	229.3

*Specimens designated by water content of ammonia test media.

Test Results are shown for the sample tubes shown in the diagram. Following the 90-day exposure period, the brazed tubes were vented. The tubes were emptied, rinsed with distilled water, and dried for sectioning and subsequent examination. The rinse fluids were retained for copper determination by atomic adsorption spectrophotometry. Tensile strength was measured with Riehle tensile tested at 0.05 inch per minute.

N/m^2). Examinations of the sectioned braze joints and analysis of the residual ammonia for copper were performed to show any evidence of reaction with the brazed alloy. In addition, mechanical properties tests were run to show any change in the strength of the braze joints.

Results (see tables) show that no significant degradation occurred on brazed CRES tubing after a 90-day exposure, which indicates that the alloy is compatible with ammonia.

This work was done by Vernon Diaz, Jr., of Rockwell International Corp. for **Johnson Space Center.** *No further documentation is available.*
MSC-16864

Antistatic Additive for Polyimide Films

Lithium salts may keep thin polymeric films static-free at temperatures up to 300° C.

NASA's Jet Propulsion Laboratory, Pasadena, California

Thin polyimide films and other polar polymeric films are given excellent antistatic properties, even at high temperatures, by low-level loading with lithium salts. In contrast, the organic antistatic agents commonly used in polyimide films (quaternary ammonium compounds, amine derivatives, phosphate esters, derivatives of polyhydric alcohols, and polyglycol esters of fatty acids) are only marginally effective even at room temperatures. This is one reason that many household and industrial plastic films are quilted or ribbed (making it easier to handle them).

The lithium-loaded films retain their physical properties and smoothness, but their electrical conductivity is sharply raised so that electric charge is dissipated quickly. In addition, the radiation resistance of the films is expected to remain unchanged.

Films containing 1 to 10 percent by weight of lithium are being tested for thermal stability and antistatic behavior up to 300° C.

The lithium-filled films were originally developed for the NASA Solar Sail program, where a light, smooth, thin, static-free, radiation-resistant film was needed. They were selected since they are known to help solubilizing polymers in the textile industry and are expected to remain stable for very high temperature service. The low atomic weight of lithium makes a high concentration of dense positive ions possible with a fairly low weight penalty (compared, for example, with sodium or potassium salts).

When lithium nitrate was tried as an additive in a polyimide film, it produced remarkable results. The film was essentially static-free; it could be easily rolled and unrolled, without sticking to itself or adjacent surfaces. Its conductivity was greater than that of unfilled polyimide films, for a loading no greater than 10 percent by weight of lithium salt. Tests with lithium chloride produced similar results.

Lithium salts are extremely hygroscopic and apparently act as antistatic agents by absorbing a layer of atmospheric water. This layer provides a conductive path that allows charges to dissipate.

This work was done by Mohammad N. Sarbolouki of Caltech for **NASA's Jet Propulsion Laboratory.** *For further information, Circle 36 on the TSP Request Card.*
NPO-14232

Brazed Boron-Silicon Carbide/Aluminum Structural Panels

Process minimizes degradation of mechanical properties of composite.

Langley Research Center, Hampton, Virginia

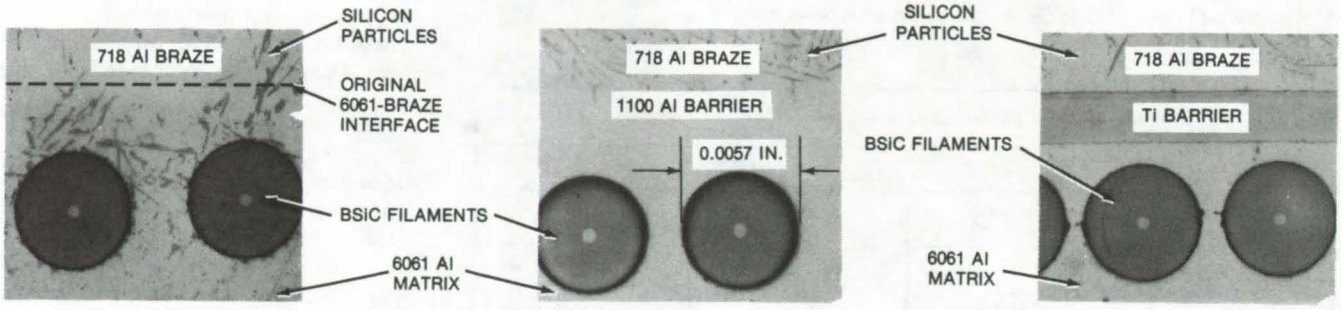

[a] CONVENTIONAL BSiC/Al-BRAZE INTERACTION. **[b] 1100 Al-CLAD BSiC/Al INTERACTION.** **[c] Ti-CLAD BSiC/Al INTERACTION.**

Metal-Matrix Interaction with the Braze Alloy is shown for a BSiC/Al composite. Conventionally, the braze alloy diffuses into the composite matrix and lowers its strength **[a]**; composite with an outer surface of 1100 Al **[b]** or a cladding of titanium **[c]** does not suffer the diffusion during brazing.

A fluxless brazing process developed at Langley Research Center minimizes degradation of the mechanical properties a composite material of silicon carbide coated boron fibers in an aluminum matrix (BSiC/Al). The process is being used to fabricate full-scale BSiC/aluminum-titanium honeycomb-core panels for Mach 3 flight testing on the NASA YF-12 aircraft and for ground testing in support of the Supersonic Cruise Aircraft Research (SCAR) program.

In the metal-matrix class of high structural efficiency composites, both B/Al and BSiC/Al have been under development for several years, but very few applications have been found because of high material costs and limited fabricability. Factors limiting fabricability are the hard and brittle nature of the boron and boron/silicon carbide filaments and degradation of the mechanical properties of the composites due to thermal processing.

In the current work, brazing was selected as the process with the greatest potential for fabricating efficient, complex structures; and BSiC/Al was selected rather than B/Al because it is less affected by exposure to the brazing environment. Initial attempts to join BSiC/Al by brazing resulted in severe degradation of mechanical properties of the composite. Metallurgical examination revealed that extensive interaction between the braze alloy and the constituents of the composite occurred during brazing. As in the photomicrograph (a) in the figure, silicon from the 718 aluminum braze alloy diffused into the composite to interact with both the BSiC filaments and the 6061 aluminum alloy matrix of the composite. Diffusion, or interaction, occurs because the brazing temperature of 1,100° F (595° C) exceeds the incipient melting temperature of the 6061 aluminum matrix by approximately 30° F (17° C), thereby permitting rapid liquid-phase diffusion between the brazing alloy and the matrix of the composite.

To alleviate the interaction problem, BSiC/Al was obtained with 1100 aluminum alloy on the outer surface of the composite. The 1100 aluminum was selected because its incipient melting temperature is approximately 100° F (55° C) higher than the brazing temperature. It would therefore serve as a diffusion barrier between the 718 aluminum alloy braze and the composite. The effectiveness of this concept is shown in the figure in part (b). The silicon particles of the braze alloy stop abruptly at the 1100 aluminum interface, showing that the braze-composite interaction was successfully prevented. This observation was verified by test data that indicated little or no degradation in the mechanical properties of the 1100 aluminum-clad BSiC/Al following brazing.

Using the 1100 aluminum clad BSiC/Al concept, BSiC/Al-titanium honeycomb-core panels for flight service evaluation on the NASA Mach 3 YF-12 airplane were fabricated. Picture-frame shear tests conducted on flight-qualification panels indicated that little degradation resulted from brazing. Ultimate shear strengths of 414 to 448 MPa (60 to 65 ksi) were realized in the brazed BSiC/Al skins during testing.

The diffusion barrier was further exploited by titanium cladding the BSiC/Al. A photomicrograph of Ti-clad BSiC/Al exposed to molten 718 aluminum braze alloy is shown in part (c) of the figure. The titanium cladding has been shown to offer increased wear and abrasion resistance as well as to provide an effective diffusion barrier. Titanium-clad BSiC/Al skin-stringer panels have been fabricated and are being evaluated prior to flight service testing on the YF-12 airplane.

This work was done by Winfrey E. Arnold, Jr., Thomas T. Bales, Troy G. Brooks, Ashby G. Lawson, Powell D. Mitchell, and Dick M. Royster of **Langley Research Center** *and H. Ross Wiant of Vought Corp. Further information may be found in NASA TM-X-3432, "Brazed Borsic/Aluminum Structural Panels," which may be obtained at cost from the North Carolina Science and Technology Research Center* *[see page A7]*.

LAR-12244

Pulse-Echo Probe of Rock Permeability Near Oil Wells

An acoustic technique determines the permeability of rock formations surrounding an oil-well borehole.

NASA's Jet Propulsion Laboratory, Pasadena, California

The ability to extract oil partly depends on the permeability to fluid flow of rock formations surrounding an oil-well borehole. One determinant of permeability is the porosity of the rock, which can be measured by a number of methods, including radioactivity, resistivity, and acoustic backscatter logging. However, porosity alone is not the only indicator. Low-porosity formations may also be permeable if there are microfractures in the rock that can provide short-range drainage and effective flow paths to the borehole.

In a new proposal, the acoustic backscatter signals would be processed to extract information about the microfracture environment at distances of up to 10 meters. The new processing method, which is similar to the pulse-echo technique used in materials testing, involves sequential insonifications of the borehole wall at a number of different frequencies. The return signals are normalized in amplitude, and the rms (root-mean-square) value of each signal is determined. These rms values can be processed to yield information on the size and the number density of microfractures at various depths in the rock matrix by using averaging methods developed for the pulse-echo technique. Several frequencies are used because the different pulse frequencies are sensitive to cracks of different sizes and can penetrate to different depths.

Figure 1 (top) shows the type of return signal obtained after an insonification burst. The decaying-amplitude envelope represents attenuation of the signal reflected from microfractures at different distances from the borehole. More distant fractures give signals that take longer to return and are therefore farther out on the time axis; they are also lower in amplitude because of spreading of the waves. The peak signals extending above the broken line represent reflections from large fractures or other solid objects (such as boulders).

A possible system for extracting the microfracture data is shown in Figure 2. The acoustic source is fed by a frequency generator controlled by the programer. The programer sets the duration of each burst and also sequences the designated frequencies of the search signal. The bursts are produced for discrete intervals followed by longer intervals of silence to obtain the reflection returns.

The signals gathered by the receiver are then processed by an amplifier having the response curve shown. The amplified signals are processed through a limiter that cuts off the large peaks at a level somewhat above the highest expected amplitude of the microfracture return signal. The normalized signals are then fed to an rms detector. The resulting data are either stored or displayed and are combined to determine the microfracture distribution. The processed signal is shown at the bottom of Figure 1.

This work was done by Keshavaiyengar Y. Narasimhan and Shakkottai P. Parthasarathy of Caltech for **NASA's Jet Propulsion Laboratory.** *For further information, Circle 37 on the TSP Request Card.*

Inquiries concerning rights for the commercial use of this invention should be addressed to the Patent Counsel, NASA Resident Legal Office-JPL [see page A8]. Refer to NPO-14192.

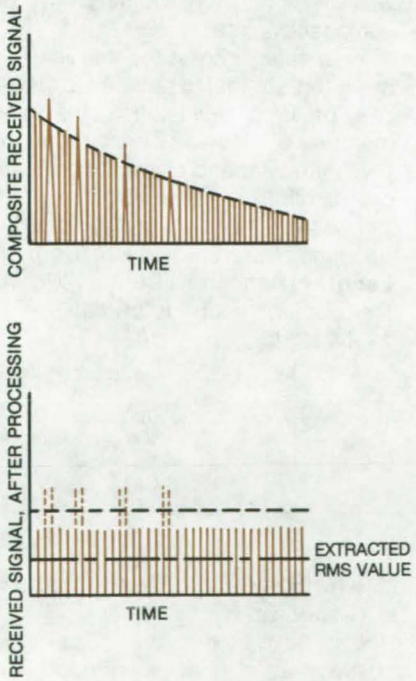

Figure 1. **Acoustic Backscatter Signal** (top) is clipped and normalized (bottom) to yield the rms value of the reflected signal from microstructural cracks (at a given frequency) around an oil-well borehole. Signals farther out along the time axis are the returns from the more distant fractures.

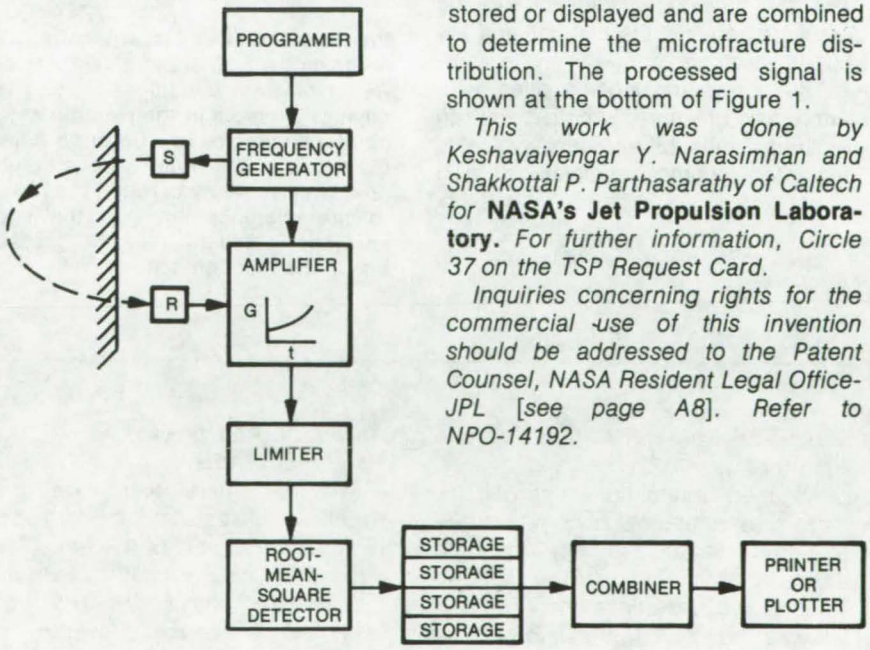

Figure 2. **Proposed Electronics** are shown in this block diagram. In the "combiner," conventional pulse-echo analysis used in the nondestructive testing of material is applied to the rms signals to yield the size and density of microcracks.

Pressure-Sensitive Glass Reaction Cell

Bourdon tube is used to measure pressure in sealed chamber.

Langley Research Center, Hampton, Virginia

Hydrazine fuel stored for lengthy periods is known to decompose slightly with time according to the following reaction:

$$2N_2H_4 \rightleftharpoons 2NH_3 + N_2 + H_2$$

The rate of decomposition is strongly influenced by the material in contact with the hydrazine.

To determine the catalytic effect of various materials on hydrazine decomposition, a special all-glass vessel has been developed. It was necessary because strain gages were not sensitive enough for this application and pressure sensors must be isolated from the reaction chamber. This device could be used in the laboratory to monitor pressure of other reactions as well.

The vessel as shown includes a gastight reaction cell that contains hydrazine with a test sample. The cell is connected to a Bourdon tube constructed of Pyrex, or equivalent, glass. The thin tube detects the differential pressure between the test cell and the upper envelope.

The upper envelope is filled with reference pressure supplied by an ordinary bottle of nitrogen, which is regulated to pressure below 20 psig (140×10^3 N/m^2). The Bourdon tube is sensitive to 0.1 psi (0.7×10^3 N/m^2) and is rated to withstand a 2-psi (14×10^3-N/m^2) differential pressure.

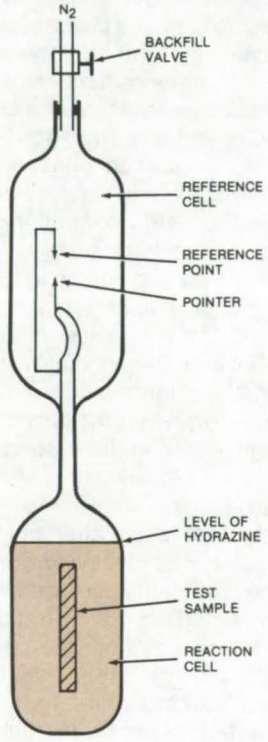

Pressure-Sensitive Glass Reaction Cell contains hydrazine and a test sample. As hydrazine decomposes and increases pressure in the reaction cell, a pointer connected to a Bourdon tube is distended to the right. The measured pressure necessary to return the pointer to the reference point in the upper envelope is identical to the pressure inside the reaction cell.

The decomposition rate of hydrazine is determined by periodically measuring pressures generated within the reaction cell. As the test sample causes hydrazine decomposition, the resulting gases raise pressure in the Bourdon tube, making the pointer move to the right. Once a week the upper cavity is filled with nitrogen through the backfill valve until the pointer returns to reference, indicating zero differential pressure across the Bourdon glass membrane. This indicates that the pressure in the upper envelope is equal to that in the cell. A standard pressure gage applied to the backfill valve will record this pressure, which will be proportional to the decomposition rate.

As a safety measure, the vessel is designed so that a sudden pressure rise or drop will cause the glass membrane to break, connecting the two chambers and distributing the gas over a relatively large volume.

This work was done by Robert T. Anselmi of Martin Marietta Corp. for **Langley Research Center.** *No further documentation is available.*
LAR-11256

Mass-Spectrometer Calibration Standard

An inert calibration material for mass spectrometers is a commercially available mixture of perfluorinated alkane and alkyl ethers. The liquid is volatile and noncontaminating, providing a series of reproducible reference peaks over a broad range of mass numbers from 1 to 200.
(See page 258.)

Antistatic Additive for Polyimide Films

Thin polyimide films are given excellent antistatic properties, even at high temperatures, by low-level loading with lithium salts. Extremely hygroscopic, these salts absorb a layer of atmospheric water that provides a conductive path allowing charges to dissipate.
(See page 227.)

Measuring Metallic Concentrations in Glycol Solutions

A study of atomic absorption spectroscopy as a possible nonobtrusive corrosion indicator for solar-energy systems is described in a new report. Procedures were tested for determining low levels of metallic concentrations in aqueous glycol formulations. Other methods for determining corrosion are suggested.
(See page 218.)

Improved Alkali-Metal/Silicate Binders

A process for producing stable, water-insoluble paint binders

Goddard Space Flight Center, Greenbelt, Maryland

Inorganic paint binders can protect ferrous metals and aluminum alloys from corrosion in salt environments better than most organic binders. Many alkali-metal/silicate inorganic paint compositions use ingredients such as lithium hydroxide to stabilize high silicon dioxide mole-ratio compositions and to provide a good water-insoluble coating immediately after drying. However, lithium compounds are expensive and degrade the adhesive qualities of the paint.

A new family of inorganic binders utilizes a potassium or sodium oxide/silicate dispersion and employs a high mole ratio of silicon dioxide to alkali-metal binder. They are stable, inexpensive, extremely water-resistant, and easy to apply. Moreover, no lithium compounds are required in the formulations.

The compositions are formed by mixing a starter alkali-metal/silicate solution with silicon dioxide hydrogel, water, and a silicone compound such as methyl trimethoxysilane. The starter solution is produced by taking silicon dioxide and potassium hydroxide and/or sodium hydroxide, adding water, and stirring while heating under pressure. The added silicone acts as a nucleation moiety for silicic acid during the mixing, forming a surface-hydrated and bulk-hydrated colloid. The final product contains a high molar ratio of silicon dioxide in the form of a hydrated sol, an alkali-metal oxide, water, and the silicone.

An easily prepared binder with a mole ratio of 5.3:1 and with an inorganic solids content of from 20 to 22 percent is composed of the following materials:

•potassium hydroxide:	4.53 to 4.99 percent
•silicon dioxide:	15.2 to 16.8 percent
•water:	77.0 to 79.1 percent
•methyl trimethoxysilane:	1.12 to 1.23 percent

Other compositions have silicon dioxide mole ratios ranging from about 4.8:1 to 6.01:1. The higher the mole ratio, the more water-insoluble the final product will be. However, as the mole ratio increases, the time required for the silicon to dissolve also increases.

This work was done by John Schutt of **Goddard Space Flight Center.** *For further information, Circle 38 on the TSP Request Card.*

This invention is owned by NASA, and a patent application has been filed. Inquiries concerning nonexclusive or exclusive license for its commercial development should be addressed to the Patent Counsel, Goddard Space Flight Center [see page A8]. *Refer to GSC-12303*

Improved Epoxy Adhesive With Radiographic Tracer

Tungsten powder enhances the radiographic contrast without degrading the epoxy flow properties.

Lyndon B. Johnson Space Center, Houston, Texas

Nonmetallic composites, such as fiber/resin matrix laminates and adhesive-bonded sandwich assemblies, sometimes contain air bubbles, fractures, delaminations, dimensional mismatches, and other defects. Radiography and ultrasonic inspection are often used to detect these defects and to evaluate the effectiveness of repairs.

The epoxy adhesives most often used for repairs are unfilled (i.e., they do not contain metallic fillers) and have low viscosity to help them flow into thin voids. In many cases, however, the adhesive layer does not absorb radiation sufficiently (in comparison to the composite material) to be detected in a radiograph. Moreover, ultrasonic methods may be unreliable, particularly for linear (ribbonlike) voids. Epoxy adhesives that contain metallic fillers (usually aluminum powder) are available; however, these compounds have a paste-like, high-viscosity consistency and do not readily flow into thin voids.

In an improved method for the nondestructive testing of nonmetallic structures, tungsten powder, in the amount of only 4 percent by volume, is added to a low-viscosity adhesive epoxy. The relative volume of tungsten is sufficiently small so that the epoxy retains its low viscosity and flows readily into voids, yet the tungsten is sufficiently large in relative mass (40 percent by weight) to give good radiographic contrast for X-ray inspection and to improve the resolution of ultrasonic testing.

The repair material is prepared by mixing a commercially-available low-viscosity epoxy adhesive with tungsten powder. In one application, the mixture was heated to approximately 110° F (43.3° C) to improve its flow properties and then was introduced into the void by using a hypodermic syringe.

This work was done by Robert G. Campbell of McDonnell Douglas Corp. for **Johnson Space Center.** *No further documentation is available.*

Inquiries concerning rights for the commercial use of this invention should be addressed to the Patent Counsel, Johnson Space Center [see page A8]. *Refer to MSC-18020.*

Repairing Silicon Carbide Coatings

A simple technique uses commercially available materials for repairing silicon carbide coatings.

Lyndon B. Johnson Space Center, Houston, Texas

Silicon carbide coatings, usually applied by vapor deposition, improve the oxidation resistance, wear, and chemical resistance of carbon-carbon parts by a factor of 4 or more. The coated carbon is used in alloying and brazing fixtures, epitaxial furnace susceptors, crucibles, and in ceramic composites. A relatively simple procedure has now been developed for repairing coated carbon-carbon parts when the coating has been damaged.

The repair procedure uses a commercial binder (Sermetel Sermabond Liquid, or equivalent) that contains a blended powder mixture. The powder blend, also commercially available, comprises a 50/50 mixture by weight of RA 1200 silicon carbide (green or black) and ground silicon carbide felt material. The silicon carbide felt is a graphite felt that has been converted to silicon carbide. It is a byproduct of a standard coating process and is blended and ground in a ball mill prior to the addition of the RA 1200 silicon carbide.

The resulting slurry is applied at points where the coating has been damaged. After curing, the repaired area is impregnated with tetraethylorthosilicate (TEOS) to seal any porosity that develops during the curing procedure. The TEOS is subsequently converted to silicon oxide at 600° F (315° C). The resulting coating gives more strength and reduces craze of the repaired area, prolonging the service life of the carbon parts.

This work was done by David M. Shuford of Vought Corp. for **Johnson Space Center.** *No further documentation is available.*
MSC-18033

Books and Reports

These reports, studies, and handbooks are available from NASA as Technical Support Packages (TSP's) when a Request Card number is cited; otherwise they are available from one of NASA's Industrial Application Centers or the National Technical Information Service.

Corrosion Detection and Evaluation

A study of nondestructive methods of detecting and evaluating corrosion

A 90-page report details a comprehensive study of nondestructive methods for detecting and/or evaluating up to six different types of corrosion: general, galvanic, filiform, pitting, intergranular, and stress corrosion.

Among the nondestructive methods examined in the study were:

- visual/optical (direct-viewing) inspection,
- radiography,
- penetrant inspection,
- analysis by polarized light,
- electrical conductivity (eddy-current) measurements,
- pH analysis,
- chemical spot tests,
- visual/optical (remote-viewing) inspection, and
- ultrasonic tests, including compression-wave, delta-principle, shear-wave, and surface-wave.

Results of the study indicate that except for areas that have both surfaces readily accessible for direct observation by visual/optical methods, most of the methods require skilled technicians or engineers to perform the analysis. Surfaces that are readily accessible are best examined by visual/optical inspection techniques. Difficult-to-reach surfaces can be inspected by using remote-viewing probes and closed-circuit television.

Penetrant-inspection techniques are successfully used to detect pitting and crack corrosion. They are limited by possible contamination of an area by the penetrant and the inapplicability of the method on rough surfaces that would prevent effective post-cleaning operations.

Polarized light is effective for detecting scratches in protective coatings, which could lead to corrosion. Electrical conductivity, radiography, and radiation-scintillation techniques are used primarily in detecting structural cracks that are frequently the result of corrosion.

Chemical spot tests and pH analysis are not used in the direct detection of corrosion. Rather, they are used to establish the activity and presence of corroding agents.

Ultrasonic techniques, in which the wave mode is optimized for the specific conditions of each test, are probably the best overall method of detecting and evaluating the effects of corrosion, provided access is possible for the ultrasonic transducers. A wide range of materials can be inspected, and most types of corrosion effects can be detected.

Data accumulated during the study also revealed potential methods for measuring material property changes caused by corrosion, fatigue, and heat treatment. Three such methods are ultrasonic velocity measurement, real-time X-ray diffraction, and eddy-current measurement.

This work was done by Calvin C. Kammerer, Fred H. Stuckenberg, and Frank E. Sugg of Rockwell International Corp. for **Marshall Space Flight Center.** *For further information, Circle 39 on the TSP Request Card.*
MFS-24436

Response of Graphite/ Epoxy Composites to Moisture

Comparative absorption and desorption data for three epoxy matrix composites

The effect of moisture on the high-temperature strength of graphite/epoxy composites is an important design parameter. Moisture is known to lower the glass-transition temperature of epoxy composites, thereby diminishing the strength of critical properties of the matrix at temperatures above the reduced glass-transition temperature.

A report presents comparative absorption and desorption data obtained from experiments with Fiberite 934, Narmco 5208, and Hexcel F-263 epoxy-resin systems in cross-piled collimated laminates containing Thornel-300 graphite fibers. In these experiments, samples were moisturized at 140° F (56° C) and 95 percent relative humidity over arbitrary exposure periods from 31 to 38 days; they were dried at 250° F (120° C) for 11 days. In addition, Fiberite 934/T-300 laminates were humidified to 0.6 percent, 0.8 percent, and 1 percent moisture levels and then were thermally spiked at 350° F (175° C) up to 100 times. The moisture response of thermally spiked specimens was compared with that of the unspiked specimens.

Results of the study show that all three composites are similar in their response to moisture; thus, a common set of values may be used in preliminary predictions of performance for all three systems. Resin content, it was determined, is a significant variable in absorption and desorption. Another finding shows that the ratio of edge-to-surface area of a composite may significantly impact absorption and desorption rates unless the edges are effectively sealed. Finally, the moisture response of Fiberite 934/T-300 is not as severely affected by 100 thermal spikes occurring at moisture levels of up to 1 percent, as had been originally thought.

The report includes a number of graphs and tables to explain the results.

This report was written by Howard Powell and Denis J. Zigrang of Rockwell International Corp. for **Johnson Space Center.** *To obtain a copy of the report, Circle 40 on the TSP Request Card.*
MSC-16899

Mechanical Properties of 18-2 Mn Stainless Steel

Behavior under cryogenic and corrosive environments

The mechanical properties of 18-2 Mn (Nitronic 32) stainless steel are detailed in a report released by Marshall Space Flight Center. The report includes experimental data obtained at cryogenic temperatures and data on stress-corrosion resistance at ambient temperatures. Hot-rolled, centerless-ground bar material was used in the tests.

The 18-2 Mn steel is a member of a new family of stainless steels in which manganese and nitrogen are substituted for part of the usual nickel content [see related article "Mechanical Properties of Low-Nickel Stainless Steel" (MFS-23543) on page 494, Vol. 2, No. 4, of *NASA Tech Briefs.*] This is an iron-based alloy containing approximately 18 percent Cr, 1.6 percent Ni, 12 percent Mn, 0.5 percent Si, 0.1 percent C, and 0.34 percent N. Hot-rolled bars of 18-2 MN are unusually strong and resist corrosion and galling. The alloy is lighter than most stainless steels and less expensive than type 304.

Some general conclusions in the report are:

- 18-2 Mn can be used where the corrosion resistance of a 300-series stainless steel is needed, but additional strength is required; and
- It can be used in tension applications at temperatures as low as -200° F (144 K).

The mechanical tests were conducted at several temperatures ranging from 75° F (297 K) to -423° F (20 K). Smooth specimens were tested for ultimate strength, modulus of elasticity, elongation, and reduction of area. Notched specimens were tested to determine notched tensile strength, notched/unnotched tensile-strength ratio, and Charpy impact strength.

The properties of the smooth specimens improved with decreasing temperature. However, the notched specimens showed the opposite behavior: Properties degraded moderately as temperature dropped below -200° F and drastically between liquid-nitrogen and liquid-hydrogen temperatures. Samples under tension became greatly elongated and their areas greatly reduced below 144 K. The Charpy V-notched impact energy decreased steadily as the temperature dropped.

In the stress-corrosion tests, bars and C-rings were exposed to periodic immersion in a salt solution, high humidity, and salt spray while stressed at 75 and 90 percent of yield strength. The bars showed no corrosion in the tests. Only minor effects were noted on the C-rings: shallow etching from immersion and pitting from the salt spray. No evidence of the "branching" associated with stress corrosion could be found when the test specimens were examined metallographically.

This work was done by J. W. Montano of **Marshall Space Flight Center.** *Further information may be found in NASA TM-X-73375 [N77-21214], "The Stress Corrosion Resistance and the Cryogenic Temperature Mechanical Properties of Hot Rolled Nitronic 32 Bar Material," a copy of which may be obtained at cost from the New England Research Application Center* *[see page A7]*.
MFS-23843

Nitronic 60: A New Alloy

Tests demonstrate attractive mechanical and stress-corrosion properties down to very low temperatures.

Mechanical and stress-corrosion properties of Nitronic 60 stainless-steel alloy are presented in a report of tests performed at NASA's Marshall Space Flight Center. Nitronic 60 is another member of a family of stainless steels in which manganese and iron are substituted for part of the usual nickel content.

This alloy, with a composition of 17 percent Cr, 8.5 percent Ni, 8.0 percent Mn, 3.5 percent Si, 0.07

percent C, and 0.1 percent N, has high yield strength, good corrosion resistance, and excellent antigalling properties. It is also slightly lighter than most stainless steels, and has good metal-to-metal abrasion resistance, excellent oxidation resistance, and subzero impact strength.

The mechanical tests were performed at temperatures ranging from 70° F (24° C) down to -423° F (20 K) on specimens manufactured from an annealed bar 1.00 in. (2.54 cm) in diameter. A variety of conclusions can be drawn from the test results. The alloy can be applied in tension applications at temperatures ranging from ambient down to liquid-hydrogen (20 K). The material is suitable for use at liquid-hydrogen temperature even though ductility decreases considerably in that range.

Stress-corrosion tests involved 180-day alternate immersion, humidity, and salt-spray tests on longitudinal tensile and transverse C-ring specimens. The alloy showed excellent resistance to stress-corrosion cracking when tested in the longitudinal direction, even when stressed to 90 percent of the 0.2-percent yield strength. However, this was not the case for the C-rings. Their design made them vulnerable to an end-grain attack that caused pitting after they were exposed to alternate immersion and salt spray. Metallurgical examination of the surface pits revealed the branching phenomenon associated with stress-corrosion cracking.

Stress-corrosion tests were also performed on transverse tensile specimens. These were stressed to 90 percent of yield strength and were exposed for 90 days to alternate immersion and salt spray. There were no failures.

The report includes design details of the alloy specimens and the test procedures. Four tables describe the chemical properties of Nitronic 60 and the measurements made during smooth and V-notched tensile and Charpy V-notched impact tests. Also included are drawings of the test specimens and microphotographs of the alloy.

This work was done by J. W. Montano of **Marshall Space Flight Center.** *Further information may be found in NASA TM-X-73359 [N77-16149], "The Stress Corrosion Resistance and the Cryogenic Temperature Mechanical Properties of Annealed Nitronic 60 Bar Material," a copy of which may be obtained at cost from the New England Research Application Center [see page A7].*

[See related articles "Mechanical Properties of 18-2 Mn Stainless Steel" [MFS-23843] the preceding article in this issue and "Mechanical Properties of Low-Nickel Stainless Steel" [MFS-23543] on page 494, Vol. 2, No. 4 of NASA Tech Briefs.]
MFS-23844

Hydrogen Embrittlement of Nickel

Report on a comprehensive study

A new report describes a comprehensive study of hydrogen embrittlement in high-purity single-crystal and polycrystalline nickel at temperatures from -130° to 20° C. Because hydrogen embrittlement is a serious problem in the metallurgical and chemical industries (in coal gasification, for example, embrittlement can cause structural failure of gasification reactors), the report should be valuable to workers in these fields.

The report details the results of studies of the behavior under tension of the nickel specimens. Briefly, the findings are:

- Notched single crystals are severely embrittled by hydrogen. The reduction in elongation to failure is roughly 35 percent.
- Smooth single crystals are not embrittled (instead, they fail by ductile shear).
- Coarse-grained polycrystals are embrittled, failing by intergranular separation.
- Fine-grained polycrystals are apparently not embrittled.

From the experimental data, it is suggested that molecular hydrogen dissociates to monatomic hydrogen on "clean" surfaces created by plastic deformation under tension. A clean surface may form near a crack tip, for example. In this model, the action of the monatomic hydrogen at the clean surface reduces cohesion in the nickel and thereby embrittles it.

For the study, rods of single-crystal nickel were grown in an electron-beam, floating-zone furnace. Tensile-test specimens (2- by 1.4-millimeter cross sections, 2-centimeter-long gage sections) were cut from the rods.

The polycrystalline tensile-test specimens (3- by 1.5-millimeter cross sections, 15-millimeter gage lengths) were machined from nickel sheet. The specimens were heat treated at 900° C for 5 hours to produce fine grains (about 0.001-millimeter grain size) or at 1,100° C for 70 hours to produce coarse grains (about 0.1-millimeter grain size).

Specimens were tested in a stainless-steel chamber installed in a tensile-test machine. The chamber was filled with hydrogen (or nitrogen) at 550 torr (Tests were done in hydrogen and in nitrogen for comparison.) The chamber was cooled by liquid nitrogen.

Each specimen was tested in tension to failure at a displacement rate in the range of 0.0005 to 100 cm/min at a given temperature between -130° and 20° C. Elongation at failure was determined from a load-displacement curve. Fractured specimens were examined optically and in a scanning electron microscope.

This work was done by M. H. Kamdar of **Ames Research Center.** *To obtain a copy of the report, Circle 41 on the TSP Request Card.*
ARC-10966

Life Sciences

Hardware, Techniques, and Processes

237 Rapid Measurement of Bacteria in Water
238 Monitoring System for Community Water Supplies
240 Data Processing for Water Monitor System
241 Water Sample-Collection and Distribution System
243 Automated Electrochemical Detection of Coliforms
244 Chemiluminescence and Bioluminescence Microbe Detection
245 Chemical Measurement of Urine Volume
246 Artificial Leg With Natural Gait
247 Boosting Production Yields of Biomedical Peptides
248 Positively Charged Membrane for Urea Dialysis
248 A Probe for Blood-Vessel and Spinal Interiors
250 Stacked Solar Cells Measure X-Ray Exposure
251 In Vivo Blood-Flow Mapping
252 Biological Sampling and Cleaning Device
253 Automatic Primate Feeder
253 Improvements in Microelectrophoresis Apparatus

Rapid Measurement of Bacteria in Water

Automated system quantitatively determines live and dead bacterial concentrations within a few hours.

Goddard Space Flight Center, Greenbelt, Maryland

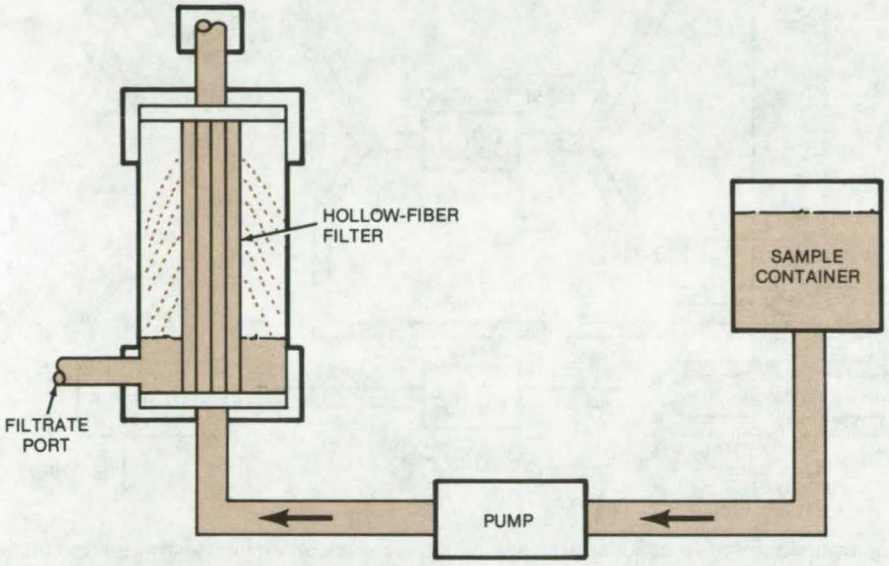

Figure 1. Hollow-Fiber Concentrator uses a commercially-available hollow-fiber bundle to separate bacteria from the aqueous sample. The sample is pumped at about 15 psi (105×10^3 N/m^2) to force the water through the fiber wall and out the filtrate port. After the water is removed, the filters are backwashed with sterile deionized water pumped through the effluent port.

An automated analysis system has been designed for detecting bacteria in saltwater, freshwater, sewage effluent, and other aqueous media. This system was used in the design of NASA's water monitor system described on page 238 of this issue. It could, of course, be used with some variations in clinical environments and other water-testing applications.

The system concentrates bacteria in a water sample with a hollow-fiber filter/concentrator. Then, bioluminescent and chemiluminscent techniques are used to measure live and dead bacteria. The samples are moved through the system and analyzed automatically. The light emitted by the luminescent reactions is measured by a photometer that outputs a signal representative of bacterial concentrations.

Typically, the sampled water will be prefiltered to remove macroparticles. However, some bacteria may be filtered out by this step, and its advisability will depend upon the particular applications. The prefiltered sample is next concentrated in a hollow fiber as illustrated in Figure 2. Pressure is used to force water out of the closed system while retaining the filtered bacteria. The filters are backwashed under pressure to remove the bacteria. The concentrator can reduce a 10-liter sample to 100 ml (100 to 1).

For samples containing saltwater bacteria, a vacuum membrane filter is used. Saltwater bacteria are easily destroyed under the pressure used in the hollow-fiber filter concentration and are damaged by the freshwater backwash.

The two assay techniques, bioluminescence and chemiluminescence, use 10-ml portions of the concentrated sample. The bioluminescence is a test for the adenosine triphosphate present in all life forms. The cells are ruptured by treatment with nitric acid solution and are reacted with the firefly enzyme luciferase and with luciferin in the presence of a divalent metal ion such as magnesium. The reaction is carried out in a lighttight chamber containing a photocell, and the amount of light emitted is related to the amount of ATP and thus the number of bacteria present.

The assay is performed on a blank, a standard with a known amount of bacteria, and on the sample. These readings are compared to obtain a quantitative measure of the bacteria present.

The chemiluminescent method used is an assay for iron porphyrins, which are present in bacteria and also in solution in the sample. As in the ATP method, a blank and a standard are used. A luminol reagent, dilute hydrogen peroxide, and sodium hydroxide are reacted with the sample. The emitted light is not measured until 6 seconds after luminescence begins. This circumvents the effects of the inorganic iron in solution, which are "used up" in the first 6 seconds of the reactions. After this period, the emitted light is related to nonporphyrins only.

When the sample is pretreated with hydrogen peroxide, iron porphyrins in both live and dead bacteria react. If the sample is treated by bubbling through carbon monoxide, only the iron porphyrins in the dead bacteria react to produce light. Thus the two types of assays may be used to determine the viability of the bacteria, as well as their quantity.

Automated systems have been designed for concentration of the sample and the various assays. As was actually done with NASA's Water-Monitoring System, this type of system can be adapted for computer control. Figure 2 illustrates the portion of the automated system for the chemiluminescence test. Reservoirs containing the test sample, a blank solution, and a standard are sequentially sampled with a system of valves and peristaltic pumps. The sample is pretreated with hydrogen peroxide and then mixed with the luminol reagent. The light emitted is measured in a photometer.

(continued next page)

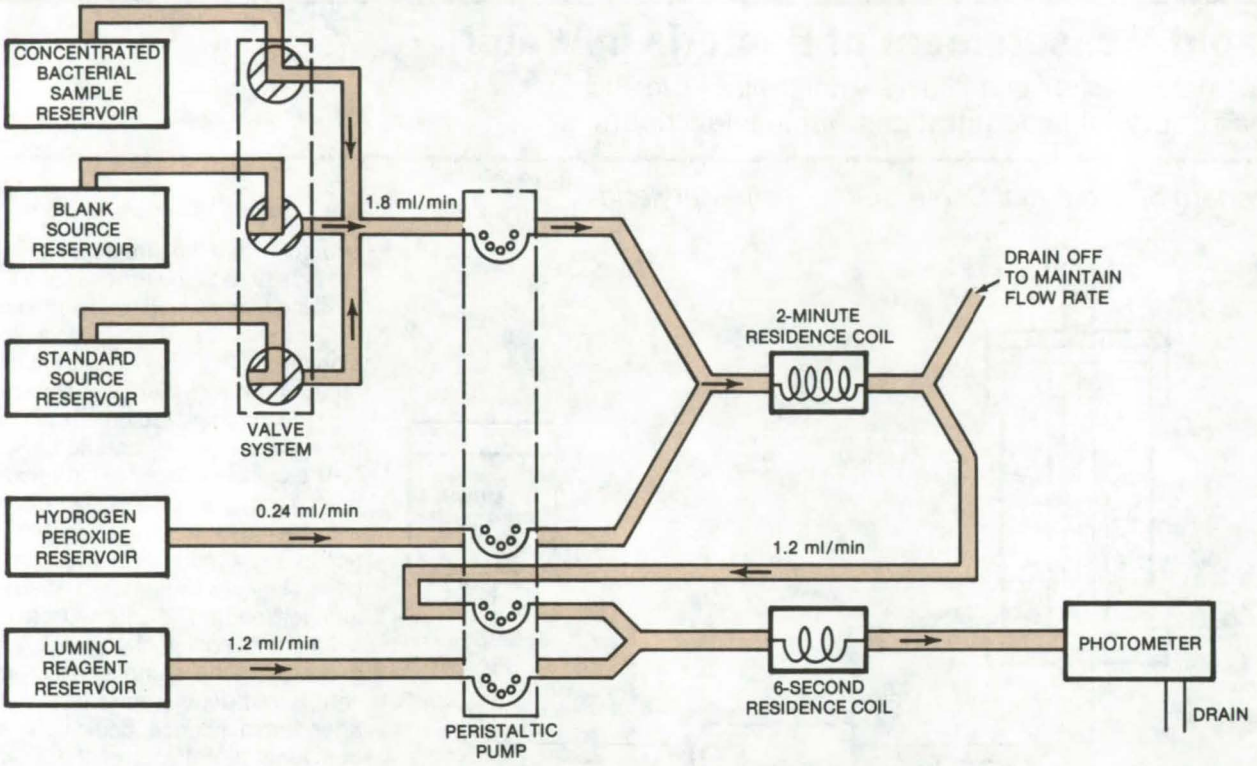

Figure 2. **Automated Chemiluminescence Apparatus** analyzes a concentrated sample of bacteria-containing freshwater and blank and standard solutions. A valve system selects the sample that is mixed with hydrogen peroxide and pumped through a 2-minute residence coil to allow time to complete the pretreatment. The pretreated sample is mixed with luminol reagent and pumped through a 6-second residence coil to allow all of the soluble metal-ion iron porphyrins to react. The remaining light-emitting reaction occurs in the photometer cell, where the light produced depends on the number of live and dead bacteria present.

This work was done by Emmet Chappelle, Jody Deming, and Grace L. Picciolo of **Goddard Space Flight Center** *and Eldon Jeffers and Richard R. Thomas of The Boeing Aerospace Co. For further information, Circle 42 on the TSP Request Card.*

This invention is owned by NASA, and a patent application has been filed. Inquiries concerning nonexclusive or exclusive license for its commercial development should be addressed to the Patent Counsel, Goddard Space Flight Center [see page A8]. *Refer to GSC-12158.*

Monitoring System for Community Water Supplies

Integrated system of sample collectors, sensors, analyzers, and data-acquisition and display equipment automatically monitors water quality.

Lyndon B. Johnson Space Center, Houston, Texas

In many areas of the United States, city planners are seriously considering facilities for the reconversion of waste water into safe, potable water to be reintroduced into the water supply. A key requirement for such a system is the thorough and continuous monitoring of the water quality. These water reclamation systems now under development are not the only requirements for improved water-quality monitoring. With today's increased population and industrial activity, many existing water-supply systems are becoming more subject to possible contamination, and continuous monitoring may become increasingly necessary in numerous municipalities.

NASA has faced related problems in monitoring water recovered in closed-loop systems such as spacecraft cabins. Because the National Aeronautics and Space Act of 1958 directs NASA to make the widest possible dissemination and transfer of aerospace technology, efforts have been undertaken to apply aerospace water-monitoring technology to the needs of community water supplies. At the Lyndon B. Johnson Space Center, in Houston, Texas, NASA has established, in cooperation with the Department of Housing and Urban Development, a test facility to develop an automated water-quality monitoring and control system to insure the safety and quality of treated waste water.

This water-monitoring system (WMS) includes equipment and tech-

NASA's Water Monitor System is installed in a mobile trailer that houses the data-acquisition system, sensors, sample conditioning/distribution system, and the report generation system.

niques for collecting samples of waste water; sensors for determining the level of micro-organisms, oxygen, chlorine, and many other important parameters; and a data-acquisition and display system that allows the information about the water quality to be computed and displayed to operating engineers in real time. This system, along with many of its component parts, is described in this and several other articles in this issue of *NASA Tech Briefs*. In addition, documentation describing the WMS in more detail can also be obtained as explained at the end of this article.

The entire system is currently installed in a mobile trailer at the Johnson Space Center in Houston, Texas, as shown in the figure. Major elements are described below.

- **Data-Acquisition System** (DAS) — The DAS comprises two separate data-collection and display subsystems: a computer and a back-up hard-wired, fixed-format device. Using preprogramed decisions, the computer initiates water sampling and up to 40 analog measurements of water quality. The resulting data are collected, sorted, and converted into displayed parameters. The information is also stored in the memory where it is directly accessible for at least 24 hours.
- **Sample-Collection and Distribution System** — The sample-collection and distribution system is designed to take test samples at six different locations throughout a waste-water treatment facility. Both filtered and unfiltered portions of the collected sample are delivered quickly to the various analytical sensors.
- **Sensors** ("Nonbiological") — Water samples are directed to several sensors. These include sensors for "nonbiological" parameters, including total organic carbon, total oxygen demand, pH, Cl^-, NH_4^+, Na^+, hardness, dissolved oxygen, turbidity, nitrate, specific conductance, and total residual chlorine. Most of these are commercially available devices that have been integrated into the WMS.
- **Biosensors** — Rapid sensors for the detection of micro-organisms in on-line flow sensors are an area of interest for many applications, but satisfactory real-time sensors are not now generally available. Using techniques developed for the detection of extraterrestrial life on unmanned planetary missions, NASA scientists have developed three nearly-real-time biological sensors for online flow systems. These "biosensors" employ three different approaches for the detection of microbes. Chemluminescence and bioluminescence sensors utilize photomultiplier tubes to sense light emitted by the reaction of cells with the respective reagent. The chemiluminescence sensor detects total bacteria, living and dead, by measuring the light emitted when bacterial porphyrins catalyze a luminol/hydrogen peroxide reaction. The bioluminescence sensor detects the ATP in living cells by measuring the light emitted in a biochemical process emulating the firefly. A third, electrochemical, sensor detects coliform, either total or fecal, by measuring with an electrode the hydrogen gas produced as a byproduct of metabolism.

This work was done by Reuben E. Taylor of **Johnson Space Center** *and Richard R. Brooks, Eldon L. Jeffers, Arthur T. Linton, and Gerald D. Poel of The Boeing Aerospace Co. Additional documentation, NASA TM-X-58179 [N77-13909], "Water Monitor System: Phase I Test Report" [$5.50], may be obtained [prepayment required] from the National Technical Information Service, Springfield, Virginia 22151. For further information, Circle 43 on the TSP Request Card.*

This invention is owned by NASA, and a patent application has been filed. Inquiries concerning nonexclusive or exclusive license for its commercial development should be addressed to the Patent Counsel, Johnson Space Center [see page A8]. Refer to MSC-16778.

Data Processing for Water Monitor System

Data acquisition, storage, and processing
for water-quality instrumentation

Lyndon B. Johnson Space Center, Houston, Texas

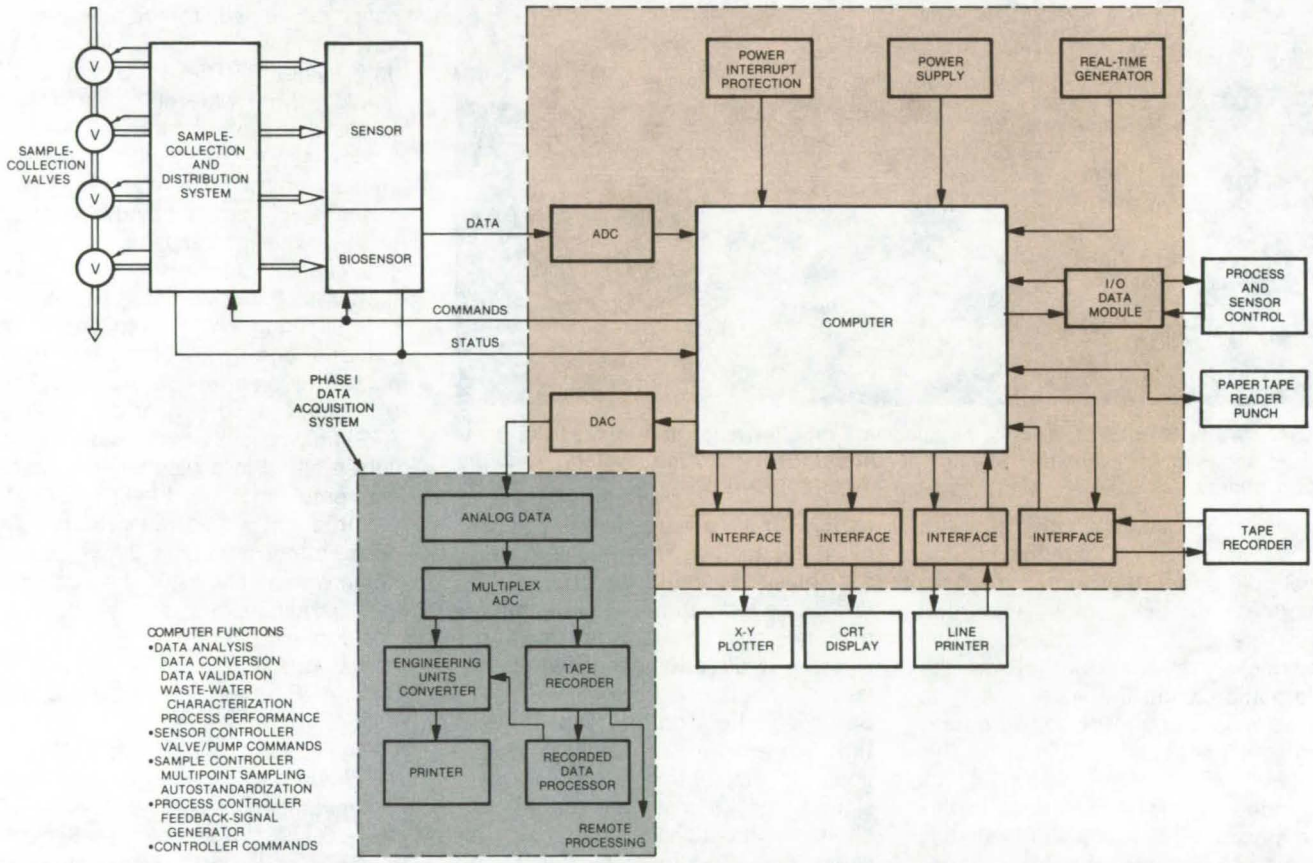

Figure 1. The **Water-Monitoring Data-Acquisition System** is structured about a central computer that controls sampling and sensor operation and analyzes and displays data in real time. A hard-wired backup system, the Phase I Data-Acquisition System, can be used independently or as a backup.

The data-acquisition equipment used with the water monitor system described on page 238 of this issue presented several requirements that precluded the direct adoption of any commercially available system. The sampling rates had to be slow, inexpensive data storage for long periods of time and with minimum operator involvement was desired, and historical data playback with processing was required.

The system developed is described in Figure 1. There are essentially two separate systems shown: the computer system and a hard-wired system, which may function separately or with the computer.

The computerized digital and analog system is based on the NOVA 1200 CPU and a nine-track magnetic tape unit. The digital section provides for a video display, a teletype terminal, a paper-tape reader, and a keypunch. The analog sections consist of an analog-to-digital converter, a scanner, a clock, and a computer-interface expansion chassis.

The computer allows automated monitoring and control of the system, real-time display of operational parameters, and the automated control of equipment through the use of preprogramed decisions. It can continuously record and display 40 analog measurements. Data are sorted within the memory and are directly accessible for a period of 24 hours minimum. Specific system capabilities include: sensor status determination, sample-source selection and identification, instantaneous data-value determinations, out-of-limit alarms, out-of-limit confirmations, the time and the level of high and low values, recording-rate adjustment, sensor-drift determinations, and the production of data reports.

The other subsystem, the Phase I DAS, is hard wired and can be manually operated. It can be used with the computer or by itself. The Phase I DAS consists of an analog section, a digital section, a tape recorder, and

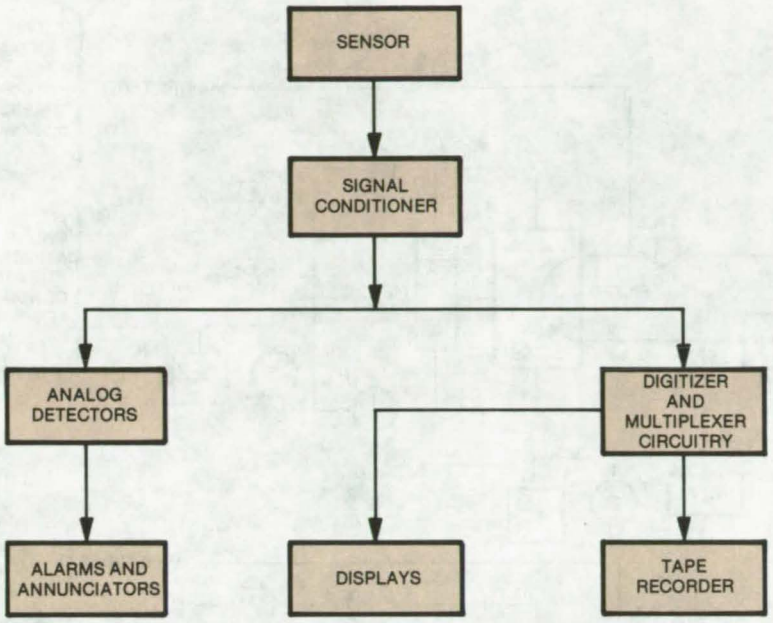

Figure 2. The **Phase I Data-Acquisition System** signal flow, when used independently, is outlined in the simplified diagram above.

appropriate power supplies. The analog section consists of input buffers, level detectors, special signal conditioning, a diode matrix, master alarm circuitry, and out-of-limit annunciator, and analog meters. The digital section includes a clock assembly, a multiplexer, an analog/digital converter, data storage buffers, control circuitry, and displays.

A typical signal flow for the Phase I DAS is shown in Figure 2. The central part of the system is a digitizer assembly that samples 25 analog data channels at an operator-selectable rate of once per second or once per 12 seconds. In the "digitizer and multiplexer circuitry," 75 samples are acquired in a storage register; then a frame leader containing a sync word and time and date information is affixed. The data frame is output to an incremental/digital cassette tape recorder. Data transfer occurs in about 6 seconds, which results in a time compression of 150:1. Therefore, one cassette can store about 75 hours of data. A biphase recording technique is used so that bit-error rates with a standard digital cassette are extremely low.

The recorded cassettes may be played back through a processor that converts the digital data to a form that is printed on a line printer. A complete frame of data (75 time slots) is printed in 38 seconds. A PROM memory bank is included to convert the printed data to engineering units.

The system also includes out-of-limit annunciators for each of the 25 analog channels, analog data displays, a time-of-day and day-of-year clock, and a power failure warning.

This work was done by Leo Monford of **Johnson Space Center** *and A. T. Linton of The Boeing Aerospace Co. The Water Monitor System [WMS] is described on page 238 of this issue and in several succeeding articles. Further information on the Phase I data-acquisition system, along with other information on the WMS, may be found in NASA TM-X-58179 [N77-13909], "Water Monitor System: Phase I Test Report" [$5.50], a copy of which may be obtained [prepayment required] from the National Technical Information Service, Springfield, Virginia 22151.*
MSC-16842

Water Sample-Collection and Distribution System

Automated equipment for use with NASA's water-monitor system

Lyndon B. Johnson Space Center, Houston, Texas

NASA's water-monitor system (described on page 238 of this issue) includes automatic sample-collection and distribution equipment. This equipment is housed in a mobile trailer, along with numerous sensors that analyze the water. In addition, a data-acquisition, processing, and display computer can operate the sample collector automatically, or it may be operated manually.

Samples are collected from any of six sampling points, filtered if desired, and delivered to the various analytical sensors. A minimum of maintenance is required; 10-micron and 0.45-micron filters are kept clean by backflushing, and the system has operated for up to 6 weeks without any maintenance.

As illustrated in the figure, samples are collected from any one of six different points by a manifold arrangement consisting of air-operated Red Valves (or equivalent) connected to two Mayno (or equivalent) pumps. The particular valves used were chosen because they are able to pass large particles without becoming clogged. This is possible because they use a rubber liner that is inflated to create a watertight seal. The valves may be operated manually or by computer.

The pumps are progressive-capacity pumps and are not susceptible to damage by the large particles that occur in unfiltered sewage. One pump is used for five multipointsample lines that are sampled periodically, and the other pumps effluent that is sampled continuously. The multipoint pump can be switched automatically to pump

(continued next page)

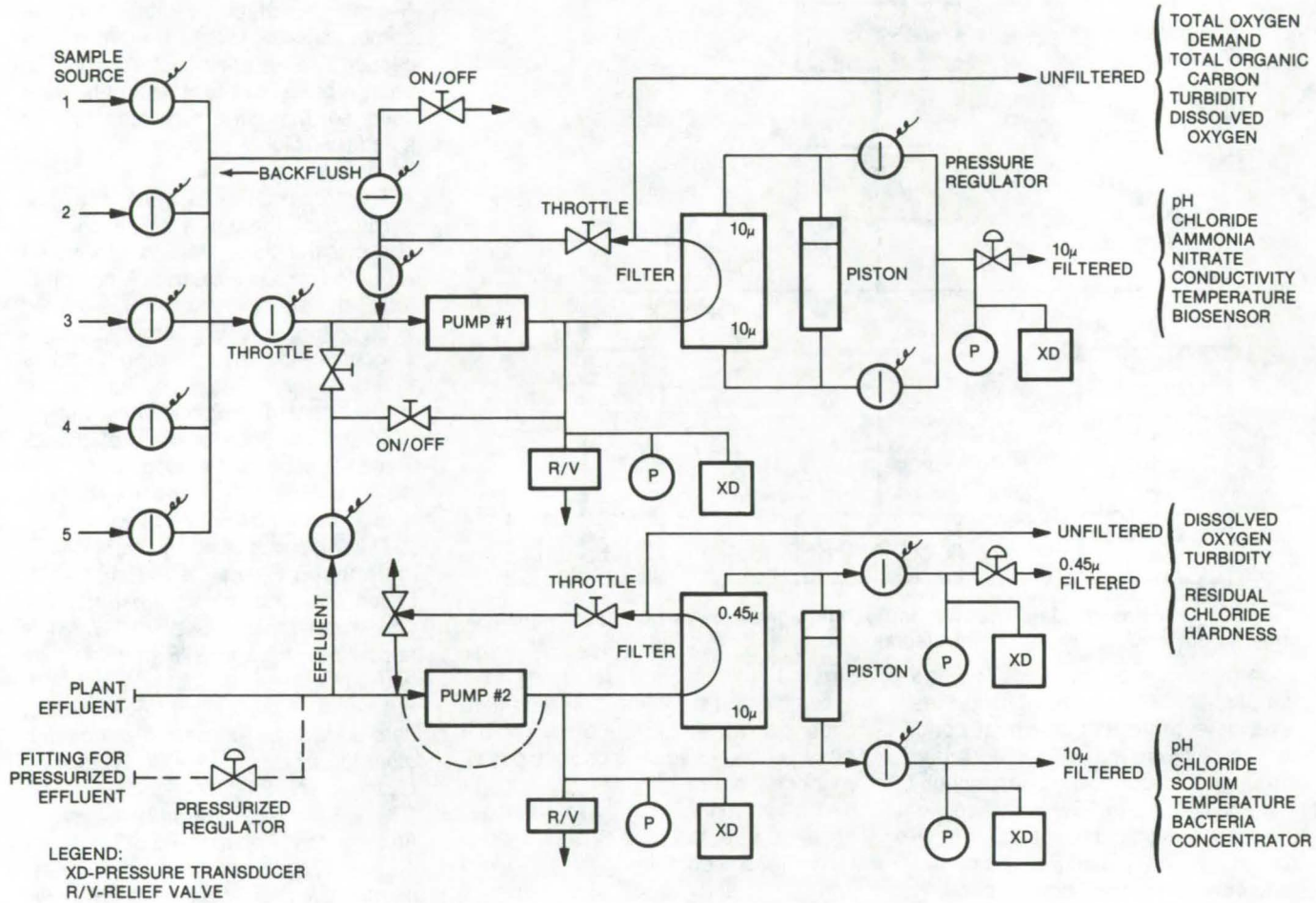

Sample-Collection and Distribution Equipment for NASA's water-monitoring system can be controlled manually or by computer. Samples are taken continuously from two of six possible sample points and are distributed to sensors that determine various water-quality parameters. Each sample is available to the sensor packages in either a filtered or an unfiltered state.

effluent from the line leading to the effluent pump.

It is also possible to use effluent to backflush each of the multipoint lines. This capability is useful for priming the multipoint lines and cleaning them.

Each pump has a bypass loop that allows adjustment of the amount of new sample being pumped to the filters. Collins Swirlklean (or equivalent) filters are used with a backflush system modified by the addition of four time-controlled solenoid valves that increase output. One filter unit is attached to the multipoint pump; both sides of that filter contain 10-micron stainless-steel woven filters.

The filter attached to the plant effluent pump contains two different filter sizes: 10-micron and 0.45-micron. Thus there are five different sample lines from the filter:

- Unfiltered multipoint,
- 10-micron-filtered multipoint,
- Unfiltered effluent,
- 10-micron-filtered effluent, and
- 0.45-micron-filtered effluent.

In the water monitor trailer, each of these various samples is piped down both sides of the trailer behind sensors that can tap into all samples. In addition to the sample lines, there is a water line, a deionized-water line, and a compressed-air line along both sides of the trailer. Once a portion of sample has flowed through a sensor, it is passed to a drain manifold.

This work was done by Richard Brooks of The Boeing Aerospace Co. for **Johnson Space Center.** *For further information, Circle 44 on the TSP Request Card.*

This invention is owned by NASA, and a patent application has been filed. Inquiries concerning nonexclusive or exclusive license for its commercial development should be addressed to the Patent Counsel, Johnson Space Center [see page A8]. *Refer to MSC-16841.*

Automated Electrochemical Detection of Coliforms

Computer-controlled detection of metabolically released hydrogen quantifies coliform organisms in waste water.

Lyndon B. Johnson Space Center, Houston, Texas

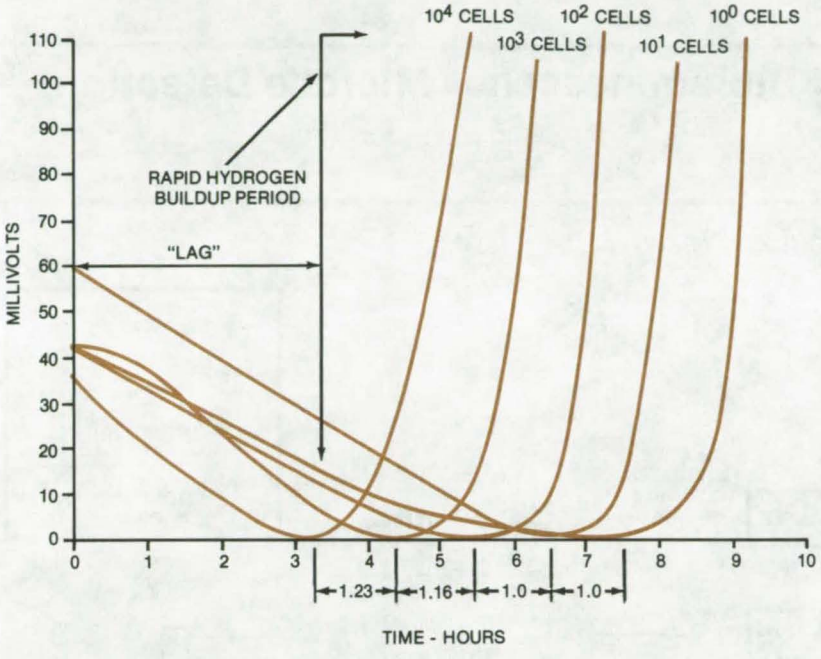

The Response of Platinum/Calomel Electrodes to E. coli metabolic hydrogen is shown for serial dilution inoculation ranging from 10^0 to 10^4 total cells.

An automated sensor for the detection of coliforms has been designed for use with NASA's water-monitor system (WMS) (developed at Johnson Space Center and described on page 238 of this issue of *NASA Tech Briefs*). The coliform test is a sensitive and widely used indicator of general bacterial levels in water. The usual coliform tests, the most probable number (MPN) and membrane filtration (ME) techniques, are laborious laboratory procedures requiring at least 24 hours to complete.

The automated coliform sensor in the WMS was based on a more rapid technique developed recently by researchers at NASA's Langley Research Center and the University of Virginia. (See Wilkens, Stoner, and Boykin, "Microbial Detection Method Based on Sensing Molecular Hydrogen," *Applied Microbiology,* May 1974, and id., "Electrochemical Method for Early Detection and Monitoring of Coliforms." *Journal AWWA,* May 1976.)

This more rapid analysis approach employs a platinum/calomel electrode to measure the hydrogen gas produced by the coliform group during the metabolism of lactose. This reaction distinguishes the coli from other micro-organisms; further differentiation within the coliform group is possible since under incubation at 44.5° C only fecal coliforms produce H_2, and at 35° C all coliforms produce H_2. The hydrogen-sensing technique is much faster (2 to 10 hours depending on concentration) than the MPN or ME tests and was thus chosen as a method for automation with the WMS.

The hydrogen evolved during the reproduction of coliforms follows the equilibrium shown below:

$$H_2 \overset{Pt}{\rightleftharpoons} 2H^+ + 2e^-$$

Using the platinum/calomel electrode, the time from inoculation to the detection of hydrogen is inversely proportional to the amount of coliforms present. This is illustrated in the graph.

The automated sensor utilizing this principle is packaged in a standard 19-in. (48-cm) cabinet. The sensor includes four subsystems:

- A manual and an automatic control switch,
- Eight incubator cells,
- Fluid-storage and transfer equipment, and
- Instrumentation.

The sensor system may be controlled manually or by computer. In the WMS, the central computer is programed to charge each cell with a measured volume of fresh nutrient at the required temperature. Each cell is inoculated automatically, and the detection time is determined. Initial coliform concentrations are determined using calibration equations.

The eight incubator cells are serially connected to a common fluid-fill and drain manifold by four-way Teflon valves. The cells are 25- by 125-mm Teflon-coated test tubes with bottom drains. The top of each cell is fitted with a stopper molded for two fill-and-vent tubes, the electrode, and a thermometer.

Each cell is immersed in an individually-temperature-controlled mineral-oil bath that can be set at 35° C (total coliforms), 44.5° C (fecal coliforms), or 85° C (bacteriostat). The bath is heated with electrical resistance heaters and is controlled with solid-state devices.

Fluid-storage and handling equipment include valves, a peristaltic pump, reagent storage, and regulated air and hot-water supplies. Air supplies are filtered to 0.45 micron and are washed in 0.1 N nitric acid. Water is sterilized at 100° C for 30 minutes.

Organism growth is monitored with one combination electrode per cell. The electrode signal is conditioned with high-impedance amplification and is multiplexed to the computer for display and printout.

(continued next page)

An important part of the sensor is the automated cleanup of sample cells. Cleanup procedures include a 15-minute flush with deionized water at 100° C and a 15-minute cleaning with an air/sodium hypochlorite mixture. The cleanup procedure incorporates external sterilization of each of the sensor interfaces with working fluids as well as the cell interiors.

This work was done by Reuben E. Taylor of **Johnson Space Center** *and W. Preston Dill and Eldon L. Jeffers of The Boeing Aerospace Co. For further information, Circle 45 on the TSP Request Card.*

This invention is owned by NASA, and a patent application has been filed. Inquiries concerning nonexclusive or exclusive license for its commercial development should be addressed to the Patent Counsel, Johnson Space Center [see page A8]. Refer to MSC-16777.

Chemiluminescence and Bioluminescence Microbe Detection

Automated biosensors for online use with NASA's water-monitor system

Lyndon B. Johnson Space Center, Houston, Texas

NASA's water-monitor system (WMS), developed at Johnson Space Center, automatically samples, analyzes, and displays water-quality parameters on a nearly-real-time basis. [This system is described on page 238 of this issue in "Monitoring System for Community Water Supplies" (MSC-16599, MSC-16778).] One of the major problems in development was the incorporation of a sensor to measure microbe contamination rapidly. Standard laboratory procedures require 24 hours and longer — much too lengthy for use with the WMS.

Faster systems have been developed by NASA as part of work on methods of detecting extraterrestrial life. Two of these, a bioluminescence technique developed with scientists at NASA's Goddard Space Flight Center and a chemiluminescence technique, were selected for the WMS. The bioluminescence technique employs an enzyme extracted from firefly tails; it reacts with the adenosine triphosphate (ATP) present in all living cells to produce light. The chemiluminescence sensor detects bacteria, living or dead, by measuring the light emitted when bacterial porphyrins catalyze a luminol/hydrogen peroxide reaction.

The major components of the online WMS sensors using these techniques are similar (see Figures 1 and 2). They include a fluid transport system, a light-detection photomultiplier tube with a proximal reaction cell, and a strip-chart recorder. The fluid transport hardware includes peristaltic pumps and the associated valves and plumbing for the transport of samples and reagents to the test cells and then to disposal.

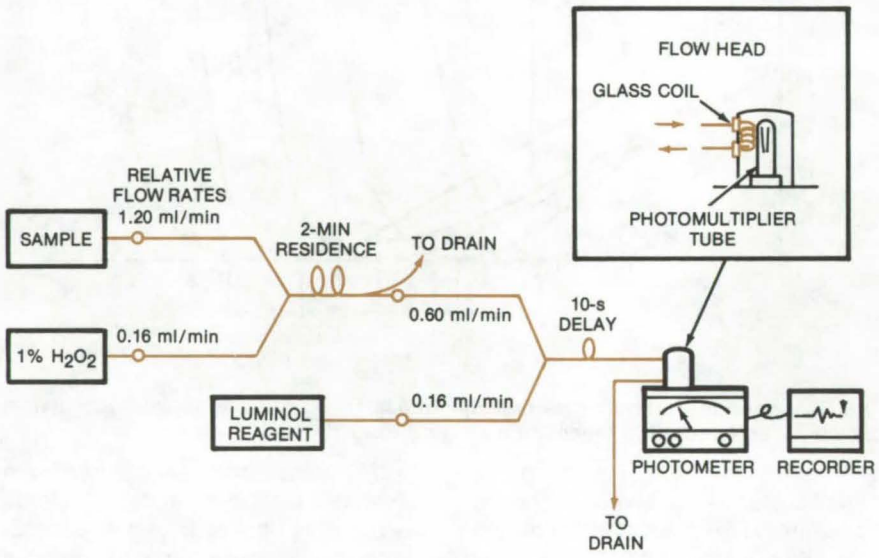

Figure 1. The **Automated Chemiluminescence Flow System** incorporates hydrogen peroxide pretreatment and reaction-rate resolution to eliminate interference from soluble porphyrins and from metal ions.

The chemiluminescence technique is based on the reaction:

$$\text{luminol} + H_2O_2 \xrightarrow[\text{metal ions, superoxide}]{\text{porphyrins}} \text{excited luminol} \rightarrow \text{product} + \text{light}$$

A sample pretreatment with dilute hydrogen peroxide is used to eliminate interference caused by soluble porphyrins such as catalase and hemoglobin. The bacterial porphyrins remain intact and react with the luminol only after the cells are ruptured by the sodium hydroxide in the luminol reagent. Metal ions can also interfere by reacting with the luminol, but metal-ion-produced light can be distinguished on the basis of reaction rates. After about 10 seconds, bacteria continue to react and produce light, but the metal-ion reaction will have been completed.

The chemiluminescence is linear with concentrations above 10^4 cells per ml, and in the WMS, the response time is 10 minutes.

The bioluminescence sensor is based on the reaction:

$$E + LH_2 + ATP \xrightarrow{Mg+2} E{\bullet}LH_2{\bullet}AMP + PP$$

$$E{\bullet}LH_2{\bullet}AMP + O_2 \rightarrow E + AMP + CO_2 + h\nu + T$$

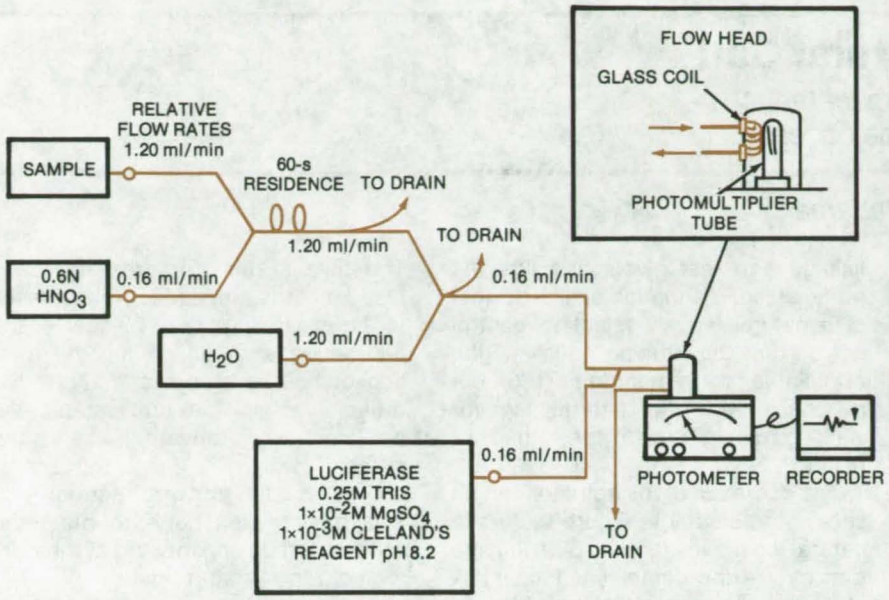

Figure 2. The **Automated Bioluminescence Flow System** employs firefly luciferase to detect bacterial ATP. Nitric acid is used to extract the cells.

where

E = firefly luciferase,
LH_2 = reduced luciferin,
PP = pyrophosphate,
AMP = adenosine monophosphate,
hv = light at 550 nm, and
T = thiazolinone (dehydroluciferin).

The bacterial ATP is extracted by rupturing the cell wall with nitric acid. The sample is then mixed with enzyme in view of the photomultiplier tube. The reaction peaks within 1 second, and when there is an excess of reagents, the intensity is proportional to the amount of ATP present.

ATP has a short survival time after cell death and is thus a specific indicator of cell viability. Sensor response is linear above 10^6 cells per ml, and the response time in the WMS is 10 minutes.

Although not shown in the illustrations, a concentration step is also necessary to prepare the sample for the biosensors. It is typically necessary to concentrate a sample containing 1,000 cells per ml to 10^6 cells per ml or greater. Several concentration techniques were investigated, and the most successful one for this application was filtering, using hollow-fiber membranes. Used in a multiple backwash mode, particle recovery was better than 80 percent at concentrations up to 600-fold.

This work was done by Reuben E. Taylor of **Johnson Space Center,** *Emmet Chappelle of Goddard Space Flight Center, Grace L. Picciolo of the U.S. Food and Drug Administration, and Eldon Jeffers and Richard R. Thomas of The Boeing Aerospace Co. For further information, Circle 46 on the TSP Request Card.*

This invention is owned by NASA, and a patent application has been filed. Inquiries concerning nonexclusive or exclusive license for its commercial development should be addressed to the Patent Counsel, Johnson Space Center *[see page A8].* *Refer to MSC-16779.*

Chemical Measurement of Urine Volume

Lithium chloride dilution technique is fast, accurate, and does not interfere with analyses.

Lyndon B. Johnson Space Center, Houston, Texas

A chemical method of measuring the volume of urine samples has proved more accurate than standard volumetric or specific gravity/weight techniques. The method was applied for urinalysis requiring accurate volume determinations aboard the Skylab and Apollo 17, where weight or volumetric measurements were not possible. This adaptation of a standard laboratory technique to urinalysis could prove generally practical for hospital mineral-balance and catecholamine determinations, which require accurate knowledge of the sample size.

The method is quite straightforward. A precisely known quantity of an inorganic salt (inert in the urine) is added to the total sample. The "doped" sample is thoroughly mixed, and a small portion (10 ml or less) of the original urine volume is drawn off for analysis. A standard analytic procedure is used to measure the inorganic salt concentration in the drawn-off portion. Knowing the concentration of the salt solution and the amount added, the volume of the original sample may be calculated.

In Skylab, lithium chloride was used as the inorganic salt, since it does not interfere with the urinalysis. It was added to the sample with a syringe containing an accurately known solution of reagent-grade lithium chloride in water. The lithium concentration was determined by atomic spectroscopy. Accuracy depends primarily on the accuracy of the atomic absorption analysis and the precision of lithium chloride solution.

This work was done by Richard L. Sauer of **Johnson Space Center.** *No further documentation is available. MSC-16585*

Artificial Leg With Natural Gait

Energy transfer by fluid displacement reduces gait distortion and increases stride cadence.

Marshall Space Flight Center, Alabama

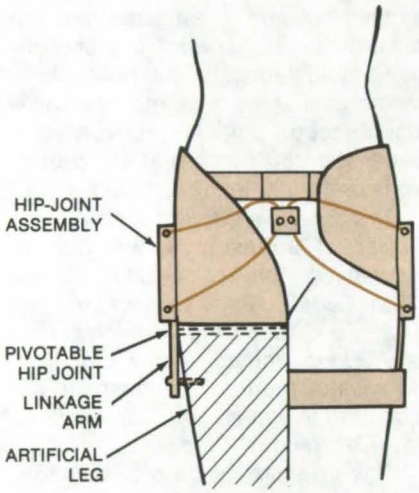

Figure 1. The **Prosthesis Actuator** is carried about the wearer's waist by a belt. Motion of the natural leg is picked up by a linkage arm and pushes a fluid in the hip-joint assembly. The fluid is transferred to the artificial leg where it powers a linkage arm on that side to produce a nearly natural gait when walking.

An improved artificial leg and hip joint reduce gait distortion by transferring energy from the normal leg to assist movement of the artificial one. With most artificial legs, the wearer must elevate his hip and swing the leg slightly to the side when taking a step. This awkward gait is necessary because most artificial legs do not flex at the hip and knee as do natural legs. The new prosthetic employs an actuator that stores energy from the movement of the natural leg and uses it to pivot the artificial hip joint in the ensuing step.

The actuator and artificial leg are worn as shown in Figure 1. The actuator consists primarily of two hip-joint assemblies, each containing a pair of bladders that are connected across the body by tubing. The bladders contain a fluid that is pumped across the body as the normal leg moves. The pressured fluid entering a bladder in the artificial leg rotates a linkage arm that pivots and lifts the artificial leg in a motion similar to that of a natural leg. A selection control valve on the tubing allows the artificial-leg movement to be 180° out of phase with the natural leg for walking, or in phase for sitting or rising.

The operation of the actuator can be seen more clearly in Figure 2. As the natural leg moves forward, the linkage arm moves the center shaft counterclockwise. The movable lobe attached to the center shaft compresses the lower bladder and expands the upper bladder in the natural-leg side. This pumps fluid through the tubing and into the upper bladder of the artificial-leg side (upper or lower bladder selection by control-valve setting).

As the upper bladder on the artificial-leg side expands, it pushes its movable lobe counterclockwise, along with the attached center shaft. The fluid in the compressing lower bladder of the artificial-leg side passes to the expanding upper bladder of the natural-leg side, enhancing the rotation of both center shafts. Thus the artificial-leg linkage arm rotates the artificial leg forward when the person's weight is supported almost entirely by the forward natural leg. This motion then helps to bring the artificial leg up and forward at the right moment for a natural gait.

This work was done by John L. Burch of **Marshall Space Flight Center.** *For further information, Circle 47 on the TSP Request Card.*

This invention has been patented by NASA [U.S. Patent No. 3,995,324]. Inquiries concerning nonexclusive or exclusive license for its commercial development should be addressed to the Patent Counsel, Marshall Space Flight Center [see page A8]. Refer to MFS-23225.

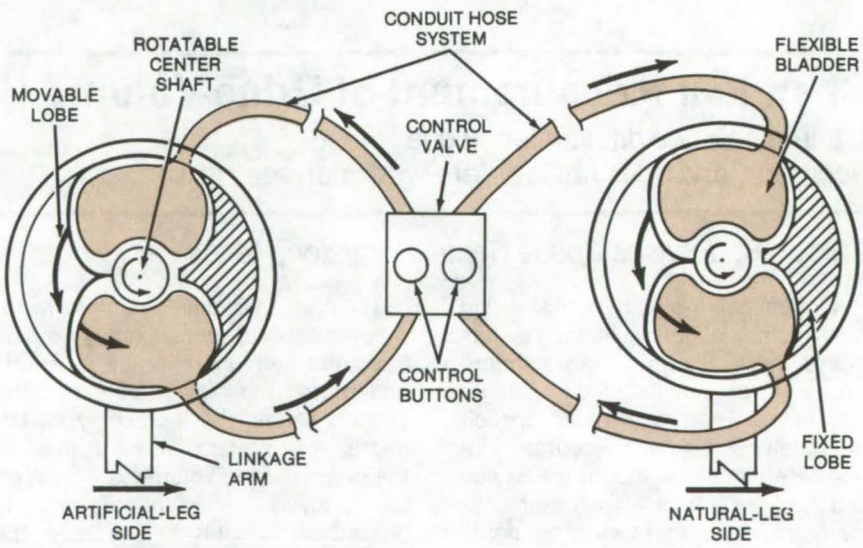

Figure 2. The **Hip-Joint Assemblies** of Figure 1 are shown here laid out on a single plane to demonstrate their operation. As the natural leg moves forward, the center shafts and movable lobes rotate counterclockwise, and the fluid is pumped in the direction of the arrows. The movable lobe compresses the lower natural-leg bladder and forces fluid into the upper artificial-leg bladder. Expansion of that bladder moves the artificial-leg movable lobe and center shaft counterclockwise to move the linkage arm on that side.

Boosting Production Yields of Biomedical Peptides

NMR can be used to monitor syntheses of insulin, ACTH, and other peptides.

NASA's Jet Propulsion Laboratory, Pasadena, California

Improved production yields of insulin, ACTH, growth hormone, and other biomedical peptides are possible by monitoring the syntheses with nuclear magnetic resonance (NMR) techniques. This approach is being applied to peptide synthesis by the Merrifield method, in which polystyrene beads are the starting material for a complex chemical sequence.

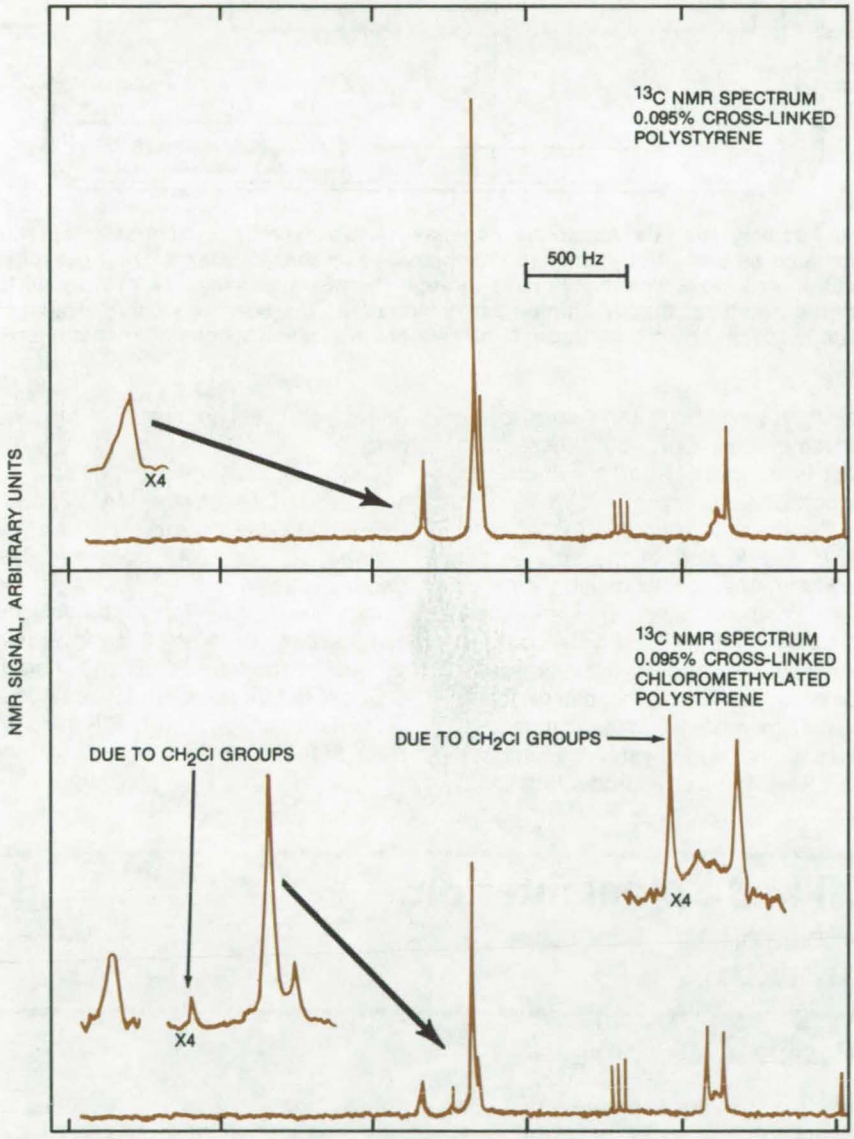

Several Peaks Appear in the NMR spectrum of polystyrene after chloromethylation. These peaks are identified with the substitution of CH_2Cl groups on the aromatic ring of the polystyrene. These spectra were taken on model 0.095-percent cross-linked resins; similar results were obtained on commercially-available polystyrene beads used in peptide synthesis.

Until now, there has been no simple and precise method for determining the extent of cross-linking in the beads. This is important information since the Merrifield method is optimized when the polystyrene is about 1 percent cross-linked. In addition, there has been no widely accepted nondestructive test for determining the degree of chloromethylation of the cross-linked polystyrene — the first step in the synthesis.

It has now been found that polystyrene, in a solvent that swells the resin, exhibits useful carbon-13 NMR signals that have line widths that can indicate the extent of cross-linking. Thus, it is possible to measure the cross-linking of bulk polystyrene before it is used in the time-consuming synthesis, to determine whether it is at the optimum 1 percent.

Carbon-13 and proton NMR spectra can also give the degree of chloromethylation. A number of NMR peaks that can be associated with the attachment of CH_2Cl groups to the aromatic ring of the polystyrene can be easily identified (see figure) and used to monitor the reaction.

The research also shows that NMR may provide information on the structure of the chloromethylated styrenes and the nature of the CH_2Cl groups. For example NMR has indicated that the chloromethylation reaction substitutes only on the 4 position of the aromatic ring of a polystyrene. This is believed to be the first evidence that only one position has been substituted.

This work was done by Stanley L. Manatt of Caltech for **NASA's Jet Propulsion Laboratory.** *For further information, Circle 48 on the TSP Request Card.*
NPO-14142

Positively Charged Membrane for Urea Dialysis

Membrane prevents toxic ammonium ions formed in urease dialysis from reentering body.

NASA's Jet Propulsion Laboratory, Pasadena, California

Urease decomposition has proved an effective method of converting urea to soluble products in dialysis, or kidney, machines.

In the urease dialysis chamber as presently designed, toxic ammonium ions are formed during the conversion of urea to soluble products and must be removed. This has been done by adding large amounts of a zirconium salt to precipitate the ammonium. This procedure requires frequent replacement of the precipitating agent and limits the potential compactness and portability of the urease technique for dialysis.

In the new system, the single dialysis chamber is replaced with two chambers separated by a porous membrane with fixed positive-charge centers. Neutral urea molecules will pass through the positively charged membrane and will be converted to soluble products in the urease chamber. However, the positively-charged ammonium ions are repelled by the membrane and will not reenter the dialyzate chamber. The only regeneration required will be replacement of the urease. Positively charged ions in the dialyzate will not enter the urease chamber and thus need not be replaced. Bicarbonate ions formed in the urease chamber can return to the dialyzate chamber, but these are readily removed from the body as carbon dioxide.

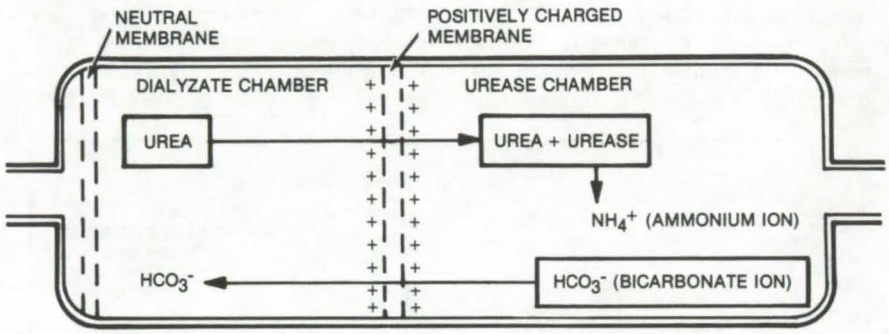

The Auxiliary Dialysis Apparatus consists of two cylindrical chambers that are separated by a positively charged membrane. Each chamber has a 30-ml capacity. Neutral urea molecules readily pass through the membrane and are hydrolyzed to soluble products, mainly ammonium bicarbonate. The positively-charged ammonium ion cannot pass back through the membrane because the positive centers repel them.

It is possible that this system will allow a reduction in the size of the dialyzate chambers, making smaller units possible. Another speculative application of the positively charged membrane concept is the encapsulation of urease in microcapsules made of the membrane. When ingested, these could conceivably decompose the urea into soluble products without releasing toxic ammonium into the body.

This work was done by William A. Mueller of Caltech for **NASA's Jet Propulsion Laboratory.** *For further information, Circle 49 on the TSP Request Card.*

Inquiries concerning rights for the commercial use of this invention should be addressed to the Patent Counsel, NASA Resident Legal Office-JPL [see page A8]. Refer to NPO-14101.

A Probe for Blood-Vessel and Spinal Interiors

In vivo colorimetric oximetry and mapping of the lumen of body vessels, using a new probe

NASA's Jet Propulsion Laboratory, Pasadena, California

A new probe is designed for insertion into the lumen of blood vessels to perform oximetry and to investigate plaque on interior vessel walls. The probe is more accurate than the standard oximetry procedure of determining the degree of oxygenation (hemoglobin-to-oxyhemoglobin ratio) of the circulating blood. The standard procedure of measuring light transmitted through the patient's earlobe is subject to errors because the circulation serving the earlobe may be lessened due to shock or anesthesia.

The proposed probe can be constructed in two ways. One version shown in Figure 1 uses two fiber-optics channels inside a thin catheter. The catheter has a small inflatable balloon tip. A similar probe can be built into the inflatable cuff of the endotracheal tube or the distal end of the esophageal stethoscope.

A second version without the fiber optics shown in Figure 2 includes at least two light-emitting diodes (LED's) and a photodiode. The photodiode detects light reflected from the vessel walls.

In use, the probe is guided into the lumen of a blood vessel in the tracheal region. The process is observed through a fluoroscope. Once the area of interest is reached, the balloon tip is inflated, and the vessel wall is investigated.

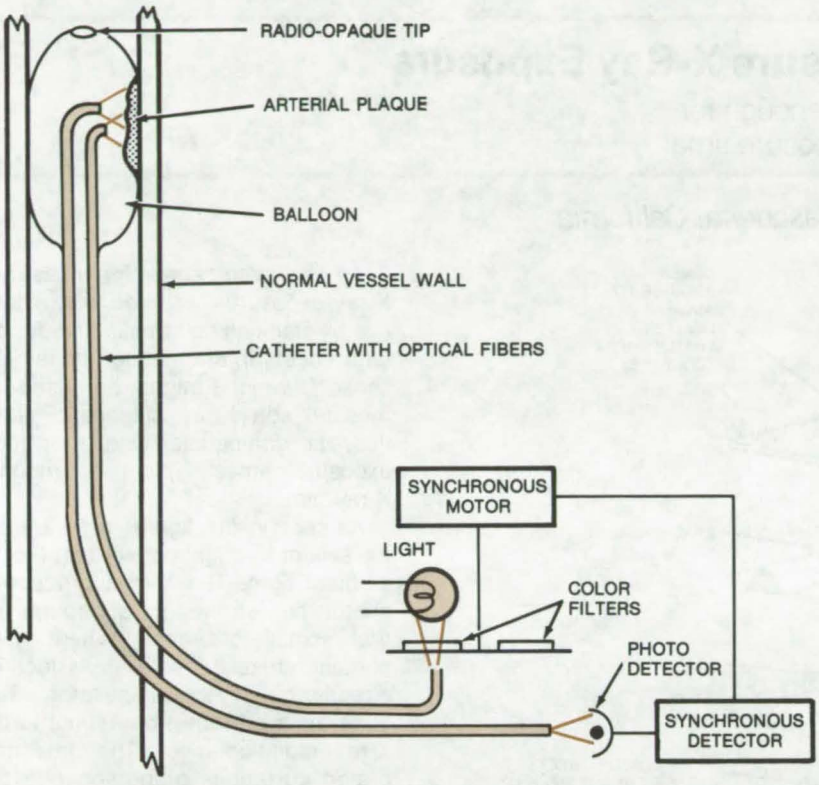

Figure 1. The **Probe Using Two Optical Fibers** is shown inside the lumen of a blood vessel. The radio-opaque tip is readily observed through a fluoroscope, which is used for accurate probe positioning. Several color filters mounted on a rotating color wheel provide an alternating-color source. The returned wavelengths are sensed by a photodetector and transmitted to a ratio indicator for final processing. The intensities at several wavelengths indicate the color of the observed object.

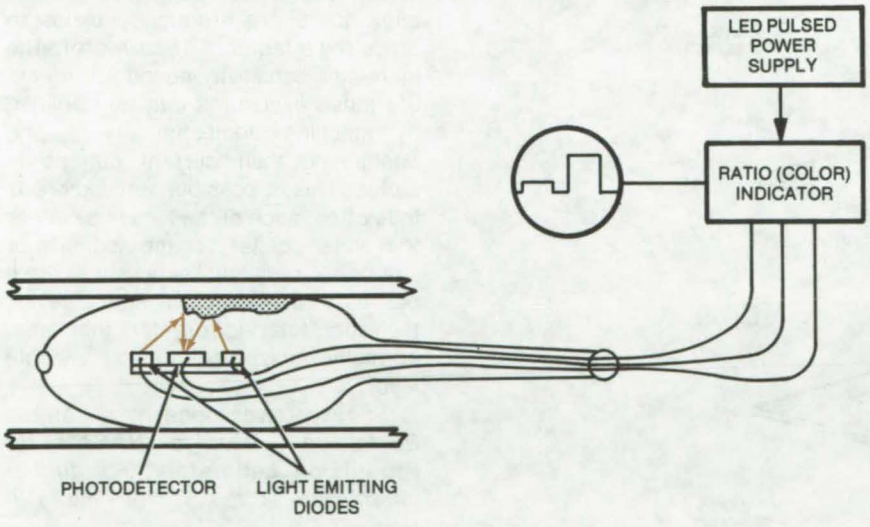

Figure 2. The **Second Version of the Probe** utilizes at least two LED's and a photodetector. The LED's emit light of known frequencies. The reflected light is sensed by a photodetector for direct processing by the ratio indicator.

In the model using fiber optics, light is directed by one channel onto the vessel wall. Separate color filters provide an alternating color input source. The reflected light is returned by the second channel for analysis by conventional photodetectors. From the analysis of returned light frequencies, it is possible to determine the ratio of hemoglobin to oxyhemoglobin and to assess the nature and extent of plaque on the surrounding walls.

Identical results are obtained with the second probe. However, a photodiode is used instead of the fiber optics to measure the reflected light.

The fiber-optics model using a very thin catheter of 1 to 2 mm in diameter can be applied in endothecal colorimetric surveys of theca medullar spinalis in spinal lumen mapping. As in the previous arrangement, the light would be incident on the lumen or neighboring nerve bundles, and the reflected wavelengths are picked up by adjacent fibers and are returned to an external sensor.

The returned light is viewed through appropriate filters or through several filters interposed in the illuminating or returning optical path in rapid succession. The intensity at several wavelengths gives an indication of the color of the object after appropriate ratios of electrical signals are determined. The colorimetric data or maps greatly facilitate diagnostic interpretation when they are correlated with angiograms, ultrasonic profiling, and thermal mapping.

This work was done by Robert E. Frazer of Caltech for **NASA's Jet Propulsion Laboratory.** *For further information, Circle 50 on the TSP Request Card.*
NPO-14132

Stacked Solar Cells Measure X-Ray Exposure

Stacked cells make sensor sensitive enough for new medical X-ray film with short exposure time.

NASA's Jet Propulsion Laboratory, Pasadena, California

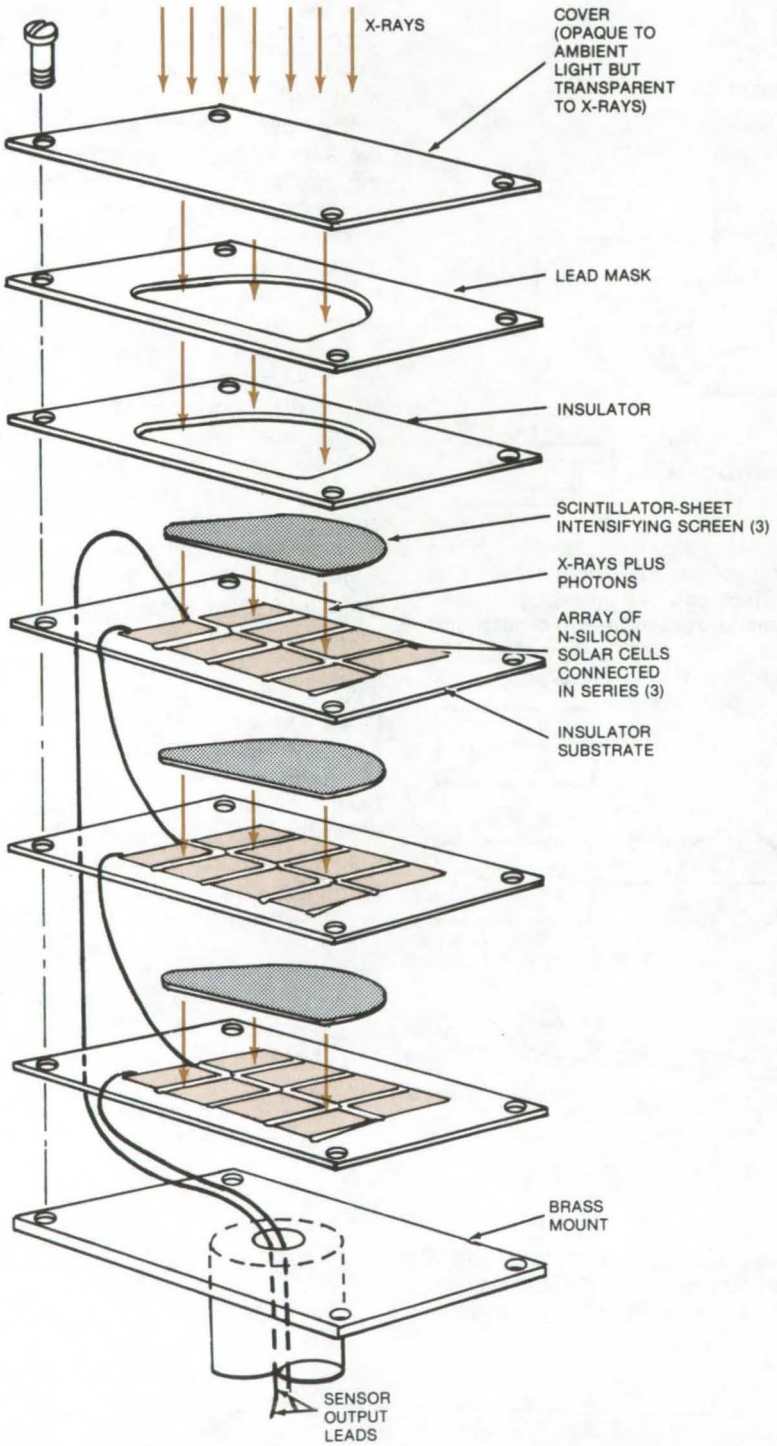

X-Ray-Exposure Sensor is made more sensitive by stacking layers of scintillator sheets and solar cells and by adding the output currents from the solar cells. The X-rays suffer only slight attenuation as they pass through the layers.

An improved sensor for measuring X-ray exposures is made very sensitive by stacking solar cells and scintillator sheets in alternating layers. The sensor, which might be used in medical soft X-ray diagnostic facilities, is compatible with the short exposure times typical of modern X-ray film.

As seen in the figure, X-rays enter the sensor through a cover that blocks ambient light. The X-rays produce a photon flux as they pass through the first scintillator sheet. When these photons strike the solar cells located directly below the scintillator, they generate a current proportional to the X-ray radiation level. The time-integrated current is proportional to the exposure.

A single scintillator/solar-cell layer suffices to measure the relatively long exposures previously required for X-ray films. Recently, however, much faster film has been developed, allowing sharply-reduced exposure times (by a factor of 15 or more). The increased sensitivity needed to measure these exposures can be obtained by stacking additional layers and connecting their current outputs in series. This is possible since there is little attenuation of the X-rays by either the solar cells or the scintillator sheets. X-radiation diminishes as it passes through each layer; however, the sum total is greater than that normally realized from using a single layer.

This work was done by C. Martin Berdahl of Caltech for **NASA's Jet Propulsion Laboratory.** *For further information, Circle 51 on the TSP Request Card.*
NPO-13954

In Vivo Blood-Flow Mapping

Doppler technique uses a fiber-optics probe inserted in the blood vessel.

NASA's Jet Propulsion Laboratory, Pasadena, California

A new proposal for blood-flow monitoring suggests the combination of commercially-available low-loss optical fibers and laser-Doppler techniques to read the blood-flow velocity directly in tiny blood vessels. As shown in Figure 1, a small 1- or 2-mm fiber-optics element, with or without a housing, can be inserted into a blood vessel. Its position can be monitored with a fluoroscope.

The fiber optic tube is connected to a laser, so that it shines a tiny beam of light inside the blood vessel. When this beam is reflected by a moving particle in the blood stream its frequency is shifted by what is known as the laser-Doppler effect. This frequency shift is then measured to determine the velocity of the particle. The principle is the same as that used to check auto speeds with police radar.

The reflected light is transmitted out of the blood vessel by the same fiber optic tube used to pipe the light into the vessel. The mixture of original and reflected light falling on a photodetector produces a beat frequency that is linearly related to the particle velocity. Conventional electronics can convert the detected signal into a blood-flow velocity map.

Radiographic data can be correlated with the blood-flow map to give more accurate blood vessel diameters and possibly velocity and pressure waves through the vascular system. In addition, any arterial plaque will sharply reduce the diameter of the vessel wall and will increase the flow rate at that point. By pinpointing otherwise-undetectable plaque locations, the system can provide precision data for each millimeter of the vessel wall as the catheter travels through the vessel.

Several shapes of the waveguide tip are possible (Figure 2). The best results are obtained when the angle and shape of the fiber cause the laser light to exit from the tip surface at a grazing angle.

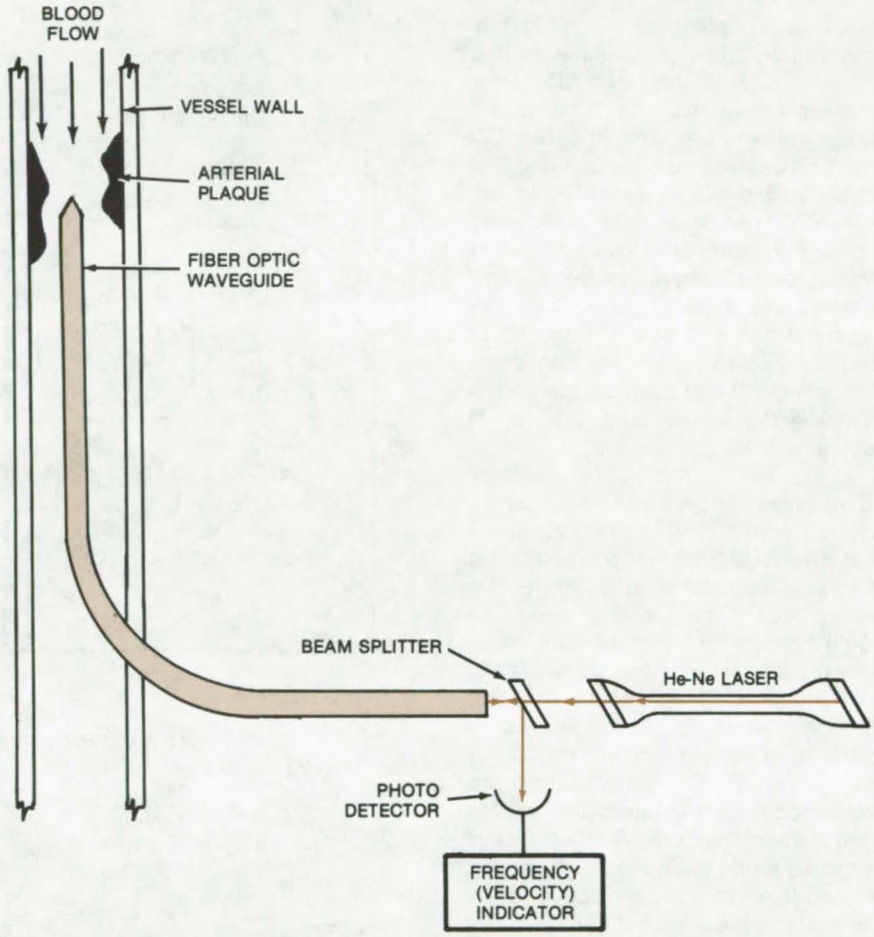

Figure 1. **Proposed Doppler Blood-Flow-Velocity Mapping System** has a 1- or 2-mm fiber-optics element inserted into the blood vessel. Laser light is propagated through the fibers and is reflected back at a different frequency by moving particles in the blood. The interaction of original and reflected light falling on the detector gives a beat frequency that is linearly related to the particle velocity.

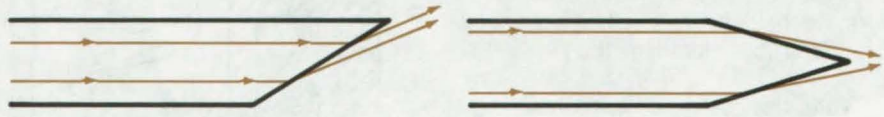

Figure 2. The **Fiber-Optics Waveguide Tip** is optimally shaped when the laser light emerges from the tip surface at a grazing angle. Two possibilities are shown. In these designs, a separate member may form the fiber-optics tip; both the shape and the refractive index of the member cooperate to give the desired grazing angle.

This work was done by Robert E. Frazer of Caltech for **NASA's Jet Propulsion Laboratory.** *For further information, Circle 52 on the TSP Request Card.*
NPO-14133

Biological Sampling and Cleaning Device

High-speed flow of liquid and vacuum-vortex removal dislodge and recover particulates.

NASA's Jet Propulsion Laboratory, Pasadena, California

A new "washing machine" gently removes biological particulates from a surface, and retains them for later analysis. It leaves the surface extremely clean, removing 98 percent of the particulates and recovering 90 percent of them. If recovery is not required, it can be adapted to cleaning alone. For example, it can be used in "clean rooms" where electronic components are manufactured. With appropriate solvents, it can be used to prepare metal surfaces for adhesives or coatings. It can even be adapted to cleaning the interior and exterior of tubing.

In the device (see figure), a jet of liquid impinges on an inclined plane, where it forms a rapidly moving sheet that sweeps across the surface to be cleaned, dislodging and entraining particulates. The flowing sheet of liquid enters a vacuum chamber where the vacuum draws off the liquid and particles in two counterrotating vortexes. When the device is used to gather a biological sample (instead of for cleaning), the particulates are separated from the drawn-off liquid by conventional methods. As the cleaner is moved along the surface, it sweeps in enough air at sufficient speed to dry the surface it leaves behind.

The moving sheet of liquid removes particulates most efficiently at the point where it initially contacts the surface to be cleaned. When contamination is particularly resistant, moving the point of initial contact back and forth is helpful. This effect can be produced by vibrating the inclined plane.

Water has been used as the working fluid in a prototype of the cleaner, although for particular applications, other solvents can be used.

Previous methods for removing biological samples from a surface are slow and expensive by comparison with the new flowing-film device. Older methods that depend on the

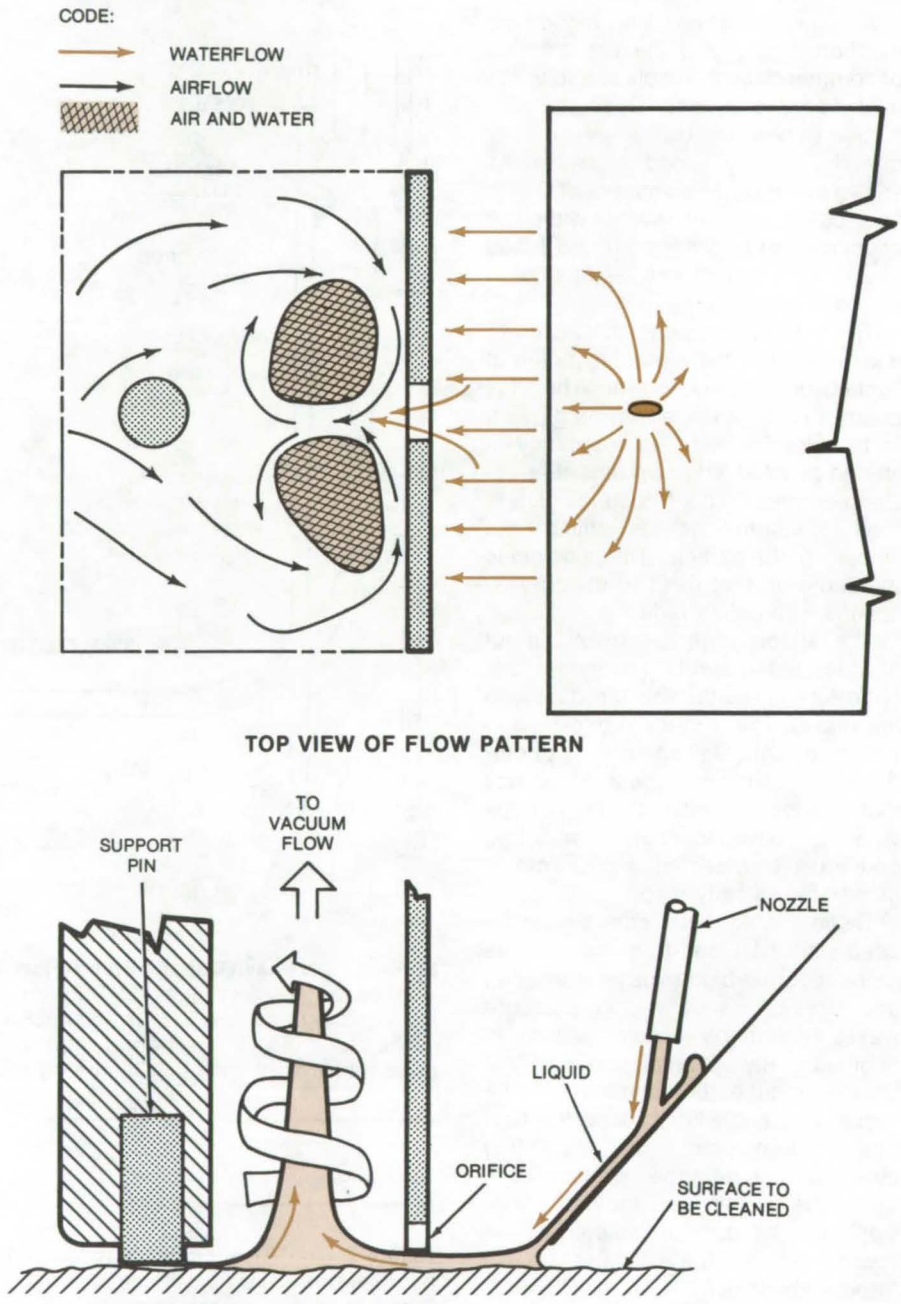

Flowing-Liquid Cleaner dislodges surface particles gently and effectively. A liquid jet from the nozzle strikes the inclined plane and spreads into a thin film that flows down and across the surface to be cleaned. Liquid and particles are swept into a vacuum chamber. The flow is directed into two counterrotating vortexes that remove the contaminant with the liquid and leave a dry surface. In addition to its use as a biological sampler and cleaner, the device could be manufactured on a larger scale for cleaning large arrays of solar cells and windows on high-rise buildings.

operator's skill can also give large sample-to-sample variations. Some of these, for example a small probe connected to a vacuum that sucks up a biological specimen, tend to damage or even kill the biological sample. The new device is gentle by comparison.

This work was done by Horst W. Schneider of Caltech for **NASA's Jet Propulsion Laboratory.** *For further information, Circle 53 on the TSP Request Card.*

Inquiries concerning rights for the commercial use of this invention should be addressed to the Patent Counsel, NASA Resident Legal Office-JPL [see page A8]. Refer to NPO-14010.

Automatic Primate Feeder

Zippered tubing and rotating wheel dispense food pellets reliably, without contamination.

Langley Research Center, Hampton, Virginia

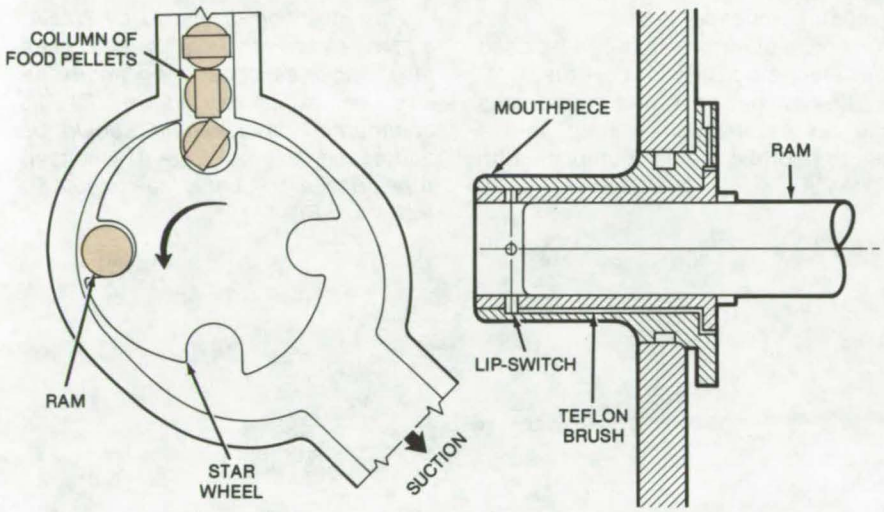

An **Automatic Primate Feeder** dispenses one food pellet at a time.

A feeder, developed for long-term experiments with monkeys, dispenses food pellets with little or no maintenance. The dispenser prevents contamination of the food, delivers it at a preset speed and rate, is not jammed by the food or feces, and can store large quantities of food.

The primate feeder uses pellets encapsulated in a plastic zippered tube to prevent contamination. After dispensing a pellet into the delivery mechanism, the unzippered tube is wound flat on a takeup reel. The food pellet is forced into one of four equally spaced notches in a star transfer wheel shown in the figure and then into a mouthpiece for delivery to the animal.

To begin a feed cycle, a ram that occupies the previously used notch is retracted. This exposes a lip-switch pressure-transducer mechanism in the mouthpiece. Upon activation of the switch by the animal, the star wheel rotates and delivers the pellet to the ram, which pushes it through the mouthpiece and into the primate's mouth. The ram stays in the extended position, sealing the mouthpiece while the system is not operating.

This system, which was originally designed to feed primates in orbit, can also be used terrestrially for the training of animals where a stimulus/response system would determine whether or not a pellet would be dispensed. It could also be used to store small parts, retaining their cleanliness, and then dispensing them as needed.

This work was done by A. R. Gandy of Northrop Corp. for **Langley Research Center.** *For further information, Circle 54 on the TSP Request Card.*
LAR-11586

Improvements in Microelectrophoresis Apparatus

Accessories for electrophoresis simplify clinical diagnoses and allow rapid, standardized separations.

Ames Research Center, Moffett Field, California

Electrophoresis is often used to separate and identify large electrically charged molecules such as proteins. In a clinical setting, this nondestructive tool makes rapid, standardized determinations of enzyme or protein mixtures for diagnosing medical conditions; it is also widely used in genetic and immunological studies in research and in forensic science.

In a conventional microelectrophoresis setup, molecules are placed on a rigid membrane or gel and are wetted by an electrolyte. When a direct current is applied, the proteins migrate toward one of the poles at a rate that depends on their charge, shape, and chemical nature. The various

(continued next page)

components can be made visible by indicator dyes or by reacting them with specific substrates that indirectly render them visible.

A number of novel improvements to a conventional electrophoresis apparatus, that can simplify and standardize clinical diagnoses, have been developed. The improvements, which include special trays, tray and cell covers, membranes, and temperature controls, can speed the diagnoses by allowing many samples to be analyzed simultaneously.

Specifically, the improvements include:

- designs that allow the use of either a membrane or a gel with the same basic apparatus;
- square trays and covers that can be rotated by 90° with respect to the electrodes to give two-dimensional separations;
- dividing the gel tray into parallel compartments by ribs or baffles, making it possible to analyze up to 10 samples at once without the need to create depressions in the gel to receive the samples;
- permanently recording the electrophoretic results by placing a slotted membrane over the gel — the membrane is preimpregnated with dyes or enzyme substrates so that a visible pattern is recorded for permanent identification and evaluation;
- improved temperature control in gel-type separations by using liquid-cooled plates next to the gel trays — this sharpens the electrophoretic separation bands; and
- a special electrode that can be used for electrofocusing in a pH gradient.

The new gel trays and membranes can be assembled as ready-to-use electrophoretic media, complete with dyes on substrates, to reduce inconsistent or faulty analyses. They can also be used for crossover electrophoresis involving antigens and antiserum samples that migrate toward each other to form visible precipitates. These precipitin bands can be indicative of present or past infectious diseases. In forensic investigations the precipitins may also be used for identification of species.

This work was done by Benjamin W. Grunbaum of the University of California, Berkeley, for **Ames Research Center.** *For further information, Circle 55 on the TSP Request Card.*

This invention is owned by NASA, and a patent application has been filed. Inquiries concerning nonexclusive or exclusive license for its commercial development should be addressed to the Patent Counsel, Ames Research Center [see page A8]. *Refer to ARC-11121.*

Mechanics

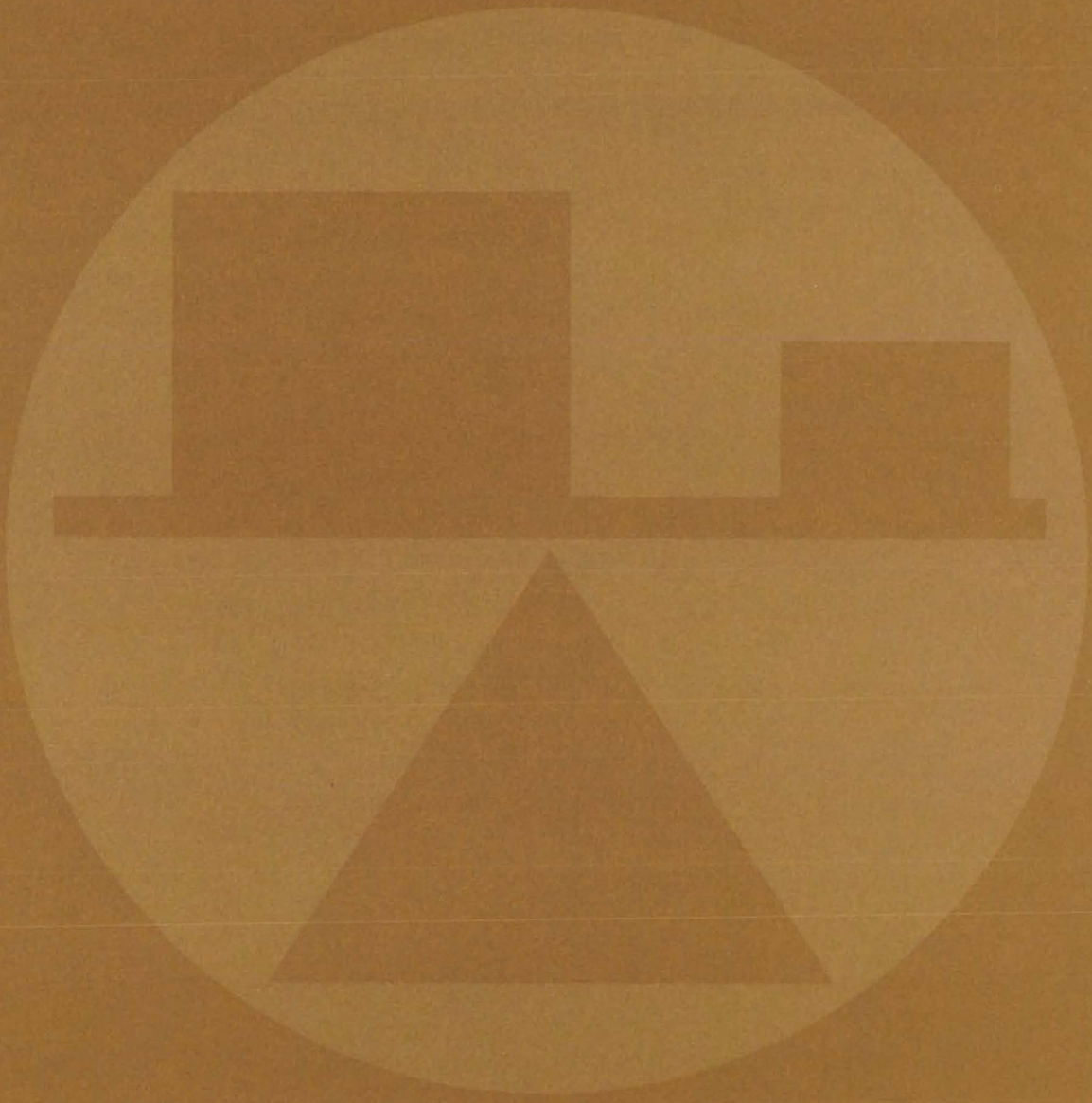

Hardware, Techniques, and Processes

257 Pseudo-Continuous-Wave Acoustic Instrument
258 Mass-Spectrometer Calibration Standard
258 Damage-Detection System for LNG Carriers
260 Free-Air Content in Fluid Systems
260 Testing Composite Sheets at High Temperatures
261 Fluidic-Oscillator Gas Analyzer
261 Improved Electron-Beam Probe for Hypersonic Flows
263 Detection of Boundary-Layer Transitions in Wind Tunnels
264 Helicopter Position Stabilizing System
265 Airframe Design for Reducing Cabin Noise

Books and Reports

267 Predicting Damage from Exploding Vessels

Computer Programs

267 Air-Cushion Landing System
268 Internal and External 2-D Boundary-Layer Flows
268 Stress Analysis Under Component-Relative Interference Fit
269 Edge Geometry of Turbomachine Blades
269 Thermal Performance of Shaft Bearing Systems
270 Structural Performance Analysis and Redesign
271 Thermal Hydraulic Analyzer
271 Analysis of Linear Viscoelastic Structures

Pseudo-Continuous-Wave Acoustic Instrument

Ultrasonic instrument measures acoustic properties of liquids, gases, and solids.

Langley Research Center, Hampton, Virginia

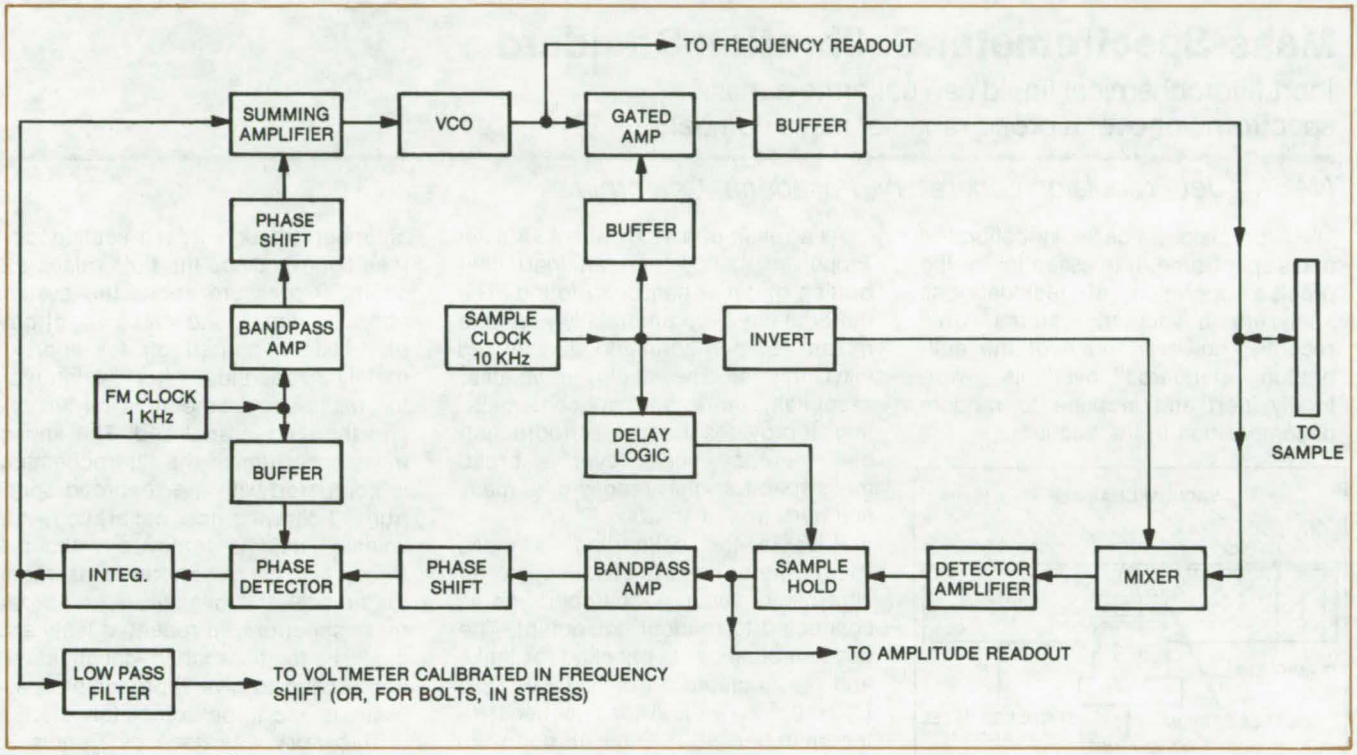

Pseudo-Continuous-Wave monitor can be used to measure any parameter detected as a resonant-frequency change or an amplitude change in the acoustic signal.

A simple, inexpensive, and portable ultrasonic device accurately measures acoustic properties of liquids, gases, and solids. The system uses pseudo-continuous-wave responses from samples to measure the change in resonant frequency or amplitude in the acoustic signal.

The two methods of ultrasonic measurement generally used, pulse echo and continuous wave (CW), both have shortcomings for certain measurements that are eliminated with the pseudo-continuous-wave (PCW) technique. In pulse echo the acoustic wave is not monochromatic, i.e., it is a broadband measurement containing many frequencies and phases. In addition, measurements suffer from duty-cycle effects; the system is not a real time system but is pulsed. Furthermore, pulse-echo techniques usually require very fast rise time electronics and higher peak powers leading to instrument complexity and expense. Standard CW techniques require care to isolate the receiving transducer from the transmitting transducer to minimize electrical leakage "crosstalk", which complicates measurement interpretation. Sampled CW has provided the best compromise to date but is still duty-cycle bound.

The PCW technique is narrow band, monochromatic, phase coherent, and nearly 100 percent duty cycle. It does not suffer from crosstalk and employs a low cost, simple electronic system.

The electronic circuitry is indicated in the block diagram. A tuned VCO provides an initial FM radio frequency that is amplified in a gated amplifier, buffered to drive a low impedance, and fed to a transducer to convert the electrical signal to an acoustic stress wave. The amplifier is then gated off by the fall of a clock for a brief period during which time some of the acoustic energy in the sample is converted back to an electrical signal; then it is passed through the mixer, detected, amplified, sampled and held. The output of the sample-and-hold circuit is amplified, band-passed to remove noise, phase shifted, and fed to one leg of a phase comparator circuit. The other leg of the phase comparator is a reference phase signal derived from the FM clock properly buffered.

A sharp 180° phase shift occurs at the peak of resonance and is used as a feedback to lock the oscillator to a frequency corresponding to the center of a mechanical resonance. Therefore, the system tracks any amplitude peak in the spectral response of the sample. The tracking system can measure both amplitude and frequency.

The PCW technique can measure essentially any parameter that manifests itself either as a resonant-frequency change or as an amplitude change in the acoustic signal obtained

(continued next page)

from the sample material. It should prove valuable in the nondestructive testing of materials under stress. One embodiment of this instrument is a bolt preload monitor that could lead to a new tightening standard for bolts, based on stress rather than torque.

This work was done by Joseph S. Heyman and F. D. Stone of **Langley Research Center.** *For further information, Circle 56 on the TSP Request Card.*

This invention is owned by NASA, and a patent application has been filed. Inquiries concerning nonexclusive or exclusive license for its commercial development should be addressed to the Patent Counsel, Langley Research Center [see page A8]. *Refer to LAR-12260.*

Mass-Spectrometer Calibration Standard

Inert fluorochemical liquid can calibrate a mass spectrometer over a broad range of mass numbers.

NASA's Jet Propulsion Laboratory, Pasadena, California

A precision, carefully-calibrated mass spectrometer is essential for the precise operation of residual gas analyzers in vacuum systems. Until recently, however, none of the calibration standards available were totally inert and immune to random decomposition in the vacuum.

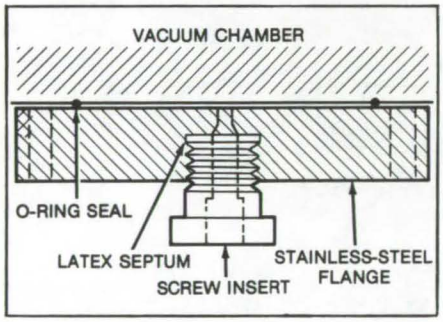

Fluorochemical Liquid is introduced through the self-sealing port. The liquid, which is highly volatile and inert, serves as a mass-spectrometer calibration standard over a broad mass range.

As a result of a study at NASA's Jet Propulsion Laboratory, an inert calibration material has been found. The material is a commercially-available mixture of perfluorinated alkane and alkyl ethers. The liquid is volatile, essentially inert, and noncontaminating. It provides a series of reproducible reference peaks over a broad mass spectrum that ranges over mass numbers from 1 to 200.

Prior to the calibration, a mass spectrometer head is installed into an ultra-clean vacuum chamber and is connected to readout equipment. The vacuum chamber is checked for leaks and evacuated to 1×10^{-6} torr (1.3×10^{-4} N/m^2). After a bakeout of the chamber (150° C for 48 hours) to remove condensable gases such as H_2O, the chamber is allowed to cool to ambient temperature.

After cooling, the calibration is initiated by injecting a small quantity of the fluorochemical fluid into the chamber through a self-sealing port (see figure). Since the fluid raises the chamber pressure above the system operating limits, the mass spectrometer head is turned off for approximately 30 seconds. After the interval, the mass spectrometer is turned on, and the fluid is analyzed. The known mass spectrum of the fluorochemical is compared with the recorded spectrum. Following the calibration, the volatile liquid is removed without a trace, and the spectrometer is ready for the detection of gases over a broad mass spectrum. In repeated tests and analyses the fluorochemical liquid has been found to give reproducible calibrations and to be completely inert.

This work was done by Dennis S. Ross of Caltech for **NASA's Jet Propulsion Laboratory.** *For further information, including sources of the standard, Circle 57 on the TSP Request Card.*
NPO-14097.

Damage-Detection System for LNG Carriers

An acoustical damage-detection system for safer LNG carriers

Langley Research Center, Hampton, Virginia

A new damage-detection system uses an array of acoustical transducers to detect cracks and leaks in liquefied natural gas (LNG) containers onboard ships. The system not only detects leaks but also indicates their location and their leak rate. It is more sensitive and precise than conventional gas-sampling methods and can be used on both a Conch gas-containment system and Moss-Rosenberg spherical tanks.

The new system as shown in the simplified diagram detects an ultrasonic wave generated in the insulation or metal wall by a dynamic flaw, leak, or impact. The wave, typically a high-frequency emission, is sensed by an array of three or more transducers, and triangulation is used to locate the leak or crack without visual inspection. In this method the first transducer sensing the signal becomes a reference. The arrival-time differences of the other transducers are compared with the reference and are converted into path-length differ-

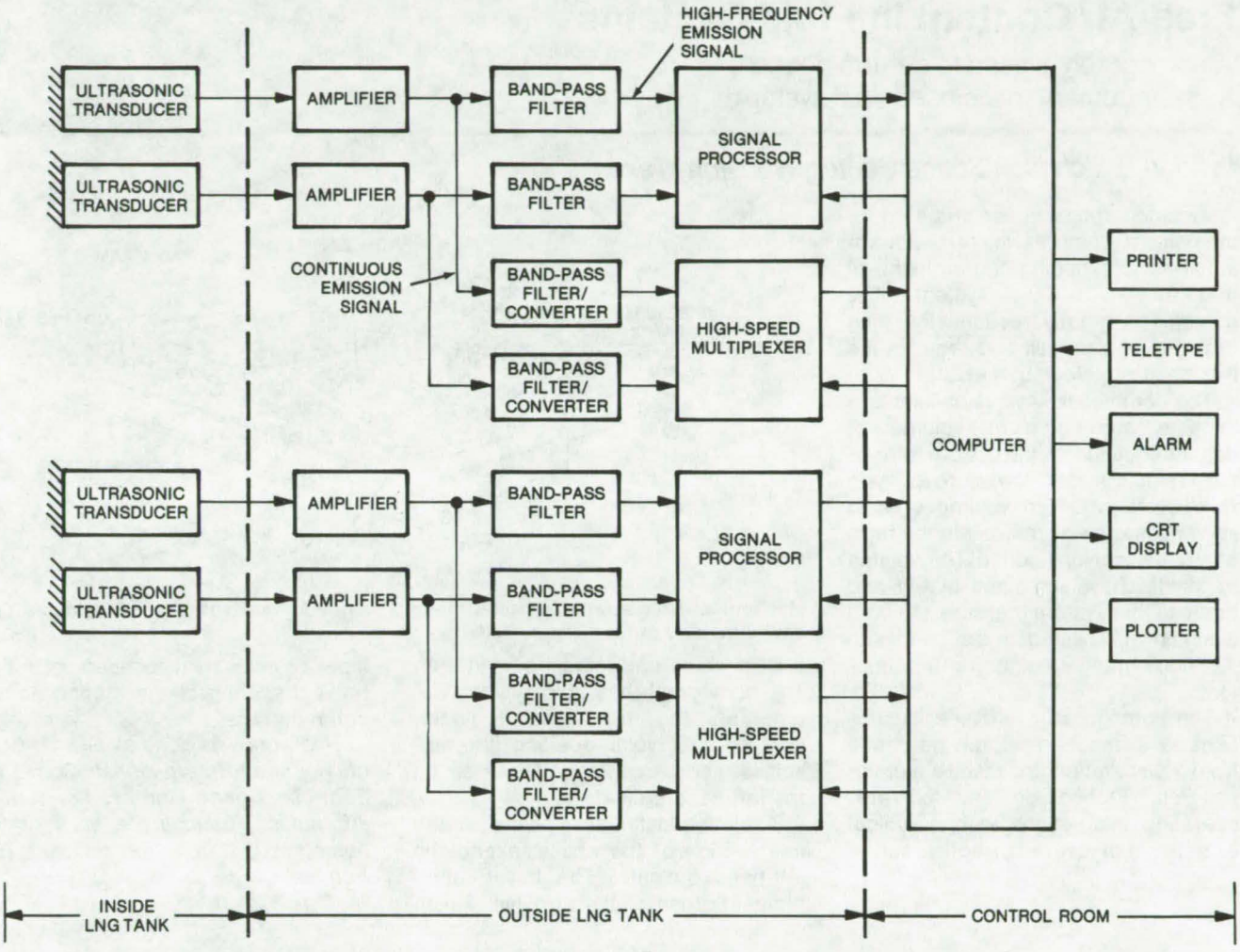

The **Acoustic Damage-Detection System** is connected to an onboard computer. The transducers are piezoelectric and can be bonded, held in place by magnets, or bolted to the wall. The signals are separated, depending on whether the source is a crack, a weakened flawed area, and the like or whether the leakage is continuous, for example, through a crack in the inner hull. In either case the computer triggers an alarm.

ences. A set of hyperbolas is generated from the loci of these constant-distance differences, and the calculated impact point occurs at the intersection of the hyperbolas.

After locating the leak, it is possible to determine the leak rate by measuring the continuous signal (true root-mean-square, V_{trms}) of the transducer closest to the leak. The measured leak rate is a function of distance of transducer from the leak and the value of V_{trms}.

Leakage of LNG through the inner hull or leakage of seawater into insulation foam is continuous in nature and exhibits signatures of characteristic frequencies. The source is located also by triangulation, except that signal attenuation is used rather than the time delay. These signals are sent through a band-pass filter/converter to a high-speed multiplexer and to a computer, as shown.

This work was done by John R. Mastandrea and Maurice V. Scherb of McDonnell Douglas Corp. for **Langley Research Center.** *For further information, Circle 58 on the TSP Request Card.*

LAR-11463

Free-Air Content in Fluid Systems

A nomograph is used to determine the free-air content in a closed fluid system.

Lyndon B. Johnson Space Center, Houston, Texas

A nomograph has been prepared for use with a compressibility tester for automatically finding the amount of free air in a fluid system. The nomograph greatly reduces the time required for this task and reduces the likelihood of calculation errors.

The compressibility tester injects a variable but sufficient volume of deaerated fluid into the system to raise the residual system pressure 10 psig (69×10^3 N/m^2). The volume of fluid injected is known precisely in the form of a dimensionless count. The volume of the fluid system being tested and the resultant system pressure are both also known. These data are used with the nomograph to find free-air content.

The nomograph itself (see illustration) is a mechanical device made from a piece of photosensitive aluminum foil. Etched on the foil are: operating instructions with a typical example, a pressure correction curve, and a three-parameter nomograph. The nomograph has fluid-system volume on the right-hand ordinate, injected-fluid volume along the abscissa, and percentage of free air on the left-hand ordinate.

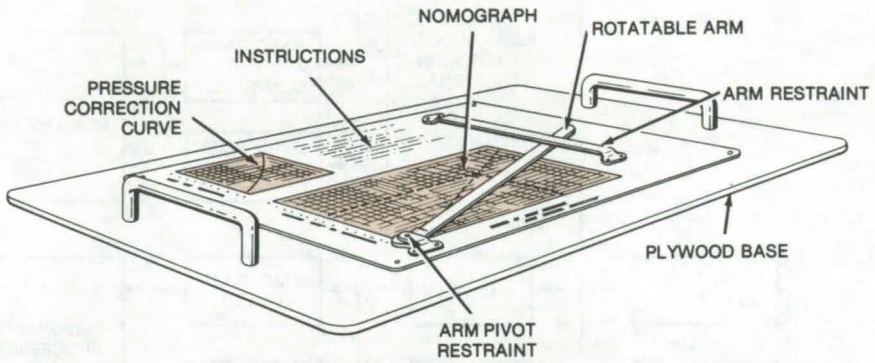

Mechanical Nomograph for determining the free-air content of fluid systems can save time and reduce errors.

A clear plastic arm pivots at the intersection of the abscissa and the left-hand ordinate. The lower longitudinal portion of the arm has Teflon tape, or equivalent, bonded onto it to prevent scoring of the etched nomograph surface.

This work was done by Guy R. Gum of Rockwell International Corp. for **Johnson Space Center.** *For further information, including a copy of the nomograph, Circle 59 on the TSP Request Card.*
MSC-16703

Testing Composite Sheets at High Temperatures

Structural skins can be flexed in tension or compression at 500° F or higher.

Lyndon B. Johnson Space Center, Houston, Texas

Candidate materials for the skins of flexural sandwich beams can be compressive- or tensile-tested at high temperature by using corrosion-resistant steel (CRES) for the core material. Previously, test temperatures were limited to 400° F (204° C) because the aluminum or epoxy core materials that have been used tended to weaken above that temperature. With the CRES core, however, tests have been made at 500° F (260° C), and it is expected that temperatures above 700° F (371° C) will be permissible. A detailed study of graphite/polyimide facesheets has been made using this new test technique.

For tensile tests above 400° F, a CRES core is sandwiched between a CRES sheet and a skin of the material to be tested. The loading is applied to the steel sheet. For compressive tests, loading is applied to CRES bearing sleeves inserted through the core. In both bases, the CRES core is bonded to the surface sheets by a polyimide adhesive. Strain is measured with strain gages bonded to the material under test.

During testing, strain loads are applied at 0.05 to 0.1 inch per minute (1.27 to 2.54 mm per minute) after the temperature has been allowed to stabilize for 10 minutes. The actual temperature is monitored by a thermocouple inside the outer cells of the core.

This work was done by John S. Jones and Bobby J. Payne of Rockwell International Corp. for **Johnson Space Center.** *For further information, Circle 60 on the TSP Request Card.*
MSC-16237

Fluidic-Oscillator Gas Analyzer

A fluidic oscillator identifies hazardous single and multicomponent gases.

John F. Kennedy Space Center, Florida

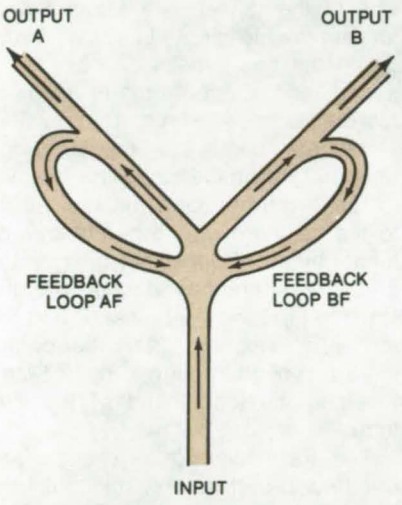

In a **Fluidic-Oscillator Gas Analyzer,** all channel diameters are carefully determined to give the desired frequencies for particular gases. The device is simpler and faster than gas chromotography, mass spectrometers, and catalytic converters.

A typical fluidic oscillator has one input channel that branches out into two output channels. Feedback loops connect each output back to the input, as shown in the figure. When a gas enters the input channel either by applying pressure at the input or by applying a vacuum at one of the output ports, the stream will enter one output channel. For example, if the stream starts through channel A, part of the flow will return through feedback loop AF. The feedback will direct the incoming stream to channel B, which also has a feedback loop BF that pushes it back to A. In this way, an oscillation is established that can reach thousands of hertz.

Because the frequency of the oscillation is inversely proportional to the gas density (i.e., low-density gases produce high frequencies), gas samples can be identified very quickly by measuring the frequency. In some applications the frequency can be detected with a low-cost earphone. Mixed gases having two components of different densities are also easily identified. For more than two components, absorption filters and two or more oscillators can be used.

Since the oscillator has no moving parts, it is highly reliable. It can also be safely used to detect explosive gases. In tests, these oscillators were able to detect 50 ppm of hydrogen in air.

This work was done by Erich A. Farber of the University of Florida for **Kennedy Space Center.** *For further information, Circle 61 on the TSP Request Card.*
KSC-11014

Improved Electron-Beam Probe for Hypersonic Flows

Boundary layers can be investigated at higher currents and for longer periods.

NASA's Jet Propulsion Laboratory, Pasadena, California

New techniques and apparatus, using electron-beam probes, may help aerodynamics' researchers studying the effects of aerodynamic drag and heat transfer at hypersonic speeds. Investigations of hypersonic boundary layers, using conventional static and pitot pressure probes or hot-wire anemometry, have yielded only an indirect determination of static temperature, density, and density fluctuations in the turbulent layer. Electron-beam studies can give more direct information; however, until recently they have been limited by the short test durations in shock or blowdown tunnels and the short-range penetration of the electrons into the boundary layers.

One problem that limits the use of electron-beam fluorescence in hypersonic wind tunnels is that the relatively high gas density in the tunnel must be interfaced with the low-pressure environment around the filament that produces the stream of electrons. Inadequate interfacing causes rapid burnout of the filament.

The new electron-beam, hypersonic-wind-tunnel test facility uses a differentially-pumped drift tube to connect the high- and low-pressure regions, thereby allowing higher gas densities to be studied. In addition, the use of higher beam voltages (50 kV) and currents (1 mA delivered to the gas) allows penetration of up to 6 inches (15.2 cm) into the boundary layers. With the facility, test durations have been extended to hour from the millisecond studies previously possible.

A schematic description of the improved apparatus is shown in the figure. A well-collimated, 1-mm-diameter beam of 50-kV electrons generated by an electron-beam welding gun is injected into the test chamber through a ceiling plate. The beam

(continued next page)

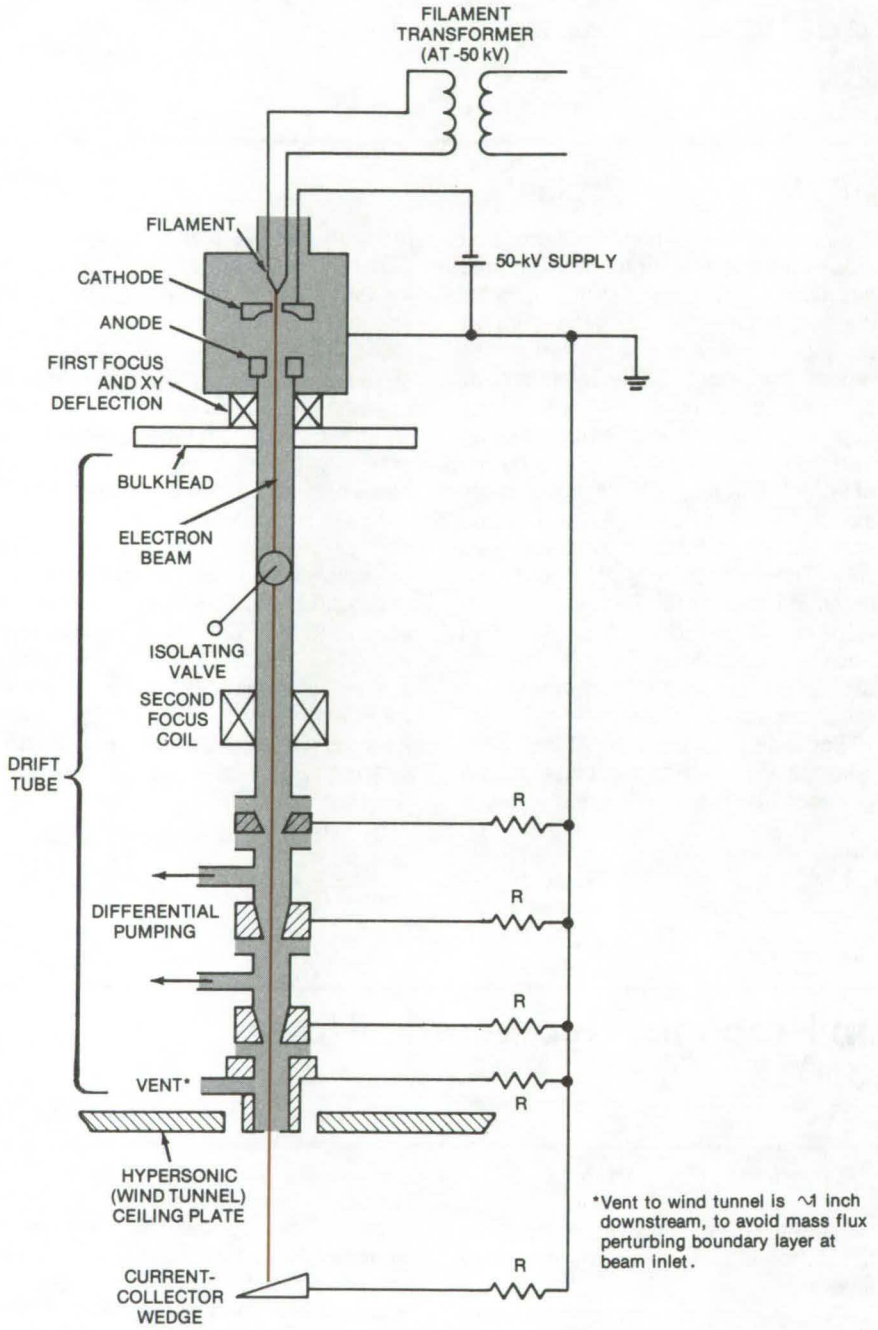

Electron Beam Is Injected into a hypersonic wind tunnel (mach 9.4, typical) through a drift tube 2 ft (0.6 m) in length. The flanges in the tube are electrically insulated from each other and tied to ground through the sensing resistors, R. The voltages across these resistors are monitored to help aline the beam.

penetrates the boundary layer, gradually spreads and attenuates due to collisions with the gas molecules, and is collected in a wedge-shaped Faraday cup at the center of the tunnel. The gas along the beam is excited and radiates light that is characteristic of the gas. The light is viewed through a window in the side wall of the tunnel. A photomultiplier measures the light intensity, from which the gas density can be determined; and a spectrometer resolves rotational lines within the excited vibrational bands to measure the temperature profile along the beam.

The electron-beam gun is coupled to the ceiling of the hypersonic wind tunnel by a drift tube that bridges the pressure differential between the gun (at 10^{-4} torr) and the tunnel (0.3 to 1.3 torr). Two steps of differential pumping are applied through 1-in. (2.5-cm) tubes at the tunnel end of the drift tube.

The Faraday cup is shaped and oriented to perturb only minimally the hypersonic flow stream. The cup is heated both by the beam (up to 50 W) and by the gas stream (stagnation temperature 820 K). Rather than adding a cooling system, the wedge is fabricated out of copper for good thermal conductivity and is replaced if eroded by local heating.

This work was done by Angus D. McRonald of Caltech for **NASA's Jet Propulsion Laboratory.** *For further information, Circle 62 on the TSP Request Card.*
NPO-13793

Detection of Boundary-Layer Transitions in Wind Tunnels

Use of accelerometer to detect laminar-to-turbulent boundary-layer transition has distinct advantages.

Langley Research Center, Hampton, Virginia

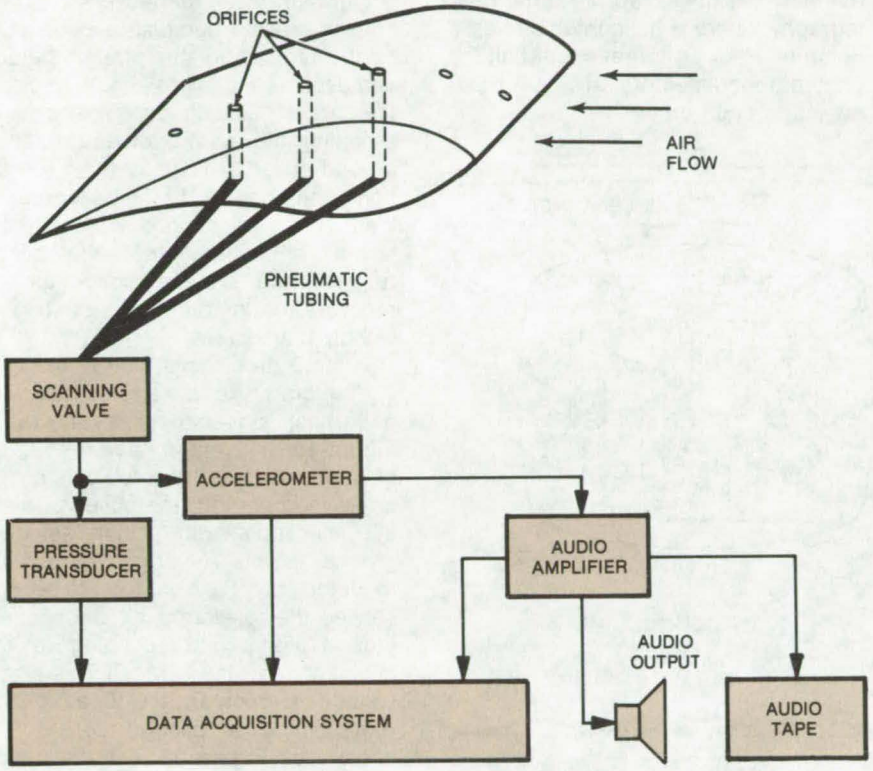

Accelerometer Detects Boundary-Layer Transitions on wind-tunnel models. Actually a small microphone, the accelerometer introduces no leaks into the system and allows pressure and boundary-layer data to be taken simultaneously.

Commonly applied techniques for detecting laminar-to-turbulent boundary-layer transitions on wind-tunnel models have included both the observation of oil flow over the model surfaces and the use of a stethoscope to detect noise changes along test-surface orifices. An accelerometer, actually a small microphone, used in place of the stethoscope at Langley Research Center has demonstrated several significant advantages over these previous methods.

In the oil-flow method, the upper surface of the model is actually coated with oil, and visual observations must be made to determine the location as well as the nature of the laminar-to-turbulent boundary-layer transition. With the stethoscope, an operator must be physically in the tunnel to connect his stethoscope to individual orifices along the test surface, starting at the leading edge and progressing from orifice to orifice until he reaches the trailing edge. The beginning of the turbulent boundary layer is detected as an increase in noise level over that for the laminar boundary layer.

The new technique replaces the stethoscope with an inexpensive accelerometer having several distinct advantages. First, data from the pressure transducer (see diagram) can be taken simultaneously with data from the accelerometer. Simultaneous data acquisitions were not possible previously because of the leak in the system introduced by the stethoscope, which is an open tube. Two separate runs were required to obtain both pressure and transition data. Secondly, the accelerometer allows measurements to be made at pressures above and below atmospheric, since a human operator is not required inside the tunnel as with a stethoscope. Thirdly, the electrical output of the accelerometer permits data inputs to a multitude of systems, such as to a computer for data reduction and storage or through an amplifier to an audio output or recording tape.

The system has been used successfuly in various applications, such as in laminar separation bubble studies; further extension of this technique is planned at Langley Research Center and at other installations.

This work was done by William R. Hood and Dan M. Somers of **Langley Research Center.** *No further documentation is available.*

Inquiries concerning rights for the commercial use of this invention should be addressed to the Patent Counsel, Langley Research Center [see page A8]. Refer to LAR-12261.

Helicopter Position Stabilizing System

A vertical gyroscope and a telescope help a helicopter fly in precise circles over a fixed ground target.

Langley Research Center, Hampton, Virginia

Helicopters used in measuring aerosol distribution from a ground source must be flown in precise circles over this source while pointing the sensor at the center of the target. A similar maneuver is necessary in aerial photography where a helicopter circles a common tracking target so that all the photographed sectors are at proper angles to each other.

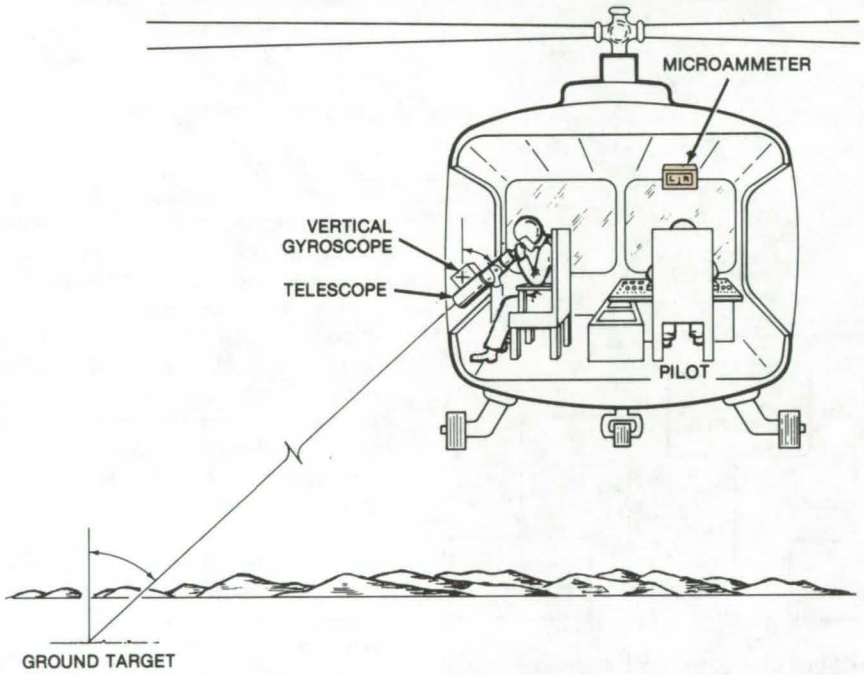

Figure 1. In this **Helicopter Position Stabilizing System,** the observer aims the telescope at a selected ground target. Once the pilot is informed that the telescope is on the target, he assumes the proper roll angle for circling the target. A null position on the microammeter tells the pilot that his angle is correct.

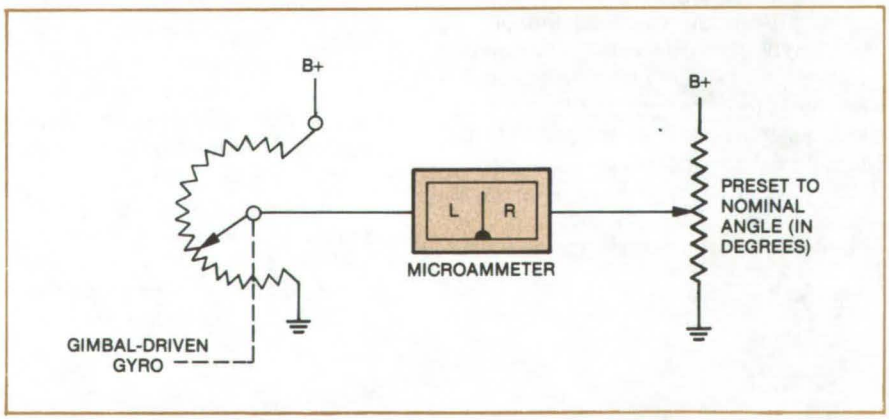

Figure 2. This **Control Circuit** compares the gyroscope output voltage with the selected reference voltage. When the voltages are equal, the microammeter is at null, indicating that the helicopter is at the proper angle.

Normally these maneuvers are difficult to execute because a pilot must bring his craft to the proper altitude and assume a fixed roll angle to circle the target. Conventional methods of assisting the pilot include either a ground observer to radio the information or an observer in the helicopter to instruct the pilot while watching the target. In either case, the pilot's reflexes are slowed down as he receives the instructions, resulting in wobbly meneuvers.

A more precise method of stabilizing the craft is to use a telescope with a vertical gyroscope, as shown in Figure 1. The system has one degree of freedom around the roll axis of the craft. In operation, the observer aims the telescope sight at the selected ground target. A vertical gyroscope mounted on top of the telescope senses the telescope tilt and generates a signal corresponding to the deviation from the vertical. This signal voltage is compared with a voltage representing a desired preset roll angle (see Figure 2). The difference between the two voltage values is displayed by a microammeter in front of the pilot. The objective is to maintain the ammeter at null position by steering right or left while circling the target.

A more complex system can be made by adding a directional gyroscope and a corresponding display, giving a second degree of freedom. The pilot will then be able to hover over an invisible target with known coordinates. Other possible uses include cargo discharge or pickup without a ground controller.

This work was done by Keith R. Jenkin of TRW, Inc., for **Langley Research Center.** *No further documentation is available.*
LAR-11670

Airframe Design for Reducing Cabin Noise

Low-frequency noise might be reduced by stiffness-control design of airframe structure.

Langley Research Center, Hampton, Virginia

Noise levels in the interiors of passenger aircraft are conventionally controlled with insulating materials such as fiberglass blankets and damping tapes. However, interior noise is rarely a major consideration when designing the airframe itself. This practice of leaving noise control to "parasitic materials" forces designers to trade off payload capacity and performance with passenger comfort.

This design approach with its drawbacks for conventional aircraft is even less acceptable with short-takeoff-and-landing aircraft with power-augmented lift systems such as blown flaps. These are aerodynamically designed with the engines tucked in close to the fuselage. STOL aircraft cabin noise is on the order of 20 dB higher than for conventional jets, and the peak of the noise spectrum is shifted toward lower frequencies because of the jet entrailment peculiar to STOL aircraft. The weight of adequate acoustic insulation would be prohibitive, and better ways are needed to reduce the low-frequency noise.

A promising solution is through "stiffness control" of the airframe. Most commercial aircraft cabins, structurally designed to handle operational loads, have major resonances in the 100- to 150-Hz range where noise due to powered-lift augmentation may be greatest. Structural responses above resonance are essentially inertial, and acoustic transmission loss is provided by the well-known "mass law." Below the resonance frequencies, structural responses can be controlled by structural stiffness, which can significantly reduce acoustic transmission. Thus, "stiffness control" implies a design wherein the aircraft structure can carry the required operational loads but where fundamental resonances are well above the frequency regime associated with maximum noise intensity. Such structures must be adequately stiff, strong, and light.

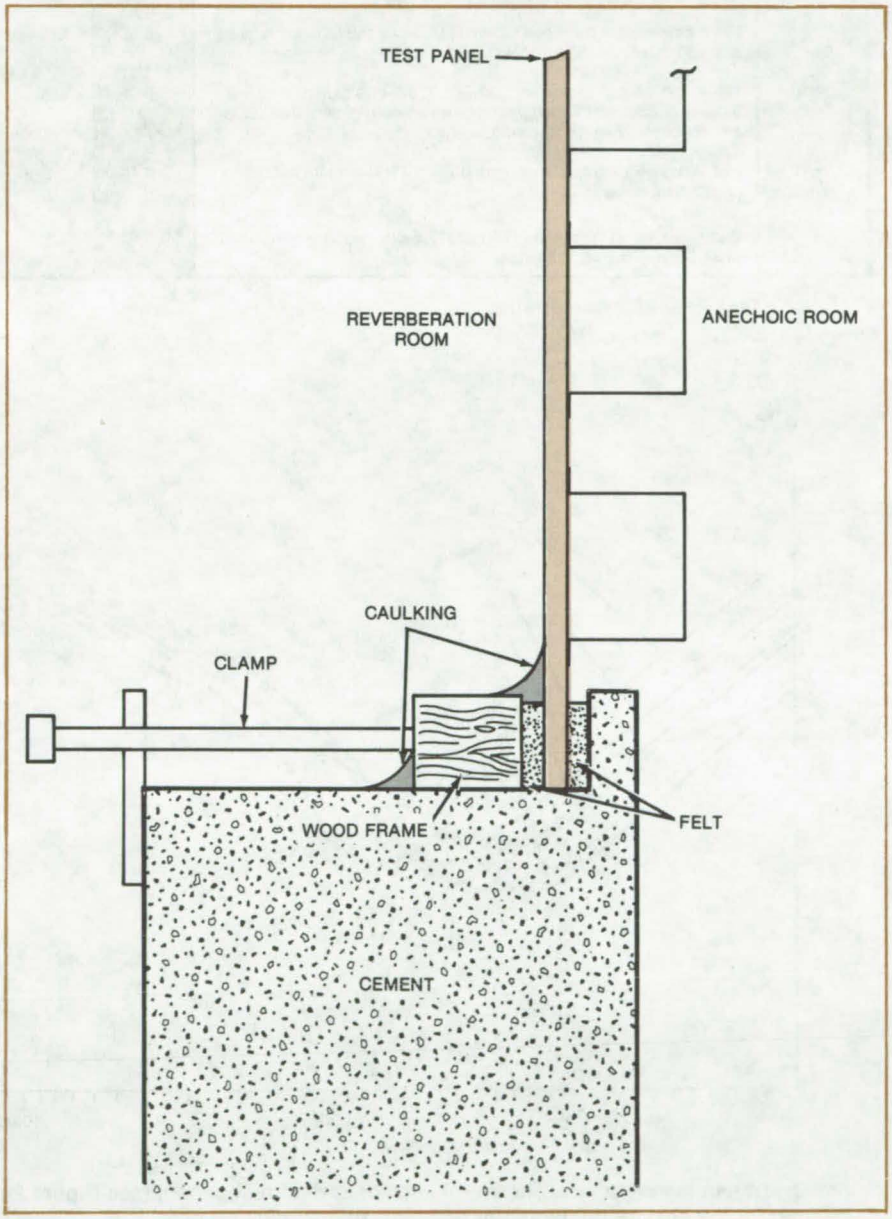

Figure 1. **Test Setup** for vibrational and acoustic tests was used to study aluminum and graphite/epoxy panels for STOL aircraft.

Vibration and acoustic tests (the acoustic test setup is shown in Figure 1) where made on a series of aluminum alloy and graphite/epoxy panels, all 30 by 40 in. (76 by 102 cm) with constructions and surface densities within a practical range for both STOL and conventional aircraft.

(continued next page)

Panel No.	Description [Note: All frames are along 30.0-in. (76.2-cm) dimensions.]	Surface Density (kg/m^2)	f_{11} (Hz)
a	Flat, 0.06-in. (1.524-mm) Al skin, Al hat frames 4 in. (10.16 cm) deep at 6.5-in. (16.5-cm) spacing	10.74	410 est.
a.1	Same as a, but also has 0.03-in. (0.762-mm) graphite/epoxy strips on Al frame caps	11.08	500
b	Same as a, except frames are all graphite/epoxy	8.00	820
c	Same as b, except panel has 125-in. (317.5-cm) radius of curvature along 30-in. (76.2-cm) dimension	8.00	815
d	125-in. (317.5-cm) radius along 30.0-in. (76.2-cm) dimension, 0.06-in. (1.524-mm) Al skin, graphite/epoxy corrugations 2 in. (5.08 cm) deep at 3.25-in. (8.26-cm) spacing	8.30	465
e	Flat, Al honeycomb sandwich, core 0.75-in. (1.91-cm) thick, 0.03-in. (0.762-mm) faces	6.44	225
f	Same as e, except panel has 125-in. (317.5-cm) radius of curvature along 30-in. (76.2-cm) dimension	6.44	420

Figure 2. **Test Panel Characteristics**

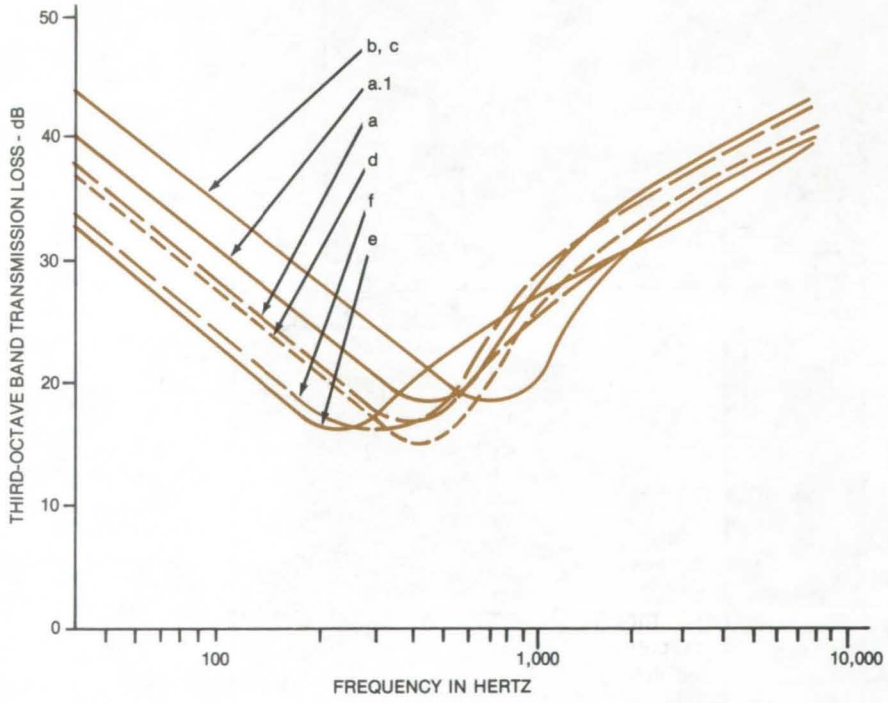

Figure 3. **Transmission Loss** is shown for each of several test panels (see Figure 2). Curve minimums are the fundamental resonant frequencies.

Figure 2 shows the physical characteristics of the test panels and the fundamental resonant frequencies, f_{11}. The tests were designed to obtain parametric information in the form of acoustic transmission loss curves at 31.5 to 8,000 Hz; a full-scale frequency range from well below the fundamental resonances of the materials (stiffness-controlled region) to well above resonance (mass-controlled region).

The tests show that below resonance, structural response is effectively a function of the stiffness of the system. Transmission-loss curves for all the test panels are shown in Figure 3. Significant decreases in noise can be obtained through stiffness control at all frequencies below about 400 Hz, with essentially no degradation of noise-reduction characteristics above 400 Hz. It appears, therefore, that stiffness control can effectively reduce low-frequency noise at acceptable structural weight. However, since relatively small panels were used in these tests, more comprehensive work with full-scale aircraft cabin designs would be required to examine adequately the attendant complexities related to matching dynamically the stiffness properties of such airframe components as skins, ring frames, and longitudinal stiffeners.

This work was done by Gordon L. Getline of General Dynamics for **Langley Research Center.** *Further information may be found in NASA CR-145104 [N77-15029], "Low-Frequency Noise Reduction of Lightweight Airframe Structures," a copy of which may be obtained at cost from the North Carolina Science & Technology Research Center* *[see page A7]*.

Inquiries concerning rights for the commercial use of this invention should be addressed to the Patent Counsel, Langley Research Center *[see page A8]*. *Refer to LAR-12097.*

Books and Reports

These reports, studies, and handbooks are available from NASA as Technical Support Packages (TSP's) when a Request Card number is cited; otherwise they are available from one of NASA's Industrial Application Centers or the National Technical Information Service.

Predicting Damage from Exploding Vessels

Pressure-Wave and Fragment Effects

A workbook has been written which provides the designer and safety engineer with the best currently available technology for predicting damage and hazards from explosions of propellant tanks and bursts of pressure vessels. This workbook provides the safety engineer with relatively simple yet comprehensive methods for estimating blast and fragment hazards for accidental explosions in flight vehicles and in flight designed systems. The information is presented in the form of graphs, tables, and nomographs that allow easy calculations without reverting to difficult mathematical procedures or the use of extensive computer programs. Complex methods used to develop simple prediction aids are fully described in the appendexes.

The material in the handbook is based on previous studies of fragmentation from bursting pressure vessels and on the literature on characteristics and effects of blast waves and fragment impacts. Publications are identified that present methods for estimating blast yields of liquid propellant accidents.

The subjects covered and special features in the workbook include:

- prediction of blast wave characteristics for gas vessel bursts,
- estimates of explosive yields,
- characteristics of pressure waves,
- effects of pressure waves and extensive applications of the pressure-impulse damage concept to a wide variety of structures and to humans,
- characteristics of fragments and the effects of fragment impact on structures, and
- risk assessment and integrated effects.

The estimates of hazards and damages should also apply to boilers.

The workbook also contains an extensive bibliography as well as detailed solutions to specific problems.

This work was done by W. E. Baker, Roger L. Bessey, James J. Kulesz, Gary A. Oldham, Van B. Parr, Randall E. Ricker, and Peter S. Westine of Southwest Research Institute for **Lewis Research Center.** *Copies of the workbook, NASA CR-134906 [N76-19296] "Workbook for Predicting Pressure Wave and Fragment Effects of Exploding Propellant Tanks and Gas Storage Vessels", may be obtained at cost from the New England Research Application Center* [see page A7].

LEW-13042

Computer Programs

These programs may be obtained at very reasonable cost from COSMIC, a facility sponsored by NASA to make new programs available to the public. For information on program price, size, and availability, circle the reference letter on the COSMIC Request Card in this issue.

Air-Cushion Landing System

Aids designers with static and dynamic predictions

The static and dynamic performance of an air cushion landing system (ACLS), is simulated in a computer program that treats four primary ACLS subsystems: the fan, the feeding system, the trunk, and the cushion. The configuration of these systems is sufficiently general to represent a variety of practical designs.

Air from the fan flows through the ducts and plenum (feeding system) and enters the trunk. The trunk has several rows of orifices that communicate both with the cushion and the atmosphere. One component of airflow from the trunk enters the cushion and another leads directly to the atmosphere. The cushion flow exhausts to the atmosphere through the clearance gap between the trunk and the ground.

For increased model generality, direct flow from plenum to cushion and plenum bleed flow to atmosphere through a pressure relief valve were included. A dynamic fan model was developed based on static pressure-flow characteristics and physical dimensions of the fan. A hybrid trunk model was also developed, wherein the curved trunk sections at bow and stern were modeled as frozen sections, while the straight sidewalls were modeled as flexible members. The total simulation was shown to have good correlaton with experimental model tests. Thus, the program should prove very useful in the design and analysis of future air cushion landing systems.

In the static simulation, the equilibrium conditions for the ACLS are calculated. These include the position of the aircraft center of gravity; orientation (pitch and roll angles); equilibrium pressures in the trunk, cushion, and plenum; equilibrium flows in various parts; and the theoretical operating power required.

If the particular design considered is physically infeasible, an error indication is produced. In addition, the static simulation generates load maps that are useful in evaluating the behavior of the ACLS in pure heave, pitch, and roll modes. The load map for the heave mode consists of values of center-of-gravity elevation, trunk and cushion pressures, fan-pressure rise and flow, gap area, and trunk-ground contact area as a function of aircraft weight. The load maps for the pitch and roll modes are similar to the heave load map, with weight replaced

(continued next page)

by respective moment, and center-of-gravity elevation replaced by the pitch or roll angle. These load maps can be used to evaluate stiffness of the ACLS in all three modes.

The dynamic simulation predicts behavior of the ACLS when it is in motion. ACLS operations that can be simulated include: landing, taxiing over an airfield, negotiating a bump or a ditch, negotiating a ramp, moment-release tests, and drop tests. For many of these operations, the dynamic simulation evaluates key ACLS parameters such as location of the aircraft center of gravity, pitch and roll orientation of the aircraft (yaw is assumed to be absent), trunk and cushion pressures, fan flow, trunk-cushion flow, trunk-atmosphere flow, cushion-atmosphere flow, sink rate, heave acceleration, and gap area as a function of time. Plots of these parameters versus time can also be produced.

This program is written in FORTRAN IV for the CDC RUN compiler and has been implemented on CDC 6400 with a central memory requirement of approximately 72K octal of 60-bit words. For plotted output, a CALCOMP plotter is required.

This program was written by A. B. Boghani, K. M. Captain, and R. B. Fish of Foster-Miller Associates, Inc. for **Langley Research Center.** *For further information, Circle A on the COSMIC Request Card.*
LAR-12303

Internal and External 2-D Boundary-Layer Flows

Numerical computation by finite difference

The computer program STAN 5 was developed to compute general two-dimensional turbulent boundary-layer flow using finite-difference techniques. It has proved accurate and useful in experimental turbulent boundary-layer research. The program is able to handle a large variety of boundary-layer problems without requiring any modifications to the program code. Two-dimensional flows that can be accommodated include boundary layers on a flat plate, flow inside nozzles and diffusers (for a prescribed flow distribution), flow over axisymmetric bodies, and developing or fully developed flow inside circular pipes and flat ducts. The structure also allows for user modification of the code to accommodate unique problems. This program should prove useful in many applications where accurate boundary-layer flow calculations are required.

The types of flows modeled are those described by the parabolic differential boundary-layer equations, which include the continuity, momentum, and stagnation enthalpy equations. These equations are written in a coordinate system for describing the flow of a turbulent compressible fluid over an axisymmetric body. Viscous dissipation in the energy equation is included as an option so that high-velocity flows can be readily solved. Provision is also made for introducing axial body forces and internal heat generation.

Turbulence modeling can include a Prandtl mixing scheme throughout the flow, a turbulent kinetic-energy scheme for flow outside the sublayer region, and an eddy diffusivity function in the outer part of the boundary layer. Laminar flow can also be modeled, in which case the turbulent stress and heat flux are ignored. Provisions are made for a transition from a laminar to a turbulent boundary layer based on a momentum-thickness Reynolds number criterion. Fluid properties may be treated as constant, with values being input directly, or as variables, with values generated by a user-supplied subroutine. Binary diffusion problems can readily be solved including heat transfer.

A fully-implicit differencing scheme is employed for all the dependent variables except for fluid and turbulence properties, which are handled explicitly. The implicit scheme, along with the conservation equations, allows large forward steps without stability problems. The explicit scheme requires no iteration but may have relatively small forward steps when the fluid and turbulence properties are changing rapidly. This restriction to relatively small forward steps (typically about one or two boundary-layer thicknesses) allows for the easy handling of variable boundary conditions and for the frequent output of data, such as heat flux, when desired.

Input begins with a description of the type of flow problem to be solved. This includes geometric information, flow type, fluid properties, number of boundary-layer equations to be solved, and the grid structure size. Further input provides the modeling and solution scheme controls, body forces, and initial profiles. Output consists of user-selected data, such as velocity, enthalpy, mass concentration, shear stress at a wall, heat flux, entrainment rates, eddy viscosity, momentum thickness, Reynolds number, and pertinent profiles.

This program is written in FORTRAN IV for the IBM FORTRAN H compiler and has been implemented in batch mode on an IBM 360 computer with a central memory requirement of approximately 120K of 8-bit bytes.

This program was written by M. E. Crawford and William M. Kays of Stanford University for **Lewis Research Center.** *For further information, Circle B on the COSMIC Request Card.*
LEW-13009

Stress Analysis Under Component Relative Interference Fit

Finite-element program for axisymmetric loading

A finite-element computer program has been developed that enables the analysis of distortions and stresses occurring in components having a relative interference. The program is limited to situations in which the loading is axisymmetric. External, inertial, and thermal loads may be applied in addition to forces arising from an interference condition. The components under investigation may comprise different homogeneous isotropic materials with properties that may be temperature dependent.

The ability of the engineer to undertake the analysis of deformations and stresses occurring in the structures and components with which he deals has changed remarkably in the last 15 years. The development of finite-element approximation techniques, coupled with the widespread availability of digital computers, has paved the way for detailed examination of the behavior of loaded structures and machine parts of quite complex geometry. Some of the more recently developed programs enable the study of situations in which three-dimensional loading pertains.

This program restricts itself to simple elements and axisymmetric loading situations. Unlike most finite-element programs, however, it can undertake a direct analysis of components that have relative interference. It is a frequent engineering practice to mate or prestress parts using shrink or press-fitting techniques. The analysis of such situations has, in general, been limited to axially-invariant axisymmetric situations. The program enables the solution of problems in which statically indeterminate conditions occur as a result of interference fits. It enables one node in a finite-element mesh to be displaced by a specified amount relative to another without having to know how the two nodes move in relation to some fixed coordinate system.

The finite-element types incorporated into the program are axisymmetric trapezoidal and triangular elements. A linear displacement model within the elements was assumed, enabling the stiffness characteristics in matrix form to be determined by analytic integration of the strain energy integrals. The unknowns are normally node displacements in the radial and axial directions. The output comprises the input information, nodal distortons, element stresses, and details of the interference contact conditions. The running of multiple cases, with one or a number of different geometries, is also possible.

The program is written in FORTRAN and has been developed on a UNIVAC 1100 machine with a FORTRAN V compiler.

This program was written by Christopher M. Taylor of the University of Leeds, England, for **Lewis Research Center.** *For further information, Circle C on the COSMIC Request Card.*
LEW-12911

Edge Geometry of Turbomachine Blades

Iterative procedure simplifies input specification.

A computer program has been written that calculates leading- and trailing-edge circle radii, tangency angles on the leading- and trailing-edge circles, and stagger angle of turbomachinery blade sections, using only spline points defining the blade surfaces. The program also shifts the origin of the blade coordinates to the leading edge of the blade.

In recent years, several computer programs have been written that calculate the velocities on a blade-to-blade surface of a turbomachine. These programs require an accurate geometrical description of the blade since spline-fit curves are used to define the blade surfaces. The inputs required include blade chord, blade stagger, leading- and trailing-edge circle radii, angles of tangency on the leading- and trailing-edge circles, and intermediate spline points. These inputs are usually obtained from measurements made on a physical layout of the blade or from a meridional flow analysis program. In either case, it is difficult to specify these inputs with the degree of accuracy necessary to insure a smooth blade shape without using a costly and time-consuming trial-and-error procedure with the computer.

Small errors in any of the input can result in a spline fit through the given input spline points in which the first and second derivatives of the curve do not vary smoothly. Since the computation of surface velocities is highly dependent on the blade surface curvatures, it is important that the geometry input be specified accurately. If the first and second derivatives are not smooth, unrealistic peaks and valleys in the surface velocity distribution will occur.

This new computer program overcomes these difficulties by using an iterative procedure. The blade surface input coordinates are defined by meridional distance, m, and the angle of rotation, Θ. The origin for both the m and Θ coordinates may be anywhere since it will be shifted by the program to the leading edge of the blade.

Also required as input are the radii from the axes of rotation of the leading and trailing edges. Since spline-fit curves are used to define the two blade surfaces, the input spline points do not reflect the leading- and trailing-edge circle curvatures but instead define a smooth blade with the surface extrapolated to the leading and trailing edges. This is the type of blade definition obtained from a known mean camber line and tangential thickness distribution.

The iterative procedure used fits a circle in the region bounded by the two blade surfaces and the leading or trailing edge. The requirement that the circle be tangent to all three boundaries leads to a unique solution. Once the radius of this circle is determined, the remaining geometry is easily calculated.

The output from this program may be used directly as the geometrical input for a NASA-developed program for calculating transonic velocities on a blade-to-blade stream surface of a turbomachine (TSONIC) (LEW-10977). The program may be used for axial, radial, and mixed-flow turbomachine blades.

This program can also be used in conjunction with a physical layout since it is often difficult to measure angles and leading- and trailing-edge radii with any degree of accuracy, while it is a relatively easy task to obtain five or six spline points on the blade surfaces that will yield a smooth blade shape.

The program is written in FORTRAN IV for use on the IBM TSS/360-67 or UNIVAC 1110.

This program was written by Lawrence F. Schumann of the U.S. Army Air Mobility R&D Laboratory for **Lewis Research Center.** *For further information, Circle D on the COSMIC Request Card.*
LEW-12979

Thermal Performance of Shaft Bearing Systems

Program SHABERTH calculates loads, torques, temperatures, and fatigue lives.

A computer program, called SHABERTH, was developed to predict the steady-state and transient thermal performance of a multibearing shaft system operating with either wet or dry friction. SHABERTH is a design analysis tool with which the thermal performance characteristics of a shaft bearing system can be determined. SHABERTH calculates the loads, torques, temperatures, and fatigue lives for ball and/or roller bearings on a single shaft. The comprehensive nature of this program allows for the study of many causes of bearing instability. The program also allows for

(continued next page)

an analysis of the system reaction to the termination of lubricant supply to the bearings and other lubricated mechanical elements. SHABERTH should prove to be a valuable tool in the design and analysis of shaft bearing systems.

The SHABERTH program is structured with four nested calculation schemes. The thermal scheme performs steady-state and transient temperature calculations that predict system temperatures for a given operating state. The bearing dimensional-equilibrium scheme uses the bearing temperatures, predicted by the temperature mapping subprograms, and the rolling-element raceway load distribution, predicted by the bearing subprogram, to calculate bearing diametral clearance for a given operating state. The shaft-bearing system load equilibrium scheme calculates bearing inner-ring positions relative to the respective outer rings such that the external loading applied to the shaft is brought into equilibrium by the rolling-element loads, which develop at each bearing inner ring for a given operating state. The bearing rolling-element and cage-load equilibrium scheme calculates the rolling-element and cage equilibrium positions and rotational speeds based on the relative inner/outer ring positions, inertia effects, and friction conditions. The ball bearing subprograms in the current SHABERTH program have several model enhancements over similar programs. These enhancements include an elastohydrodynamic (EHD) film-thickness model that accounts for thermal heating in the contact area and lubricant film starvation; a new model for traction in concentrated contacts based on a semiempirical model for fluid traction combined with an asperity load-sharing model; a model for the hydrodynamic rolling and shear forces in the inlet zone of lubricated contacts, which accounts for the degree of lubricant film starvation; a modeling of the normal and friction forces between a ball and a cage pocket, which accounts for the transition between the hydrodynamic and elastohydrodynamic regimes of lubrication; and a model of the effect on fatigue life of the ratio of the EHD plateau film thickness to the composite surface roughness.

SHABERTH is intended to be as general as possible. The models in SHABERTH allow for the complete mathematical simulation of real physical systems. Systems are limited to a maximum of 5 bearings supporting the shaft, a maximum of 30 rolling elements per bearing, and a maximum of 100 temperature nodes. The SHABERTH program structure is modular and has been designed to permit refinement and replacement of various component models as the need and opportunities develop.

This program is written in FORTRAN IV and has been implemented on a UNIVAC 1100-series computer with a central memory requirement of approximately 86K of 36-bit words.

This program was written by William Crecelius of SKF Industries, Inc., for **Lewis Research Center.** *For further information, Circle E on the COSMIC Request Card.*
LEW-12761

Structural Performance Analysis and Redesign

Group of programs for systems with over 50,000 DOF

SPAR is a system of computer programs designed to perform stress, buckling, and vibrational analyses of large, linear, finite-element systems in excess of 50,000 degrees of freedom. Processing costs, execution time, central memory storage, and secondary data storage requirements are kept reasonable through the use of sparse matrix solution techniques and other computational and data management procedures designed for problems of very large size.

Efficient eigensolver techniques often allow the same finite-element model to be used for both static and dynamic analyses. For static stress analysis, SPAR accepts applied loading data in any or all of the following categories:

- Point forces and moments acting on joints,
- Directly-specified joint motion components,
- Inertial loading,
- Nodal (joint) temperatures,
- Nodal (joint) pressures,
- Thermal loading defined for individual structural elements,
- Dislocational (initial mismatch) loading defined for individual elements, and
- Pressure loading defined for individual elements.

The finite elements currently available with SPAR include various formulations of bars, beams, triangular and quadrilateral membranes, shear panels, and fluid elements. Elements may be defined singly or through a variety of network generators, or combinations thereof, by specifying the joints to which they are connected and pointers to applicable entries in tables of section properties, material constants, and the like.

In linear vibration and bifurcation buckling problems, the eigenvalue and vector extraction procedure employs an iterative process consisting of a simultaneous iteration procedure followed by a Rayleigh-Ritz procedure, followed by a second simultaneous iteration procedure, etc., resulting in successively refined approximations. The eigensolver component of SPAR can also be used to solve 'shifted' vibrational eigenproblems, which is useful when computing the vibrational modes associated with eigenvalues in the neighborhood of specified constant values.

Input to SPAR is free-field. A command-oriented executive control language allows the user to design execution sequences suited to the requirements of each individual application. Facilities are also provided for automated mesh generation and input data validity checking. Plotting capability is available for inclusion in SPAR or to be set up as a stand-alone program to operate from previously generated data. The graphics capabilities include undeformed, deformed, and vibration mode plots of the structure and plots of structure modeling including node and element labeling. The plot routines are written for an SC 4020 in the UNIVAC version and a CALCOMP in the CDC versions.

Level 11 of SPAR includes several new capabilities as well as operational enhancements over previous levels of SPAR. Fluid elements have been included along with a hydroelastic mesh generator. One of the most important new features of level 11 is the ability to handle composite and laminated shell elements. Individual laminate stresses can be recovered,

even for thermal loadings such as occur in fabrication and curing.

SPAR is available for implementation on CDC 6000 or CYBER Series machines operating under SCOPE (LAR-12213) or NOS (LAR-12234) and on UNIVAC 1100 Series machines operating under EXEC 8 (MFS-23182). SPAR has a minimum central memory requirement of approximately 20K to 30K (decimal) words. During the course of a run, the central memory field length can be modified dynamically to permit additional memory resources to be acquired temporarily for the duration of the specific computational activity.

This program was written by W. D. Whetstone of Engineering Information Systems, Inc., for **Langley Research Center** *and Larry Kiefling of* **Marshall Space Flight Center.** *For further information, Circle F [CDC 6000 Series], Circle G [CYBER Series], or Circle H [UNIVAC 1100 Series], on the COSMIC Request Card.*
LAR-12213, LAR-12234, MFS-23944

Thermal Hydraulic Analyzer

Transient and steady-state problems solved with lumped-parameter representation

The Thermal Hydraulic Analyzer Program (THAP) allows the user to solve thermal problems, hydraulic problems, and combined thermal and hydraulic problems. The program solves both transient and steady-state thermal problems, steady-state hydraulic problems, and combined thermal and hydraulic transient or steady-state problems. The physical system is approximated to the desired degree of accuracy with a lumped-parameter representation, using the elements provided by the program.

Any complex thermal/hydraulic system can be modeled by proper synthesis of program elements connected between nodes. Elements are provided to handle conduction, radiation, heat inputs, line-pressure drops, pumps, flow-rate inputs, film conduction, fluid-motion heat conduction, and fluid-flow heat capacity. At the node points between elements, the dependent variables (temperature and pressure) are calculated. Material properties or fluid properties can be input by means of curves. A variables block allows the user to do unique calculations and testing, using the program parameters, program keywords, and curve data. The output block allows selective printing of the required output. It also allows the user to obtain graphic output when using CRT's.

Several innovative techniques make this program more accurate and less costly to run. The one-and-a-half "step method" has been developed for steady-state iterative solution of both thermal and hydraulic problems. The methods use next-neighbor nodes for those already calculated in the current iteration and next-neighbor plus next-to-next neighbor nodes for those nodes not yet calculated in this iteration. This allows the errors to be reduced much more rapidly throughout the steady-state network, and convergence time is likewise reduced.

A forward option is provided for thermal fluid-flow transient problems; it has been shown to allow time-increment steps to 100 times the fluid-flow time between adjacent nodes with less than 5 percent error in the results. Additional techniques include the alternating-direction method for the thermal transient calculation and the matrix method for the steady-state hydraulic solutions. Also the matrix method can be used as the first approximation to the nonlinear steady-state hydraulic equations followed by use of the iterative method until convergence occurs. Many non-branched pipes can be combined into a larger pseudoelement to reduce significantly the computer time required to balance the hydraulic system.

The user's input defines the thermal/hydraulic model, initial conditions, and control information. The input has been made as natural, simple, and compact as possible to reduce the input error and document references.

The IBM version of THAP is written in FORTRAN and IBM OS Assembler. The program has been implemented on an IBM 370 computer with a central memory requirement of approximately 390K 8-bit bytes.

The UNIVAC version of THAP is written in FORTRAN V and requires an included relocatable library. The program has been implemented on a UNIVAC 1110 with a central memory requirement of approximately 60K of 36-bit words.

The CDC version of THAP is written in FORTRAN IV for the CDC FTN compiler and requires an included relocatable library. The program has been implemented on a CDC 6000-series machine with a central memory requirement of approximately 150K octal of 60-bit words and is overlaid.

This program was written by Erculano E. Garcia and Robert W. Santen of Rockwell International Corp. for **Johnson Space Center.** *For further information, Circle J [IBM Version], Circle K [UNIVAC Version], or Circle L [CDC Version] on the COSMIC Request Card.*
MSC-18014, MSC-16797, MSC-16877

Analysis of Linear Viscoelastic Structures

Program for a wide variety of structures and materials

VISCEL is a general-purpose program for solving equilibrium problems associated with one-, two-, or three-dimensional linear thermoviscoelastic structures. It is an updated and extended version of the linear equilibrium problem solver ELAS (COSMIC Program NPO-10598/NPO-11555). A synchronized material property concept utilizing incremental time steps and the finite-element displacement approach are used. VISCEL can be used to analyze a wide variety of structures having elastic or viscoelastic properties and constructed of any isotropic, orthotropic, or anisotropic material.

The fundamental equilibrium problem in structural analysis can be formulated as differential equations with appropriate boundary conditions, or an equivalent extremum formulation based on the principle of minimal potential energy and its complement can be used. In this program, structural discretization is achieved by the finite-element displacement-matrix technique. This is a variant of

(continued next page)

the well-known Ritz method for the minimization of the total potential energy function associated with the admissible displacement trial functions.

The admissible functions are restricted to be sufficiently smooth and are required to satisfy essential boundary conditions arising from the requirement of geometric compatibility. This is achieved by expressing the trial solution in terms of a set of linearly-independent known functions and undetermined parameters and then by minimizing the functional with respect to those parameters.

In the finite-element method that VISCEL uses, a structure is discretized by a suitable mesh of node points and a family of connecting elements. The parameters to be determined by potential energy minimization are the nodal point displacements; the fundamental assumption in the procedure is that the total potential energy of the entire structure is equal to the sum of the potential energies of the individual elements.

Almost any structure can be handled by VISCEL because of the availability of linear, triangular, quadrilateral, tetrahedral, hexahedral, conical, triangular torus, and quadrilateral torus elements. In viscoelasticity, the creep strain rate or the relaxation stress response depends not only on the current stress and strain state but also on the entire history of its development in the time domain. In VISCEL the viscoelastic equations are developed as finite-difference equations in time and as finite-element matrix equations in space. An option allows the employment of constant time steps in the logarithmic scale, thereby reducing computational efforts resulting from accumulative material memory effects.

Inputs to VISCEL consist of the coordinates of the mesh points, the connecting mesh elements, material properties, and loads. Outputs include deflections and stresses at the mesh points. Other features are dynamic memory allocation, an optional node-relabeling scheme, and boundary condition imposition during assembly of the stiffness matrix.

The program is written in FORTRAN V and has been implemented on a UNIVAC 1108 computer under control of EXEC 8 with a central memory requirement of 12K (decimal) of 36-bit words. It is divided into four segments: input, generation, deflection, and stress.

This program was written by Kajal K. Gupta and Ewald Heer of Caltech for **NASA's Jet Propulsion Laboratory** *and F. A. Akyuz of the Technical University of Istanbul, Turkey. For further information, Circle M on the COSMIC Request Card.*
NPO-13197

Machinery

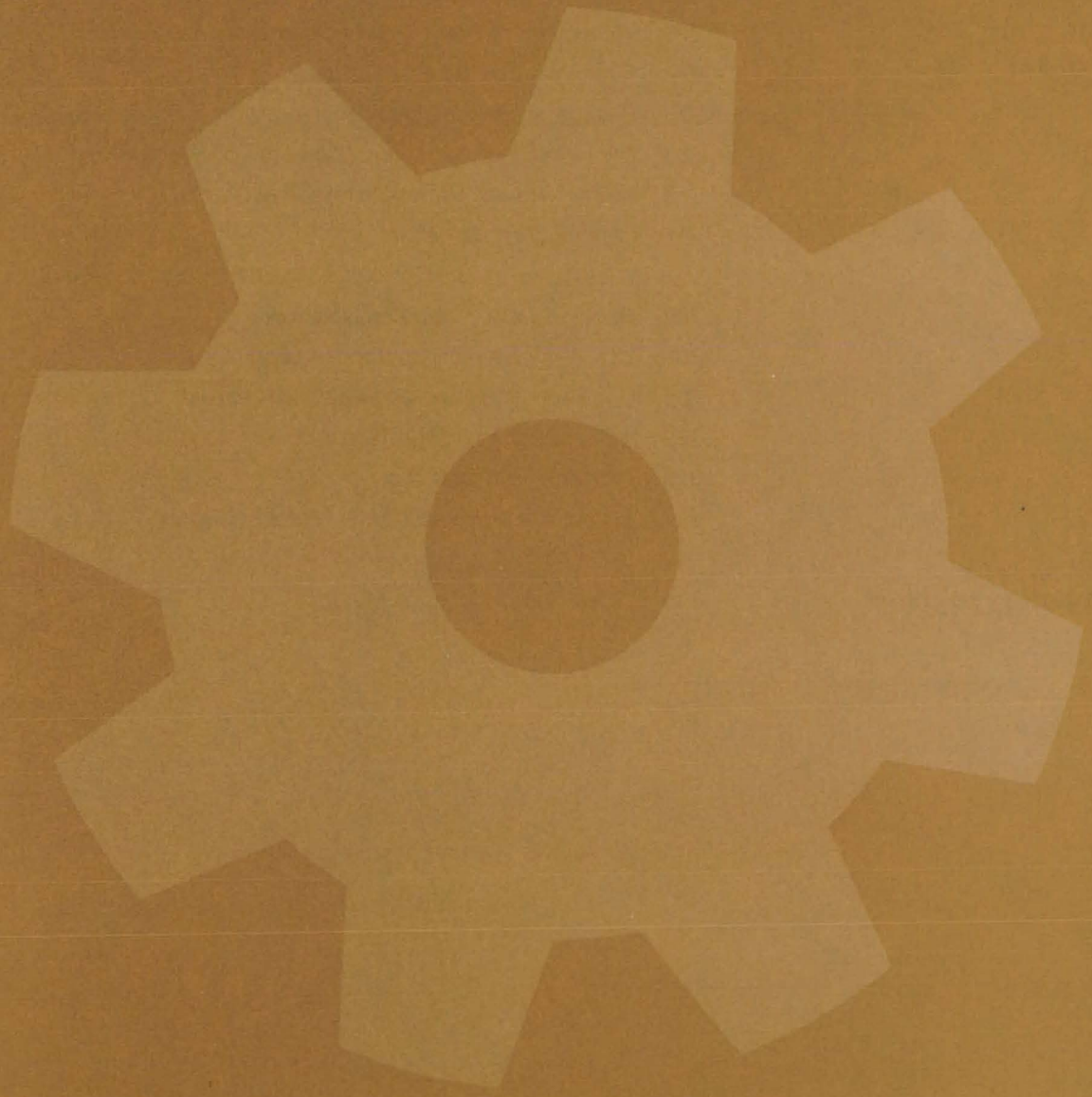

Hardware, Techniques, and Processes

275 Meter for Very Slow Flows
276 Wind-Wheel Electric-Power Generator
277 Subminiature Hydraulic Actuator
278 Emergency Escape Device
278 Ultrasonic Extensometer Measures Bolt Preload
280 Aircraft Trailing Vortex Hazard Alleviators
281 Compact Ratchet Wrench
281 Wide-Temperature Corrosion-Resistant Pressure Regulator
282 Low-Frequency Vibration Isolation
283 Simpler Valve for Reciprocating Engines
285 Dual-Action Expand-and-Latch Mechanism
285 A Sharp Knife for High Temperatures
286 Adhesive-Removal Tool
287 Collapsible Module Extends Tenfold in Height

Computer Programs

288 Three-Phase Induction Motors

Meter for Very Slow Flows

Nonprotruding sensor detects flows up to 0.5 ml/min with sensitivity of 0.01 ml/min.

Lyndon B. Johnson Space Center, Houston, Texas

A solid-state sensing unit developed for use with NASA's Water-Quality Monitoring System (see page 238) can detect small velocity changes in a slowly moving fluid. This nonprotruding sensor should be useful in numerous other applications requiring sensitive measurement of slow flows.

In the Water-Quality Monitoring System, chemicals are injected into the flowing sample stream at 0.2 and 0.05 ml/min. The reagent input flow is monitored as an indicator of pump, tubing, or other fluidic failures. The sensor cannot protrude into the fluid-flow stream where it might interfere with the flow.

The flowmeter developed for this purpose is outlined in Figure 1. It has a sensitivity of 0.01 ml/min. Two thermistors and a small resistance heater are encapsulated in an epoxy block.

The first thermistor measures the "ambient" fluid temperature, and the second measures the temperature of the heated platinum tube. An external power supply is used to keep a constant temperature differential between the two thermistors. The power required is a measure of the flow rate. A typical response curve is shown in Figure 2.

The device is easily made by placing the components on a piece of polyethylene tubing and casting them in place with epoxy. The tubing is then pulled out, leaving a smooth channel for fluid flow with excellent thermal contact between the fluid and platinum tubes.

This work was done by Wilfred J. Baxter, Jr., Martin S. Frant, and Steven J. West of Orion Research Inc. for **Johnson Space Center.** *For a copy of the thermal control schematic, Circle 63 on the TSP Request Card.*
MSC-18112

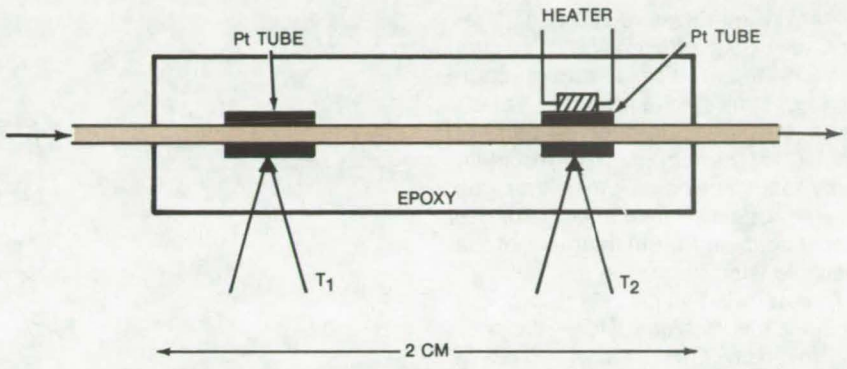

Figure 1. **Very-Slow-Flow Fluid Monitor** is an epoxy box cast with a smooth channel including a platinum-and-thermistor sensor section and a platinum-heater-and-thermistor section. The power required to maintain a constant temperature differential between the two sections is a measure of the flow rate.

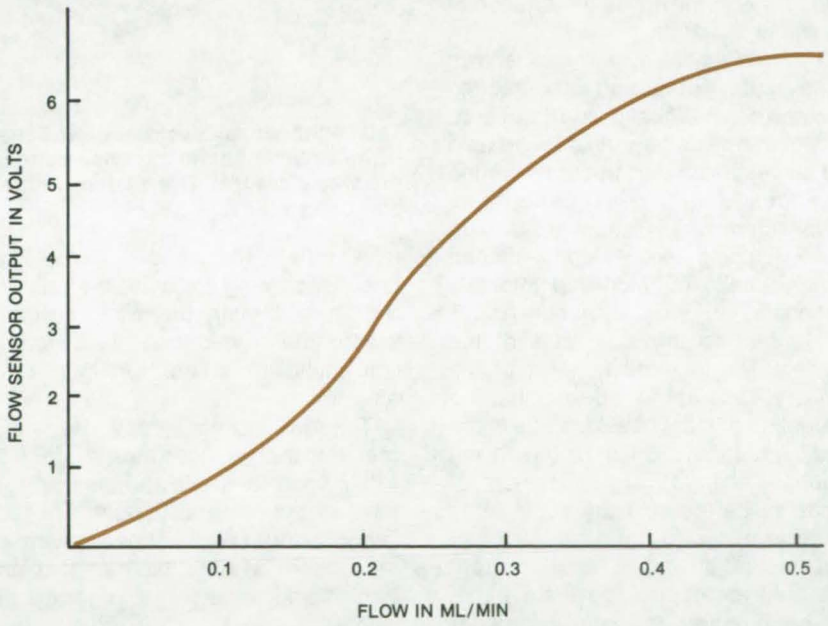

Figure 2. **Typical Sensor-Output vs. Flow Curve** is shown for the detector in Figure 1.

Wind-Wheel Electric-Power Generator

A rotor mounted in a special housing utilizes wind currents to generate electric power.

Marshall Space Flight Center, Alabama

Many wind-driven electric generators have poor efficiency and require frequent repair. For example, common windmills often sustain blade damage from winds directed perpendicular to the direction of rotation. Many other devices are either too large for effective maintenance or are simply not built for efficient use of the available wind forces.

A new wind-wheel electric-power generator is designed for efficiency and reliability. The new wheel has a rotor mounted in a housing designed with a number of ducts. These ducts capture the wind currents, which drive the bladed rotor. The ducts are configured to integrate the effect of all the wind forces to maximize the rotation of the wheel.

The wind-wheel system, as shown in the figure, rotates about a bearing mounted on a vertical support column. The column rests on a rigid foundation and serves as an axis about which the system can turn into the direction of prevailing winds. The forward portion of the housing has a funnel-shaped primary intake duct divided into two sections. Two auxiliary intake ducts are located on the side walls of the housing. The longitudinal axes of the auxiliary ducts are flared to adjust the orientation of the wheel for shifts in the wind direction. Should the wind direction change, an imbalance of forces inside the auxiliary ducts turns the system toward the wind.

In operation, the wind current enters all the ducts. The main thrust will be directed through the upper section of the primary duct. This section, designed using venturi principles and with a nozzle that arcs up toward the wheel blades, directs a high-velocity airflow to turn the wheel. A second vent below this nozzle and a deflecting plate direct additional air toward the blades, adding to the total force. A cowling on top of the primary duct also directs the wind currents toward the blades and at the same time shields the wheel from interfering wind forces.

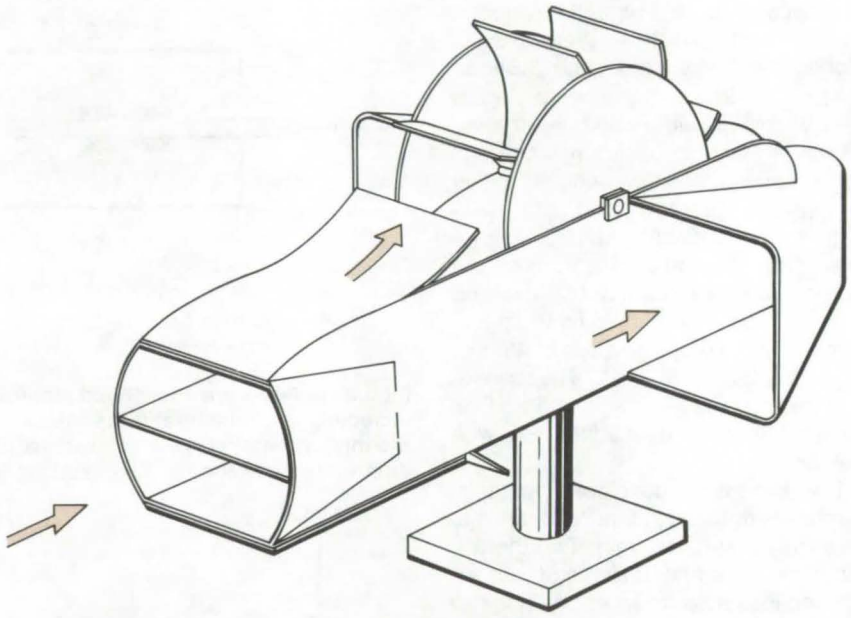

This **Wind-Wheel Electric-Power Generator** maximizes the use of the available wind, using a number of ducts. Wind currents captured by the ducts are directed against the wheel blades. The system rotates around its supporting column to face the prevailing winds.

The two auxiliary ducts lead to a manifold that includes a separator wall to eliminate possible turbulence from the two opposing air inputs. The two separate airflows are aimed upward by the bottom wall of the manifold and furnish additional force to rotate the wheel.

The wheel is mounted on an axle perpendicular to the main airflow. It includes a number of curved blades (between 3 and 16) extending radially. Each blade is oriented at a 45° angle with respect to the wheel radius for optimum capture of the wind forces.

The wheel may be connected to a generator using conventional couplings at the ends of the wheel axle. Alternatively, the wheel can be modified to serve as a primary generator. The system is best suited to work with a variable-speed dc generator, although an ac generator may also be used.

This work was done by John W. Kaufman of **Marshall Space Flight Center.** *For further information, Circle 64 on the TSP Request Card.*

This invention is owned by NASA, and a patent application has been filed. Inquiries concerning nonexclusive or exclusive license for its commercial development should be addressed to the Patent Counsel, Marshall Space Flight Center [see page A8]. *Refer to MFS-23515.*

Subminiature Hydraulic Actuator

A single-vane rotary actuator for wind-tunnel test-model control-surface actuation systems

Langley Research Center, Hampton, Virginia

A subminiature, single-vane rotary actuator suitable for wind-tunnel test-model control-surface actuation systems and other applications has been designed, fabricated, and breadboard-tested. Two of these actuators were installed at Langley Research Center in a 1/17-scale supersonic-transport wing model to drive leading- and trailing-edge control surfaces during wind-tunnel tests. This model presented severe torque and system band-pass requirements with stringent space and weight limitations.

In this application, the single-vane rotary actuator (see figure) was designed to produce 41 lb-in. (460 N-cm) peak torque with two-thirds of the 1,000-psi (6.9×10^6-N/m^2) supply pressure across the vane. The actuator can be operated at any supply pressure up to 1,000 psi, with proportional capability below maximum torque. The design can be easily altered to permit a larger shaft diameter, greater shaft angular displacements, and higher torque capability by increasing the vane area (with some size and weight penalty).

The moving part of the actuator is a steel shaft with an attached vane. The vane is installed within a cavity in the body, dividing it into upper and lower sections for the hydraulic fluid; end caps, sealed by copper gaskets, close the sides of the cavity. An effective low-friction seal is formed by molding urethane rubber around the vane edge. A straight section of rubber blocks leakage of the fluid from one side of the vane to the other side around the back of the shaft. The fluid is admitted to the cavity through ports in the end caps.

The shaft is supported by precision ball bearings in the end caps; O-rings in glands seal the shaft. The gasket seals between the end caps and the actuator body are formed by two loops of copper wire around the vane cavity edge. Each end cap is secured to the actuator body by two screws, using sufficient preload to maintain the gasket seal. Special washers (not shown) were designed for the screws to retain the bearings and O-rings while the cavity is pressurized. The actuators were static pressure-tested to 1,200 psi (8.3×10^6 N/m^2) after assembly to insure satisfactory performance up to the full 1,000-psi supply pressure.

The primary advantages of the actuator are its small size and weight [2.5 oz (70 g)] for a relatively-high maximum torque capability. The actuator has very low leakage of fluid from one side of the vane to the other, permitting its use in precision position servosystems. The sealing of the actuator prevents external leakage of hydraulic fluid, which could contaminate the wind-tunnel test medium.

This work was done by Francis D. Sevart of The Boeing Co. for **Langley Research Center.** *For further information, Circle 65 on the TSP Request Card.*
LAR-11522

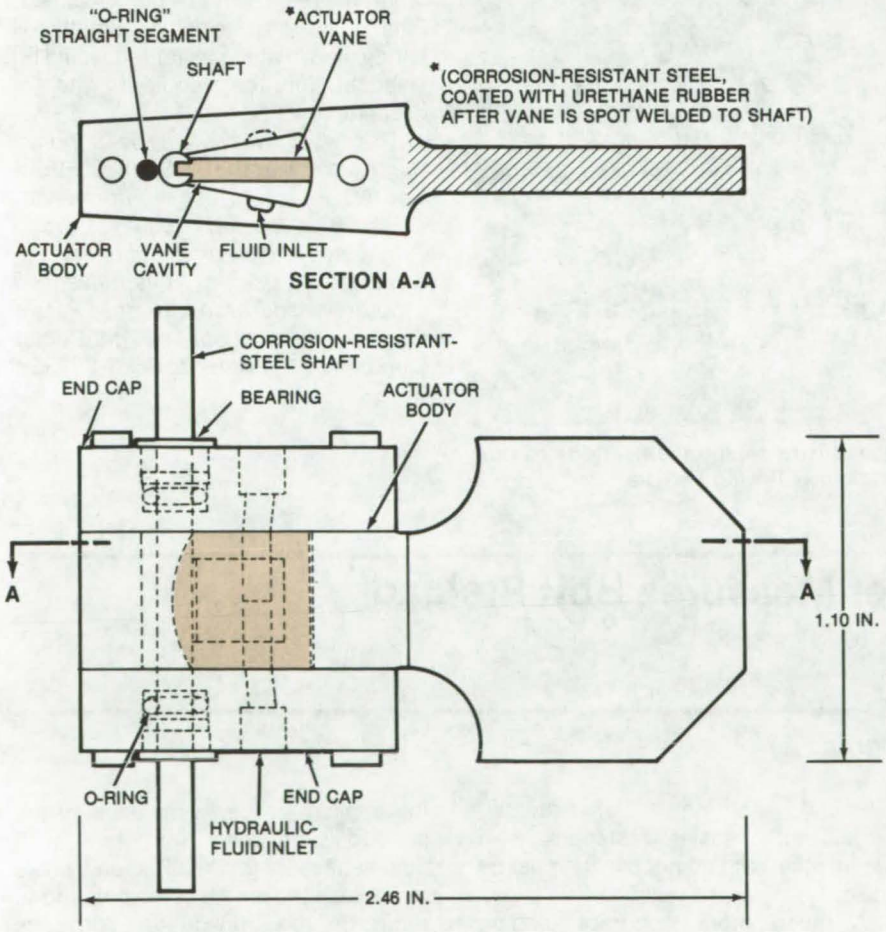

The **Actuator Body and End Caps** are machined from 2024 aluminum alloy to minimize weight. The vane cavity is contained in the actuator body, permitting ±10° vane displacements.

Emergency Escape Device

The mechanism that deployed the Lunar Rover could be adapted to handle man-sized loads.

Marshall Space Flight Center, Alabama

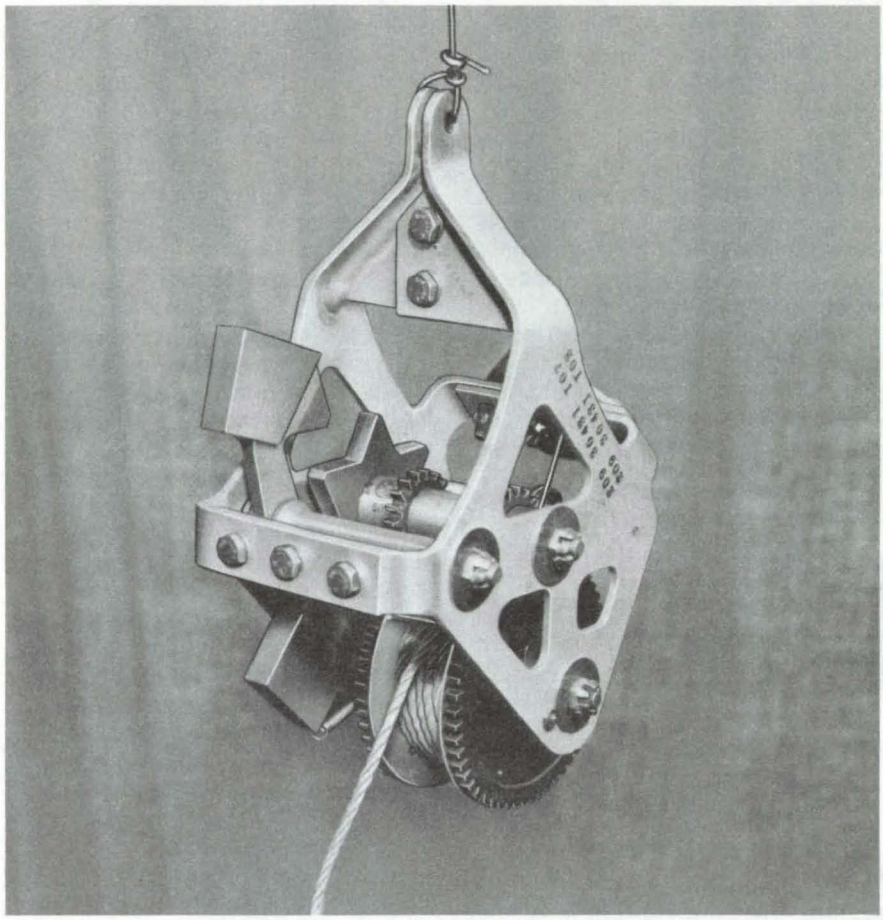

An **Emergency Escape Device** could be designed with small modifications to this egress mechanism, originally designed for the Lunar Roving Vehicle.

With a few modifications, the device used to control the descent of the Lunar Roving Vehicle from the Lunar Module on the Moon's surface could be used in construction, shipping, safety exits, amusement parks, and other applications to gently lower people or equipment several hundred feet.

To adapt the basic unit, shown in the figure, a storage reel for a small-diameter flexible aircraft cable would be added. Then, in order to guide the cable to and from the storage reel and to insure that the cable enters and wraps parallel turns across the reel or the device, a cable guider and a tapered reel would be installed. Finally, the tension in the small coil spring shown at the lower left would be selected for the required rate of descent.

This work was done by John L. Burch of **Marshall Space Flight Center.** *For further information, Circle 66 on the TSP Request Card.*

Inquiries concerning rights for the commercial use of this invention should be addressed to the Patent Counsel, Marshall Space Flight Center [*see page A8*]. *Refer to MFS-23235.*

Ultrasonic Extensometer Measures Bolt Preload

An ultrasonic device is more accurate than conventional torque wrenches.

Marshall Space Flight Center, Alabama

Conventional torque wrenches are relatively inaccurate when applying specified preloads to bolts and other threaded fasteners. A typical torque wrench has an inaccuracy of about ±25 percent because of the variation in the coefficient of friction between the mating parts. This limits the loading of fasteners to well below their ultimate strength. Consequently, larger and heavier fasteners than would otherwise be necessary must be used.

A much more accurate loading method uses ultrasonic pulse reflection to measure elongations in tightened bolts and studs. Since the elongation is directly proportional to the applied torque, a measure of the preload is obtained from the transit time necessary for the ultrasonic pulse to traverse the length of the bolt and to return to the transducer. With this method, the fastener load can be predicted to within ±10 percent, making it possible to use lighter, smaller diameter bolts in a given

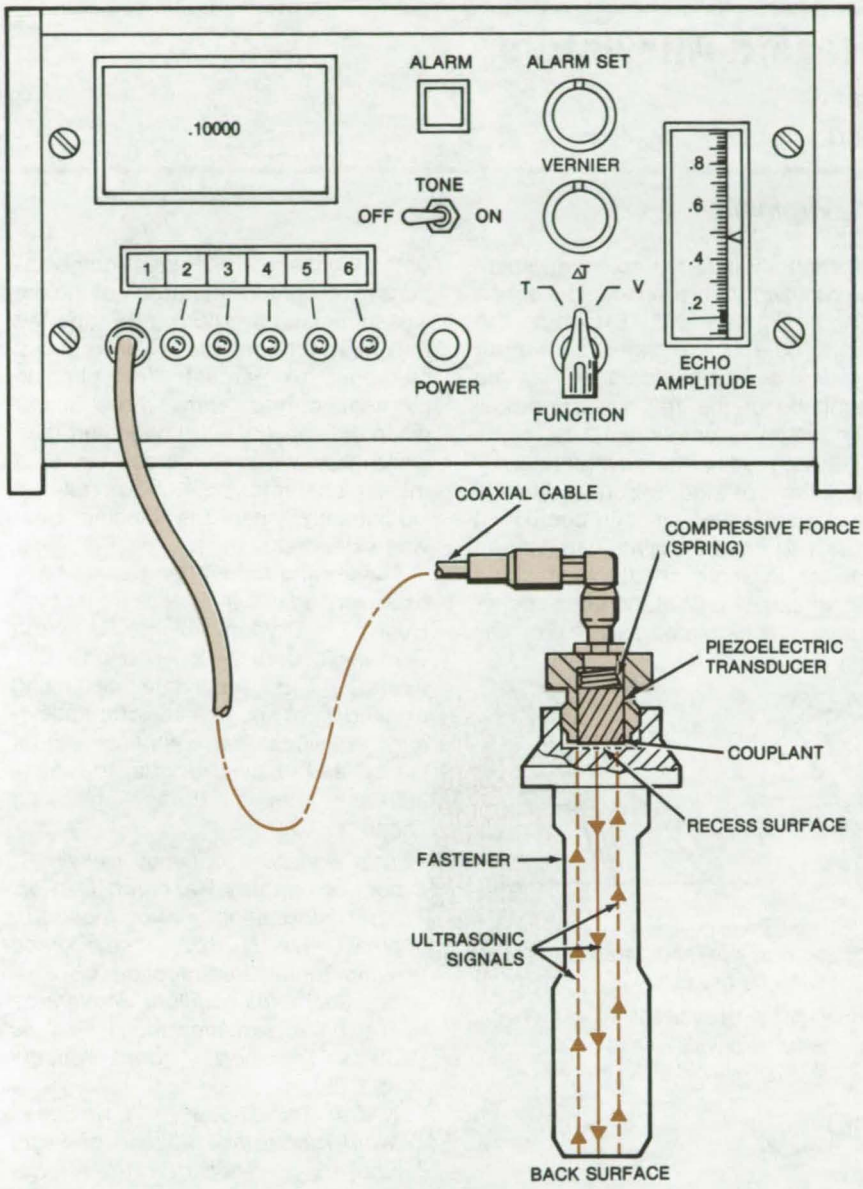

Figure 1. This **Ultrasonic Extensometer** is used to determine if proper torque is applied to a threaded stud or bolt. The instrument measures the transit time necessary for an ultrasonic pulse to traverse the length of the fastener and to return to the transducer. This time is proportional to the fastener elongation and to the applied torque.

application. In the main engine of the Space Shuttle, for example, bolts could be safely loaded to 60 percent of their ultimate strength (rather than 20 percent, the limit when torque wrenches were used). An overall weight savings of 1,000 lb (453 kg) out of 6,700 lb (3,035 kg) was realized by using lighter bolts.

The ultrasonic extensometer, as shown in Figure 1, incorporates a piezoelectric transducer in an adapter that fits the head of the fastener to be measured. A couplant is used to improve the contact between the transducer and the bolt. The instrument energizes the piezoelectric element, which transmits an ultrasonic pulse into the fastener. This pulse is reflected from the back surface of the fastener and returns to the transducer. The total pulse transit time is directly proportional to the fastener length and is shown on a digital display.

In operation (Figure 2) the instrument can be used with the lobe wrench shown. Initially, the extensometer is calibrated by using a standard bolt and a calibration block.

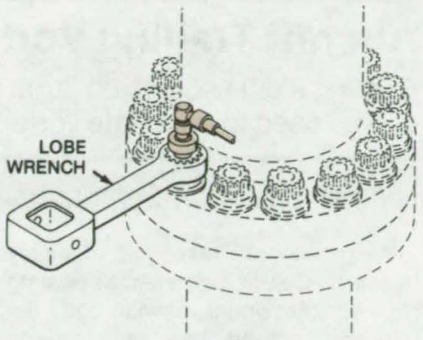

Figure 2. In a **Typical Application,** the ultrasonic extensometer is monitored as the lobe wrench tightens the bolt.

In addition to measuring preloads during assembly, the extensometer can also be used for quick measurements throughout the life of studs and bolts, to see if these fasteners maintain the proper load. With appropriate couplers, the extensometer can be adapted to a fastener of almost any size.

This work was done by C. M. Daniels of Rockwell International Corp. for **Marshall Space Flight Center.** *For further information, Circle 67 on the TSP Request Card.*

Inquiries concerning rights for the commercial use of this invention should be addressed to the Patent Counsel, Marshall Space Flight Center [*see page A8*]. *Refer to MFS-19337*

Aircraft Trailing Vortex Hazard Alleviators

Existing flight spoilers on large aircraft can be used to attenuate vortex hazard.

Langley Research Center, Hampton, Virginia

Wind tunnel tests at Langley Research Center indicate that existing flight spoilers on large, wide-body, jet transport aircraft can be used to reduce the vortex hazard for trailing aircraft. Various combinations of existing flight spoilers on models of three wide-body transport aircraft were investigated; all effectively reduced the induced rolling-moment on the trailing wing model by from 30 to 70 percent (see figure).

Wind-tunnel tests over a flight-spoiler deflection range of from 0° to 60° indicate that essentially all the reduction in induced rolling-moment was realized with a spoiler deflection of approximately 30°. Extending the landing gear of the transport aircraft models did not significantly affect the magnitude of the trailing-wing-model rolling-moment coefficient.

The longitudinal aerodynamic characteristics of the aircraft models indicated that a nominal lift coefficient ($C_L \cong 1.2$) can be maintained with an increase in angle of attack of about 2.5° when any pair of the flight spoiler segments is deflected to 45°. For any of the flight spoiler segment combinations investigated, the drag coefficient was increased by about 0.04, and the maximum lift coefficient was reduced by about 10 percent. The pitching moment curves were more linear when the spoilers were deflected than when they were retracted. None of these characteristics was altered significantly when the landing gear was extended.

These wind tunnel test results have been verified in full-scale flight tests at Hugh L. Dryden Flight Research Center with both the B-747 and L-1011 aircraft. This technique of using existing flight spoilers as vortex alleviation devices can enhance flight safety and allow airports to safely increase their traffic handling capacity.

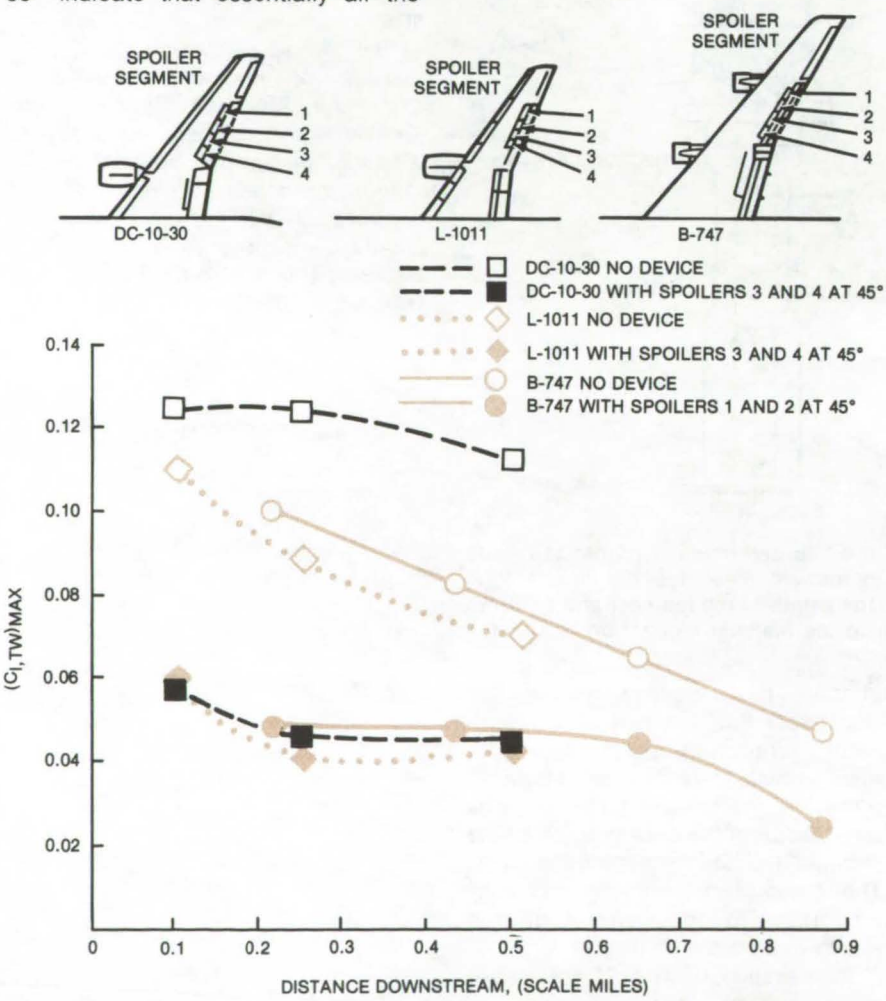

Trailing-Wing Rolling-Moment Coefficient varies as shown above with downstream distance behind the B-747, DC-10-30, and L-1011 airplane models with and without spoiler trailing-vortex alleviators. Landing flap configuration, $C_{L,trim} = 1.2$.

This work was done by Delwin R. Croom of **Langley Research Center.** *Further information may be found in:*

NASA TN D-8162, "Low-Speed Wind-Tunnel Investigation of Various Segments of Flight Spoilers as Trailing-Vortex-Alleviation Devices on a Transport Aircraft Model" [$3.25];

NASA TN D-8360, "Low-Speed Wind-Tunnel Investigation of Flight Spoilers as Trailing-Vortex-Alleviation Devices on a Medium-Range Wide-Body Tri-Jet Airplane Model" [$3.75];

NASA TN D-8373, "Low-Speed Wind-Tunnel Investigation of Flight Spoilers as Trailing-Vortex-Alleviation Devices on an Extended-Range Wide-Body Tri-Jet Airplane Model" [$4.25]; and

NASA SP-409, "Wake Vortex Minimization" [$10.50].

Copies may be purchased [prepayment required] from the National Technical Information Service, Springfield, Virginia 22161.

Inquiries concerning rights for the commercial use of this invention should be addressed to the Patent Counsel, Langley Research Center [see page A8]. Refer to LAR-12034.

Compact Ratchet Wrench

A round ratchet-wrench handle would simplify work in tight areas.

Marshall Space Flight Center, Alabama

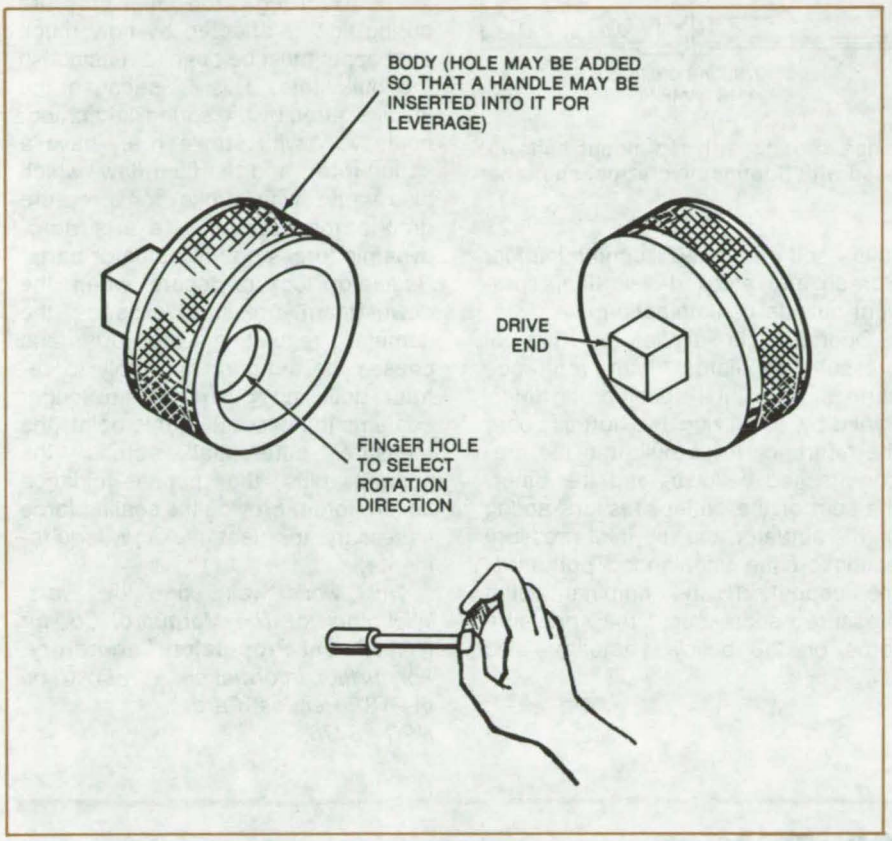

A **Round Ratchet Wrench** is used for work in tight areas. The drive end would be adapted to fit all the standard ratchet attachments. A finger is inserted in the hole to select the turning direction.

Many ratchet wrenches have long handles that make them difficult to manipulate in confined areas. This type of work would be easily handled by a proposed round ratchet wrench that fits the palm of a hand. Because the handle is small, the wrench could be inserted into most areas that are inaccessible to conventional wrenches.

The wrench, as shown in the illustration, would operate like conventional ratchet wrenches. The only change is the round handle operated by a simple twist of the wrist to install or remove a nut or bolt.

This work was done by Eugene J. Stringer of Rockwell International Corp. for **Marshall Space Flight Center.** *For further information, Circle 68 on the TSP Request Card.*
MFS-24252

Wide-Temperature Corrosion-Resistant Pressure Regulator

Simplified design and all-metal-and-ceramic construction make pressure regulator ideal for hot corrosive fluids.

NASA's Jet Propulsion Laboratory, Pasadena, California

By combining several new but well-proved techniques, a new pressure regulator has been designed with a number of advantageous features. Flexure guidance eliminates hysteresis and reduces friction and self-generated contamination enough to produce a nearly-unlimited maintenance-free lifetime. Metal and ceramic components (no organics) make the regulator compatible with corrosives such as fluorine and hydrazine and extend the operating-temperature range.

The regulator, as illustrated, is nearly frictionless and employs only solid and gas damping. Most components are of Inco 718, except for the screen and stacked-disk filters (304L stainless steel) and the poppet and seat interfaces (tungsten carbide). These materials allow operation from about -420° F (25 K) up to a temperature depending upon fluid compatibility; e.g., over 300° F (420 K) for fluorine and hydrazine.

A redundant bellows eliminates the need for reference springs and simplifies design. Two identical bellows (one in compression, one in tension)

(continued next page)

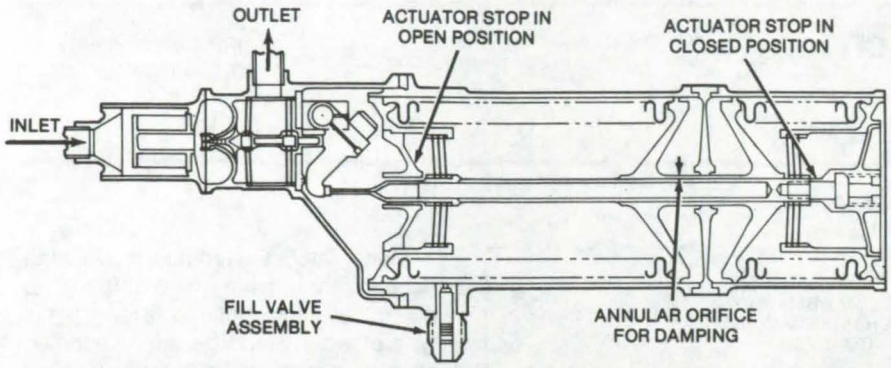

Improved Pressure Regulator replaces reference springs with redundant bellows. Made of metals and ceramics only, it can be used with fluorine, hydrazine, and other corrosives over a wide temperature range.

provide a reference force equal to the nominal outlet pressure times the effective bellows area. The moving ends of the bellows are attached to the actuator shaft, which is guided by two flexure assemblies.

When the actuator shaft moves, there is a pumping action at the annular damping orifice. The cavity containing the damping orifice will be prepressurized to the nominal outlet pressure with helium entering through a fill valve.

Several flexure assemblies are used in the regulator to reduce friction and thus self-generated contamination. Screen and stacked-disk filters prevent outside contamination.

Operation is similar to that of pressure regulators with reference springs. The "null" position is determined by equalizing two forces: one, the reference force built into the precompressed bellows, and the other, the sum of the outlet pressure acting on the actuator and the inlet pressure acting on the unbalanced portion of the poppet. If the nominal outlet pressure decreases, the pressure force on the bellows actuator also decreases and is overcome by the precompression force of the bellows. This causes the actuator shaft to move and the poppet to open. The open poppet results in flow into the regulator outlet and a corresponding increase in the regulator-outlet pressure.

The exact regulator-outlet pressure during flow is affected by how much the poppet must be open to reestablish the null state. This is because the loads exerted by the springlike components vary with stroke (i.e., have a spring rate); and the fluid flow, which also varies with stroke and pressure drop across the unit, exerts aerodynamic forces on the actuator parts. Regulator lockup occurs when the downstream pressure exceeds the nominal regulating pressure and causes the actuator assembly to retract until the push rod no longer contacts the poppet. At this point, the pressure differential across the poppet, plus the poppet-guidance flexure force, provide the sealing force necessary to meet leakage requirements.

This work was done by Horst Wichmann of The Marquardt Co. for **NASA's Jet Propulsion Laboratory.** *For further information, Circle 69 on the TSP Request Card.*
NPO-13776

Low-Frequency Vibration Isolation

Viscoelastic washers damp out very small deflections at frequencies in the neighborhood of 1 Hz.

NASA's Jet Propulsion Laboratory, Pasadena, California

Microinch deflections resulting from low-frequency vibration can be eliminated with the aid of viscoelastic shear dampers (see figure). Originally developed to remove oscillations that cause blurry television pictures from the Mariner spacecraft boom-mounted camera, the dampers should find other applications in which vibration isolation is critical. In audio engineering, for example, they might be used to control tones and resonances in record players and turntables.

The dampers used in the Mariner spacecraft were designed to provide at least 4 percent of critical damping at displacements ranging from 0.0025 inch to 100 microinches (0.006 to 0.0003 cm) and frequencies from 1.28 to 0.16 Hz. They consist of viscoelastic polyurethane washers sandwiched between inner and outer flanged sleeves. The washers are bonded to both flanges; the inner sleeve is a stationary base, and the outer sleeve moves with the load.

The key to the successful performance of a viscoelastic shear damper is in selecting the washer material and size. In general, the material should have a high loss-tangent value over the expected temperature and frequency range. (Loss-tangent value is a parameter that describes the ability of a material to absorb energy.) However, washer size (which determines the total shear area and thickness) and material selection are interrelated.

At the outset, the frequency and damping constraints must be known. For example, one of the booms on the Mariner spacecraft is 9 feet (2.7 m) long, weighs 250 pounds (113 kg), and requires a damping factor (frequency

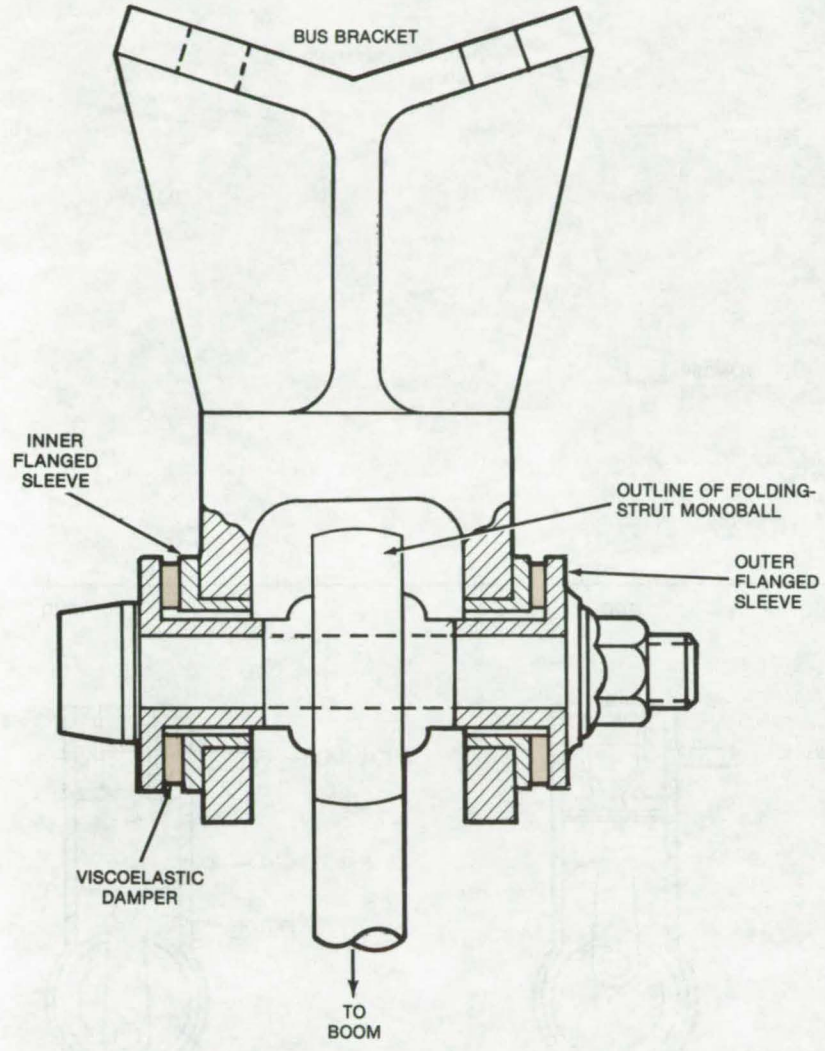

Microinch Deflection Damper on the Mariner spacecraft consists of a viscoelastic washer sandwiched between inner and outer flanges.

times fraction of critical damping) of at least 0.05 Hz during damper deflection of 0.0001 to 0.0005 in. (0.0003 to 0.0013 cm) over a 50° to 85° F (10° to 29° C) temperature range. The lowest acceptable damped boom frequency is 1.28 Hz, which requires the damping to exceed 4 percent of critical to meet the 0.05-Hz minimum damping factor. The resulting boom requirements include a damper stiffness of at least 2,600 pounds/inch (4,553 newtons/cm) and a loss-tangent value of at least 0.5.

The elastomeric material selected has a peak loss-tangent value near the 67° F (19° C) average temperature and 1.28-Hz frequency requirements. The thickness was set at 0.050 in. (0.13 cm) to give at least 0.1 percent strain at 0.0001 in. minimum deflection. The area was set at 0.123 in.^{2} (0.79 cm^2) to give the minimum allowable damper stiffness over the expected temperature range.

This work was done by David C. Miller and David H. Otth of Caltech for **NASA's Jet Propulsion Laboratory.** *For further information, Circle 70 on the TSP Request Card.*
NPO-13915

Simpler Valve for Reciprocating Engines

Moving piston and pressure-controlled valve eliminate camshaft.

Lyndon B. Johnson Space Center, Houston, Texas

No camshaft, cams, or mechanical springs are required in a new valve concept for reciprocating engines. The piston and a novel "pneumatic spring" that is controlled by static gas-pressure differentials operate the valve over an anticipated wide range of engine speeds and gas pressures. The new design, which was originally proposed for hydrazine-powered reciprocating engines, is expected to improve the efficiency and decrease the weight of reciprocating engines in the range up to 50 horsepower. The simpler design should also improve their reliability.

Other engine designs that eliminate cam-operated valves have been proposed. However, these have depended on the flow of gas into and out of the cylinder to close the valve. In contrast, the new valve relies on static pressure differentials to hold the valve poppet against the piston during the entire "open" phase. In this design, the force of the moving piston itself operates the valve. This should be considerably more reliable, since in the previous designs it was difficult to control the motion of the poppet in the midst of the hot flowing gas. In the new concept, the positive-locking action of the valve against the piston prevents "chattering" and decreases valve wear.

As shown in the figure, the upper surface of the valve poppet slides in a chamber within the inlet-gas storage plenum. The lower surface of the

(continued next page)

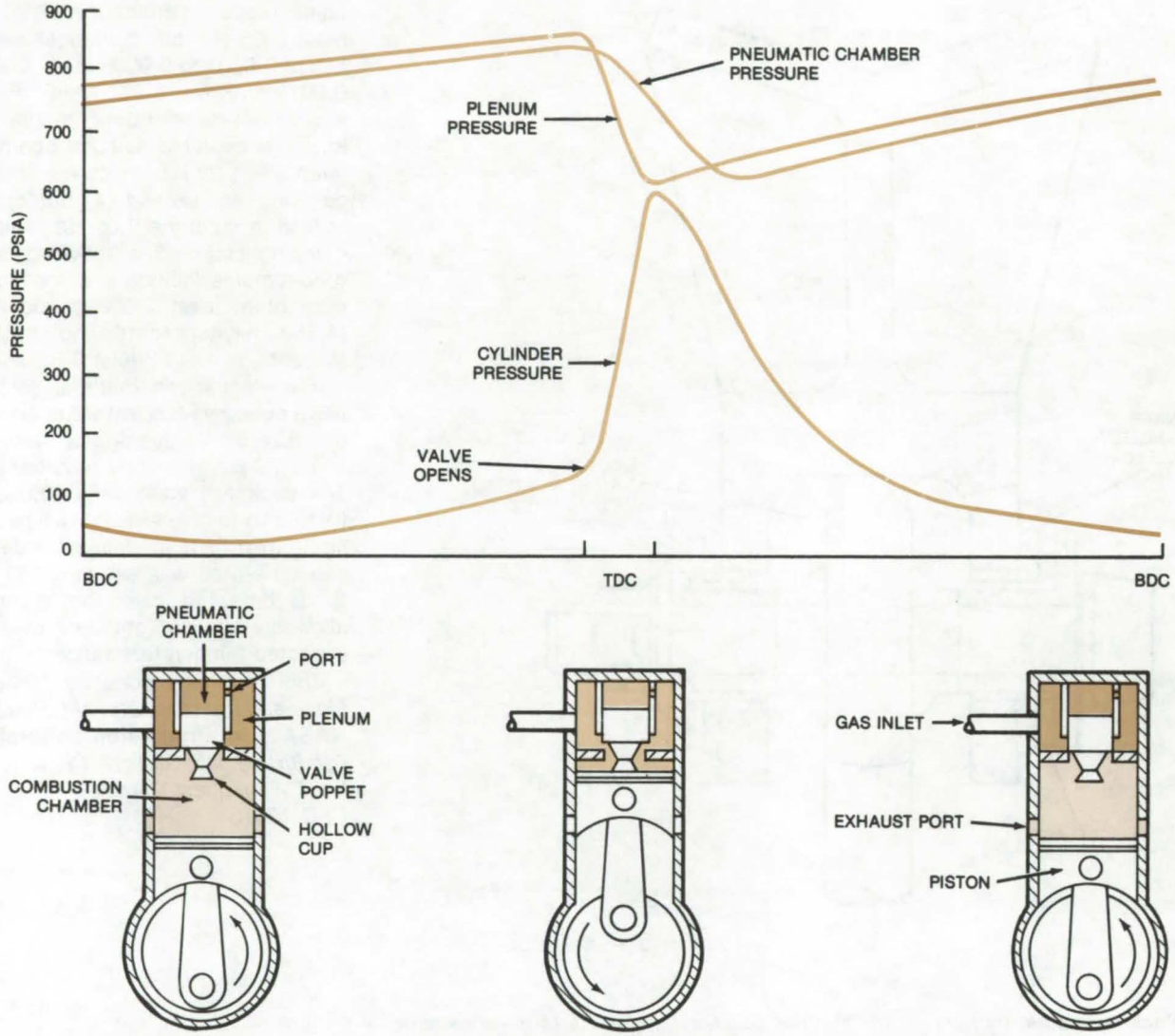

Proposed Valve for reciprocating engines is held closed (lower left) by the pressure differential between the pneumatic chamber and the combustion chamber. It is opened (lower center) as the piston moves up to its top-dead-center (TDC) position. Relatively-low-pressure gas remains trapped in the cup on the bottom surface of the valve poppet so that the piston remains in contact with the valve until it closes on the downstroke (lower right).

poppet has a hollow cup at its center. The three illustrations at the bottom of the figure show how the valve moves during a complete cycle; pressure variations within the system are shown in the graph.

With the piston at its bottom-dead-center (BDC) position, the plenum pressure is high, and the cylinder pressure is low as the combustion products of the previous cycle have exited through the exhaust ports. At this point in the cycle, the pressure differential between the chamber and the cylinder acts like a pneumatic spring that holds the valve closed.

As the piston moves up to its top-dead-center (TDC) position, it pushes up the poppet to open the valve. This traps relatively-low-pressure gas between the piston head and the hollow cup. The gas remains trapped even as the high-pressure gas from the plenum fills the chamber. On the downstroke, the poppet remains in contact with the piston because of the pressure differential between the chamber above the poppet and the hollow cup below. The lag in pressure drop between the plenum and the pneumatic chamber is controlled by the size of the port on the wall of the chamber. This permits the valve to remain in contact with the piston until the valve closes.

While many questions concerning the choice of materials, fabrication methods, and wear rate must be answered before the valve becomes practical, its potential for low weight, efficiency, and reliability make it attractive for further development.

This work was done by James W. Akkerman of **Johnson Space Center.** *For further information, Circle 71 on the TSP Request Card.*

This invention is owned by NASA, and a patent application has been filed. Inquiries concerning nonexclusive or exclusive license for its commercial development should be addressed to the Patent Counsel, Johnson Space Center [see page A8]. *Refer to MSC-16239.*

Dual-Action Expand-and-Latch Mechanism

A single drive actuator operates both the expansion mechanism and the latch.

Marshall Space Flight Center, Alabama

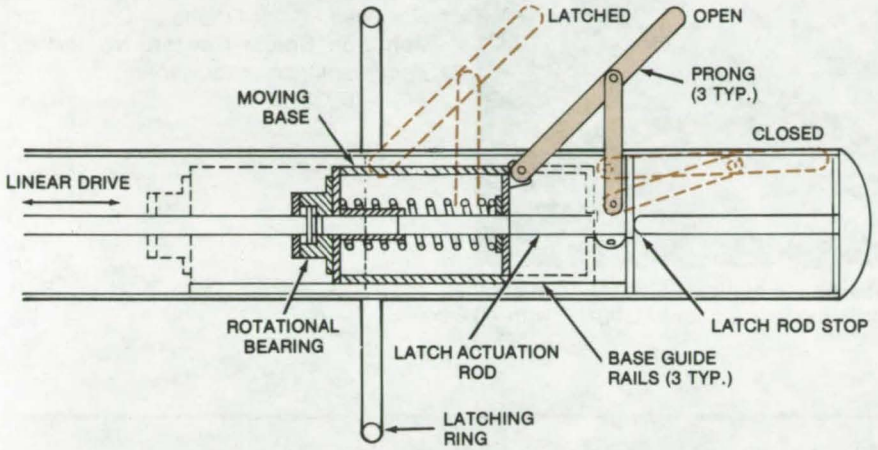

Dual-Action Device expands and latches to secure two objects together. The latching ring provides a stop that rests against the surface of the panel on which the mechanism is mounted.

A single drive actuator operates a novel mechanism that expands, deploys three prongs to attach to an object, and then withdraws to latch the object firmly to another part. The packaging is extremely simple and compact and eliminates the need for precision machined parts or close tolerances.

As shown in the figure, the device has three positions: closed, open, and latched. Starting from the closed position, the linear drive moves to the left, pulling the moving base with it, while the latch-actuation rod remains stationary. This causes the prongs to deploy to an angle of approximately 45° at the open position. In this position, the linkages are slightly over center, enabling large latch forces to be transmitted. Subsequent travel of the linear drive translates the complete assembly to the left, resulting in the latched configuration.

As shown, the right side of the spring is pinned to the latch actuation rod. Its primary function is to provide the force to deploy the linkage assembly during the closed-to-open actuation interval. Also, during this same interval, the prongs are backdrivable. This prevents large loads from being transmitted by the mechanism if initial misalinements with the latch interfaces exist.

The dimensions of a prototype device are 4 in. (10 cm) in diameter and 22 in. (55 cm) in length. These can be changed to accommodate particular design requirements.

The actuator may be used in industrial manipulator systems or cargo-handling devices. Other applications include train and trailer coupling systems and remotely-operated fluid or electrical connectors.

This work was done by R. A. Spencer, J. R. Tewell, and W. H. Tobey of Martin Marietta Corp. for **Marshall Space Flight Center.** *For further information, Circle 72 on the TSP Request Card.*

Inquiries concerning rights for the commercial use of this invention should be addressed to the Patent Counsel, Marshall Space Flight Center [see page A8]. Refer to MFS-23557.

A Sharp Knife for High Temperatures

Electrically heated knife of nickel-chrome steel maintains its edge while cutting at temperature of 1,700° F.

Lyndon B. Johnson Space Center, Houston, Texas

Heat-resistant plastic felts and similar materials can be cut with relative ease, using an electrically heated blade made of a newly-developed nickel-chrome-steel alloy. The blade is loop shaped and retains its edge at temperatures as high as 1,700° F (927° C). The conventional-steel-alloy hot knives used previously oxidized and lost their toughness at 1,200° F (649° C).

The blade is made of a commercially available alloy, RA 330 (equivalent alloys might be used but have not been tested), manufactured originally for high-temperature furnaces. It was applied in the hot knife to slice tiles of silicone-faced heat-resistant nylon pads during the fabrication of exterior insulation on the Space Shuttle. The tiles are 8- by 8-in. (20- by 20-cm) pieces of insulation that must conform to the Shuttle shape and structural deflections. Slits for flexure relief are cut in the tile surface with a hot knife.

Conventional hot knives, used at a lower temperature, required considerable force to slice into the tiles. Moreover, the felt would debond along the tile edges. The new knife cuts with relatively little force, and the debonding is eliminated. It is mounted easily on a temperature-resistant handle, as

(continued next page)

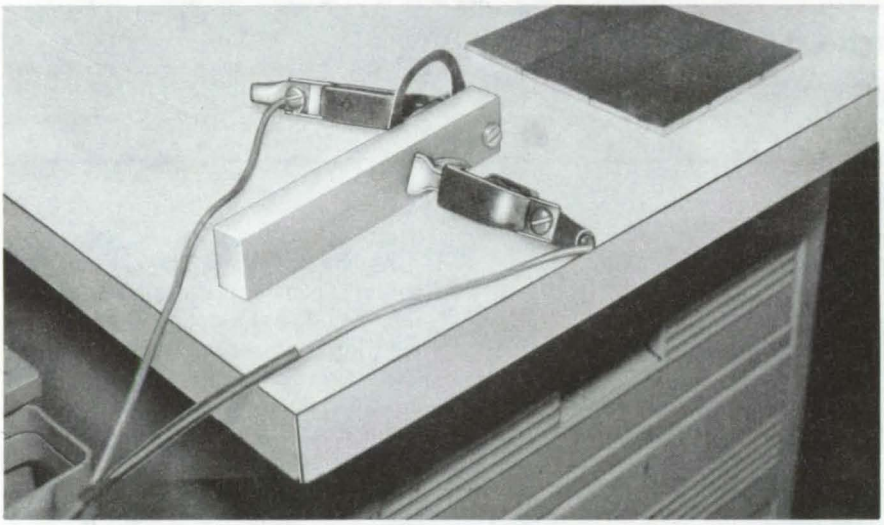

Hot-Knife Tile Cutter utilizes a loop-shaped blade made of nickel-chrome-steel alloy fastened to an insulating epoxy-glass base. It is heated to about 1,700° F with 40 amperes at 10 volts.

shown. The power required is about 40 amperes at 10 volts and is applied through the screw terminals on the handle. Heating of the blade can be controlled by varying the applied power as well as by widening or narrowing the blade itself.

This work was done by Robert M. Heisman and William F. Iceland of Rockwell International Corp. for **Johnson Space Center.** *No further documentation is available.*
MSC-16932

Adhesive-Removal Tool

An air-motor-driven hand-held tool with an acrylic cutting blade efficiently removes adhesive and paint from surfaces.

Lyndon B. Johnson Space Center, Houston, Texas

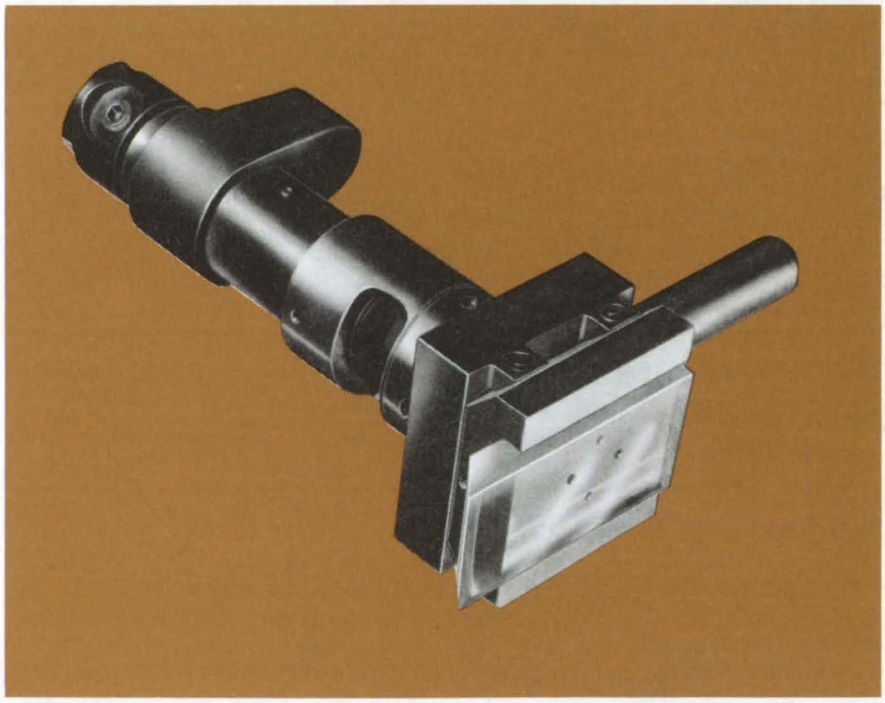

A new **Adhesive-Removal Tool** is driven by an air motor. The acrylic blade is held in a reciprocating head that moves parallel to the blade edge. Shearing motion removes adhesive and paint quickly and efficiently.

When cleaning coated surfaces, it is often necessary to scrape away adhesive or paint remaining after treatment with a solvent. Any such residual coating can be removed rapidly and without damaging the underlying material, by using the air-powered handtool shown in the photograph. The tool moves a sharpened acrylic cutter over the surface in a shearing sidewise motion.

Several experimental cutters were tested on silicone-rubber adhesive. Of these, the design shown here was found to be the most effective. The sidewise-slicing cutter was more efficient than conventional orbital-motion cutters, particularly when scraping very resilient materials that can cause an orbital cutter to "bounce." This tendency is eliminated with the new cutter.

This work was done by Cyrus C. Haynie of Rockwell International Corp. for **Johnson Space Center.** *For further information, Circle 73 on the TSP Request Card.*
MSC-19498

Collapsible Module Extends Tenfold in Height

An easily transportable module rapidly converts into an elevated platform for field applications.

NASA's Jet Propulsion Laboratory, Pasadena, California

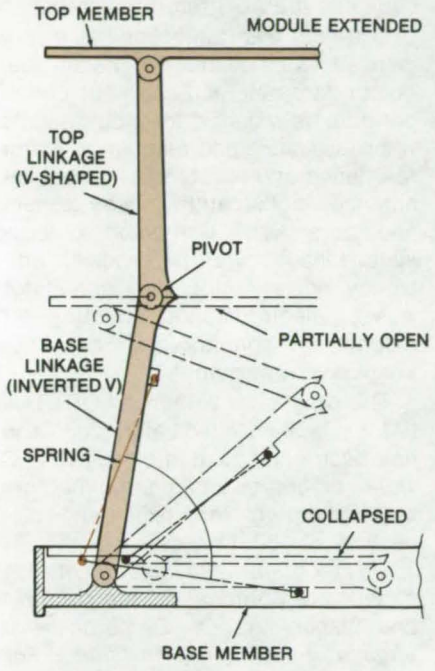

Figure 1. A **Collapsible Module** is shown in its extended, partially open, and collapsed positions. The top member can serve as an elevated platform for equipment or people. The "knee" of the pivot can be machined for any desired angle between the top and base linkages in the fully extended position. With the pivot right of center, as shown here, the module can be collapsed by hand pressure on the platform; if it were left of center, it would be able to sustain a heavy load without collapsing.

A new low-cost hollow module expands to 10 times its height by simply shifting a lever. The module can support a platform or tower for deployment in field applications. For example, it can serve as an elevated support for communications antennas or for TV or movie cameras operated by news reporters. Alternatively, it can be used as an extendable boom on vehicles.

The module consists of rigid top and base members (see Figure 1). Three or more foldable linkages, connected between the top and the base, support the top platform (only one linkage is shown). The linkages are locked in place with spring tension. When the structure is collapsed, the V-shaped top linkage nests within the base linkage (also V-shaped, but inverted) and is held in position with simple ball detents, latches, or pins.

The key to the module operation is in the base, which includes a lever-operated cam/ring mechanism. This mechanism (see Figure 2) shifts the position of the bottom of the spring, thus directing the spring tension either to open or close the linkages.

To extend the module, the top member is released by opening the latches, lockpins, or ball detents. This action permits the linkage springs to extend the module part of the way. Next, the lever-operated cam ring is shifted, moving the spring cams to their locked-open positions. This places tension on the linkages, causing them to extend and lock into place, elevating the top platform to its working position.

The module is collapsed by operating the lever to position the spring cams into an unlocked position. This folds the linkages. The module is closed by manually pushing the top member into the base.

This work was done by Allan R. McDougal of Caltech for **NASA's Jet Propulsion Laboratory.** *For further information, Circle 74 on the TSP Request Card.*
NPO-13371

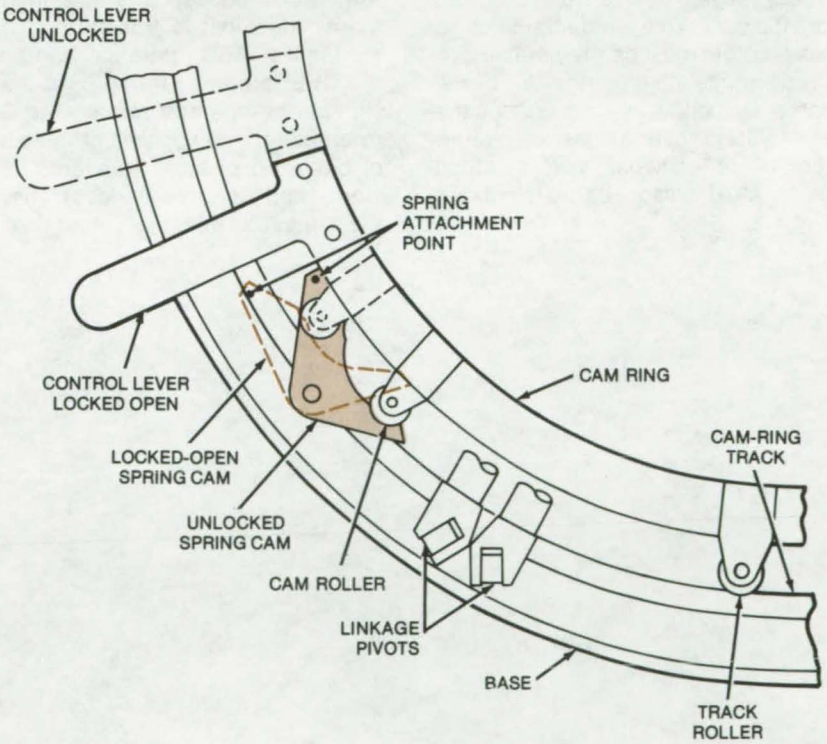

Figure 2. The **Cam/Ring Assembly** is positioned in the base plane and is operated by manually shifting the control lever. The lever shifts the spring cam into its locked-open or unlocked position to elevate or compress the structure.

Computer Programs

These programs may be obtained at very reasonable cost from COSMIC, a facility sponsored by NASA to make new programs available to the public. For information on program price, size, and availability, circle the reference letter on the COSMIC Request Card in this issue.

Three-Phase Induction Motors

Predict motor performance under diverse conditions.

A new program simulates the performance characteristics of three-phase induction motors under normal conditions and under extreme temperature, frequency, voltage magnitude, and voltage balance. The program was written to aid in design of the Shuttle Orbiter, which contains approximately 250 three-phase induction motors ranging in size from 1/50 to 2 horsepower. The characteristics of these motors must be predictable over a wide range of electrical and environmental conditions to assure satisfactory performance under all circumstances. In addition, their electrical loads must also be predictable, because they represent the major portion of the load on the inverters and the ac distribution system of the Shuttle.

This program readily predicts the characteristics of three-phase induction motors under normal operating conditions as well as severe conditions, such as temperature extremes [-100° to +250° F (73° to 121° C)] and unbalanced input voltages, including complete loss of one phase. Laboratory tests have confirmed the accuracy of the program over a wide range of conditions. It should be useful for the analysis of three-phase induction motors in energy systems, industrial load-drive studies, and many other applications.

The computer model uses the Thevenin's equivalent circuit for induction motors to calculate the motor currents using Kirchhoff's laws. The method of symmetrical components is used to handle unbalanced conditions. Kirchhoff's equations are written in matrix form that is transformed from the familiar ABC reference frame into the OFB reference frame by a matrix with vector-operator terms. The OFB reference frame consists of three sets of balanced phasors (forward, backward, and zero sequences), having the same total effect as the original set of unbalanced phasors. This permits Kirchhoff's current laws to be applied to the Thevenin equivalent circuit using balanced phasors to solve for the currents with standard procedures. All results are transformed back into the ABC reference frame.

Classical electromechanical theory is used to calculate the mechanical output parameters. Equivalent circuit parameters required for input include rotor resistance and reactance, stator resistance and reactance, mutual reactance, friction and windage losses, and core loss. Computed outputs include input power, horsepower, efficiency, power factor, rotor and stator losses, electromagnetic torque, net mechanical torque, and net mechanical power output.

This program is written in FORTRAN IV for execution in the batch mode and has been implemented on a UNIVAC 1108 computer with a central memory requirement of approximately 10K decimal of 36-bit words.

This program was written by Marion E. Wood of **Johnson Space Center** *and Nabeel A. O. Demerdash of Virginia Polytechnic Institute. For further information, Circle N on the COSMIC Request Card.*
MSC-16904

Fabrication Technology

Hardware, Techniques, and Processes

291 Improved Transformer-Winding Method
292 Bonding Core Mating Surfaces Improves Transformer
292 Fabrication of Thick Laminates
293 Void-Free Bends in Laminated Structures
294 Protective Coating for Copper in Aluminum Heat Exchangers
294 High-Strength Blind Rivet
295 Special Weave for Insulating Fabrics
296 Installing Fiber Insulation in Tight Spaces
297 Verifying the Fit of Mating Contoured Surfaces
298 Gentle Support Stands for Fluid-Line Mockups
299 Microcircuit-Cleaning Machine
300 Slurry-Powder Sintering Furnace

Improved Transformer-Winding Method

Better transformers made by installing the windings directly on the core.

NASA's Jet Propulsion Laboratory, Pasadena, California

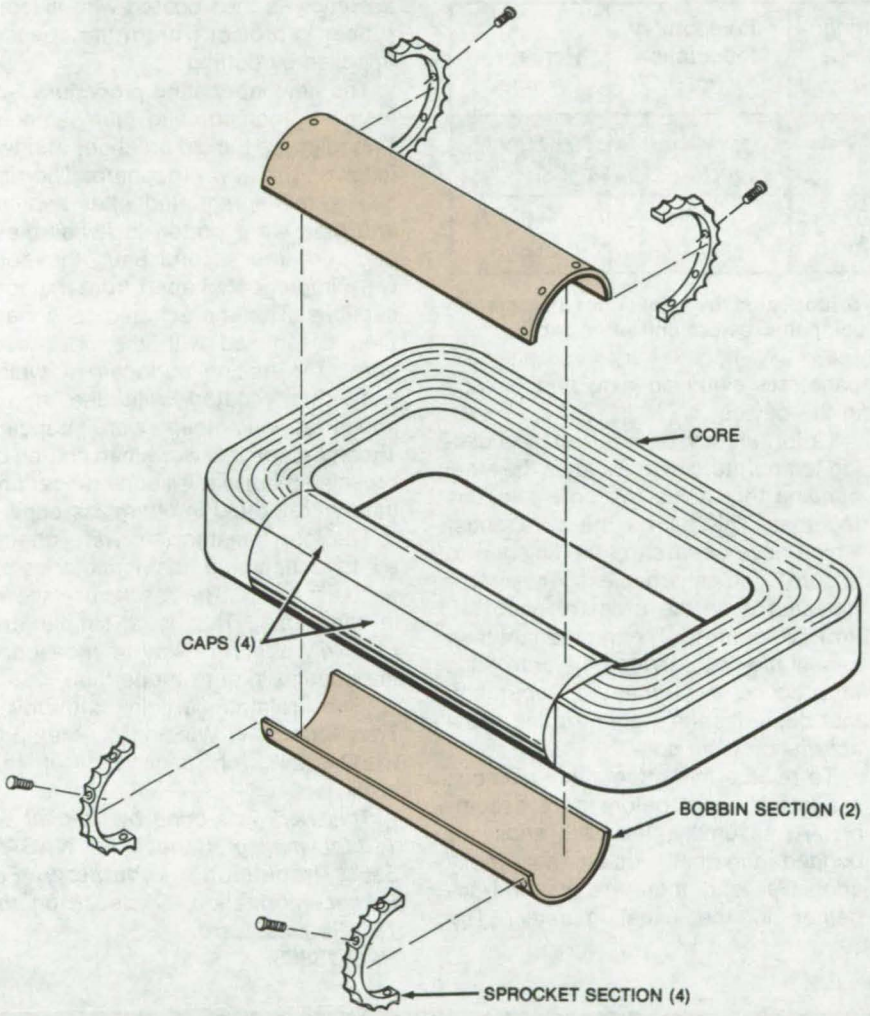

A **Gapless Transformer Core** is possible if the copper wire is wound directly on the core. After assembly of the parts, the bobbin is rotated around the end caps by a chain drive around the sprockets.

In conventional transformer assembly, the core is formed from a continuous ribbon, and the copper windings are wound separately on a bobbin. The core is then cut, disassembled, and bent open so that it can be placed through the winding.

A proposed new technique does not require that the core be cut. Instead a special bobbin and fixture are installed so that the copper wire can be wound directly on the core. The core can be shaped and impregnated to form a rigid structure before winding. By eliminating the gaps produced during conventional transformer assembly, the new method would improve the stacking factor from 0.9 to 0.95 or better, and the core would retain exactly the same shape that it had after annealing (since disassembly and reassembly of the laminations would not be necessary). The resulting core would be quieter, there would be no localized heating because of lamination spacing or distortion, and the core would have higher permeability.

As shown in the figure, four semicircular caps are cemented to a leg of the core assembly to form a circular cross section. A split bobbin fits around the capped core as shown. This bobbin will receive the winding and will be rotated in the winding operation. To reduce friction, a lubricant is applied to the outer surface of the caps or to the inner surface of the bobbin.

To rotate the bobbin there are threaded inserts at each end, and split sprockets are attached to these inserts by anchor bolts. A chain could be used to engage the sprocket and rotate the bobbin.

[See related article "Bonding Core Mating Surfaces Improves Transformer" (NPO-13855) on page 292 of this issue.]

This work was done by Colonel W. T. McLyman of Caltech for **NASA's Jet Propulsion Laboratory.** *For further information, Circle 75 on the TSP Request Card.*

NPO-14243

Bonding Core Mating Surfaces Improves Transformer

Preimpregnation and other measures produce virtually no inductance changes during potting.

NASA's Jet Propulsion Laboratory, Pasadena, California

Device	Fabrication Method	Prepotting Inductance (mH)	Postpotting Inductance (mH)	Percent Change
1	Conventional	92.5	48.3	-52
2	Conventional	86.5	74.5	-14
3	Bonded Ends	73.8	76	+3
4	Bonded Ends	81.5	83	+2

The Inductances of Four Transformers (two fabricated by conventional assembly methods and two by the new method) are compared before and after potting.

New modifications in assembly procedures for C-core transformers involve the impregnation of the windings before core assembly, epoxy bonding the core ends at assembly, and coating the assembly with silicone rubber before final potting. These modifications virtually eliminate changes in the core end gaps due to temperature cycling during the impregnation and potting stages, thus stabilizing the magnetization properties of the core.

In the conventional assembly of C-core type transformers, the impregnation and final potting steps are carried out by a vacuum process at an elevated temperature that lowers the viscosity of the impregnation and potting compounds. This improves their flow characteristics so that they penetrate every opening and crevice in the device.

Unfortunately, the raised processing temperature also expands the steel banding that holds the core sections together. This allows the core ends, which have been carefully finished to ensure almost gapless assembly (spacing is on the order of about 10 μm), to separate. The impregnant then can fill the gap between the core ends to produce a permanent separation that degrades the magnetization characteristic of the core.

To reduce this effect, the windings are impregnated before core assembly. At assembly, the core ends are bonded together, using an epoxy adhesive, and then are banded together in the usual manner. The assembly is then coated with silicone rubber to protect it from the stresses imposed by potting.

The new fabricating procedure was tested by constructing four samples. Two followed the old practice, and two followed the new procedure. The first two were impregnated after banding and then were potted in a fiberglass cup. For the second pair, the coils were impregnated apart from the core sections. The impregnated coils were then assembled with the core sections, the mating surfaces of which were first coated with the epoxy adhesive, and then were banded. These assemblies were then coated by brushing them with silicone rubber and then were potted in fiberglass cups.

The four transformers were checked by measuring the inductance of each assembly. The results are shown in the table. This is a simple and relatively accurate way of measuring the change in core properties.

[See related article "Improved Transformer Winding Method" (NPO-14243) on page 291 of this issue.]

This work was done by Colonel W. T. McLyman of Caltech for **NASA's Jet Propulsion Laboratory.** *For further information, Circle 76 on the TSP Request Card.*
NPO-13855

Fabrication of Thick Laminates

A method for fabricating thick laminates from resin-impregnated monofilament composite tape

Langley Research Center, Hampton, Virginia

A new fabrication technique improves the properties of thick laminated structures. The process, which was developed for the layup of composites with selected directional properties by the controlled orientation of monofilaments, improves fiber alinement and reduces overall void content. It is readily applicable to structures that contain thick sections (ribs, channels, bosses, and the like) joined to thin stems of the same material.

Processes used in the past applied chiefly to the curing of thin laminates. One reason for this was that when thicker laminates were cured, air or polymer byproducts became trapped because the perimeter areas cured too soon. Another reason was that as the thicker laminate was warmed and became less viscous, the applied pressure usually caused more resin flow than was desired. This created a disorientation of the fibers (washing effect) that lowered directional strength. Finally, as thick laminates were cured, the chemical reaction of

the polymer created heat faster than the surrounding surfaces could dissipate it. This caused the polymer to boil off byproducts faster than they could escape, trapping bubbles inside the laminate.

In the new process, the preimpregnated fibers are first layed up in thin sections consistent with the manufacturer's recommended procedures. The prescribed curing cycle is followed with some important modifications: The time and/or the temperature specified for the final curing are sustained only until the fibers are locked in place, voids are eliminated, and the laminates are capable of physical handling and cutting. Next, the laminates are stacked to the desired final thickness with two layers of raw (uncured) preimpregnated fibers between each laminate. This combination is then cured by following the manufacturer's prescribed cycle.

Because the entire assembly is final cured together, neither additional bonding nor the application of additional thermal and mechanical stresses are necessary.

This work was done by George E. Dickerson of **Langley Research Center.** *Further information may be found in the U.S. Patent referenced below, which may be purchased from the U.S. Patent and Trademark Office, Washington, D.C. 20231 for $0.50 a copy.*

This invention has been patented by NASA [U.S. Patent No. 4,065,340]. Inquiries concerning nonexclusive or exclusive license for its commercial development should be addressed to the Patent Counsel, Langley Research Center [see page A8]. Refer to LAR-12019.

Void-Free Bends in Laminated Structures

Improved layup techniques control wrinkles and pores.

Lyndon B. Johnson Space Center, Houston, Texas

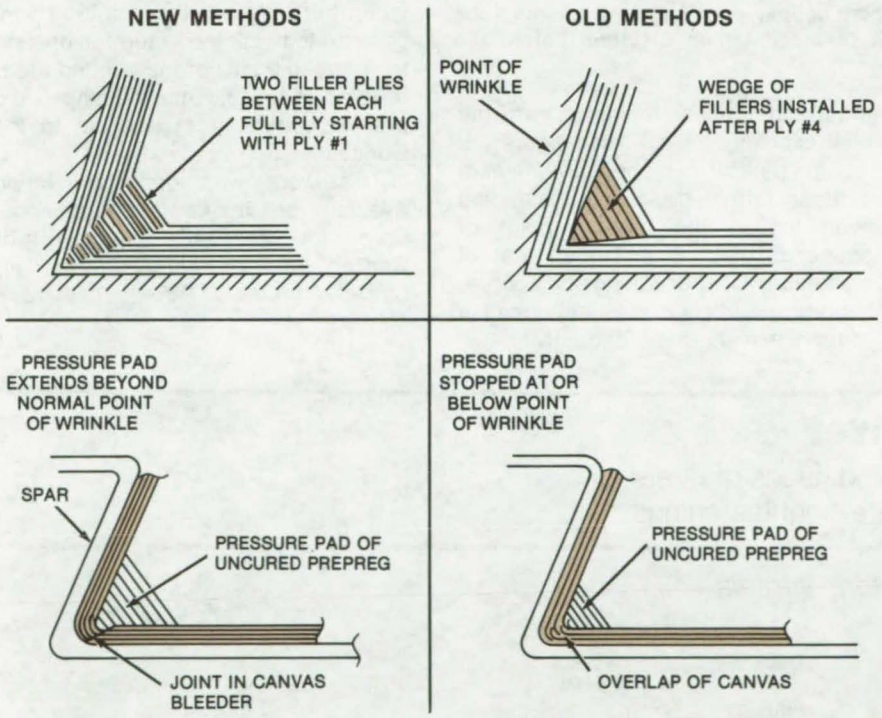

Bends Are Better when new layup methods are used. Two filler plies between each full ply (top left) do not tend to shift and cause wrinkles as did a single block of fillers (top right). Wrinkling and overlap of the canvas in the apex of the bend (bottom right) are prevented by cutting the canvas bleeder below the apex (bottom left).

Defects at sharp bends in laminated materials can be reduced by using special layup techniques originally developed to improve a spar-to-web assembly (see figure). The new methods, shown compared with previous layup techniques, involve the repositioning of filler plies and the redesign of the bleeder pressure pad. Wrinkles in the spar plies, which had tended to develop 3/4 in. (1.91 cm) above the 0.06-in. (0.15-cm) bend radius, were eliminated, as were tubular voids and pores and the tendency of the plies to "bridge" along the outside of the bend radius.

Rather than locating the filler plies as a block following ply number 4, two filler plies are inserted between each ply, starting with ply number 1. This keeps the fillers from slipping as a unit and causing the adjacent plies to wrinkle. Pressure is distributed more evenly since the sharp bend is smoothed out starting at ply number 1 (rather than at ply number 4).

Bridging is prevented by splitting the canvas bleeder pad and forming a tapered joint adjacent to the bend radius. An uncured-prepreg 10-to-16-ply layup is placed over the canvas to contain the wrinkle.

This work was done by Stephen W. Rice, Francis A. Schwind, and James H. Wilson of Vought Corp. for **Johnson Space Center.** *No further documentation is available.*
MSC-16998

Protective Coating for Copper in Aluminum Heat Exchangers

Molybdenum disulfide prevents the formation of a copper/aluminum eutectic, but does not impede heat transfer.

Marshall Space Flight Center, Alabama

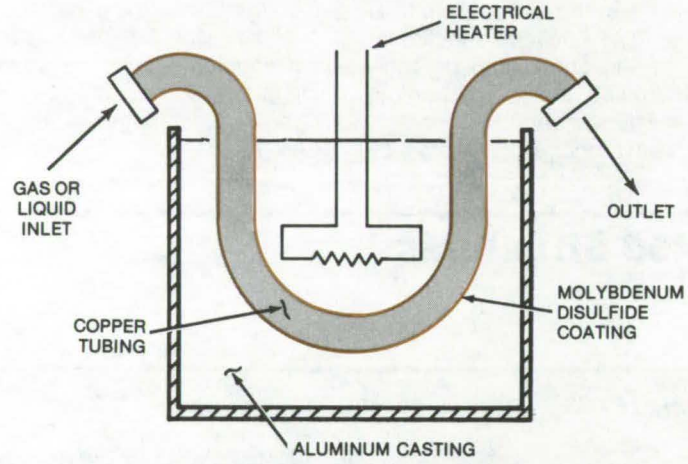

In an Aluminum Heat-Sink Heat Exchanger, copper may be used as the tube material, if it is coated with a thin layer of molybdenum disulfide before the aluminum is cast.

Copper tubing can now be used in cast-aluminum heat exchangers, if the tubing is first coated with an ultrathin layer of molybdenum disulfide. Previously, stainless-steel tubing had to be used in this application because copper deteriorates in aluminum. When molten aluminum is poured around the copper tubing to form the heat-exchanger block (see figure), a low-temperature copper/aluminum eutectic forms, dissolving the tubing even though the melting point of copper is much higher than that of aluminum. Copper tubing, of course, is preferred to stainless steel because of its higher thermal conductivity.

Attempts to protect the copper by nickel or silver plating do not work since these materials also form a low-temperature eutectic with aluminum. It was discovered, however, that a coating of molybdenum disulfide only 0.001 inch (0.0025 cm) in thickness was sufficient to protect the tubing. Moreover, the coating is thin enough so that it does not significantly reduce the thermal conductivity of the copper-to-aluminum interface.

Molybdenum disulfide may be useful in other applications where the formation of a eutectic prevents a material with otherwise desirable properties from being used. In another type of application, the coating might be used to mask a surface for brazing to control the size of the bonded area. In vacuum brazing, the coating could prevent platens from bonding to the workpiece.

This work was done by Ralph Avazian of Rockwell International Corp. for **Marshall Space Flight Center.** *For further information, Circle 77 on the TSP Request Card. MFS-19334*

High-Strength Blind Rivet

A new method for upsetting the blind heads of rivets produces reliable, strong, pressure-tight fastenings.

Langley Research Center, Hampton, Virginia

Some rivet fasteners use a pin or explosive to form the blind head. These rivets do not have a filled rivet body or they do not snugly fill the rivet hole. Consequently they are not high-strength fasteners.

High-strength blind fasteners incorporate a shank through their centers, that upsets the blind head when pulled. The tapered rivet body snugly fills the rivet hole, and the shank fills the rivet body.

This system has several shortcomings. The fasteners are not

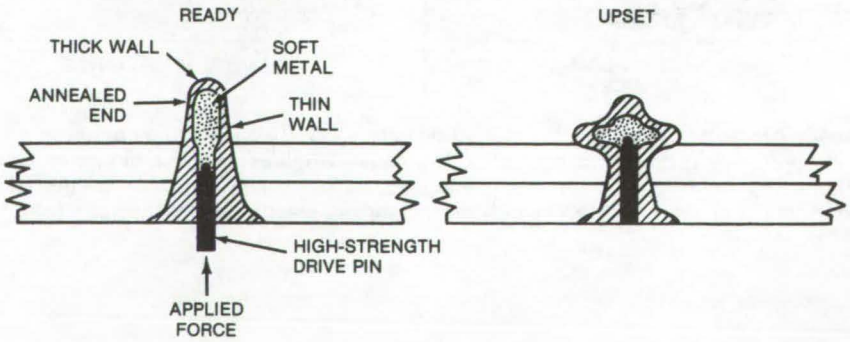

Sectional View of Fastener shows the initial and final upset condition. An optional preinstalled collar, over the annealed end, can give tensile strengths equivalent to threaded fasteners.

suitable for pressure vessel applications, as the hole through the center (for the shank) is not pressure-tight. The pullthrough of the shank not only forms the head but also deforms or tightens a tapered body in order to fill the holes. The magnitude of the hole fillings is controlled by the tensile strength of the shank, which does not allow good quality control. The fasteners are heavier than conventional rivets, and since they usually extend farther into the hole, they can create clearance problems.

A pressure-tight attachment with precisely-controlled mechanical properties can be obtained with a rivet that utilizes a new method of upsetting the blind head. The head is upset by using mechanical pressure to plastically deform a ductile material, such as soft aluminum, contained within a cavity. The ductile material is compressed by a force applied to a mandrel or drive pin that protrudes from the preformed head prior to installation. The drive pin has a head that is pressed into the soft material during manufacture so that it is retained by the soft material.

The compression of the material within the cavity in the annealed end of the rivet generates a uniform internal pressure. This pressure causes the rivet head material to yield at the point of highest stress. This point is controlled by selectively thinning the walls of the cavity within the annealed end of the rivet. The total deformation of the head is controlled by the volume of the protruding part of the mandrel. When the mandrel is driven flush with the surface of the preformed head, the upset head is completely formed, and the tapered rivet body has been pulled snugly into the hole by the forming of the blind head.

This work was done by L. Robert Jackson of **Langley Research Center** *and Allan H. Taylor of Vought Corp. No further documentation is available.*
LAR-12154

Special Weave for Insulating Fabrics

Harder, abrasion-resistant material can be woven without fracturing.

Lyndon B. Johnson Space Center, Houston, Texas

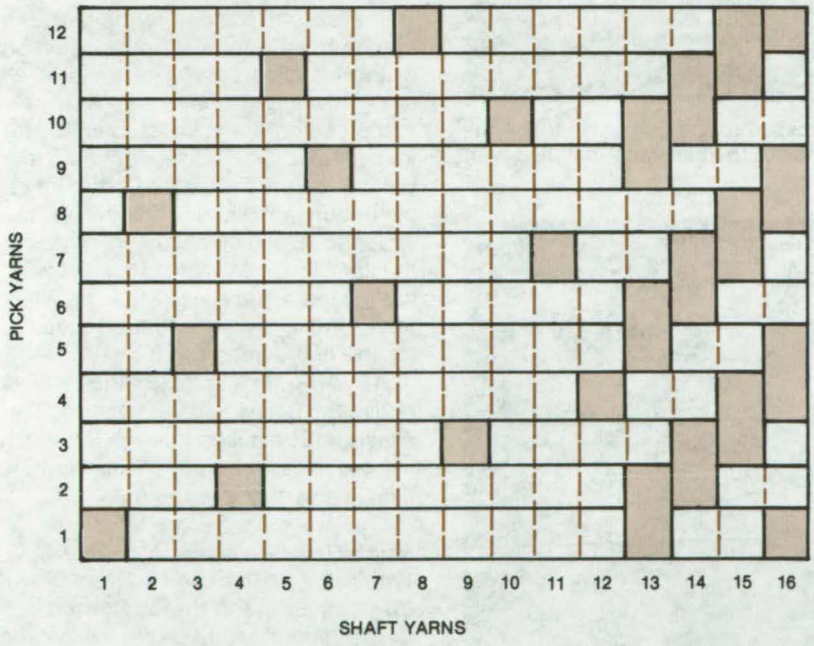

This Special Weave forms a tight fabric for high-alumina-content alumina/boria/silica fibers, without leading to excessive filament fracture during the weaving process. The abrasion-resistant material is superior to conventional insulating materials at elevated temperatures.

The abrasion resistance of alumina/boria/silica fabric, used as high-temperature insulation, can be significantly improved if high-alumina-content fibers are substituted for the high-silica materials commonly available. However, the harder, alumina-enriched filaments are also more brittle and susceptible to fracture if conventional weave patterns are used.

A special weave pattern, developed during the testing of insulating materials for the Space Shuttle, tightens the high-alumina fibers, without causing excessive breakage during weaving. The new pattern, shown in the figure, is a 12-harness irregular satin weave having a warp-and-fill yarn count of approximately 46 and 42, respectively, and a thickness of approximately 0.026 in. (0.066 cm). Each yarn is composed of two twisted 390-filament strands to form a 390-1/2-4z yarn.

As shown in the figure, shaft yarn #1 goes over pick yarn #1 and under picks #2 through #12; shaft #2 goes over pick #8 and under the other 11 picks; shaft #3 goes over pick #5 and under the others; and so on, through shaft #12. Shafts #13 through #16 represent the selvage-edge pattern. The patterns repeat for larger fabrics.

This work was done by John A. Frye of Rockwell International Corp. and Richard H. Pusch of HITCO for **Johnson Space Center.** *No further documentaton is available.*
MSC-16380

Installing Fiber Insulation in Tight Spaces

Fugitive binder and film simplify the installation of fiber batting.

Lyndon B. Johnson Space Center, Houston, Texas

Lightweight high-temperature insulation, such as alumina/zirconia fiber batting, is particularly difficult to handle and install. The fibers are fragile and easily broken, and it is difficult to shape the batting to conform to hollow tubes and enclosures.

Two new techniques for handling fiber batting have been used with considerable success in high-temperature seals around the thruster nozzle of the Space Shuttle. In one method, the batting is impregnated with an organic resin binder that is burned off cleanly after the insulation has been installed. As the resin is volatilized, the batting expands to fill the cavity in which it has been placed. This approach can be used for enclosures of almost any shape.

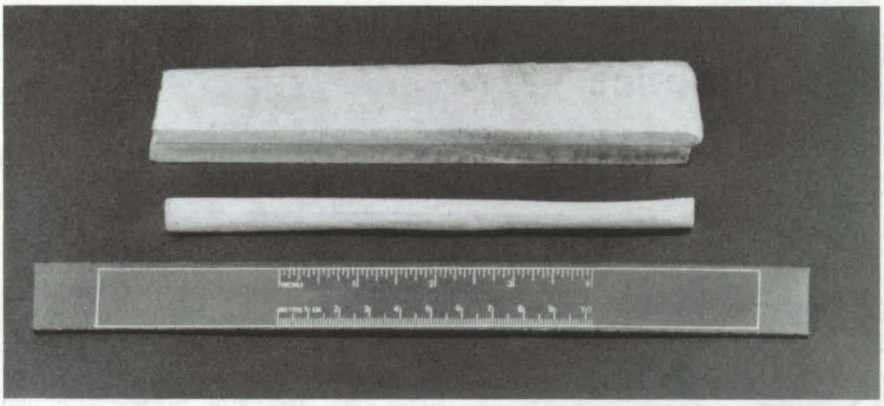

Figure 1. **Resin-Filled Insulation Batting** is compressed to a much smaller volume than the dry batting. The compressed batting can be cut to shape and installed with comparative ease.

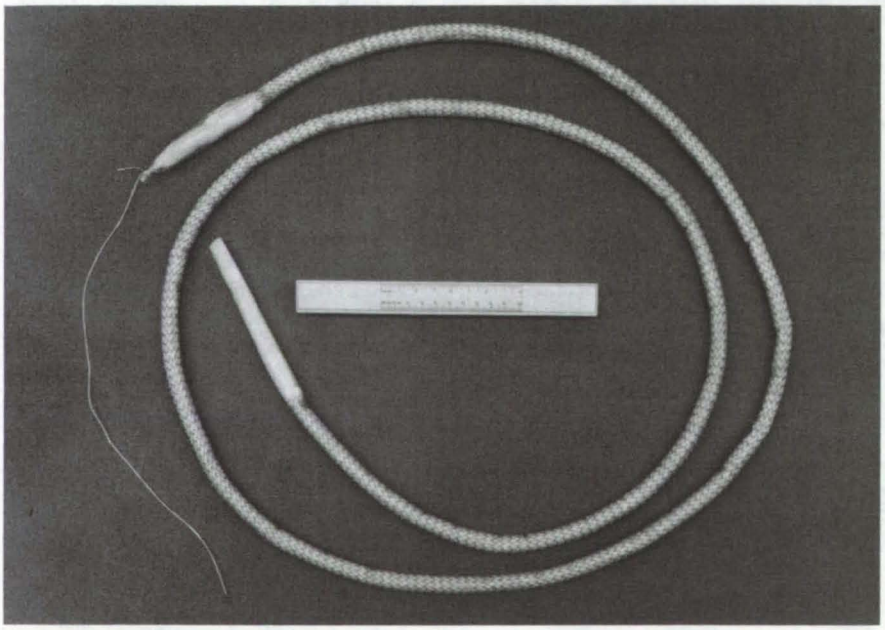

Figure 2. **Plastic-Wrapped Batting** is drawn through a mesh sleeve. This method is simpler than that of Figure 1 and can be used if the mesh is to be installed in an enclosure that has a uniform cross section.

The binder material that makes the insulation rigid in the first method is a water-based solution of an acrylic polymer resin. This solution is diluted further with distilled water to a 5-percent solids solution. The batting is then compressed in a mold, dried, and cured at 250° to 300° F (121° to 149° C). Once cured, the compressed and rigid batting may be cut to the shape and dimensions that are required (see Figure 1). This done, the rigidizing resin is burned off by oven-heating at 800° F (427° C).

The second method is simpler and can be used if the final cross section of the installed batting is uniform all along its length and if extreme precompression is not required for installation. In these cases, the batting can be wrapped in a thin, clean-burning plastic film. After the wrapped insulation has been installed, the film is burned off. This process has worked very well for installing fiber batting in tubular-mesh sleeves for the high-temperature seals.

As shown in Figure 2, the leading end of the film is tied with a string that allows it to be pulled through the mesh sleeve. After burnoff, the batting expands evenly into the mesh.

This work was done by Bhanu C. Patel, David S. Wang, and Aubrey D. Warren of Rockwell International Corp. for **Johnson Space Center.** *For further information, Circle 78 on the TSP Request Card.*

Inquiries concerning rights for the commercial use of this invention should be addressed to the Patent Counsel, Johnson Space Center [see page A8]. Refer to MSC-16934.

Verifying the Fit of Mating Contoured Surfaces

An inexpensive vacuum-and-heat process to verify fit between mated contoured metal surfaces

Langley Research Center, Hampton, Virginia

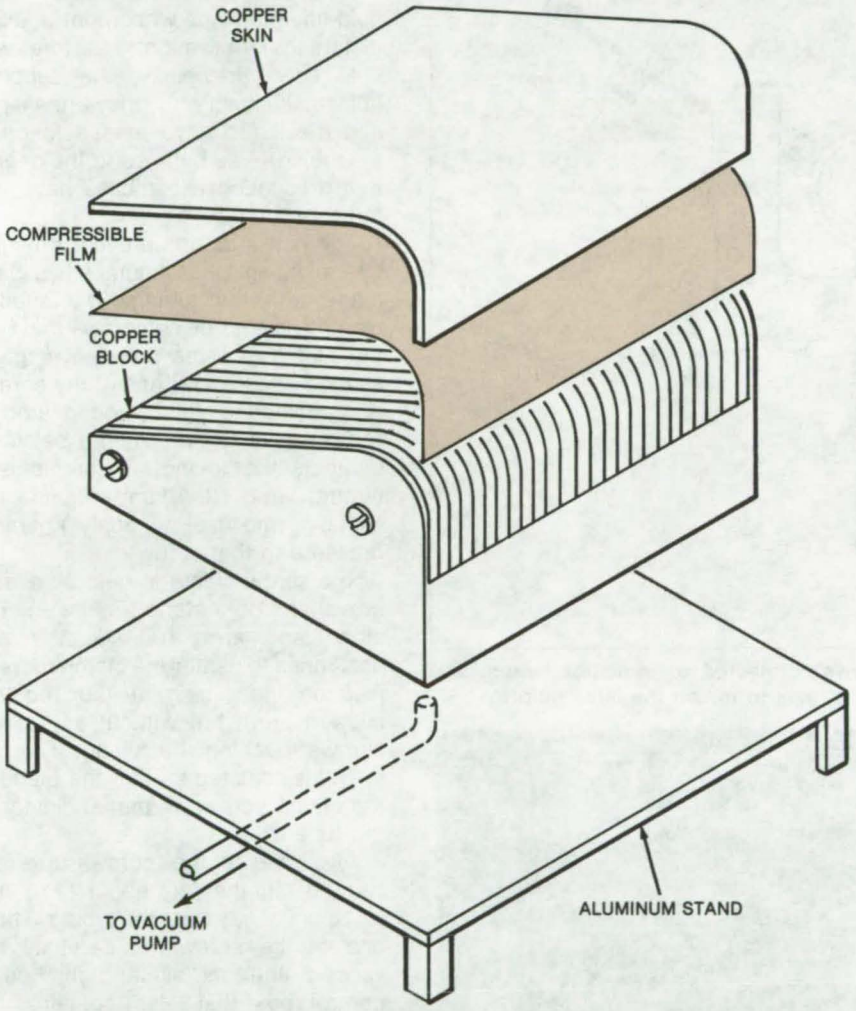

The **Fit Between a Copper Skin and a Mating Copper Block** is verified by using a thin compressible film. The entire setup is covered by a heat-resistant plastic envelope and then evacuated as it is baked in a furnace at 225° F. The film holds its shape after cooling, so that dimensional variations can be measured.

A simple, inexpensive process uses a commercially-available compressible film to verify the fit between mating metal surfaces within 0.003 in. (0.08 mm) to 0.005 in. (0.13 mm). In one application, the method was used successfully to fit a copper cover skin to a copper nozzle block for a jet engine.

The new procedure uses a vacuum-bag setup, an oven, and the compressible film (ranging in thickness between 0.003 and 0.005 in.). The arrangement is shown in the illustration.

To check the final fit between the skin and the nozzle block, the following procedure is used:

1. The copper block is placed on an aluminum stand, and a sheet of the film is placed over the block.
2. Next, a thin [0.0005-in. (0.013-mm)] polyester film is placed on the compressible film to prevent the skin from bonding to the compressible film; the copper sheet is then placed on top of the layup.
3. The entire setup, covered by a heat-resistant-plastic vacuum envelope, is evacuated and heated to 225° F (107° C).
4. After being held in the oven for 90 minutes, the parts are removed, the vacuum is disconnected, and the film is inspected for dimensional variations after cooling to room temperature.

In the jet-engine nozzle application, poorly fitting areas can usually be identified by a visual inspection. However, more sophisticated electrical and mechanical devices could be used to measure the dimensional differences in other applications.

This work was done by W. Dorton Leonard, Paul G. Sandefur, Jr., and Leland E. Wilkinson of **Langley Research Center.** *No further documentation is available.*
LAR-11731

Gentle Support Stands for Fluid-Line Mockups

Clamps with indicator lamps
hold tubing without deforming it.

Lyndon B. Johnson Space Center, Houston, Texas

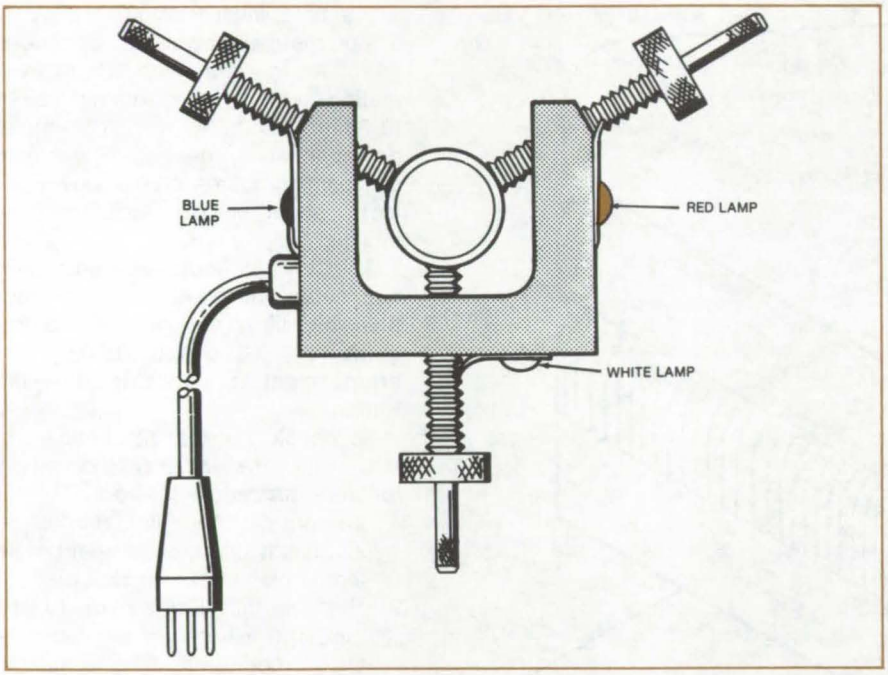

Figure 1. **Gentle Clamp** has three setscrews connected to indicator lamps. The clamp is painted with red, blue, and white stripes to match the lamp colors.

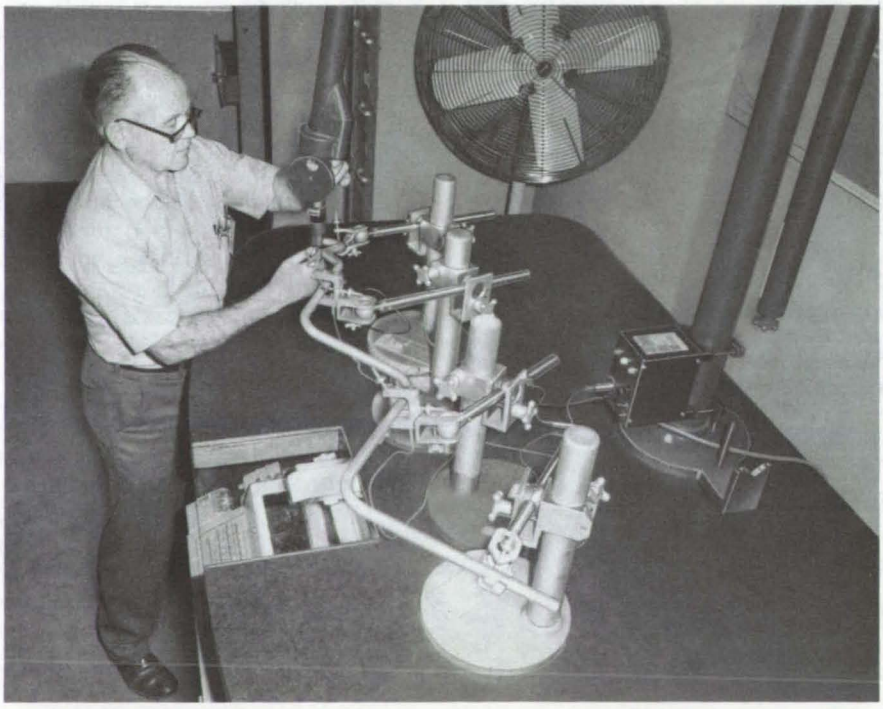

Figure 2. **Several Stands and Clamps** are used to support a fluid-line mockup while its bends are measured. The power supply and control box are at the rear of the table, and the keyboard of the bend-measurement machine is at the front.

New clamps and stands hold fluid-line mockups without introducing distortions that might interfere with fluid flow. Previously, the supports holding the lines while they are shaped and measured have tended to crush the tubing — sometimes to the degree that production assemblies have had to be reworked.

The new supports prevent crushing by indicating when contact has been made with the tubing. The support clamps have three setscrews that hold the tubing at three points in a given section (Figure 1). Each of the screws is connected to a color-coded lamp — red, blue, or white. When a setscrew contacts the tubing, it completes a circuit, and its lamp lights up, signaling the user to apply no more pressure to that screw.

The screw clamp is held by a ball-swivel arm on a stand (Figure 2). The stand and arm are adjusted and positioned to center the clamp more or less on the tubing at the required support area, but without any of the screws touching the tubing. The ball swivel is adjusted so that the plane of the clamp screws is perpendicular to the tube axis.

All three of the screws are advanced until they are about 1/16 inch (0.16 cm) away from the tubing. Then, one of the screws is carefully advanced until its signal light (on a control box that also contains the power supply) shows that it has made contact with the tubing. After the first screw has made contact, the same procedure is followed with the other two clamp screws. Then the power supply and control box are connected to the next support stand, and the entire procedure is repeated.

Normally, several support stands are used for the mockup. It is important to use enough stands so that the tubing is not distorted by its own weight when the bends are measured. The ends of the screws and the area of the tubing that they touch should be cleaned to ensure good electrical contact.

At the extreme ends of the tubing, a single screw clamp is used instead of the triple screw clamp. These end clamps have large swivels that automatically aline the clamp with the tubing without introducing strain in the tube.

The new tube-clamping system was designed for use with a computer-aided vector machine to obtain bend data from fluid-line mockups for the Space Shuttle. However, it can also be used for manual measurements on surface tables.

This work was done by Alma U. Millett and John A. Stein of Rockwell International Corp. for **Johnson Space Center.** *For further information, Circle 79 on the TSP Request Card.*
MSC-16479

Microcircuit-Cleaning Machine

Shaker knocks loose debris off hybrid microcircuit packages before they are sealed.

Lyndon B. Johnson Space Center, Houston, Texas

A circuit shaker for removing loose particles from hybrid microcircuits is easily constructed and could be manufactured for distribution as a kit. In operation, this machine can reduce rejections from particle-impact noise determination (PIND) tests to less than 7 percent.

Figure 1. Microcircuit-Cleaning Machine ready for operation — when the circuits are inserted, the stop pin is partially withdrawn to allow the arm to be raised 180°. During the actual operation, the stop pin is reinserted to restrict the arm elevation to 90°.

The shaker (Figure 1), which works like a pendulum, consists of an upright block bolted to a baseplate. The plate has four holes to bolt the entire machine to a workbench.

The upright block includes a support block that holds a bearing-supported pivot shaft. A swing arm is press-fitted through this shaft. The lower end of this arm carries a circuit-mounting block that holds two 1.18- by 1.18-in. (3- by 3-cm) circuit packages. Smaller circuit packages also can be mounted, using two small packing plates supplied with the machine (Figure 2).

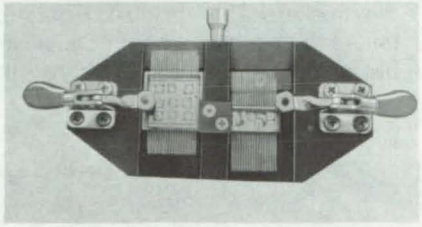

Figure 2. Mounting Block with circuit packages in position

The machine is loaded by raising the arm 180°. The technician inserts two standard-size circuits to the bottom end of the mounting block and secures them with two clamps on opposite sides of the block. Smaller circuits are held by screwed-on packing plates. The arm then is lowered, and the stop pin is reinserted.

The circuits are cleaned by raising the arm 90° and dropping it. The procedure is repeated three times. Loose particles are removed by shock from impact between the support and upright blocks.

Clean-room gloves and tweezers are used in handling the circuits during the entire procedure to prevent extra contamination. A clean filter paper is used to collect the dislodged particles, which can then be identified to help devise cleaner fabrication procedures.

This work was done by Wilf Robinson and Jack C. Williamson of Sperry Rand Corp. for **Johnson Space Center.** *For further information, Circle 80 on the TSP Request Card.*
MSC-16060

Fire-Retardant Epoxy Polymers

Phosphorus atoms in the molecular structure of new epoxies make them fire-retardant without degrading their adhesive strength. Moreover, the polymers are transparent, unlike compounds that contain arsenic or other inorganics. They have been used to bond polyvinylfluoride and polyether sulfone films onto polyimide glass laminates.
(See page 225.)

Repairing Silicon Carbide Coatings

Damaged silicon carbide coatings are easily repaired by applying a slurry that contains silicon carbide and a binder. The slurry is cured and impregnated with tetraethylorthosilicate to seal any residual porosity, prolonging the service life of silicon carbide coated parts.
(See page 232.)

Adhesive-Removal Tool

Paint and adhesive can be scraped from surfaces by using an air-powered handtool that moves an acrylic cutter in a shearing sidewise motion. The tool has been found to be more effective than sanders, particularly when scraping very resilient materials that cause other tools to "bounce."
(See page 286.)

Slurry-Powder Sintering Furnace

Furnace design and filler material allow uniform sintered nickel plaque to be manufactured reliably.

Langley Research Center, Hampton, Virginia

The production of large nickel-cadmium cells requires the manufacture of uniform, blemish-free nickel plaque. This plaque is obtained by the sintering of nickel powder. At temperatures around 900° C, under the proper conditions, the metal powder particles form spot surface bonds to adjoining particles, creating a porous solid.

In previous methods of sintering, a slurry made up of a binder (a water/alcohol mixture), a pore former, and the metal powder was applied to a carrier sheet (e.g., woven screen fabric). The slurry and carrier were sintered in a furnace containing a moist atmosphere that had to be controlled precisely. Without the moisture, the point-to-point adhesion would vary, and the plaque would have an oversintered surface and an undersintered interior with poor adhesion to the carrier.

A new sintering furnace eliminates the difficulties created by the stringent moisture-control requirements. The furnace has an entrance zone with a temperature lower than that of the adjoining sintering zone (see figure). Oxygen (instead of water vapor) introduced in the entrance zone, forms an oxide layer on the surface of the nickel. The oxidized material enters the hot zone, which contains a hydrogen atmosphere, where the oxides are reduced and sintering proceeds. Because the reactions are chemical, rather than physical, the bonding of the nickel-particles to adjacent particles and to the grid is exceptionally strong.

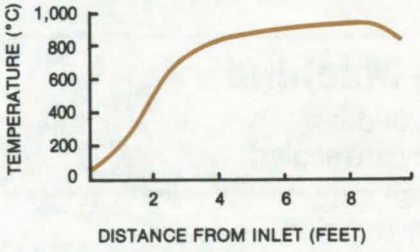

Temperature Profile of an improved slurry-powder sintering furnace defines two zones. In the lower-temperature entrance zone, oxygen is introduced to form an oxide layer on the powder. When the higher temperature region is reached, the oxide is reduced by dry hydrogen gas. This profile was taken on a nickel-plaque sintering furnace 28 feet (8.53 m) long.

A further advance in the sintering technique is the use of an insolubilized form of ammonium carbonate (oxamide) as the pore-former material. It does not absorb water, has the appropriate particle size, and decomposes at 419° C to leave little or no residue. It is also readily available and inexpensive.

The sintered material produced by this technique adheres well to the carrier, and the sintering is uniform throughout the plaque. The plaque itself is strong and has a high conductivity.

This work was done by James Bene of **Langley Research Center** *and J. Frederik Jansen and Harvey N. Seiger of Heliotek Corp. For further information, Circle 81 on the TSP Request Card.*

LAR-11423 and LAR-11426

Mathematics and Information Sciences

Hardware, Techniques, and Processes

303 Detecting and Correcting Bit Errors on Magnetic Tape

303 Fabrication of Sea-Floor Models

Books and Reports

305 Marshall System for Aerospace Simulation

Detecting and Correcting Bit Errors on Magnetic Tape

A means for remedying errors in data after long-term storage on magnetic tape

NASA's Jet Propulsion Laboratory, Pasadena, California

A new procedure for detecting and correcting errors in data held for long-term storage on magnetic tape involves recording and storing identical data strings at several locations on the tape reel. A computer verifies and upgrades the fidelity of the recorded data, using a comparison-and-rerecord process.

The data system in which this procedure is implemented includes a magnetic-tape unit, a computer, and a control sequencer. The system can be operated after long periods of inactivity and may be subjected to extreme environments. (It was originally intended for use aboard a Mars-Jupiter-Saturn space probe.) The computer, in addition to data handling, encodes the data in a BCH (Bose-Chaudhuri-Hocquenghem) error-detection code. These encoded data are stored at several positions on the tape.

When the system is reactivated, the computer decodes the stored data at playback. If there are independent or dependent (burst) errors, the computer requests a retransmission of the same data stored at another of the several tape positions. This retransmission is requested only if an error is detected. The computer then operates in combination with the control sequencer to execute the (correct) instructions recorded on the tape.

The system detects both independent and dependent errors. Errors in the received word are independent if channel noise affects each bit of a transmitted code word independently (i.e., the probability that a particular bit is in error is independent of the effect of the channel on previous bits). When channel noise affects a group of bits within a region of consecutive bits, the errors in the corresponding received word are dependent. Dependent-error patterns are known as burst-error patterns or simply "bursts."

The system can detect errors by using either a software or a hardware approach. A hardware encoder consists of control switches (flip-flops) and a feedback shift register (FSR). The FSR effectively multiplies the information polynomial, q(x) (the coefficients of which are represented by k information bits), by a fixed generator polynomial, g(x), of degree r. The resulting polynomial, $C(x) = q(x)g(x)$, is represented by a coefficient sequence having $n = k + r$ bits.

The corresponding decoder is an FSR that divides the received polynomial by the generator polynomial g(x). If the received polynomial is a valid code polynomial C(x), a zero remainder polynomial results. If the code polynomial contains a detectable error, a nonzero remainder polynomial results.

This work was done by Marvin Perlman of Caltech for **NASA's Jet Propulsion Laboratory.** *For further information, Circle 82 on the TSP Request Card.*
NPO-13842

Fabrication of Sea-Floor Models

Sea-floor models are fabricated simply and inexpensively by using a programed milling machine.

NASA's Jet Propulsion Laboratory, Pasadena, California

Sea-floor models are frequently used in evaluating marine construction projects. Typically, the seabed around a planned construction site is mapped by conventional soundings, and a scale model of the bed is built on the bottom of a large tank. The tank is then filled with water, and sea conditions are simulated to determine the water-wave mechanics of the area.

To date, sea-floor models have been built manually. Nails were driven to carefully measured heights in the wooden tank bottom to match the sea-bottom contours. Later, cement or concrete was poured, and the floor was hand-troweled to the levels established by the nails. After testing, the model was usually destroyed by using jackhammers.

In one newly proposed method (Figure 1) the sea-floor model is cut automatically with a programable milling head mounted on a carriage that rides on rails above the tank top. In this technique, a mixture of cement and vermiculite is poured on the tank floor. After the mixture sets, it is machined by the milling head, using standard cutters. The numerically-controlled milling head is programed using a tape from the sounding data; the machine is guided to produce a scale model of the ocean floor.

A key advantage of this process is that the model can be reused by pouring a fresh mixture and cutting a different contour for the next surface study. A typical end product of the method is shown in Figure 2.

(continued next page)

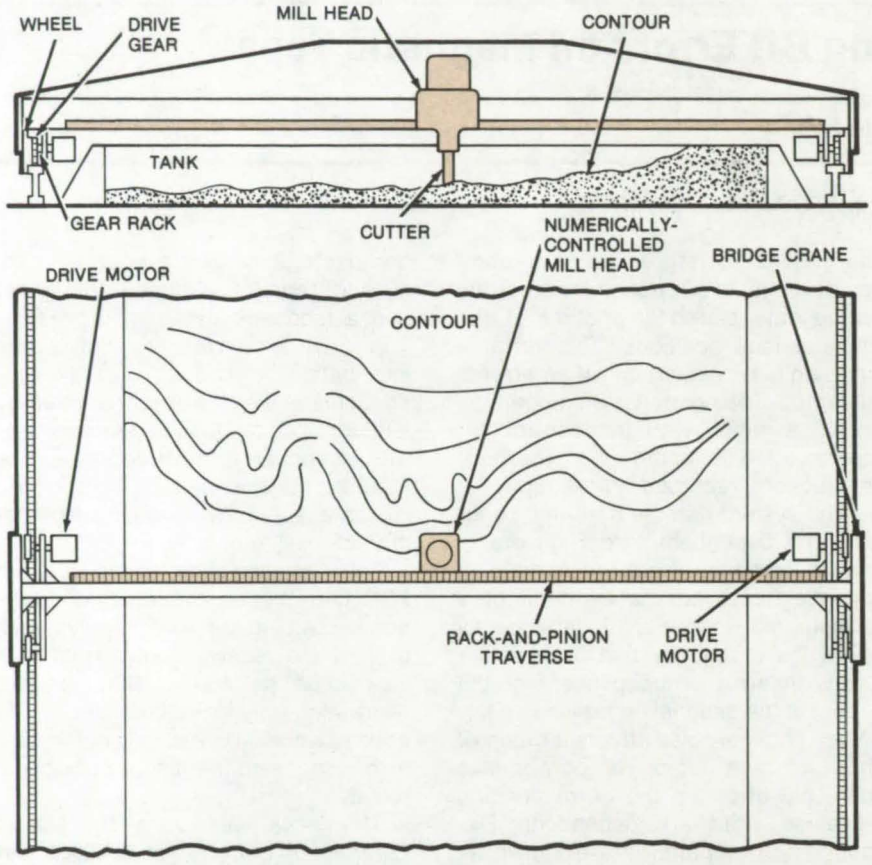

Figure 1. A **Programed Numerically-Controlled Cutter** moves in three dimensions. The sea-floor contour is reproduced, using sounding data to program the mill head.

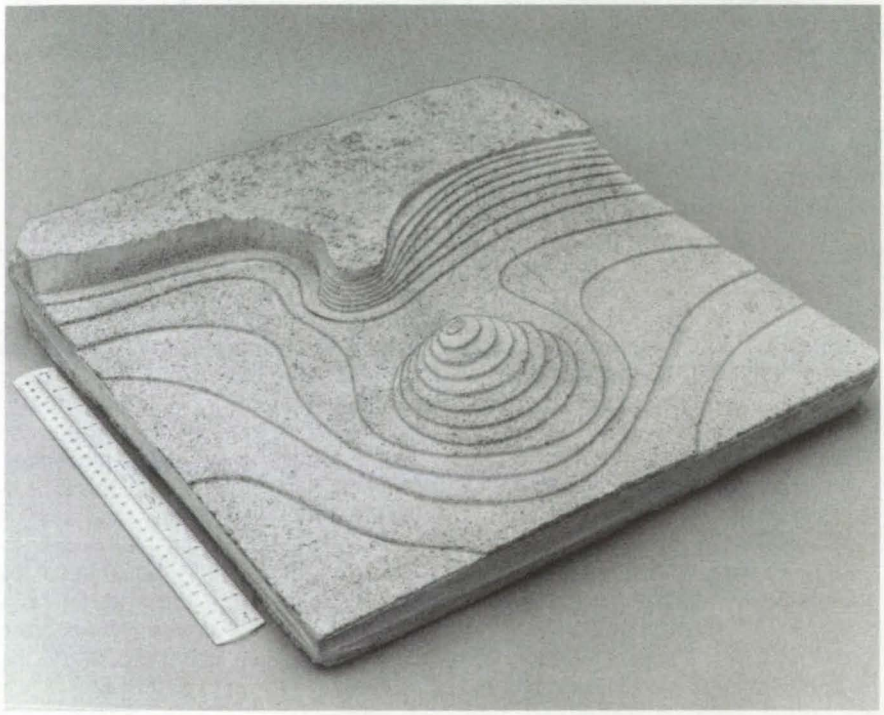

Figure 2. This **Sea-Floor Contour** was machined by using apparatus similar to that shown in Figure 1. The model can be filled and recut to generate a different contour.

A modified version of this procedure uses a fixed-bridge arrangement. The bridge is indexed in large increments and pinned. A small, traversing, trolley unit moves the milling head in a horizontal plane to create contours within a limited area. After completing an area, the bridge and trolley are indexed to the next position to work on another contour area. A third proposed method is to machine separate sections in a machine shop. The machined sea-floor sections would be transported to the tank site and fitted together to make the complete bottom.

The cement and vermiculite mixture sets well enough for machining in 2 days and can be walked on in from 3 to 7 days. The mixture can be poured or blown, is heavier than water, and does not redissolve in water. Its primary characteristic is that it is easily machinable.

This work was done by Gary L. Hale, Clarence E. Levoe, and Ralph E. Renner of Caltech for **NASA's Jet Propulsion Laboratory.** *For further information, Circle 83 on the TSP Request Card.*
NPO-13554

Computer Programs

These programs may be obtained at very reasonable cost from COSMIC, a facility sponsored by NASA to make new programs available to the public. For information on program price, size, and availability, circle the reference letter on the COSMIC Request Card in this issue.

Marshall System for Aerospace Simulation

Easily used system for engineering analysis

MARSYAS (Marshall System for Aerospace Simulation) was developed by NASA's Computation Laboratory at Marshall Space Flight Center to furnish engineers with a software system for quick and relatively easy simulations of physical systems on a digital computer. MARSYAS is a simple flexible language that can be coded by people who are unfamiliar with computer programing. With MARSYAS, even an engineer with little experience in simulation can simulate large physical systems. The language can be used to solve a system of differential equations or to simulate control systems including analog-computer block diagrams, or both simultaneously. Thus, one can mix differential equations with diagrams in a model.

In a MARSYAS model consisting of equations, the equations are expressed in a form that is similar to FORTRAN but allows explicit differentiation and the inclusion of special devices such as relays and switches directly in the equations. A block-diagram model specifies elements such as adders, integrators, and multiple input/output nonlinear devices and their interconnections. Either type of model may be treated as a submodel of a larger system, and the submodels may be nested to any degree required.

DEVICE and FUNCTION statement operators allow the user to construct unusual elements or excitation functions that do not appear in the library of Standard Elements and Excitation Functions. Other features include a Functional Data Base capability for storage of often-used models, a CHANGE operator for multiple stacked simulations without rewriting or resubmitting the program, and a CONTINUATION capability for changes at the object level, in the parameters and constraints of the problem, but not the physical model.

A versatile plotting system in the MARSYAS language allows nearly unlimited flexibility in specifying graphical output. Typical analyses that can be made and plotted are the ROOT LOCUS obtained by varying a given gain, the frequency response of the transfer function from any input to any output, and the FAST FOURIER transfer of any output. The system Jacobian matrix can also be obtained, as well as the associated eigenvalues and eigenvectors. Automatic features of MARSYAS include the detection and solution of linear and nonlinear algebraic loops.

For problems that contain discontinuities, the MARSYAS system automatically changes integration schemes to integrate through the discontinuity, unless instructed otherwise by the user. Default options are available to cover such constraints as integration method, initial conditions on transfer functions, excitation functions, and print sample rate. The language is designed so that the user needs to submit only the information essential to describe the mathematical model and to specify the simulation constraints.

This program is written in FORTRAN and Assembler and has been implemented on a UNIVAC 1108 computer with a central memory requirement of approximately 64K of 36-bit words. Plotted output requires an SC 4020 plotter and a plot library.

This program was written by H. H. Trauboth of **Marshall Space Flight Center** *and T. L. Balentine, W. L. McCollum, R. Sevigny, and A. J. Ventre of Computer Sciences Corp. For further information, Circle P on the COSMIC Request Card.*
MFS-22672

SUBJECT INDEX

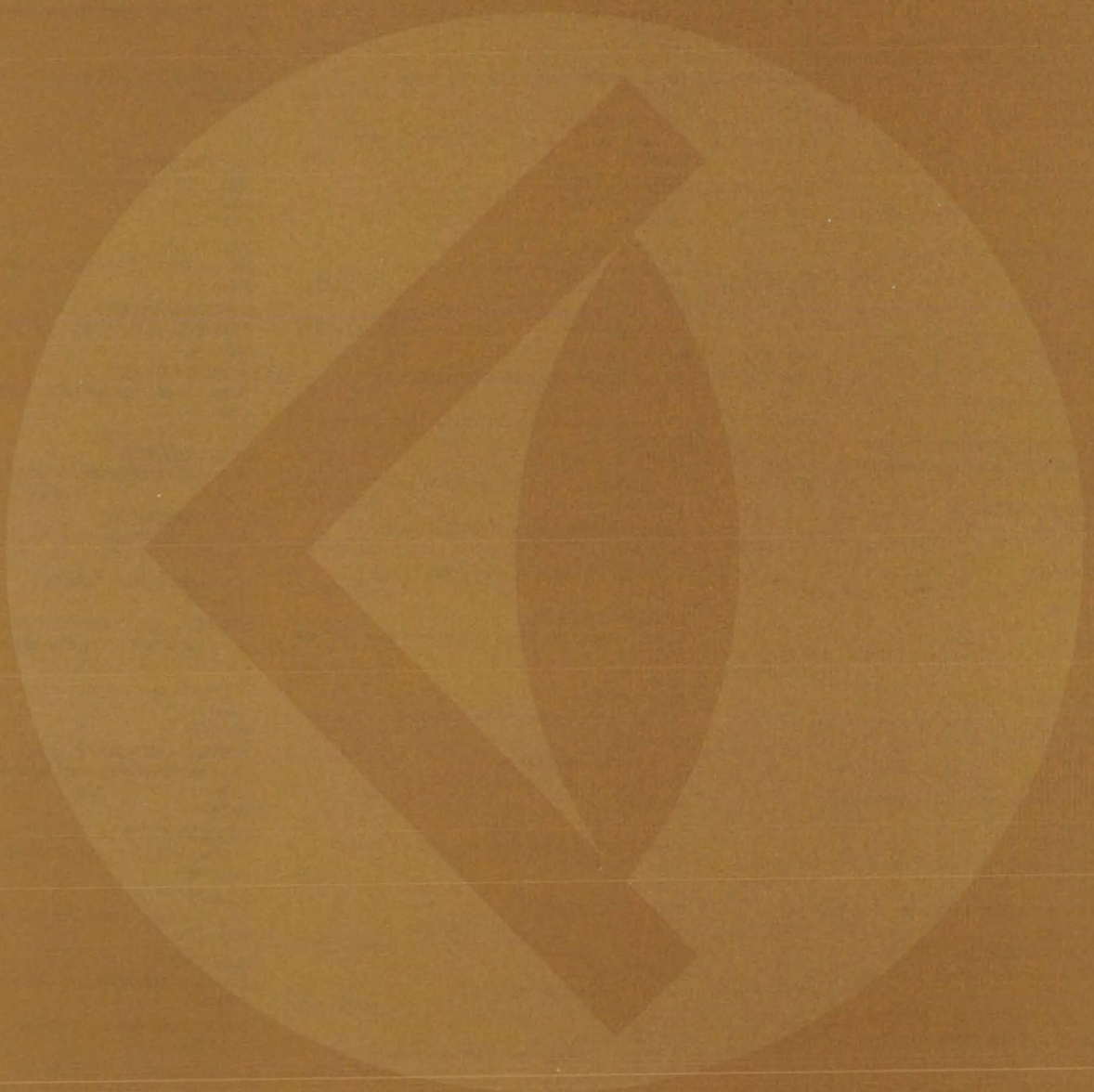

ABSORPTANCE
Selection standard for FEP films for solar energy
page 211 MSC-16999

ACCUMULATORS [COMPUTERS]
Fast differential analog-to-digital conversion
page 166 LEW-12909

ACOUSTIC MEASUREMENTS
Damage-detection system for LNG carriers
page 253 LAR-11463

Pseudo-continuous-wave acoustic instrument
page 257 LAR-12260

Pulse-echo probe of rock permeability near oil wells
page 229 NPO-14192

ACTUATORS
Subminiature hydraulic actuator
page 277 LAR-11522

ADHESIVES
Adhesive-removal tool
page 286 MSC-19498

Fire-retardant epoxy polymers
page 225 ARC-11182

Improved epoxy adhesive with radiographic tracer
page 231 MSC-18020

ADRENOCORTICOTROPIN [ACTH]
Boosting production yields of biomedical peptides
page 247 NPO-14142

AERATION
Free-air content in fluid systems
page 260 MSC-16703

AIR
Free-air content in fluid systems
page 260 MSC-16703

AIR CONDITIONING EQUIPMENT
Application of solar energy to air-conditioning
page 220 MFS-23913

AIRCRAFT GUIDANCE
Optical gyroscope
page 195 NPO-14258

AIRFRAMES
Airframe design for reducing cabin noise
page 265 LAR-12097

ALLOYS
Interactive data-processing system for metallurgy
page 224 MFS-23774

ALUMINUM ALLOYS
Brazed boron-silicon carbide/aluminum structural panels
page 228 LAR-12244

AMMETERS
Helicopter position stabilizing system
page 264 LAR-11670

AMMONIA
Compatibility of Au-Cu-Ni braze alloy with NH_3
page 226 MSC-16864

Positively charged membrane for urea dialysis
page 248 NPO-14101

AMPLITUDE MODULATION
Direct-reading group-delay measurement
page 172 NPO-13909

ANALOG TO DIGITAL CONVERTERS
Fast differential analog-to-digital conversion
page 166 LEW-12909

ANTENNA ARRAYS
Control of small phased-array antennas
page 184 MSC-14938

ANTENNAS
Human arm may act as antenna
page 179 ARC-11195

AUTOMATIC CONTROL
Improved servocontrol system
page 167 MFS-19358

AUTOMATIC TEST EQUIPMENT
Monitoring system for community water supplies
page 238 MSC-16778

Strobe-margin test for plated memory systems
page 171 MFS-23838

Water sample-collection and distribution system
page 241 MSC-16841

AUXILLIARY POWER SOURCES
Wind-wheel electric-power generator
page 276 MFS-23515

BACKGROUND NOISE
Low-background trace-gas detector
page 188 NPO-13683

BACTERIA
Automated electrochemical selection of coliforms
page 243 MSC-16777

Chemiluminescence and bioluminescence microbe detection
page 244 MSC-16779

Rapid measurement of bacteria in water
page 237 GSC-12158

BALL BEARINGS
Thermal performance of shaft bearing system
page 269 LEW-12761

BEAM SPLITTERS
Less-costly Michaelson interferometer
page 196 NPO-13999

BINDERS [MATERIALS]
Improved alkali-metal/silicate binders
page 231 GSC-12303

Installing fiber insulation in tight spaces
page 296 MSC-16934 and MSC-16973

BIOASSAY
Biological sampling and clearing device
page 252 NPO-14010

Chemiluminescence and bioluminescence microbe detection
page 244 MSC-16779

Monitoring system for community water supplies
page 238 MSC-16778

Rapid measurement of bacteria in water
page 237 GSC-12158

Water sample-collection and distribution system
page 241 MSC-16841

BIOLUMINESCENCE
Chemiluminescence and bioluminescence microbe detection
page 244 MSC-16779

BIOSYNTHESIS
Boosting production yields of biomedical peptides
page 247 NPO-14142

BIT SYNCHRONIZATION
Bit-synchronizer lock detector
page 182 MSC-16744

BITS
Detecting and correcting bit errors on magnetic tape
page 303 NPO-13842

BLADES [CUTTERS]
A sharp knife for high temperatures
page 285 MSC-16932

BLOOD FLOW
In vivo blood-flow mapping
page 251 NPO-14133

BLOOD VESSELS
A probe for blood-vessel and spinal interiors
page 248 NPO-14132

In vivo blood-flow mapping
page 251 NPO-14133

BOLTS
Ultrasonic extensometer measures bolt preload
page 278 MFS-19337

BOOMS [EQUIPMENT]
Collapsible module extends tenfold in height
page 287 NPO-13371

BORON CARBIDES
Brazed boron-silicon carbide/aluminum structural panels
page 228 LAR-12244

BOROSILICATE GLASS
Protective coating for laser diodes
page 191 LAR-11746

BOUNDARY LAYER FLOW
Detection of boundary-layer transitions in wind tunnels
page 263 LAR-12261

Internal and external 2-D boundary-layer flows
page 268 LEW-13009

BOURDON TUBES
Pressure-sensitive glass reaction cell
page 230 LAR-11256

BRAZING
Brazed boron-silicon carbide/aluminum structural panels
page 228 LAR-12244

Compatibility of Au-Cu-Ni braze alloy with NH_3
page 226 MSC-16864

CALCIUM OXIDES
High-yield process for preparing calcium superoxide
page 223 ARC-11053

CALIBRATING
Mass-spectrometer calibration standard
page 258 NPO-14097

CAMERA SHUTTERS
Wide-angle pinhole camera
page 192 LAR-11905

CARBON FIBERS
Response of graphite/epoxy composites to moisture
page 233 MSC-16899

CATECHOLAMINE
Chemical measurement of urine volume
page 245 MSC-16585

CATHETERIZATION
A probe for blood-vessel and spinal interiors
page 248 NPO-14132

In vivo blood-flow mapping
page 251 NPO-14133

CHEMICAL REACTION CONTROL
Boosting production yields of biomedical peptides
page 247 NPO-14142

High-yield process for preparing calcium superoxide
page 223 ARC-11053

CHEMILUMINESCENCE
Chemiluminescence and bioluminescence microbe detection
page 244 MSC-16779

CHROMIUM STEELS
A sharp knife for high temperatures
page 285 MSC-16932

CLAMPS
Gentle support stands for fluid-line mockups
page 298 MSC-16479

CLEANING
Biological sampling and cleaning device
page 252 NPO-14010

Microcircuit-cleaning machine
page 299 MSC-16060

CLOSED CIRCUIT TELEVISION
Infrared-enhanced TV for fire detection
page 191 MFS-19380

COATINGS
Protective coating for copper in aluminum heat exchangers
page 294 MFS-19334

Repairing silicon carbide coatings
page 232 MSC-18033

CODING
Low-noise computer link
page 178 NPO-14152

COLIFORM
Automated electrochemical selection of coliforms
page 243 MSC-16777

COLOR
Laser beam color separator
page 193 LAR-11806

COLORIMETRY
A probe for blood-vessel and spinal interiors
page 248 NPO-14132

COMBUSTION CHAMBERS
Simpler valve for reciprocating engines
page 283 MSC-16239

COMPARATORS
Automatic radio transmission monitor
page 183 NPO-13941

Femtosecond time-domain phase comparator
page 180 GSC-12228

Pseudo-continuous-wave acoustic instrument
page 257 LAR-12260

COMPENSATORS
Improved servocontrol system
page 167 MFS-19358

COMPOSITE MATERIALS
Fabrication of thick laminates
page 292 LAR-12019

Response of graphite/epoxy composites to moisture
page 233 MSC-16899

Testing composite sheets at high temperatures
page 260 MSC-16237

Void-free bends in laminated structures
page 293 MSC-16998

COMPRESSIBILITY
Verifying the fit of mating contoured surfaces
page 297 LAR-11731

COMPUTER STORAGE DEVICES
Detecting and correcting bit errors on magnetic tape
page 303 NPO-13842

Strobe-margin test for plated memory systems
page 171 MFS-23838

COMPUTERIZED DESIGN
Edge geometry of turbomachine blades
page 269 LEW-12979

Structural performance analysis and redesign
page 270 LAR-12213, LAR-12234, and MFS-23944

CONCENTRATORS
Improved conical solar concentrator
page 207 NPO-13825

CONDUCTIVE HEAT TRANSFER
Vibration-free thermal link
page 188 GSC-12297

CONTAMINATION
Low-background trace-gas detector
page 188 NPO-13683

Monitoring system for community water supplies
page 238 MSC-16778

Rapid measurement of bacteria in water
page 237 GSC-12158

CONTOURS
Verifying the fit of mating contoured surfaces
page 297 LAR-11731

CONTROL MOMENT GYROSCOPES
Helicopter position stabilizing system
page 264 LAR-11670

CONTROLLERS
Multichannel temperature controller for solar heating
page 203 MFS-23775

Programable controller for solar heating
page 204 MFS-23915

COOLING SYSTEMS
Application of solar energy to air-conditioning
page 220 MFS-23913

Protective coating for copper in aluminum heat exchangers
page 294 MFS-19334

The economics of solar-powered absorption cooling
page 219 MFS-23908

COPPER
Compatibility of Au-Cu-Ni braze alloy with NH_3
page 226 MSC-16864

Protective coating for copper in aluminum heat exchangers
page 294 MFS-19334

CORROSION
Compatibility of Au-Cu-Ni braze alloy with NH_3
page 226 MSC-16864

Corrosion detection and evaluation
page 232 MFS-24436

Corrosion inhibitors for solar heating and cooling systems
page 217 MFS-23892

Improved alkali-metal/silicate binders
page 231 GSC-12303

Measuring metallic concentrations in glycol solutions
page 218 MFS-23894

COST ANALYSIS
The economics of solar-powered absorption cooling
page 219 MFS-23908

COUNTERS
Synchronous transfer circuits for redundant systems
page 173 NPO-14162

COUPLING CIRCUITS
Human arm may act as antenna
page 179 ARC-11195

COUPLINGS
High-strength blind rivet
page 294 LAR-12154

CUSHIONS
Air-cushion landing system
page 267 LAR-12303

Low-frequency vibration isolation
page 282 NPO-13915

DAMAGE
Damage-detection system for LNG carriers
page 253 LAR-11463

Predicting damage from exploding vessels
page 267 LEW-13042

DAMPING
Low-frequency vibration isolation
page 282 NPO-13915

DATA ACQUISITION
Chopper-stabilized phase detector
page 181 MSC-16461

Data processing for water monitor system
page 240 MSC-16842

Monitoring system for community water supplies
page 238 MSC-16778

Water sample-collection and distribution system
page 241 MSC-16841

DATA LINKS
Low-noise computer link
page 178 NPO-14152

DATA PROCESSING
Interactive data-processing system for metallurgy
page 224 MFS-23774

DATA STORAGE
Automatic radio transmission monitor
page 183 NPO-13941

Water sample-collection and distribution system
page 241 MSC-16841

DATA TRANSMISSION
Detecting and correcting bit errors on magnetic tape
page 303 NPO-13842

Low-noise computer link
page 178 NPO-14152

DECONTAMINATION
Biological sampling and cleaning device
page 252 NPO-14010

DETONATION WAVES
Predicting damage from exploding vessels
page 267 LEW-13042

DIALYSIS
Positively charged membrane for urea dialysis
page 248 NPO-14101

DIGITAL SIMULATION
Electrolysis cell simulation
page 198 LEW-12740

Marshall system for aerospace simulation
page 305 MFS-22672

DIGITAL TO ANALOG CONVERTERS
Fast differential analog-to-digital conversion
page 166 LEW-12909

DISPENSERS
Automatic primate feeder
page 253 LAR-11586

DOSIMETERS
Stacked solar cells measure X-ray exposure
page 250 NPO-13954

DRILLING
Pulse-echo probe of rock permeability near oil wells
page 229 NPO-14192

ECONOMIC ANALYSIS
The economics of solar-powered absorption cooling
page 219 MFS-23908

EFFICIENCY
Pump efficiency in solar-energy systems
page 219 MFS-23934

ELASTIC PROPERTIES
Analysis of linear viscoelastic structures
page 271 NPO-13197

ELECTRIC CHOPPERS
Chopper-stabilized phase detector
page 181 MSC-16461

ELECTRIC GENERATORS
Wind-wheel electric-power generator
page 276 MFS-23515

ELECTRIC MOTORS
Three-phase induction motors
page 288 MSC-16904

ELECTRIC SWITCHES
High-power RF switch
page 168 NPO-14229

IC implementation of crossbar switches
page 170 NPO-13837

ELECTRO-OPTICS
Improved "spectrophone"
page 187 NPO-14143

ELECTROCHEMISTRY
Automated electrochemical selection of coliforms
page 243 MSC-16777

ELECTROLYSIS
Electrolysis cell simulation
page 198 LEW-12740

ELECTROMAGNETIC ABSORPTION
Selection standard for FEP films for solar energy
page 211 MSC-16999

ELECTROMAGNETIC RADIATION
Finding radiant-energy sources
page 177 GSC-12147

ELECTRON BEAMS
Improved electron-beam probe for hypersonic flows
page 261 NPO-13793

ELECTRONIC CONTROL
Programable controller for solar heating
page 204 MFS-23915

ELECTRONIC EQUIPMENT TESTS
Strobe-margin test for plated memory systems
pae 171 MFS-23838

Universal test specimen for solar cells
page 205 NPO-14062

ELECTRONIC MODULES
Safe venting for electronic components
page 171 MSC-18007

Synchronous transfer circuits for redundant systems
page 173 NPO-14162

ELECTROPHORESIS
Improvements in microelectrophoresis apparatus
page 253 ARC-11121

ELECTROSTATIC CHARGE
Antistatic additive for polyimide films
page 227 NPO-14232

ENERGY ABSORPTION FILMS
Selection standard for FEP films for solar energy
page 211 MSC-16999

ENERGY CONSERVATION
Energy conservation, using remote thermal scanning
page 197 LEW-12812

Optics for natural lighting
page 209 LAR-12333

ENERGY CONVERSION EFFICIENCY
Electrolysis cell simulation
page 198 LEW-12740

ENGINE PARTS
Edge geometry of turbomachine blades
page 269 LEW-12979

Simpler valve for reciprocating engines
page 283 MSC-16239

ENVIRONMENT MODELS
Fabrication of sea-floor models
page 303 NPO-13554

ENVIRONMENT SIMULATORS
Accelerated-weathering test system for solar cells
page 205 NPO-14061

ENVIRONMENTAL TESTS
Accelerated-weathering test system for solar cells
page 205 NPO-14061

Universal test specimen for solar cells
page 205 NPO-14062

EPOXY RESINS
Fire-retardant epoxy polymers
page 225 ARC-11182

Improved epoxy adhesive with radiographic tracer
page 231 MSC-18020

Response of graphite/epoxy composites to moisture
page 233 MSC-16899

EQUILIBRIUM EQUATIONS
Analysis of linear viscoelastic structures
page 271 NPO-13197

ERROR CORRECTING DEVICES
Detecting and correcting bit errors on magnetic tape
page 303 NPO-13842

ESCAPE SYSTEMS
Emergency escape device
page 278 MFS-23235

EXPANDABLE STRUCTURES
Collapsible module extends tenfold in height
page 287 NPO-13371

EXPLOSIONS
Predicting damage from exploding vessels
page 267 LEW-13042

EXTENSOMETERS
Ultrasonic extensometer measures bolt preload
page 278 MFS-19337

FABRICS
Special weave for insulating fabrics
page 295 MSC-16380

FAILURE ANALYSIS
Glass solar collector — materials assessment
page 218 MFS-23926

FASTENERS
High-strength blind rivet
page 294 LAR-12154

Ultrasonic extensometer measures bolt preload
page 278 MFS-19337

FEEDBACK CIRCUITS
Symmetric voltage-controlled variable resistance
page 165 MSC-16685

FEEDBACK CONTROL
Improved servocontrol system
page 167 MFS-19358

FEEDERS
Automatic primate feeder
page 253 LAR-11586

FERRITES
Temperature stabilization of microwave ferrite devices
page 169 MSC-16833

FIBER ORIENTATION
Fabrication of thick laminates
page 292 LAR-12019

FIBERS
Installing fiber insulation in tight spaces
page 296 MSC-16934 and MSC-16973

FIELD EFFECT TRANSISTORS
Symmetric voltage-controlled variable resistance
page 165 MSC-16685

FINISHES
Repairing silicon carbide coatings
page 232 MSC-18033

FIRE PREVENTION
Infrared-enhanced TV for fire detection
page 191 MFS-19380

FLEXING
Artificial leg with natural gait
page 246 MFS-23225

FLOW DISTRIBUTION
Detection of boundary-layer transitions in wind tunnels
page 263 LAR-12261

Internal and external 2-D boundary-layer flows
page 268 LEW-13009

FLOW MEASUREMENT
Aircraft trailing vortex hazard alleviators
page 280 LAR-12034

In vivo blood-flow mapping
page 251 NPO-14133

Meter for very slow flows
page 275 MSC-18112

FLUID SWITCHING ELEMENTS
Fluidic-oscillator gas analyzer
page 261 KSC-11014

FLUID TRANSMISSION LINES
Gentle support stands for fluid-line mockups
page 298 MSC-16479

FLUIDIC CIRCUITS
Fluidic-oscillator gas analyzer
page 261 KSC-11014

FOLDING STRUCTURES
Collapsible module extends tenfold in height
page 287 NPO-13371

FRAGMENTATION
Predicting damage from exploding vessels
page 267 LEW-13042

FREQUENCY MEASUREMENT
Pseudo-continuous-wave acoustic instrument
page 257 LAR-12260

FUEL VALVES
Simpler valve for reciprocating engines
page 283 MSC-16239

FURNACES
Slurry-powder sintering furnace
page 300 LAR-11423

GALLIUM ARSENIDE LASERS
Protective coating for laser diodes
page 191 LAR-11746

GAS ANALYSIS
Fluidic-oscillator gas analyzer
page 261 KSC-11014

Free-air content in fluid systems
page 260 MSC-16703

Improved "spectrophone"
page 187 NPO-14143

Low-background trace-gas detector
page 188 NPO-13683

Mass-spectrometer calibration standard
page 258 NPO-14097

GLASS
Pressure-sensitive glass reaction cell
page 230 LAR-11256

GLASS COATINGS
Protective coating for laser diodes
page 191 LAR-11746

GLYCOLS
Measuring metallic concentrations in glycol solutions
page 218 MFS-23894

GOLD ALLOYS
Compatibility of Au-Cu-Ni braze alloy with NH_3
page 226 MSC-16864

GRAPHITE
Response of graphite/epoxy composites to moisture
page 233 MSC-16899

GROUP VELOCITY
Direct-reading group-delay measurement
page 172 NPO-13909

GYROSCOPES
Optical gyroscope
page 195 NPO-14258

HEAT EXCHANGERS
Passive heat exchanger for solar heating
page 214 MFS-23914

Protective coating for copper in aluminum heat exchangers
page 294 MFS-19334

HEAT PUMPS
Practical and efficient magnetic heat pump
page 190 LEW-12508

HEATING EQUIPMENT
Multichannel temperature controller for solar heating
page 203 MFS-23775

Passive heat exchanger — installation package
page 214 MFS-23930

Passive heat exchanger for solar heating
page 214 MFS-23914

Protective coating for copper in aluminum heat exchangers
page 294 MFS-19334

Prototype residential solar-energy system
page 211 MFS-23932

Prototype residential solar-energy system-engineering analysis
page 212 MFS-23929

Prototype solar-heating system
page 201 MFS-23916

Prototype solar-heating system — engineering analysis
page 213 MFS-23910

Prototype solar-heating system — installation manual
page 213 MFS-23907

Pump efficiency in solar-energy systems
page 219 MFS-23934

Residential solar-heating system
page 202 MFS-23909

Residential solar-heating system — design brochure
page 212 MFS-23933

Solar-heating module
page 213 MFS-23925

HELICOPTER CONTROL
Helicopter position stabilizing system
page 264 LAR-11670

HIGH TEMPERATURE FLUIDS
Wide-temperature corrosion-resistant pressure regulator
page 281 NPO-13776

HOLDERS
Gentle support stands for fluid-line mockups
page 298 MSC-16479

HONEYCOMB CORES
Brazed boron-silicon carbide/aluminum structural panels
page 228 LAR-12244

HYDRAULIC EQUIPMENT
Subminiature hydraulic actuator
page 277 LAR-11522

HYDRAULIC SYSTEMS
Thermal hydraulic analyzer
page 271 MSC-18014, MSC-16797, and MSC-16877

HYDRAZINES
Pressure-sensitive glass reaction cell
page 230 LAR-11256

Wide-temperature corrosion-resistant pressure regulator
page 281 NPO-13776

HYDROGEN EMBRITTLEMENT
Hydrogen embrittlement of nickel
page 234 ARC-10966

HYDROGEN FUELS
Electrolysis cell simulation
page 198 LEW-12740

HYPERSONIC BOUNDARY LAYERS
Improved electron-beam probe for hypersonic flows
page 261 NPO-13793

INDUCTION MOTORS
Three-phase induction motors
page 288 MSC-16904

INERTIAL GUIDANCE
Optical gyroscope
page 195 NPO-14258

INFRARED IMAGERY
Infrared-enhanced TV for fire detection
page 191 MFS-19380

INHIBITORS
Corrosion inhibitors for solar heating and cooling systems
page 217 MFS-23892

INJECTION LASERS
Protective coating for laser diodes
page 191 LAR-11746

INORGANIC COATINGS
Protective coating for copper in aluminum heat exchangers
page 294 MFS-19334

INORGANIC PEROXIDES
High-yield process for preparing calcium superoxide
page 223 ARC-11053

INSTALLATION MANUALS
Flat-plate solar collector — installation package
page 214 MFS-23921

Passive heat exchanger — installation package
page 214 MFS-23930

Prototype solar-heating system — installation manual
page 213 MFS-23907

INSULATION
Installing fiber insulation in tight spaces
page 296 MSC-16934 and MSC-16973

Special weave for insulating fabrics
page 295 MSC-16380

INSULIN
Boosting production yields of biomedical peptides
page 247 NPO-14142

INTEGRATED CIRCUITS
Analyzing CMOS/SOS fabrication for LSI arrays
page 174 MFS-23788

IC implementation of crossbar switches
page 170 NPO-13837

Microcircuit-cleaning machine
page 299 MSC-16060

INTERFEROMETERS
Less-costly Michaelson interferometer
page 196 NPO-13999

LAMINATES
Fabrication of thick laminates
page 292 LAR-12019

Void-free bends in laminated structures
page 293 MSC-16998

LANDING AIDS
Air-cushion landing system
page 267 LAR-12303

LARGE SCALE INTEGRATION
Analyzing CMOS/SOS fabrication for LSI arrays
page 174 MFS-23788

LASER APPLICATIONS
Laser beam color separator
page 193 LAR-11806

Improved "spectrophone"
page 187 NPO-14143

In vivo blood-flow mapping
page 251 NPO-14133

Optical gyroscope
page 195 NPO-14258

LATCHES
Dual-action expand-and-latch mechanism
page 285 MFS-23557

LEAKAGE
Damage-detection system for LNG carriers
page 253 LAR-11463

LIGHT EMITTING DIODES
Protective coating for laser diodes
page 191 LAR-11746

LIGHT TRANSMISSION
Optics for natural lighting
page 209 LAR-12333

LINING PROCESSES
Installing fiber insulation in tight spaces
page 296 MSC-16934 and MSC-16973

LIQUEFIED GASES
Damage-detection system for LNG carriers
page 253 LAR-11463

LIQUID AMMONIA
Compatibility of Au-Cu-Ni braze alloy with NH_3
page 226 MSC-16864

LIQUID METALS
Interactive data-processing system for metallurgy
page 224 MFS-23774

LITHIUM CHLORIDES
Chemical measurement of urine volume
page 245 MSC-16585

LOW TEMPERATURE BRAZING
Compatibility of Au-Cu-Ni braze alloy with NH_3
page 226 MSC-16864

LOW TEMPERATURE TESTS
Mechanical properties of 18-2 Mn stainless steel
page 233 MFS-23843

Nitronic 60: a new alloy
page 233 MFS-23844

MAGNETIC CORES
Cost-effective method for transformer fabrication
page 291 NPO-14243

Improved fabrication method for C-core transformers
page 292 NPO-13855

MAGNETIC TAPES
Detecting and correcting bit errors on magnetic tape
page 303 NPO-13842

MASS SPECTROMETERS
Mass-spectrometer calibration standard
page 258 NPO-14097

MECHANICAL PROPERTIES
Brazed boron-silicon carbide/aluminum structural panels
page 228 LAR-12244

Hydrogen embrittlement of nickel
page 234 ARC-10966

Mechanical properties of 18-2 Mn stainless steel
page 233 MFS-23843

Nitronic 60: a new alloy
page 233 MFS-23844

Response of graphite/epoxy composites to moisture
page 233 MSC-16899

Thermal hydraulic analyzer
page 271 MSC-18014, MSC-16797, and MSC-16877

MEMBRANES
Positively charged membrane for urea dialysis
page 248 NPO-14101

Pressure-sensitive glass reaction cell
page 230 LAR-11256

METAL CRYSTALS
Hydrogen embrittlement of nickel
page 234 ARC-10966

METAL OXIDE SEMICONDUCTORS
Analyzing CMOS/SOS fabrication for LSI arrays
page 174 MFS-23788

MICHELSON INTERFEROMETERS
Less-costly Michaelson interferometer
page 196 NPO-13999

MICROWAVE EQUIPMENT
Direct-reading group-delay measurement
page 172 NPO-13909

High-power RF switch
page 168 NPO-14229

Temperature stabilization of microwave ferrite devices
page 169 MSC-16833

MIRRORS
Optics for natural lighting
page 209 LAR-12333

MODELS
Fabrication of sea-floor models
page 303 NPO-13554

MODULATION
Direct-reading group-delay measurement
page 172 NPO-13909

MODULES
Collapsible module extends tenfold in height
page 287 NPO-13371

MOISTURE CONTENT
Response of graphite/epoxy composites to moisture
page 233 MSC-16899

MOTORS
Three-phase induction motors
page 288 MSC-16904

MULTIPLEXING
IC implementation of crossbar switches
page 170 NPO-13837

NICKEL
Compatibility of Au-Cu-Ni braze alloy with NH_3
page 226 MSC-16864

Hydrogen embrittlement of nickel
page 234 ARC-10966

A sharp knife for high temperatures
page 285 MSC-16932

NOISE METERS
Pseudo-continuous-wave acoustic instrument
page 257 LAR-12260

NOISE REDUCTION
Airframe design for reducing cabin noise
page 265 LAR-12097

Low-noise computer link
page 178 NPO-14152

NOMOGRAPHS
Free-air content in fluid systems
page 260 MSC-16703

NONDESTRUCTIVE TESTS
Corrosion detection and evaluation
page 232 MFS-24436

Improved epoxy adhesive with radiographic tracer
page 231 MSC-18020

Pseudo-continuous-wave acoustic instrument
page 257 LAR-12260

NONFLAMMABLE MATERIALS
Fire-retardant epoxy polymers
page 225 ARC-11182

NUCLEAR MAGNETIC RESONANCE
Boosting production yields of biomedical peptides
page 247 NPO-14142

Pulsed NMR spectroscopy
page 194 NPO-14023

NUMERICAL CONTROL
Data processing for water monitor system
page 240 MSC-16842

OCEAN MODELS
Fabrication of sea-floor models
page 303 NPO-13554

OIL EXPLORATION
Pulse-echo probe of rock permeability near oil wells
page 229 NPO-14192

OPTICAL GYROSCOPES
Optical gyroscope
page 195 NPO-14258

OSCILLATING FLOW
Fluidic-oscillator gas analyzer
page 261 KSC-11014

OSCILLATION DAMPERS
Low-frequency vibration isolation
page 282 NPO-13915

Vibration-free thermal link
page 188 GSC-12297

OVENS
Slurry-powder sintering furnace
page 300 LAR-11423

Verifying the fit of mating contoured surfaces
page 297 LAR-11731

OXIMETRY
A probe for blood-vessel and spinal interiors
page 248 NPO-14132

OXYGEN PRODUCTION
High-yield process for preparing calcium superoxide
page 223 ARC-11053

PAINTS
Improved alkali-metal/silicate binders
page 231 GSC-12303

PANORAMIC CAMERAS
Wide-angle pinhole camera
page 192 LAR-11905

PARTICULATE SAMPLING
Biological sampling and cleaning device
page 252 NPO-14010

Water sample-collection and distribution system
page 241 MSC-16841

PEPTIDES
Boosting production yields of biomedical peptides
page 247 NPO-14142

PERFORMANCE TESTS
Flat-plate liquid solar collector
page 216 MFS-23912

Performance and structural tests of hot-air solar collectors
page 215 MFS-23911

Performance evaluation of a liquid solar collector
page 216 MFS-23931

Prototype solar-heating system — engineering analysis
page 213 MFS-23910

Strobe-margin test for plated memory systems
page 171 MFS-23838

Testing of three hot-air solar collectors
page 215 MFS-23887

Thermal performance of an air-type solar collector
page 216 MFS-23924

PHASE DETECTORS
Chopper-stabilized phase detector
page 181 MSC-16461

Femtosecond time-domain phase comparator
page 180 GSC-12228

PHASE ERROR
Bit-synchronizer lock detector
page 182 MSC-16744

Femtosecond time-domain phase comparator
page 180 GSC-12228

PHASED ARRAYS
Control of small phased-array antennas
page 184 MSC-14938

PHOSPHORUS
Fire-retardant epoxy polymers
page 225 ARC-11182

PHOTOGRAPHY
Wide-angle pinhole camera
page 192 LAR-11905

PINS
High-strength blind rivet
page 294 LAR-12154

PIPES [TUBES]
Gentle support stands for fluid-line mockups
page 298 MSC-16479

PISTON ENGINES
Simpler valve for reciprocating engines
page 283 MSC-16239

POLLUTION MONITORING
Data processing for water monitor system
page 240 MSC-16842

Monitoring system for community water supplies
page 238 MSC-16778

Rapid measurement of bacteria in water
page 237 GSC-12158

POLYIMIDES
Antistatic additive for polyimide films
page 227 NPO-14232

POLYMERIC FILMS
Selection standard for FEP films for solar energy
page 211 MSC-16999

PORPHYRINS
Chemiluminescence and bioluminescence microbe detection
page 244 MSC-16779

POSITION [LOCATION]
Helicopter position stabilizing system
page 264 LAR-11670

POSITIONING DEVICES [MACHINERY]
Collapsible module extends tenfold in height
page 287 NPO-13371

POWDER METALLURGY
Slurry-powder sintering furnace
page 300 LAR-11423

PRESSURE MEASUREMENTS
Pressure-sensitive glass reaction cell
page 230 LAR-11256

PRESSURE REGULATORS
Wide-temperature corrosion-resistant pressure regulator
page 281 NPO-13776

PRESSURE VESSELS
Predicting damage from exploding vessels
page 267 LEW-13042

PRESTRESSING
Ultrasonic extensometer measures bolt preload
page 278 MFS-19337

PRIMATES
Automatic primate feeder
page 253 LAR-11586

PRISMS
Laser beam color separator
page 193 LAR-11806

PROPELLANT TANKS
Predicting damage from exploding vessels
page 267 LEW-13042

PROSTHETIC DEVICES
Artificial leg with natural gait
page 246 MFS-23225

PROTECTIVE COATINGS
Improved alkali-metal/silicate binders
page 231 GSC-12303

Protective coating for copper in aluminum heat exchangers
page 294 MFS-19334

Protective coating for laser diodes
page 191 LAR-11746

Repairing silicon carbide coatings
page 232 MSC-18033

PULSE CODE MODULATION
Low-noise computer link
page 178 NPO-14152

PUMPS
Pump efficiency in solar-energy systems
page 219 MFS-23934

RADIATION DETECTORS
Finding radiant-energy sources
page 177 GSC-12147

Inexpensive, portable, integrating solar meter
page 208 LEW-12804

Stacked solar cells measure X-ray exposure
page 250 NPO-13954

RADIATION DOSAGE
Stacked solar cells measure X-ray exposure
page 250 NPO-13954

RADIO ANTENNAS
Human arm may act as antenna
page 179 ARC-11195

RADIO FREQUENCIES
High-power RF switch
page 168 NPO-14229

RADIO FREQUENCY INTERFERENCE
Automatic radio transmission monitor
page 183 NPO-13941

Finding radiant-energy sources
page 177 GSC-12147

RADIO TRANSMISSION
Automatic radio transmission monitor
page 183 NPO-13941

RADIOGRAPHY
Stacked solar cells measure X-ray exposure
page 250 NPO-13954
Improved epoxy adhesive with radiographic tracer
page 231 MSC-18020

REDUNDANCY ENCODING
Detecting and correcting bit errors on magnetic tape
page 303 NPO-13842

REDUNDANT COMPONENTS
Synchronous transfer circuits for redundant systems
page 173 NPO-14162

REFRIGERATORS
Practical and efficient magnetic heat pump
page 190 LEW-12508

REMOVAL
Adhesive-removal tool
page 286 MSC-19498

REPLICAS
Fabrication of sea-floor models
page 303 NPO-13554

RIGID MOUNTING
Vibration-free thermal link
page 188 GSC-12297

RIVETS
High-strength blind rivet
page 294 LAR-12154

ROLLER BEARINGS
Thermal performance of shaft bearing system
page 269 LEW-12761

ROLLING MOMENTS
Aircraft trailing vortex hazard alleviators
page 280 LAR-12034

ROTOR BLADES [TURBOMACHINERY]
Edge geometry of turbomachine blades
page 269 LEW-12979

SAFETY MANAGEMENT
Infrared-enhanced TV for fire detection
page 191 MFS-19380

SAMPLING
Biological sampling and cleaning device
page 252 NPO-14010
Monitoring system for community water supplies
page 238 MSC-16778
Rapid measurement of bacteria in water
page 237 GSC-12158
Water sample-collection and distribution system
page 241 MSC-16841

SANDWICH STRUCTURES
Fabrication of thick laminates
page 292 LAR-12019
Testing composite sheets at high temperatures
page 260 MSC-16237
Void-free bends in laminated structures
page 293 MSC-16998

SCANNING
Energy conservation, using remote thermal scanning
page 197 LEW-12812

SCRAPERS
Adhesive-removal tool
page 286 MSC-19498

SEA ROUGHNESS
Fabrication of sea-floor models
page 303 NPO-13554

SERVOCONTROL
Improved servocontrol system
page 167 MFS-19358

SHAFTS [MACHINE ELEMENTS]
Thermal performance of shaft bearing system
page 269 LEW-12761

SHAKERS
Microcircuit-cleaning machine
page 299 MSC-16060

SHOCK ABSORBERS
Low-frequency vibration isolation
page 282 NPO-13915
Vibration-free thermal link
page 188 GSC-12297

SIGNAL STABILIZATION
Chopper-stabilized phase detector
page 181 MSC-16461

SIGNAL TO NOISE RATIOS
Low-noise computer link
page 178 NPO-14152

SILICATES
Improved alkali-metal/silicate binders
page 231 GSC-12303

SILICON CARBIDES
Brazed boron-silicon carbide/aluminum structural panels
page 228 LAR-12244
Repairing silicon carbide coatings
page 232 MSC-18033

SINTERING
Slurry-powder sintering furnace
page 300 LAR-11423

SKY RADIATION
Optics for natural lighting
page 209 LAR-12333

SLURRIES
Slurry-powder sintering furnace
page 300 LAR-11423

SOLAR CELLS
Accelerated-weathering test system for solar cells
page 205 NPO-14061
Automated solar-cell-array assembly machine
page 206 NPO-13652
Universal test specimen for solar cells
page 205 NPO-14062

SOLAR ENERGY
Accelerated-weathering test system for solar cells
page 205 NPO-14061
Application of solar energy to air-conditioning
page 220 MFS-23913
Automated solar-cell-array assembly machine
page 206 NPO-13652
Corrosion inhibitors for solar heating and cooling systems
page 217 MFS-23892
Flat-plate liquid solar collector
page 216 MFS-23912
Flat-plate solar collector — installation package
page 214 MFS-23921
Glass solar collector — materials assessment
page 218 MFS-23926
Improved conical solar concentrator
page 207 NPO-13825
Indoor and outdoor tests of a liquid solar collector
page 217 MFS-23886
Inexpensive, portable, integrating solar meter
page 208 LEW-12804
Measuring metallic concentrations in glycol solutions
page 218 MFS-23894
Passive heat exchanger for solar heating
page 214 MFS-23914
Passive heat exchanger — installation package
page 214 MFS-23930
Performance and structural tests of hot-air solar collectors
page 215 MFS-23911
Performance evaluation of a liquid solar collector
page 216 MFS-23931
Performance of black-nickel and black-chrome solar collectors
page 218 MFS-23888
Programable controller for solar heating
page 204 MFS-23915
Prototype air flat-plate solar collector
page 214 MFS-23893
Prototype residential solar-energy system
page 211 MFS-23932
Prototype residential solar-energy system-engineering analysis
page 212 MFS-23929
Prototype solar-heating system
page 201 MFS-23916
Prototype solar-heating system — engineering analysis
page 213 MFS-23910
Prototype solar-heating system — installation manual
page 213 MFS-23907
Pump efficiency in solar-energy systems
page 219 MFS-23934
Residential solar-heating system
page 202 MFS-23909
Residential solar-heating system — design brochure
page 212 MFS-23933
Selection standard for FEP films for solar energy
page 211 MSC-16999
Solar-heating module
page 213 MFS-23925
Testing of three hot-air solar collectors
page 215 MFS-23887
The economics of solar-powered absorption cooling
page 219 MFS-23908
Thermal performance of a flat-plate liquid solar collector
page 217 MFS-23890
Thermal performance of a hot-air solar collector
page 215 MFS-23891
Thermal performance of an air-type solar collector
page 216 MFS-23924
Universal test specimen for solar cells
page 205 NPO-14062

SOLAR REFLECTORS
Optics for natural lighting
page 209 LAR-12333

SOLAR SIMULATORS
Accelerated-weathering test system for solar cells
page 205 NPO-14061
Flat-plate liquid solar collector
page 216 MFS-23912

SOLUBILITY
Positively charged membrane for urea dialysis
page 248 NPO-14101

SOUND TRANSMISSION
Airframe design for reducing cabin noise
page 265 LAR-12097

SPECTRAL SIGNATURES
Measuring metallic concentrations in glycol solutions
page 218 MFS-23894

SPECTROSCOPY
Pulsed NMR spectroscopy
page 194 NPO-14023

SPECTRUM ANALYSIS
Automatic radio transmission monitor
page 183 NPO-13941

SPIN RESONANCE
Pulsed NMR spectroscopy
page 194 NPO-14023

SPINDLES
Cost-effective method for transformer fabrication
page 291 NPO-14243

SPINE
A probe for blood-vessel and spinal interiors
page 248 NPO-14132

STABILIZATION
Helicopter position stabilizing system
page 264 LAR-11670

STAINLESS STEELS
Mechanical properties of 18-2 Mn stainless steel
page 233 MFS-23843
Nitronic 60: a new alloy
page 233 MFS-23844

STANDARDS
Mass-spectrometer calibration standard
page 258 NPO-14097

STARK EFFECT
Improved "spectrophone"
page 187 NPO-14143

STATIC ELECTRICITY
Antistatic additive for polyimide films
page 227 NPO-14232

STEERABLE ANTENNAS
Control of small phased-array antennas
page 184 MSC-14938

STRAPS
Human arm may act as antenna
page 179 ARC-11195

STRESS ANALYSIS
Stress analysis under component relative interference fit
page 268 LEW-12911
Structural performance analysis and redesign
page 270 LAR-12213, LAR-12234, and MFS-23944

STRESS CORROSION
Mechanical properties of 18-2 Mn stainless steel
page 233 MFS-23843
Nitronic 60: a new alloy
page 233 MFS-23844

STRUCTURAL ANALYSIS
Analysis of linear viscoelastic structures
page 271 NPO-13197
Stress analysis under component relative interference fit
page 268 LEW-12911
Structural performance analysis and redesign
page 270 LAR-12213, LAR-12234, and MFS-23944

SUBMINIATURIZATION
Subminiature hydraulic actuator
page 277 LAR-11522

SWITCHES
High-power RF switch
page 168 NPO-14229

SWITCHING CIRCUITS
IC implementation of crossbar switches
page 170 NPO-13837
Symmetric voltage-controlled variable resistance
page 165 MSC-16685

SYNCHRONISM
Chopper-stabilized phase detector
page 181 MSC-16461
Synchronous transfer circuits for redundant systems
page 173 NPO-14162

SYNCHRONIZED OSCILLATORS
Synchronous transfer circuits for redundant systems
page 173 NPO-14162

SYSTEMS FAILURES
Synchronous transfer circuits for redundant systems
page 173 NPO-14162

TANKS [CONTAINERS]
Damage-detection system for LNG carriers
page 253 LAR-11463

TEFLON [TRADEMARK]
Selection standard for FEP films for solar energy
page 211 MSC-16999

TELEVISION CAMERAS
Infrared-enhanced TV for fire detection
page 191 MFS-19380

TEMPERATURE CONTROL
Multichannel temperature controller for solar heating
page 203 MFS-23775
Prototype residential solar-energy system
page 211 MFS-23932
Prototype residential solar-energy system-engineering analysis
page 212 MFS-23929
Prototype solar-heating system
page 201 MFS-23916
Residential solar-heating system
page 202 MFS-23909
Residential solar-heating system — design brochure
page 212 MFS-23933
Solar-heating module
page 213 MFS-23925
Temperature stabilization of microwave ferrite devices
page 169 MSC-16833

TEMPERATURE EFFECTS
Testing composite sheets at high temperatures
page 260 MSC-16237

TENSILE PROPERTIES
Hydrogen embrittlement of nickel
page 234 ARC-10966
Mechanical properties of 18-2 Mn stainless steel
page 233 MFS-23843
Nitronic 60: a new alloy
page 233 MFS-23844

TENSILE STRENGTH
Hydrogen embrittlement of nickel
page 234 ARC-10966

TEST FACILITIES
Accelerated-weathering test system for solar cells
page 205 NPO-14061
Flat-plate liquid solar collector
page 216 MFS-23912
Strobe-margin test for plated memory systems
page 171 MFS-23838
Testing composite sheets at high temperatures
page 260 MSC-16237
Testing of three hot-air solar collectors
page 215 MFS-23887
Universal test specimen for solar cells
page 205 NPO-14062

TEST STANDS
Testing composite sheets at high temperatures
page 260 MSC-16237

THERMAL CONTROL COATINGS
Selection standard for FEP films for solar energy
page 211 MSC-16999

THERMAL DEGRADATION
Brazed boron-silicon carbide/aluminum structural panels
page 228 LAR-12244

THERMAL INSULATION
Installing fiber insulation in tight spaces
page 296 MSC-16934 and MSC-16973
Special weave for insulating fabrics
page 295 MSC-16380

THERMAL MAPPING
Energy conservation, using remote thermal scanning
page 197 LEW-12812

THERMODYNAMIC PROPERTIES
Thermal hydraulic analyzer
page 271 MSC-18014, MSC-16797, and MSC-16877

THERMOSETTING RESINS
Response of graphite/epoxy composites to moisture
page 233 MSC-16899

THERMOSTATS
Multichannel temperature controller for solar heating
page 203 MFS-23775

TOOLS
Adhesive-removal tool
page 286 MSC-19498
Compact ratchet wrench
page 281 MFS-24252

TORQUEMETERS
Ultrasonic extensometer measures bolt preload
page 278 MFS-19337

TRACE ELEMENTS
Improved epoxy adhesive with radiographic tracer
page 231 MSC-18020

TRACKING FILTERS
Chopper-stabilized phase detector
page 181 MSC-16461

TRANSFORMERS
Cost-effective method for transformer fabrication
page 291 NPO-14243
Improved fabrication method for C-core transformers
page 292 NPO-13855

TRANSMITTANCE
Selection standard for FEP films for solar energy
page 211 MSC-16999

TURBINE BLADES
Edge geometry of turbomachine blades
page 269 LEW-12979

TURBULENT WAKES
Aircraft trailing vortex hazard alleviators
page 280 LAR-12034

TWO DIMENSIONAL BOUNDARY LAYER
Internal and external 2-D boundary-layer flows
page 268 LEW-13009

ULTRASONIC TESTS
Ultrasonic extensometer measures bolt preload
page 278 MFS-19337

ULTRASONIC WAVE TRANSDUCERS
Damage-detection system for LNG carriers
page 253 LAR-11463

UNDERWATER ENGINEERING
Fabrication of sea-floor models
page 303 NPO-13554

UREAS
Positively charged membrane for urea dialysis
page 248 NPO-14101

URINALYSIS
Chemical measurement of urine volume
page 245 MSC-16585

VELOCITY MEASUREMENT
In vivo blood-flow mapping
page 251 NPO-14133
Meter for very slow flows
page 275 MSC-18112

VENTILATION
Safe venting for electronic components
page 171 MSC-18007

VERY HIGH FREQUENCIES
Human arm may act as antenna
page 179 ARC-11195

VIBRATION ISOLATORS
Low-frequency vibration isolation
page 282 NPO-13915
Vibration-free thermal link
page 188 GSC-12297

VIDICONS
Infrared-enhanced TV for fire detection
page 191 MFS-19380

VISCOELASTICITY
Analysis of linear viscoelastic structures
page 271 NPO-13197

VISCOUS DAMPING
Low-frequency vibration isolation
page 282 NPO-13915

VOIDS
Void-free bends in laminated structures
page 293 MSC-16998

VOLUMETRIC ANALYSIS
Chemical measurement of urine volume
page 245 MSC-16585

VORTICES
Aircraft trailing vortex hazard alleviators
page 280 LAR-12034

WALKING
Artificial leg with natural gait
page 246 MFS-23225

WASHING
Biological sampling and cleaning device
page 252 NPO-14010

WATER QUALITY
Automated electrochemical selection of coliforms
page 243 MSC-16777

Chemiluminescence and bioluminescence microbe detection
page 244 MSC-16779

Data processing for water monitor system
page 240 MSC-16842

Monitoring system for community water supplies
page 238 MSC-16778

Rapid measurement of bacteria in water
page 237 GSC-12158

Water sample-collection and distribution system
page 241 MSC-16841

WAVELENGTHS
Laser beam color separator
page 193 LAR-11806

WEATHERING
Accelerated-weathering test system for solar cells
page 205 NPO-14061

WEAVING
Special weave for insulating fabrics
page 295 MSC-16380

WELDED JOINTS
Compatibility of Au-Cu-Ni braze alloy with NH_3
page 226 MSC-16864

WIDE ANGLE LENSES
Wide-angle pinhole camera
page 192 LAR-11905

WINCHES
Emergency escape device
page 278 MFS-23235

WIND TUNNEL TESTS
Aircraft trailing vortex hazard alleviators
page 280 LAR-12034

Detection of boundary-layer transitions in wind tunnels
page 263 LAR-12261

Subminiature hydraulic actuator
page 277 LAR-11522

WINDING
Cost-effective method for transformer fabrication
page 291 NPO-14243

WINDPOWERED GENERATORS
Wind-wheel electric-power generator
page 276 MFS-23515

WIRE WINDING
Cost-effective method for transformer fabrication
page 291 NPO-14243

WRENCHES
Compact ratchet wrench
page 281 MFS-24252

X RAY INSPECTION
Improved epoxy adhesive with radiographic tracer
page 231 MSC-18020

X RAY IRRADIATION
Stacked solar cells measure X-ray exposure
page 250 NPO-13954

YARNS
Special weave for insulating fabrics
page 295 MSC-16380

ZIRCONIUM IODIDES
Positively charged membrane for urea dialysis
page 248 NPO-14101

National Aeronautics and
Space Administration

Washington, D.C.
20546

SPECIAL FOURTH-CLASS RATE
BOOK

FOURTH-CLASS MAIL
POSTAGE & FEES PAID
NASA
WASHINGTON, D.C.
PERMIT No. G 27

NASA

NASA's Water Monitor System [WMS] automatically analyzes community water supplies for chemicals and biological contaminants. Developed at NASA's Lyndon B. Johnson Space Center in Houston, Texas, in cooperation with the U.S. Department of Housing and Urban Development, the WMS transfers the technology of aerospace sensors, information processing and display, and fluid control equipment to the growing needs for quality control of community water supplies. *See page 238 for more information on the WMS.*